JYU DISSERTATIONS 606

Dhanik Reshamwala

Broad-Spectrum Antivirals from Nature

Studies on Efficacy and Molecular Mechanism

UNIVERSITY OF JYVÄSKYLÄ
FACULTY OF MATHEMATICS
AND SCIENCE

JYU DISSERTATIONS 606

Dhanik Reshamwala

Broad-Spectrum Antivirals from Nature

Studies on Efficacy and Molecular Mechanism

Esitetään Jyväskylän yliopiston matemaattis-luonnontieteellisen tiedekunnan suostumuksella
julkisesti tarkastettavaksi yliopiston Ylistönrinteen salissa YAA303
helmikuun 24. päivänä 2023 kello 12.

Academic dissertation to be publicly discussed, by permission of
the Faculty of Mathematics and Science of the University of Jyväskylä,
in Ylistönrinne, auditorium YAA303, on February 24, 2023 at 12 o'clock noon.

JYVÄSKYLÄN YLIOPISTO
UNIVERSITY OF JYVÄSKYLÄ

JYVÄSKYLÄ 2023

Editors
Matti Jalasvuori
Department of Biological and Environmental Sciences, University of Jyväskylä
Ville Korkiakangas
Open Science Centre, University of Jyväskylä

ISBN 978-951-39-9293-4 (PDF)
URN:ISBN:978-951-39-9293-4
ISSN 2489-9003

Permanent link to this publication: http://urn.fi/URN:ISBN:978-951-39-9293-4

ABSTRACT

Reshamwala, Dhanik
Broad-spectrum antivirals from nature: studies on efficacy and molecular mechanism
Jyväskylä: University of Jyväskylä, 2023, 55 p.
(JYU Dissertations
ISSN 2489-9003; 606)
ISBN 978-951-39-9293-4 (PDF)
Yhteenveto: Luonnosta löytyvien laajakirjoisten antiviraalien tehokkuuden ja molekyylimekanismien selvittäminen
Diss.

Viral diseases and their outbreaks continue to challenge our society. They are not only responsible for causing numerous infections but also disrupt the global economy and public health system. The recent COVID-19 pandemic was one of the most catastrophic event in human history that caused millions of fatalities worldwide. Enteroviruses are group of viruses that cause an array of diseases ranging from the mild, common cold to more severe infections like myocarditis and central nervous system infections. They are also associated with chronic infections such as type I diabetes. Currently, no antivirals have been clinically approved against enteroviruses and only one drug has been granted a conditional marketing authorization against coronaviruses by the European medicines agency (EMA). It has become important that one looks beyond the conventional routes and explore bioactive compounds from natural products to identify novel broad-spectrum antivirals. This study concentrates on the screening of different natural compounds for their antiviral potential against enteroviruses and coronaviruses and investigates their mechanism of action. We found broad-spectrum antiviral activity of *Salix* bark extract and *Ganoderma* sp. ferment against enveloped and non-enveloped viruses. These natural antivirals inhibited enteroviruses by stabilizing them and preventing their genome release. In contrast, the bark extract treatment led to disruption of coronaviruses. In addition, polyphenolic compounds also exhibited potent antiviral efficacy against enteroviruses and their efficacy was improved by several folds when they were functionalized on the surface of nanoparticles. Polyphenols inhibited the infection by binding at multiple sites on the virus capsid, leading to clustering and stabilization of the virus.

Keywords: Coronavirus; enterovirus; natural antivirals; polyphenols; screening; stabilization.

Dhanik Reshamwala, University of Jyväskylä, Department of Biological and Environmental Science, P.O. Box 35, FI-40014 University of Jyväskylä, Finland

TIIVISTELMÄ

Reshamwala, Dhanik
Luonnosta löytyvien laajakirjoisten antiviraalien tehokkuuden ja molekyylimekanismien selvittäminen
Jyväskylä: Jyväskylän yliopisto, 2023, 55 s.
(JYU Dissertations
ISSN 2489-9003; 606)
ISBN 978-951-39-9293-4 (PDF)
Yhteenveto: Broad-spectrum antivirals from nature: studies on efficacy and molecular mechanism
Diss.

Virustaudit ja niiden puhkeaminen haastavat edelleen yhteiskuntaamme. Ne eivät ole vain vastuussa lukuisten infektioiden aiheuttamisesta, vaan myös häiritsevät maailmantaloutta ja julkista terveydenhuoltojärjestelmää. Äskettäinen COVID-19-pandemia oli yksi katastrofaalisimmista tapahtumista ihmiskunnan historiassa, ja se aiheutti miljoonia kuolemia maailmanlaajuisesti. Enterovirukset ovat toinen virusryhmä, joka aiheuttaa joukon sairauksia, jotka vaihtelevat lievästä flunssasta vakavampiin infektioihin, kuten sydänlihastulehduksiin ja keskushermostoinfektioihin. Ne liittyvät myös kroonisiin infektioihin, kuten tyypin I diabetekseen. Tällä hetkellä enteroviruksia vastaan ei ole yhtään kliinisesti hyväksyttyä viruslääkettä, ja vain yksi lääke on hyväksytty koronaviruksiin. On tullut tärkeäksi katsoa perinteisiä reittejä pidemmälle ja tutkia myös luonnontuotteiden bioaktiivisia yhdisteitä uusien laajakirjoisten viruslääkkeiden tunnistamiseksi. Tämä tutkimus keskittyy erilaisten luonnosta peräisin olevien yhdisteiden seulomiseen niiden antiviraalisen potentiaalin suhteen enteroviruksia ja koronaviruksia vastaan sekä niiden vaikutusmekanismien tutkimiseen. Löysimme *Salix*-kuoriuutteesta ja *Ganoderma* sp. fermenteistä laajakirjoista antiviraalista aktiivisuutta vaipallisia ja vaipattomia viruksia vastaan. Nämä antiviraaliset aineet estivät enteroviruksia stabiloimalla niitä ja estämällä niiden genomin vapautumisen. Sitä vastoin kuoriuutekäsittely johti koronavirusten rakenteen muutoksiin. Lisäksi polyfenoliset yhdisteet osoittivat voimakasta antiviraalista tehoa enteroviruksia vastaan, ja niiden teho parani moninkertaiseksi, kun ne funktionalisoitiin nanopartikkelien pinnalle. Polyfenolit estivät infektiota sitoutumalla useisiin kohtiin viruskapsidissa, mikä johti viruksen klusteroitumiseen ja stabiloitumiseen.

Avainsanat: Koronavirus; enterovirus; luonnolliset viruslääkkeet; polyfenolit; seulonta; vakauttaminen.

Dhanik Reshamwala, Jyväskylän yliopisto, Bio- ja ympäristötieteiden laitos PL 35, 40014 Jyväskylän yliopisto

Author's address Dhanik Reshamwala
Department of Biological and Environmental Science
P.O. Box 35
FI-40014 University of Jyväskylä
Finland
dhanik.d.reshamwala@jyu.fi

Supervisor Prof. Varpu Marjomäki, PhD
Department of Biological and Environmental Science
P.O. Box 35
FI-40014 University of Jyväskylä
Finland

Reviewers Docent Kari Airenne, PhD
Head of Vector Development
Kuopio Centre for Gene and Cell Therapy
Microkatu 1
70210 Kuopio, Finland

Docent Tytti Vuorinen, PhD
Institute of Biomedicine
University of Turku
Kiinamyllynkatu 13
20520 Turku, Finland

Opponent Prof. Dr. Urs Greber
Department of Molecular Life Sciences
University of Zurich
Winterthurerstrasse 190
CH-8057 Zurich, Switzerland

CONTENTS

LIST OF ORIGINAL PUBLICATIONS

I Pap N., Reshamwala D., Korpinen R., Kilpeläinen P., Fidelis M., Furtado M.M., Sant'Ana A.S., Wen M., Zhang L., Hellström J., Marnilla P., Mattila P., Sarjala T., Yang B., Lima A. dos S., Azevedo L., Marjomäki V. & Granato D. 2021. Toxicological and bioactivity evaluation of blackcurrant press cake, sea buckthorn leaves and bark from Scots pine and Norway spruce extracts under a green integrated approach. *Food and Chemical Toxicology* 153: 112284

II Granato D., Reshamwala D., Korpinen R., Azevedo L., Vieira do Carmo M.A., Cruz T.M., Marques M.B., Wen M., Zhang L., Marjomäki V. & Kilpeläinen P. 2022. From the forest to the plate – Hemicelluloses, galactoglucomannan, glucuronoxylan, and phenolic-rich extracts from unconventional sources as functional food ingredients. *Food Chemistry* 381: 132284.

III Tienaho J., Reshamwala D., Karonen M., Silvan N., Korpela L., Marjomäki V. & Sarjala T. 2021. Field-Grown and In Vitro Propagated Round-Leaved Sundew (Drosera rotundifolia L.) Show Differences in Metabolic Profiles and Biological Activities. *Molecules* 26: 3581

IV Tienaho J., Reshamwala D., Sarjala T., Kilpeläinen P., Liimatainen J., Dou J., Viheriä-Aarnio A., Linnakoski R., Marjomäki V. & Jyske T. 2021. *Salix* spp. Bark Hot Water Extracts Show Antiviral, Antibacterial, and Antioxidant Activities - The Bioactive Properties of 16 Clones. *Frontiers in Bioengineering and Biotechnology* 9.

V Reshamwala D., Shroff S., Tienaho J., Liimatainen J., Laajala M., Kilpeläinen P, Viherä-Aarnio A., Jyske T & Marjomäki V. 2022. Willow (*Salix* spp.) bark hot water extracts show antiviral activity for both enveloped coronaviruses and non-enveloped enteroviruses**.** Manuscript.

VI Reshamwala D.*, Linnakoski R.*, Shroff S., Laajala M., Civra A., Francese R., Veteli P., Cortina-Escribano M., Liimatainen J., Tienaho J., Sarjala T., Lembo D., Vanhanene H. & Marjomäki V. 2022. Selected strains of *Ganoderma* sp. from Finnish forests have excellent broadly acting antiviral properties. Manuscript. *Equal contribution

VII Reshamwala D.[1], Shroff S.[1], Sheik Amamuddy O., Laquintana V., Denora N., Zacheo A., Lampinen V., Hytonen V.P., Tastan Bishop Ö., Krol S. & Marjomäki V. 2021. Polyphenols Epigallocatechin Gallate and Resveratrol, and Polyphenol-Functionalized Nanoparticles Prevent Enterovirus Infection through Clustering and Stabilization of the Viruses. *Pharmaceutics* 13: 1182. [1]Equal contribution

RESPONSIBILITIES

Article I: The original idea of research and planning was done by Daniel Granato and Nora Pap. The virology part of the study was designed by Varpu Marjomäki and me. The antiviral activity and cytotoxicity experiments were performed by me. Analysis of the data was performed by Varpu Marjomäki and me. All the authors participated in the writing process.

Article II: The original idea of research and planning was done by Petri Kilpalainen and Daniel Granato. The virology part of the study was planned by Varpu Marjomäki and me. The antiviral activity and cytotoxicity experiments were performed by me. Data analysis was performed by Varpu Marjomäki and me. All the authors were involved in the writing process.

Article III: The original idea of research and planning was done by Tytti Sarjala and Jenni Tienaho. The virology part of the study was conceptualized by Varpu Marjomaki and me. The antiviral activity and cytotoxicity experiments were carried out by me. Analysis of the data was performed by Varpu Marjomäki and me. All the authors were involved in the writing process.

Article IV: The original idea of research and planning was done by Tuula Jyske and Jenni Tienaho. The virology part of the study was designed by Varpu Marjomaki and me. The antiviral activity and cytotoxicity experiments along with the time and temperature studies were performed by me. Data analysis was performed by Varpu Marjomäki and me. All the authors contributed to the writing process.

Article V: The original idea of research and planning of the experiments were done by Varpu Marjomäki and me. All the experiments were performed by me, except the particle stability thermal release assay, sedimentation assay and TEM. Data analysis was performed by Varpu Marjomäki and me. I and Varpu wrote the paper.

Article VI: The original idea of research was done by Varpu Marjomaki and Riikka Linnakoski. The virology part of the study was conceptualized and planned by Varpu Marjomäki and me. All the virology experiments were carried out by me except the particle stability thermal release assay and TEM. Analysis of the data of the virology part was done by Varpu Marjomäki and me. All the authors participated in the writing process. Riikka Linnakoski and I contributed equally to the article.

Article VII: The original idea of research was of Varpu Marjomäki and Silke Krol. The planning of the experiments was carried out by Varpu Marjomaki, Sailee Shroff and me. I performed the intial screening experiments, tested the antiviral efficacy and cytotoxicity of the compounds in a dose-dependent manner to calculate EC50 and CC50 respectively. Also, I performed the time of addition studies and the gradient studies. I also performed studies to test compounds at diferent vitrus titers. Also I performed DLS with the help of Ville Lampinen. Data analysis was performed by Varpu Marjomäki, Sailee Shroff and me. All the authors were involved in the writing of the article. Sailee Shroff and I contributed equally to the article.

.

ABBREVIATIONS

CVA9	coxsackievirus A9
CVB	coxsackievirus B
A549	adenocarcinoma human alveolar basal epithelial cells
EV	enterovirus
CPE	cytopathic effect
ER	endoplasmic reticulum
HCoV	human coronavirus
SARS	severe acute respiratory syndrome
ACE2	angiotensin-converting enzyme 2
MRC-5	human lung fibroblast cells
SGII	sybr green II
PFU	particle forming unit
MOI	multiplicity of infection
+ssRNA	positive-sense single stranded RNA
S-protein	spike protein
HSV	herpes simplex virus
IAV	influenza A virus
EGCG	epigallocatechin gallate
RES	resveratrol
AuNPs	gold nanoparticles
EC_{50}	50% effective concentration
CC_{50}	50% cytotoxic concentration
HP	hydrophobic pocket
COPD	chronic obstructive pulmonary disease
FDA	food and drug administration
EMA	European medical agency

1 INTRODUCTION

Amongst all the emerging infections, viruses continue to pose a threat to our society. Viral outbreaks and diseases associated with them put a huge burden on the world's financial resources and public health. The recent pandemic caused by severe acute respiratory syndrome coronavirus 2 (SARS-CoV-2) has been one of the most devastating crisis in human history that has caused over 6.5 million deaths until now. Enteroviruses (EV) are group of viruses that are also responsible for millions of symptomatic infections every year all around the world. They are one the most common pathogens that infect humans of all age groups, especially immunocompromised individuals, elderly people, and young children. In addition, these viruses have also been associated with exacerbation of asthma and/or chronic obstructive pulmonary disease (COPD) and have contributed to the development of type I diabetes as well. Enteroviruses can survive in the environment and on the surfaces for a longer period than enveloped viruses and are relatively resistant to chemical disinfectants as well. Therefore, there is a dire need to tackle these viruses to reduce their spread and viral load around us. At present, only one drug has been granted a conditional marketing authorization against coronaviruses by the European medicines agency (EMA) and no antivirals have been approved against enteroviruses. It has become pertinent today to look beyond conventional routes to identify novel antivirals. One of the most sustainable ways to achieve this is to explore natural products that are an abundant source of bioactive compounds.

This thesis focuses on the screening of different natural compounds against enteroviruses and coronaviruses for their antiviral potential and investigating their mechanism of action. *Salix* bark extract and *Ganoderma* sp. ferment were found to exhibit broad-spectrum antiviral activity against enveloped and non-enveloped viruses. These natural antivirals showed their antiviral action by stabilizing the enterovirus and preventing its genome release. On the other hand, treatment with the bark extract led to disruption of coronavirus. In addition, polyphenols also inhibited enteroviruses, and its efficacy was improved by many folds when they were functionalized on

nanoparticles. Polyphenols inhibited the virus by binding at multiple sites on the capsid, causing clustering and stabilization of the virus.

2 REVIEW OF LITERATURE

2.1 Coronaviruses

Coronaviruses belong to the family of coronaviridae and infect both humans and animals. They are further divided into four genera: alpha-, beta-, gamma- and delta-coronaviruses. There are seven species of human coronaviruses (HCoVs) namely HCoV-229E, HCoV-OC43, HCoV-NL63, HCoV-HKU1, SARS-CoV, Middle East respiratory syndrome coronavirus (MERS-CoV) and SARS-CoV-2, all belonging to alpha and beta-coronaviruses genera. Of these seven, four coronaviruses (HCoV-229E, HCoV-HKU1, HCoV-OC43 and HCoV-NL63) are endemic in humans. They infect the upper respiratory tract and cause common cold. From the beginning of this century, mankind has encountered the emergence of three zoonotic coronaviruses (SARS-CoV, MERS- CoV and SARS-CoV-2) capable of infecting humans. SARS-CoV was first spotted in China, triggering an epidemic in 2003. MERS-CoV was detected in 2012 in the Middle East and still causes intermittent outbreaks there. SARS-CoV-2, responsible for COVID-19 also originated in China in 2019 and due to its highly transmissible nature, it spread all over the globe very quickly (Hui *et al.* 2020, Wu *et al.* 2020). The lower respiratory tract is the primary site of infection for these zoonotic viruses. If the innate and adaptive immunity of the host is unable to clear the virus, it enters the alveoli in the lungs and its rapid replication may trigger a cytokine storm. This eventually causes acute respiratory distress syndrome (ARDS) and respiratory failure, the major reasons for deaths in patients having COVID-19 (Huang *et al.* 2020, Mehta *et al.* 2020). The major modes of transmission for SARS-CoV-2 are through aerosol, the fecal-oral route and surface contamination (reviewed in Karia *et al.* 2020, Zhou *et al.* 2021).

HCoV-OC43 and SARS-CoV-2 belong to the same genus and are closely related genetically (Lu *et al.* 2020). Due to their shared characteristics, the American Society for Testing and Materials (ASTM) identified HCoV-OC43 as a preferred surrogate for SARS-CoV-2 (Schirtzinger *et al.* 2022). Generally, HCoV-OC43 causes common cold, and in some cases also leads to lower respiratory

infections, particularly in children, the elderly, and in immunocompromised individuals (Zhang *et al.* 2018). HCov-OC43 along with other coronaviruses have also been implicated to have neuroinvasive properties leading to neuropathogenicity (reviewed in de Assis *et al.* 2020).

2.1.1 Overview of coronavirus infection cycle

Coronaviruses are enveloped viruses with a diameter of 60-140 nm, encapsulating a positive-sense single stranded RNA (+ssRNA) genome of approximately 27-32 kilobases (reviewed in Pizzato *et al.* 2022). The virus encodes structural proteins (spike protein, nucleocapsid protein, envelope protein and membrane protein), accessory proteins and non-structural proteins (most of which play a role in viral replication and transcription complex). The overall life cycle of the seven HCoVs are similar but might vary for example in case of receptors used, the way they internalize and production of accessory genes. HCoV-OC43 binds to the cells using the receptor, N-acetyl-9-O-acetylneuraminic acid and internalizes through caveolin-1-dependent endocytosis, where the scission of the virus containing vesicle is dynamin dependent (Owczarek *et al.* 2018).

In case of SARS-CoV-2 infection, the virus attaches itself to the host receptor angiotensin-converting enzyme 2 (ACE2) via spike (S) protein to facilitate its entry inside the cells (Hoffmann *et al.* 2020). The S-protein of the virus is made of two subunits – S1 and S2. The C-terminal domain of the S1 subunit has a receptor binding domain (RBD), which is important for the virus entry (Shang *et al.* 2020). The S2 subunit plays a vital role in membrane fusion. Following the binding, conformational changes occur, and the cleavage of the S protein takes place at the S2' site with the help of host transmembrane serine protease TMPRSS2 (Hoffmann *et al.* 2020). This leads to the activation of the S2 subunit which fuses the host and viral lipid envelope; the viral ribonucleoprotein complex is thereby released into the cell. SARS-CoV-2 can also use an alternative, however less efficient endosome pathway, where cathepsins can cleave the S protein (Lamers *et al.* 2021).

After its entry in the cytoplasm, the virus releases its +ssRNA genome and initiates the production of viral polyproteins 1a and 1b, that are further processed into 16 non-structural proteins (nsps) by virus encoded proteases. Some of these nsps make the viral replication and transcription complex (RTC) from the endoplasmic reticulum membrane (Knoops *et al.* 2008). Replication of viral RNA takes place in these protective double-membrane vesicles (DMVs). Translation and transcription with the help of nsp12 (RNA dependent RNA polymerase) lead to the formation of structural proteins. These newly produced structural proteins (E, M and S) are introduced into the endoplasmic reticulum (ER), where they continue through the ER-Golgi intermediate compartment (ERGIC). The N protein forms a complex with the newly produced RNA and in ERGIC they interact with E and M proteins, leading to the assembly of viral particles. The assembled virions acquire their membrane envelope from the Golgi

compartment and use exocytosis pathway for their egress from the host cell (reviewed in Pizzato *et al.* 2022).

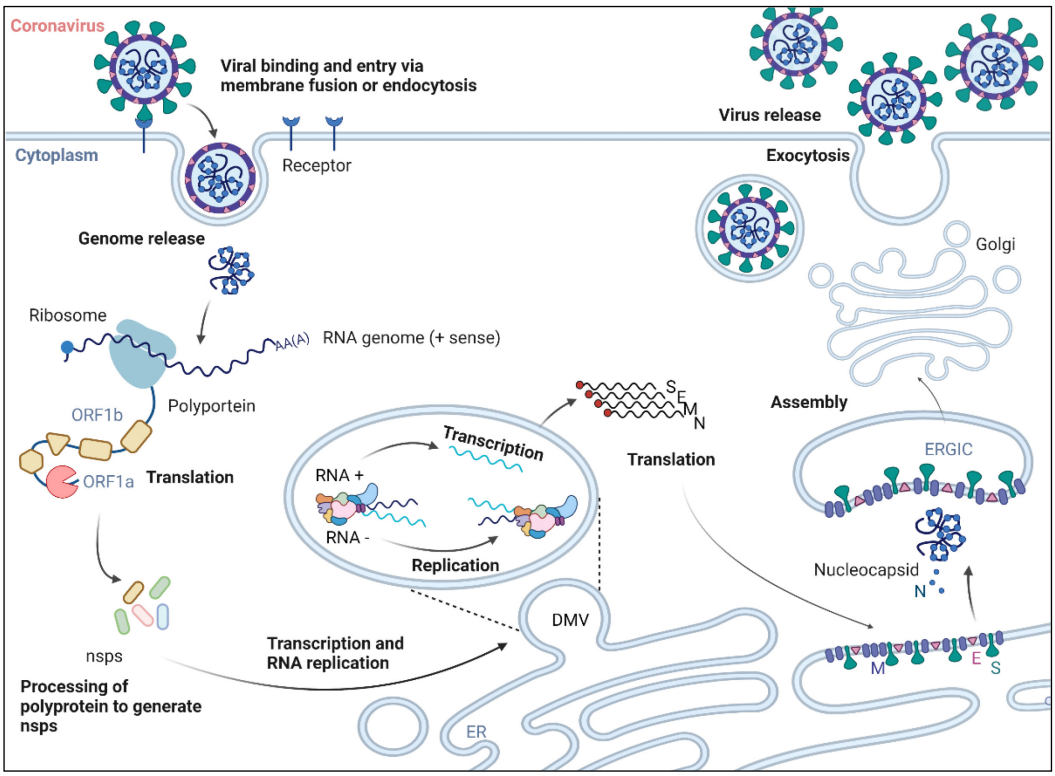

FIGURE 1 Overview of the coronavirus lifecycle. The image was modified from a review by Pizzato *et al.* 2022. The lifecycle of coronavirus begins as the virus attaches to the host cells using receptors; the severe acute respiratory syndrome (SARS) viruses use angiotensin-converting enzyme 2 (ACE2) while the human coronavirus-OC43 utilizes N-acetyl-9-O-acetylneuraminic acid. Host proteases also help in the internalization by activating the spike proteins. Depending on the species, the virus enters the host cell either through endocytosis pathway or by fusion of viral and host lipid bilayers. Once the genome is released in cytoplasm, two open reading frames, ORF1a and ORF1b are translated into polyproteins 1a and 1b. They are then cleaved into individual non-structural proteins where some of them form the double-membrane vesicles (DMVs), where viral replication and transcription takes place. Structural proteins formed after transcription and translation, are localized within the endoplasmic reticulum (ER) where they continue to pass through the ER-Golgi intermediate compartment (ERGIC). Assembly of the virion is then initiated when the genome along with the N protein interact with other structural proteins. The assembled virion acquires the membrane from the Golgi compartment and egress from the host cell through exocytosis. The figure was made with the help of BioRender image creating tool.

2.2 Enteroviruses

One of the most common viruses infecting humans are enteroviruses (EVs). Every year in the US, these viruses account for 10-15 million cases of symptomatic infections (Sandoni *et al.* 2022). Enteroviruses belong to the picornaviridae family and within that genus, there are three rhinovirus species A-C and four enterovirus species A-D, (altogether more than 100 serotypes), that are capable of infecting humans. These viruses transmit through the fecal-oral route along with the upper respiratory system and from their primary infection sites, could spread to secondary tissues and infect heart, liver, pancreas, or brain. Enteroviruses can cause an array of diseases ranging from mild flu like symptoms to more severe forms such as meningitis, pancreatitis (reviewed in Simons-Linares *et al.* 2021), and myocarditis (Bouin *et al.* 2019). They also contribute to chronic infections, such as type I diabetes (reviewed in Nekoua *et al.* 2022), and are associated with the exacerbation of asthma and/or COPD (reviewed in Kurai *et al.* 2013), making them vital clinically. The best known and most studied virus belonging to this genus, is the poliovirus. Some of the other known viruses of this genus are human rhinoviruses which are responsible for common cold; EV71 that is associated with hand, foot and mouth disease, and difficult central nervous system infections. The enterovirus species B accounts for many serotypes of coxsackieviruses and echoviruses, of which coxsackievirus B3 and A9 are important to us.

Despite their clinical importance, no vaccines are available for enteroviruses, except for poliovirus. It is also practically not possible to develop vaccines against all enteroviruses. Even though several compounds inhibiting enterovirus have been identified, none of them were able to clear the clinical trials.

2.2.1 Overview of enterovirus infection cycle

Enteroviruses are small non-enveloped viruses that are roughly 30 nm in diameter (Hogle *et al.* 1985). They possess a +ssRNA as their genome, which is approximately 7-7.5 kilobases (kb) long. The genome is enclosed in an icosahedral capsid, made of 60 copies of each of four structural proteins, VP1-VP4. Of all these proteins VP4 is present on the inner side of the capsid whereas VP1-VP3 are located on the surface. Each of these four proteins form a protomer, five such protomers combine to make one pentameric subunit of the capsid and 12 of these pentamers assemble to form the icosahedral capsid. Capsids of enteroviruses have a surface depression (canyon), surrounding each of the 12 fivefold vertices (Rossmann *et al.* 2000) which is used for receptor binding. There is a hydrophobic pocket beneath the canyon, which is occupied by a natural fatty acid (also called pocket factor). This pocket factor has been associated with the virus stability and its removal is an important criteria for the virus uncoating inside the endosome (reviewed in Smyth and Martin 2002).

The infectious life cycle of enteroviruses has been well studied (reviewed in Baggen *et al.* 2018). It begins by binding of the virus to receptor of the cell surface, leading to receptor mediated endocytosis for its entry inside the host. Different viruses use different receptors, such as poliovirus employs poliovirus receptor (PVR); CVA9 and echovirus 1 utilizes integrins whereas CVBs uses decay accelerating factor for cell attachment, followed by using coxsackievirus-adenovirus receptor (CAR) for cell entry. Also, based on the virus serotype and the host cell type, enteroviruses can use different endocytic pathways. Uncoating of the viral capsid occurs in the endosome, resulting in the release of its genome in the cytoplasm. Once in the cytosol, the viral RNA gets translated into a single large polyprotein, that is processed proteolytically by viral proteases into individual proteins. One such protein is an RNA dependent RNA polymerase ($3D^{pol}$), which initiates the replication of positive-sense viral RNA to generate a complementary negative strand, which in-turn generates more positive-sense RNA strands. The genome replication of enteroviruses occurs on virus-induced membrane structures known as replication organelles (reviewed in van der Schaar *et al.* 2016). These organelles are like DMVs mentioned in the coronavirus infection cycle (Sec. 2.1.1), as these are common membranous structures which act as a platform for genome replication of +ssRNA viruses. The nascent (+) RNA can either be used for translation and replication or packaged into newly made virions. Structural proteins VP0, VP1 and VP3 assemble into protomers and then form pentamers, which along with the newly produced RNA, produces provirions. VP0 breaks into VP2 and VP4 resulting in mature and infectious virions. Finally, the progeny virions exit the host cell through lysis (reviewed in Harris and Coyne 2014). There is also growing evidence about virions being released in vesicles through the non-lytic route prior to cell lysis (reviewed in Lai *et al.* 2016).

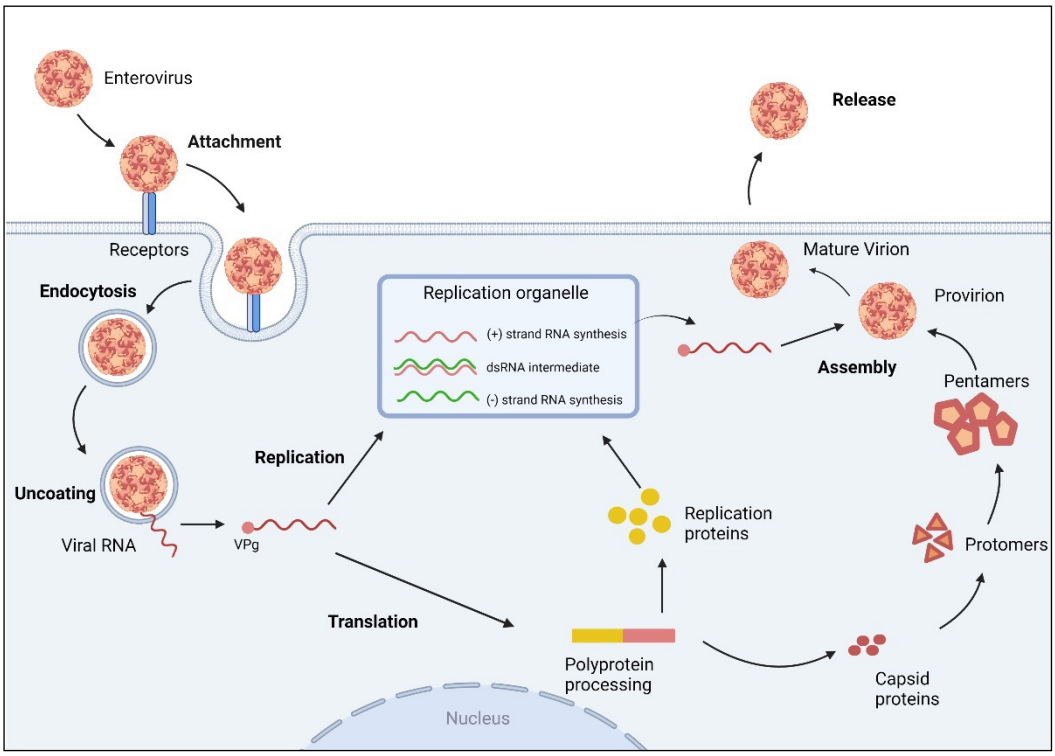

FIGURE 2 Overview of the enterovirus lifecycle. The image was modified from a review by Baggen *et al.* 2018. Enterovirus attaches to the host cell receptor and is endocytosed. Once the virion delivers the positive sense RNA genome in the cytoplasm, it is translated into a polyprotein. The polyprotein is translated to release structural and replication proteins. One such replication protein is an RNA dependent RNA polymerase ($3D^{pol}$), that replicates the positive-sense viral RNA. Viral RNA contains VPg (3B) protein which is also required for viral replication. The enterovirus replication occurs on virus-induced, and host cell-derived membrane structures known as replication organelles where positive-sense viral RNA synthesizes a complementary negative strand and through dsRNA intermediate, new copies of positive-sense RNA are made. The new positive sense RNA can either undergo another translation-replication cycle or get packaged for assembly. Structural proteins first assemble into protomers followed by forming pentamers, which together with the nascent RNA, produces provirions. Newly matured and infectious virions egress by lysing the host cell or via non-lytic route through vesicles. The figure was made with the help of BioRender image creating tool.

2.3 Stability of enveloped v/s non-enveloped viruses

An important feature distinguishing the enveloped and non-enveloped viruses is the presence of lipid envelope. This surface feature along with the virus type plays a crucial role in the stability, its survival in the environment and hence in the pathogenesis of the virus. Studies comparing the stability on surfaces have shown that non-enveloped viruses are more stable compared to enveloped

viruses and can also survive for a longer duration (reviewed in Kramer *et al.* 2006). On the contrary, enveloped viruses have been reported to be more sensitive to different antiseptics-disinfectants formulations (reviewed in Geller *et al.* 2012). One plausible explanation could be that due to impairment of the envelope (van Engelenburg *et al.* 2002), these viruses lose their ability to attach on the susceptible host cells, therefore, affecting their pathogenesis. Structural studies by Watts and colleagues reported disintegration of lipid envelope when it was subjected to ethanol, resulting in its loss of infectivity (Watts *et al.* 2021). Bushman and colleagues investigated links between virus structures and their routes of transmission by compiling database of 243 virus/host combinations and performing statistical analysis. They showed that the absence of a lipid envelope was strongly correlated to fecal-oral transmission (Bushman *et al.* 2019). A virus must survive in various chemically harsh environments when infecting through the fecal-oral route, a route used by polio and many other gastroenteritis viruses for transmission. They rationalized their finding due to the fragile nature of the lipid bilayer. As the enveloped viruses are not stable outside the human body, one of their transmission modes is via transfer of body fluids, for example hepatitis B and C viruses. In a study done on enveloped viruses such as SARS-CoV-2, the virus remained infectious for a maximum of 72 hours on surfaces like plastic and stainless steel, while it lost its infectivity within few hours on surfaces like copper and cardboard (van Doremalen *et al.* 2020). Thevenin and colleagues studied the effect of disinfectant on enveloped and non-enveloped viruses (Thevenin *et al.* 2013) . They reported that CVB4 was more resistant to the disinfectant in the suspension compared to herpes simplex virus (HSV) 1, suggesting that the protein capsids of non-enveloped viruses are more stable compared to the fragile lipid layer of enveloped viruses.

2.4 Targeting the viral life cycle

The life cycle of enteroviruses and coronaviruses consists of receptor binding, followed by cell entry or internalization. This leads to uncoating and genome release, resulting in translation, polyprotein processing, and replication. Finally, assembly occurs and virus egresses from the host cell (Fig. 1 and 2). All these steps are potential targets for inhibiting viral infection by the antivirals. Host and viral factors essential for different steps have also been studied as potential targets. Compounds targeting the viral factors have the advantage of lower cytotoxicity, whereas probability of resistance development in viruses is smaller for the compounds targeting the host factors.

2.4.1 Antivirals against enteroviruses

Majority of the enteroviruses adhere to the receptor via the canyon (reviewed in Bergelson and Coyne 2013), while some members of the genus do not use it. To give an example, CVA9 binds to the integrin receptor through an arginine–

glycine–aspartate (RGD) motif (Chang *et al.* 1989). Even though many receptors have been identified, the mechanism through which they mediate infection is still poorly understood. Hence, designing inhibitors that work against different receptors is not feasible. The next sequential step in the viral life cycle is internalization and here as well, the entry pathway varies between the viruses. Also, the virus might adapt to use another entry route if the primary one has been blocked. Therefore, due to the variability of the entry pathway employed, it is also not considered as the best target for developing broad-spectrum antiviral.

Another important group of inhibitors are the capsid binders, of which the most famous being pirodavir, vapendavir, pleconaril, OBR-5-340, and pocapavir (Andries *et al.* 1992, Pevear *et al.* 1999, Oberste *et al.* 2009, Matz 2013, Makarov *et al.* 2015). These compounds bind to the hydrophobic pocket (HP), beneath the canyon and displace the pocket factor (Pevear *et al.* 1989). This results in capsid stability and therefore, preventing receptor attachment and/or uncoating. Nevertheless, these capsid inhibitors lack effectiveness against all the different enteroviruses. Tijsma and co-workers showed lack of antiviral activity of pleconaril against EV71 (Tijsma *et al.* 2014). These compounds are also ineffective against rhinovirus C (RVC), due to its unique structure compared to other enteroviruses (Liu *et al.* 2016). Another drawback of using traditional capsid binders is the development of drug-resistant viruses (Collett *et al.* 2017). Till date, the majority of capsid binders tested were shown to bind to the HP. In a recent study, Abdelnabi and colleagues reported the binding of a compound to a pocket within a conserved VP1-VP3 interprotomer interface of the viral capsid (Abdelnabi *et al.* 2019). This compound showed antiviral efficacy against CVB1, CVB6, CVB4, CVB5 and CVA9. Furthermore, analogues of the compound were able to show broad-spectrum antiviral activity against many enteroviruses and rhinoviruses. Another group of researchers working on OBR-5-340, revealed from their cryo-EM analysis, that the compound bound to the less conserved area on surface of rhinovirus B5. Unlike most of capsid binders, it attached closer to the pocket entrance of the virus (Wald *et al.* 2019). However, due to inadequate clinical benefits, none of the capsid binders have yet made it through the clinical trials.

Another important class of inhibitors are the ones that target the viral proteases, which play a pivotal role in enterovirus infection. One such compound is rupintrivir, that targets the 3C protease of the rhinoviruses (Matthews *et al.* 1999). It was also effective in inhibiting other enteroviruses, demonstrating its potent antiviral activity (reviewed in De Palma *et al.* 2008). However, it was not successful in significantly reducing the viral load and disease severity during infection studies in patients, hence, its clinical development was stopped (Patick *et al.* 2005). In a recent study, calpains, which are cellular proteases, were shown to be required for virus polyprotein processing. This makes them a potential antiviral target as well (Laajala *et al.* 2019).

A key protein responsible for viral replication is the RNA-dependent RNA polymerase 3D (3Dpol), which serves as an important target for inhibitors as well. Ribavirin, approved by the food and drug administration (FDA) for treating hepatitis C virus infection has also shown effectiveness against

enteroviruses. It was reported that ribavirin, which is an RNA virus mutagen, worked by forcing RNA viruses into error catastrophe, leading to lethal mutagenesis (Crotty *et al.* 2001). Favipiravir is another nucleoside analog that has been reported to target the RNA polymerase of a number of RNA viruses, including enteroviruses (reviewed in Furuta *et al.* 2017). Another vital viral protein 2C, that plays an important role in replication, can also be targeted for antiviral development. Another drug, fluoxetine, targeted the replication of EV-B and D serotypes and 2C protein was identified as the target of the drug (Ulferts *et al.* 2013). Fluoxetine is already an FDA approved drug for the treatment of depression, making it easier to develop it further as an antiviral.

2.4.2 Antivirals against coronaviruses

An important step in coronavirus life cycle is the cleavage of S-protein by host proteases such as TMPRSS2, without which the viral and host lipid bilayers fusion cannot occur. Hence, TMPRSS2 could serve as a vital target for antivirals. Hoffmann and co-workers showed that SARS-CoV-2 entry was completely blocked when they used a TMPRSS2 inhibitor, making it a viable treatment option (Hoffmann *et al.* 2020). Another research group suggested the use of a combination of inhibitors as a more effective way of inhibiting the virus. When they used phosphoinositide kinase and serine protease inhibitors together, they reported a 5-fold synergistic effect in their effectiveness to inhibit the infection (Kreutzberger *et al.* 2021). Apilimod, which targets the kinase is undergoing clinical trial in the United States of America for preventing SARS-CoV-2 infection (ClinicalTrails.gov identifier NCT04446377). Camostat mesylate, targeting the serine protease TMPRSS2 is also under clinical trials on patients in France (ClinicalTrails.gov identifier NCT04608266). Another TMPRSS2 protease inhibitor nafamostat mesylate is being evaluated in Japan (Doi *et al.* 2020) and subjected to clinical trials in South Korea (ClinicalTrails.gov identifier NCT04418128).

Inhibiting the viral and host lipid fusion can also be a promising target for antivirals. Arbidol is one such compound reported to showcase a broad range of antiviral activity against a number of enveloped and non-enveloped RNA and DNA viruses (reviewed in Blaising *et al.* 2014). It has already been approved in China and Russia for treating a number of respiratory viral infections including influenza (reviewed in Debing *et al.* 2015). Previous work has shown that arbidol functions by blocking fusion of host and viral membrane, inhibiting their cell entry (Boriskin *et al.* 2006).

Like enteroviruses, viral proteases of coronaviruses are also important for infection and are possible targets for antiviral development. Even before the onset of SARS-CoV-2, antiviral activity of inhibitors targeting 3C-like proteases was reported against feline coronaviruses (Kim *et al.* 2015). The same group of researchers found a broad-spectrum antiviral compound that inhibited 3C or 3C-like (3CL) protease of enteroviruses and coronaviruses (Kim *et al.* 2012). Pfizer's oral antiviral treatment Paxlovid™ also targets SARS-CoV-2 3CL protease to inhibit the viral replication ('Pfizer's Novel COVID-19 Oral Antiviral Treatment

Candidate Reduced Risk of Hospitalization or Death by 89% in Interim Analysis of Phase 2/3 EPIC-HR Study | Pfizer'). Based on the promising results, it was granted a conditional marketing authorization by the European medicines agency (EMA) for COVID-19 treatment (EMA 2022).

Targeting the viral replication can also be an important step to inhibit the virus. Nucleoside analogues are one such class of molecules that work on that mechanism. Remdesivir, developed for Hepatitis C virus, was repurposed to check its efficacy against SARS-CoV-2. This resulted in its quick emergency use authorization (EUA) and later approval by the FDA for treating SARS-CoV-2 infection (reviewed in Puhl *et al.* 2022). Results from a trial study show that remdesivir is effective against hospitalization and death in outpatients but exhibited no clinical benefit in patients hospitalized due to COVID-19 (Ader *et al.* 2022). Remdesivir continues to be researched on ways to overcome its limitations and increase its effectiveness. In addition, it could still be combined with another drug to have a synergistic effect.

Cyclophilins are another important mediator of viral infection and therefore, are prospective targets for the antivirals. Cyclophilin inhibitors have displayed inhibition of a number of RNA and DNA viruses (reviewed in Frausto *et al.* 2013). Replication of SARS-CoV and HCoV-229E was shown to be inhibited by cyclosporin A (CsA) (de Wilde *et al.* 2011). Although a lot of work has been done with antivirals, none of them have yet made it to the market successfully. Therefore, one must look beyond the traditional routes and focus their attention on nature to find novel broad-spectrum antivirals.

2.5 Natural products

For the past decades and even now, natural products continue to be a rich source of bioactive compounds (reviewed in Newman and Cragg 2020). The biggest advantage of natural products is the unmatched, vast structural diversity and complexity they offer (reviewed in Clardy and Walsh 2004). As the natural products interact with wide range of biological macromolecules, they can regulate biological systems. In addition, they have undergone evolutionary selection so they can remain significantly beneficial to their producers. These unique traits of natural products gives them an edge over synthetic molecules and make them a pertinent source for compounds in pharmaceutical research (reviewed in Schmitt *et al.* 2011). In today's time, however, combinatorial chemistry is preferred over natural products as a source for drug discovery. But when one looks carefully at the data of the 1881 drugs that were approved between period of 1981-2019, only three new chemical entities have been reported to be discovered using combinatorial chemistry approach. On the other hand, 41.8% of drugs approved were either biological macromolecules, unaltered natural products, natural product derivatives or botanical drugs (reviewed in Newman and Cragg 2020). The contribution of natural products as a source for drug discovery in different areas has been exhaustively covered by Newman and

Cragg in their review article. Their significance in the field of infectious diseases is quite prevalent as they have provided the chemical template for the majority of antibacterial and antifungal drugs (reviewed Butler *et al.* 2013). They also have contributed substantially to the area of anti-viral drug discovery (reviewed in Martinez *et al.* 2014). Bioactive compounds from natural flora and fauna are all potential sources for antiviral compounds.

2.5.1 Fungi as a source for antivirals

Fungi kingdom consists of a rich and untapped source of bioactive natural products and could serve as a reservoir of unique compounds that might be useful against infectious agents. They are the second biggest kingdom after bacteria and it is said that the research community is only aware of 10% of its species (Singh *et al.* 2019). Penicillin is one of the most prominent example of fungi secondary metabolite used as antimicrobial agent. In the past, bioactive compounds isolated from fungi were not explored to its full potential but are now extensively studied for their antiviral activities. Cyclosporine which is widely used as an immunosuppressant also is of fungal origin. It also has been studied thoroughly for its antiviral activity against a wide range of viruses (reviewed in Martinez *et al.* 2014). Riikka and colleagues (reviewed in Linnakoski *et al.* 2018) have assembled a list, showcasing investigations of different fungi for their antiviral activities. Edible and medicinal mushrooms are one group of fungi that have been explored for their bioactive properties.

Since early times, mushrooms have served as an integral part of our food because of their nutritional value. They also have medicinal value due to their pharmacological characteristics of being antidiabetic, antioxidative, antiviral, antibacterial, hepatoprotective, and so on (reviewed in Anusiya *et al.* 2021). The genus of Ganoderma, whose bioactive compounds have been associated with medicinal properties, have been studied comprehensively (reviewed in Hapuarachchi 2017). Their antiviral properties have been linked to polysaccharides in fruiting bodies and mycelium, and secondary metabolites such as triterpenoids. Ang and co-workers evaluated the antiviral activity of *Ganoderma neo-japonicum* Imazeki (GNJI) crude extracts against different serotypes of Enterovirus species A (Ang *et al.* 2021). They reported that one of the extracts was able to effectively inhibit the infection of all the serotypes tested, when added 2 h post-infection. Not just the mushroom extracts but the secondary metabolites isolated from them have also been investigated for their antiviral potential. Zhang and his colleagues exhibited the antiviral efficacy of two triterpenoids against EV71 and revealed that the compounds interacted with the HP of the virus capsid and thereby, interfered with the virus binding to the cells (Zhang *et al.* 2014). The bioactive compounds of the mushroom have also been reported to inhibit enveloped viruses (Zhu *et al.* 2015).

2.5.2 Plants as a source for antivirals

Natural products from plants have always been considered a rich source of structurally unique compounds. Since time immemorial, plants have been known to be an invaluable source of vital bioactive compounds for the treatment of numerous diseases. There have been many studies reporting the usefulness of plant-derived secondary metabolites and their therapeutic potential (reviewed in Barbieri *et al.* 2017, Denaro *et al.* 2020). Nearly 11% of crucial drugs in the world come entirely from plants (Veeresham 2012). One of the biggest advantage of plants-derived compounds, apart from being anti-inflammatory and antioxidant is that they have either very low, or no side effects compared to synthetic molecules (reviewed in Karimi *et al.* 2015). Many phytochemicals such as flavonoids, terpenoids, polyphenols, saponins, organosulfur compounds and others have shown to affect cellular functions as well as virus life cycle. So, these compounds could be explored for treating viral diseases (reviewed in Jassim and Naji 2003, Thomford *et al.* 2018, Denaro *et al.* 2020). Purified natural products derived from plants are a wealthy source of novel compounds which could serve as a good alternative for antiviral drug development (reviewed in Lin *et al.* 2014). Triterpene compounds that are present in medicinal plants such as *Bupleurum spp., Heteromorpha spp*., and *Scrophularia scorodonia* exhibit various biological properties (Guinea *et al.* 1994). These compounds when tested for their antiviral potential, inhibited HCoV-229E infection by interfering with the viral attachment and internalization (Cheng *et al.* 2006). Lau and co-workers studied the extract of *Hottuynia cordata* against SARS-CoV and reported that the extract inhibited viral 3CL protease and also blocked the viral RNA-dependent RNA polymerase activity (Lau *et al.* 2008). Plant extracts have shown their antiviral efficacy against non-enveloped viruses as well. In a study, researchers reported the antiviral activity of *O. basilicum* extracts against EV71 and CVB1 (Chiang *et al.* 2005).

Polyphenols present in vegetables, fruits, tea and wine have garnered intrigue within the research community due to the reporting of their many pharmacological properties (reviewed in Orhan *et al.* 2010, Cushnie and Lamb 2011, Panche *et al.* 2016). They are produced by plants as secondary metabolites and one of their functions is to protect the plants from microbial infection (reviewed in Manach *et al.* 2004). Many natural products falling under polyphenols have been reported for their antiviral efficacy and should be explored for potent antivirals due to their availability, tolerability and minimal side effects (reviewed in Kumar and Pandey 2013, Goh *et al.* 2020, Chojnacka *et al.* 2021). Derksen and his colleagues studied the antiviral potential of polyphenols isolated from *Eupatorium perfoliatum* and observed that the entry of influenza virus was blocked when the virus was treated with polyphenols (Derksen *et al.* 2016). In another study, researchers reported the antiviral activity of a flavonoid derivative compound, 3(2H)-isoflavene, against poliovirus. They further studied its mechanism of action and found that the compound interfered with the virus uncoating by acting at the HP of the virus (Salvati *et al.* 2004).

3 AIMS OF THE STUDY

I To screen different natural extracts against enteroviruses to determine their antiviral potential

II To explore the broad-spectrum antiviral activity of *Salix* bark extract and *Ganoderma* sp. ferment and investigate their mechanism of action against enveloped and non-enveloped viruses

III To determine the antiviral efficacy of polyphenols and polyphenol-functionalized nanoparticles against enteroviruses and study their mechanism of action

4 SUMMARY OF THE METHODS

The methods used during this thesis are summarized in Table 1. More detailed description of these methods could be found in the original publications, depicted by Roman numerals

TABLE 1 Summary of methods used in the publication and included in thesis. Original publications are shown by Roman numerals.

Method	Publication
Antiviral assay for enteroviruses	I, II, III, IV, VI, VII
Antiviral assay for HCoV-OC43	V
Antiviral assay for SARS-CoV-2	V, VI
Antiviral assay for Zika and Rotavirus	VI
Virucidal assay or endpoint titration assay	V, VI
Time and temperature assay	IV, V, VI, VII
Time of addition studies	V, VI, VII
Thermal stability assay	V, VI, VII
Immunofluorescence and confocal microscopy	V, VI
Quantification of microscopic data	V, VI
Electron microscopy	V, VI, VII
Gradient centrifugation	VI, VII
Sedimentation assay for coronavirus	V
Real-time fluorescence uncoating assay	VII
DLS measurement	VII
Radioactive labelling of enterovirus	VII
Molecular docking studies	VII
Statistical testing	III, V, VI, VII

5 RESULTS AND DISCUSSION

5.1 Screening of different natural sources to evaluate their antiviral potential

Nature has a wide variety of plants, which are abundant in bioactive compounds that could be exploited for their antiviral activity. The idea was to screen different natural sources and identify the ones that have antiviral potential, so that they could be characterized and studied further. First, we investigated four samples that were extracted from Sea buckthorn leaves (SB), Blackcurrant press cake (BC), Norway spruce bark (NS) and Scots pine bark (SP), which were collected from different parts in Finland. The source of these samples are side streams from berries and wood industry. Various concentrations of the extracts were tested for their antiviral potential against enteroviruses using the cytopathic effect (CPE) inhibition assay where the virus was incubated with the extract before adding it on the cells. All the extracts inhibited the viral infection, even at the lowest concentration tested (I, Fig. 4A). In addition, none of the extracts were found to be toxic to the human lung adenocarcinoma (A549) cells at the concentrations tested (I, Fig. 4B). The antiviral potential of these extracts have been reported earlier for enveloped viruses. Ikuta and co-workers showed that the BC extracts were able to reduce the replication and adsorption of influenza virus A and B (IFV-A and IFV-B), respiratory syncytial virus (RSV) and HSV-1 (Ikuta *et al.* 2012). In another study, the extract from SB buds were reported to show antiviral activity against influenza virus (Torelli *et al.* 2015). Both these studies show the antiviral activity of extracts against enveloped viruses. Comparatively, enteroviruses and non-enveloped viruses in general, are more stable and can survive on surfaces for a longer duration than the enveloped viruses (reviewed in Kramer *et al.* 2006). Here, we show the ability of the extracts to inhibit the more resistant non-enveloped viruses, demonstrating the potent antiviral nature of these extracts. Determination of the chemical composition showed that the compounds belonging to the polyphenols family made up the highest proportion in each of these extracts (I, Table 2). Earlier studies have also reported the

presence of phenolic compounds from these extracts (Metsämuuronen and Sirén 2019, Tian *et al.* 2017). Correlation analysis showed that both total phenolic content (TPC) and flavonoids content were strongly associated with the antiviral activity of the extracts.

Next, we also evaluated another set of samples for their antiviral activity. Nine samples (E1-E9) were extracted from sawdust or bark of Norway spruce (*Picea abies*), birch (*Betula pendula*), or Scots pine (*Pinus sylvestris*), which were procured from sawmills in Finland (II). Samples E1-E4 and E5-E9 extracted from sawdust and bark were rich in hemicellulose and polyphenols, respectively. Various concentrations of the extracts were tested for their antiviral efficacy. All the samples rich in polyphenols (E5-E9) were able to protect the cells from viral infection. However, none of the hemicellulose extracts (E1-E4) were able to inhibit CVA9 infection even at the highest concentration tested (II, Fig. 4C and D). Commercial tannin (E10) was also tested as a reference sample to understand whether the antiviral activity of samples was dependent on their phenolic content. The reference sample was able to protect the cells against viral infection. These results implied that only those extracts that were rich in polyphenolic content showed antiviral activity. Previous studies have reported the presence of tannins, stilbenes, phenolic acids and some flavonoids from the above mentioned spruce and pine species (reviewed in Metsämuuronen and Sirén 2019). Correlation analysis of total phenolic count (II, Table 1) and antiviral activity of these extracts also indicated phenolic compounds as the major antiviral agent. All the extracts screened so far have been sourced from side streams and majority of them are showing antiviral potential, suggesting a great possibility to contribute towards circular economy. The secondary metabolites of these extracts could have value-added applications in the field of packaging, cosmetics, and medicines, as the chemical and pharmaceutical industries are always on the lookout for new materials of natural origin (Ragab *et al.* 2018).

We further evaluated the antiviral potential of round-leaved sundews (*Drosera rotundifolia* L.) against enteroviruses. The idea was to perform a comparative analysis of the antiviral activity of extracts produced in the lab (lab-grown) with the ones taken from the fields (field-grown). Both the field and lab-grown round-leaved sundews showed their antiviral activity and protected the cells from both enterovirus serotypes, CVB3 and CVA9 (III, Fig. 3A and B). However, both the extracts were more effective at inhibiting CVA9 infection compared to CVB3. Moreover, the extract prepared from the field-grown sundew was effective in inhibiting the viral infection even at lower concentration compared with the lab-grown extract. One plausible explanation could be the difference in the metabolic profile of both the extracts. The determination of the metabolite profile revealed majority of the compounds to be flavonoids or naphthoquinones (III, Table 1 and 2). Hence, it can be suggested that the antiviral activity of the sundews was due to the presence of these compounds as secondary metabolites in the extracts. The antiviral potential of polyphenols have been demonstrated previously. Lin and colleagues showed that tannins significantly reduce the infectivity of CVA16 by inactivating the viral particles and inhibiting viral binding (Lin *et al.* 2018). Another important interpretation drawn from

metabolite result was that the field-grown extract contained significantly higher amounts of flavonoids and naphthoquinones compared to the lab-grown extract. Thus, this difference in the amounts of secondary metabolites influenced the ability of field-grown extract to inhibit the viral infection even at lower concentrations.

From the selected extracts screened so far, many of them have shown the ability to inhibit the viral infection and it seems that their antiviral potential is strongly correlated with the presence of phenolic compounds as secondary metabolites in the extracts. In the future, these extract could be screened against other non-enveloped as well as enveloped viruses to evaluate its broad-spectrum antiviral activity. Moreover, the different phenolic compounds identified in these extracts could be further tested to understand if the antiviral activity was due to the synergistic effect of many of these bioactive agents or was it dependent solely on one key compound. In addition, these bioactive compounds could be further investigated to understand their antiviral mechanism of action as well.

5.2 Mushroom ferments and plant bark extracts show broad-spectrum antiviral activity

During our next phase of research, the broad-spectrum antiviral activity of *Ganoderma* sp. ferments and *Salix* spp. bark extracts were explored, and their mechanism of action was investigated against enterovirus and coronavirus.

5.2.1 Determining the antiviral activity against enveloped and non-enveloped viruses

5.2.1.1 *Salix* bark extracts

Bark of *Salix* L. species is a source of bioactively rich and diverse phenolic compounds. First, we screened the bark extracts from 16 *Salix* clones for their antiviral potency against non-enveloped enteroviruses. Treatment of the virus (CVA9) with the *Salix* bark extracts for 1 h at 37 °C, rescued the cells from viral infection (IV, Fig. 8A). We also wanted to evaluate if the bark extracts were effective against other enterovirus species-B serotype. So, we tested them against CVB3 and observed that these bark extracts were equally effective in protecting the cells from CVB3 infection (V, Fig. 4).

Next, the extracts were screened against the enveloped coronaviruses. When HCoV-OC43 was incubated with the bark extracts, it was able to protect the human lung fibroblast cells (MRC-5) from infection (V, Fig. 2A). Except for the clones 11 and 12, all the others showed antiviral activity against enveloped viruses. One major difference was observed in the antiviral efficacy of the bark extracts between enterovirus and coronavirus. The extracts were effective even at lower concentrations (0.1% v/v) against enteroviruses whereas for coronaviruses, they were effective at higher concentrations (1% v/v). None of the

extracts tested were toxic to either the A549 or MRC-5 cells at any of the concentration that were used for studying the antiviral activity.

To further verify the antiviral activity of the bark extract, confocal studies were performed where the viral infection was followed for only one infection cycle. For studying coronaviruses (OC43), the S-protein of the virus was immunolabeled. The untreated virus exhibited high amounts of newly synthesized S-protein inside the MRC-5 cells, corroborating its successful entry and infection (42%) of the cells (V, Fig. 5A middle row). But, when the virus was treated with the clone 5 or 10, one observed a drastic reduction in the amount of S-protein as only 1% and 4% of the cells were infected, respectively (V, Fig. 5A last row). Similar confocal studies were also performed for enteroviruses (CVA9) to understand whether the interaction with the extract hinders the replication or protein production of the virus. For this, the viral capsid protein VP1 and the replication intermediate, dsRNA of CVA9 were immunolabeled. The untreated CVA9 infected 37% of the A549 cells and ample amount of capsid protein and dsRNA in the cytoplasm of the cells was observed (V, Fig. 5B middle row). However, no infection was noticed when the virus was treated with the bark extracts as no signal was detected from dsRNA or VP1 protein (V, Fig. 5B last row). Overall, these results showed that the treatment with the extract, led to a significant reduction in the viral infection and protein production.

Once the antiviral nature of the bark extracts was well-established, it was also important to quantify it and hence, a virucidal assay was performed. The result exhibited a 3 to 4 log reduction in the titre of HCoV-OC43 treated with clones 8 and 10 respectively, compared to the non-treated virus (V, Table 2). This demonstrated the exceptional efficacy of the *Salix* extracts in reducing the virus infectivity. Though the antiviral activity of the bark extract against HCoV-OC43 had already been determined, it was imperative to know if the extracts could inhibit the more virulent coronavirus, SARS-CoV-2. Therefore, the antiviral efficacy of *Salix* extract was evaluated against the clinical isolate of SARS-CoV-2 at the biosafety level 3 (BSL-3) facility of the University of Helsinki. It was revealed that the amount of viral RNA was substantially reduced when SARS-CoV-2 was incubated with the bark extracts. Treatment of the extract lead to a 6-log reduction in the RNA of the virus (V, Table 3). These results depict the antiviral potency of the bark extracts and its remarkable ability to inhibit both enveloped and non-enveloped viruses.

5.2.1.2 *Ganoderma* sp. ferments

We screened 17 strains of *Ganoderma* sp. ferments for their antiviral potency against different serotypes of enteroviruses. All the ferments were able to inhibit CVA9 and CVB1 infection (VI, Fig. 2 A and B). However, only a handful of ferment strains showed modest antiviral activity against CVB3 (VI, Fig. 2C). The difference in the antiviral potency of ferments against CVB3 compared to other enterovirus serotypes could possibly be due to the variation in the HP structure, which is collapsed in the Nancy strain of CVB3 whereas CVB1 and CVA9 have a wider pocket. Hence, this would indicate HP as a potential target for the ferments. Based on the screening assay and its statistical significance result, a

couple of ferment strains that showed antiviral efficacy against all enterovirus serotypes were selected for further studies (VI, Fig 2). Confocal microscopy was also performed to study the effect of ferment on the infection cycle of CVA9, by immunolabeling the viral replication intermediate, dsRNA capsid protein. The treated virus showed no replication or production of proteins, confirming inhibition of infection (VI, Fig. 3). The antiviral efficacy of the ferments was also quantified, and it showed a 3-log reduction in the virus infectivity of ferment treated virus compared to the untreated virus (VI, Table 1). This demonstrated the exceptional antiviral potency of the ferments against enteroviruses.

Next, the antiviral activity of the ferment was evaluated against SARS-CoV-2 similarly as for the *Salix* extract. A reduction of 4-log in the viral RNA was determined when the virus was treated with the ferment compared to the untreated virus (VI, Table 2). This result showed that the ferments could also work against the enveloped viruses. To further assess the broad-spectrum antiviral nature of the ferments, they were also tested against the enveloped zikavirus and non-enveloped rotavirus. The ferments of strain MUS 18 and 23 demonstrated complete inhibition against zikavirus (VI, Fig. 10A) whereas they showed moderate antiviral activity against the rotavirus (VI, Fig. 10B). These combined studies confirm the broad-spectrum antiviral activity of *Ganoderma* sp. ferments. In addition, the ferments seemed to be more efficient in inhibiting the enveloped viruses, compared to the non-enveloped viruses. One plausible explanation could be the difference in the structure between the two virus groups. Impairment of the fragile lipid envelope makes the enveloped viruses vulnerable and affects their ability to infect (Bushman *et al.* 2019). Also, non-enveloped viruses are more stable and resistant to harsh conditions compared to enveloped viruses (Thevenin *et al.* 2013).

Overall, both the *Salix* bark extract and *Ganoderma* sp. ferments showed antiviral activity against both enveloped as well as non-enveloped viruses.

5.2.2 Suspected bioactive agents

5.2.2.1 *Salix* bark extract

The bioactive properties of *Salix* bark has traditionally been associated with salicylic acid, different salicinoids compounds and various polyphenols (reviewed in Lavola *et al.* 2018, Tyśkiewicz *et al.* 2019). Hence, we tested a couple of reference compounds to understand whether they contributed towards the antiviral activity of the bark extracts. None of the reference compounds tested were able to block the enterovirus (IV, Fig. 8B) or coronavirus (V, Fig. 2B) infection even when their concentration was ten to hundred folds higher, compared to the bark extracts concentrations. This indicated that the reference compounds were solely not responsible for the antiviral nature of the bark extracts. It also meant that other secondary metabolites, most probably belonging to the group of polyphenols, are responsible for the antiviral efficacy. In an earlier study reporting the antiviral activity of the bark extracts of *Hamamelis virginiana* against influenza A virus and human papillomavirus, the researchers found that

tannin rich fractions from the bark extract were responsible for their antiviral efficacy (Theisen *et al.* 2014). In another study, flavonoids such as luteolin and quercetin were reported to block SARS-CoV infection (Yi *et al.* 2004). Yi and his colleagues showed that the flavonoids blocked the virus entry by binding to the S-protein. In case of *Salix* bark extract, either the phenolic compounds might be acting alone or many of the secondary metabolites might have a synergistic effect in inhibiting the infection.

5.2.2.2 *Ganoderma* sp. ferments

High performance liquid chromatography (HPLC) study was performed for some of the ferment strains showing antiviral activity. Analysis of the result and comparing with the standard sample implied the presence of various triterpenoid compounds (VI, Fig. 11). Triterpenoids derived from fungi constitute one of the largest group of bioactive natural compounds (Christianson 2008). Until now, nearly 200 triterpenoids from *Ganoderma* sp. have been identified (Yang *et al.* 2019). Hence, different reference compounds were selected based on literature for testing against CVA9 to understand if they contributed towards the antiviral activity of the ferments. None of the reference samples showed any antiviral activity (VI, Fig. 12B). This indicated that the antiviral activity was not dependent on any one of the compound. It might be that several compounds together were responsible for the antiviral efficacy or other triterpenoid compounds apart from the ones tested, might have a role to play in bioactivity of the ferments. Antiviral activity of triterpenoids belonging to *Ganoderma* sp. have been reported before against enveloped (El-Mekkawy *et al.* 1998, Min *et al.* 1998) and non-enveloped viruses (Zhang *et al.* 2014).

Overall, bioactive compounds belonging to the class of polyphenols and triterpenoids are suspected to contribute towards the antiviral activity of bark extracts and ferments, respectively. Studies are currently ongoing to determine the bioactive agents.

5.2.3 Effect of time and temperature on the antiviral efficacy

For determining the antiviral activity of the bark extracts, they were incubated for 1 h at 34 °C or 37 °C with coronavirus or enterovirus, respectively. It was crucial to understand the effect of incubation time and temperature on the antiviral efficiency of the bark extracts and ferments. When selected extracts were incubated with CVA9 for a shorter time-point (5 mins) and at lower temperature (21^{o}C vs. 37 °C), the bark extracts were able to rescue the cells from CVA9 infection (IV, Fig. 9 A and B). We further tested even shorter incubation time-point (45 sec) and notably, even a short treatment of the virus with the extract at lower temperature was adequate for them to exhibit their antiviral efficacy (IV, Fig. 9 C and D). Like bark extracts, ferments also showed enterovirus inhibition at shorter incubation time (VI, Fig. 5 A and B). These results depicted that treating the virus with the extract or ferment for only a short duration and at room temperature was adequate to exhibit their antiviral efficacy.

In addition to enteroviruses, the bark extracts retained their antiviral efficacy against the enveloped HCoV-OC43 within 5 mins of incubation of the virus and extract at room temperature (V, Fig. 6A). Strikingly, the extracts also protected the cells from HCoV-OC43 infection when the incubation time-point was further lowered to 45 sec (V, Fig. 6B). Overall, the *Salix* bark extracts showed exceptional antiviral activity against HCoV-OC43 at reduced time and temperature.

5.2.4 Studies showing direct action of natural antivirals on the virus

After the antiviral potency of the bark extracts and ferments was well-established, we wanted to understand their mechanism of action. First, we wanted to investigate at which step of the virus lifecycle do these natural antivirals (extract and ferment) target. So, time of addition studies was performed for the natural antivirals against enterovirus and coronavirus. In this assay, three modes of infection were studied (V and VI, Fig. 1). In the pre-infection and post-infection modes, the antiviral was added onto the cells 1 h before and after the infection, respectively. For studying the co-infection mode, a mix of virus and the antiviral was prepared and added to the cells. These studies showed that the bark extract was unable to demonstrate its antiviral activity when it was added to the cells before or after the coronavirus infection (V, Fig. 7 A and C). However, the extract blocked the infection when it was added together with the coronavirus (V, Fig. 7B). Interestingly, the ferments also demonstrated their antiviral efficacy only when added together with the enterovirus and they were not effective in other modes of infection (VI, Fig. 6). This suggested that both *Salix* bark extract and *Ganoderma* sp. ferments do not have any intracellular effect on the host, nor does it target the late stages of the viral infection cycle. Instead, it was evident that the extract and ferment directly interact with the coronavirus and enterovirus particles, respectively.

Similar results have been reported by other research groups as well. Derksen and co-workers observed that the influenza virus infection was blocked only when it was treated with the polyphenols isolated from *Eupatorium perfoliatum* before adding it to the cells. The compounds had no antiviral effect if added post-infection (Derksen *et al.* 2016). In another study, tannic acid was shown to have antiviral activity against hepatitis C virus (Liu *et al.* 2015). The researchers claimed that tannic acid interacted directly with the virus and interfered with its entry, as the infection was only blocked when the compound was present during infection and had no effect when it was added before or after the infection. Based on time of addition studies, it was clear that the antiviral potency of both natural antivirals was due to their direct interaction with their respective virus surfaces.

5.2.5 Natural antivirals demonstrate different mode of action against enveloped and non-enveloped viruses

5.2.5.1 Non-enveloped viruses

To better understand the structural changes on the virions due to the ferment treatment, sucrose gradient studies were performed using metabolically labelled virus (^{35}SMet/Cys-CVA9). The gradient assay can distinctly separate the virions into empty, intact, and expanded/intermediate particles (Myllynen *et al.* 2016, Ruokolainen *et al.* 2019). Fresh virus control without the ferment and without any incubation gave a single peak in the lower and denser part of the gradient, which corresponds to the intact virus particles (VI, Fig. 7 A and B). If there were empty virus particles present, they would appear in fractions 8 to 10 (Ruokolainen *et al.* 2019). Another virus control without the ferment, but incubated in similar conditions as the treated virus, also exhibited similar peak of intact particles. Interestingly, incubation of the enterovirus with the ferment led to a complete loss of radioactivity (VI, Fig 7 C and D). This could be due to the clustering of the virus because of the ferment treatment, which resulted in formation of aggregates that could have either sedimented or attached on tube walls. Similar loss of radioactivity was observed by Mira and colleagues when virions were aggregated during their fractionation studies using a $CsCl_2$ gradient (Myllynen *et al.* 2016).

High resolution microscopy techniques such as transmission electron microscopy (TEM) studies was carried out to further examine the structural changes caused to the enteroviruses by the natural antivirals. The treated virus sample was negatively stained and visualized under the TEM. In case of ferment treated enteroviruses, large aggregates of virions were observed. This was unlike the untreated virus, where the virions appeared separated from one another and nicely spread on the TEM grid (VI, Fig. 9A). In addition, no empty particles were noticed on the treated virus grid. Instead, majority of the virions appeared to be intact particles like the ones observed on the grid of untreated virus (VI, Fig. 9B). Additionally, in case of virus treated with the *Salix* bark extract, large aggregates of enterovirus were observed which appeared mostly intact (V, Fig. 8B). TEM studies thus provided evidence that the enterovirus treatment with either *Salix* bark extract or *Ganoderma* sp. ferment, led to the clustering of virions and formation of aggregates.

Once the formation of virus aggregates was visually confirmed, it was important to investigate whether the treatment with the natural antivirals destabilizes or stabilizes the virus particles. For this, a thermal assay was performed where gradual heating of the virus until 90 ^{0}C would lead to its opening and genome release, which was detected using SGII as a fluorescent marker. The untreated virus showed a typical bell-shaped melt curve (VI, Fig. 8; V, Fig 9). Under normal conditions, CVA9 would release its genome when subjected to temperatures between 50 and 60 ^{0}C (Martikainen *et al.* 2015). However, when the virus was treated with the bark extract, genome release was not observed (V, Fig. 9). A similar result was observed when the virus was treated

with the ferment (VI, Fig. 8). This suggested a stabilization effect of these natural antivirals on enteroviruses. The HP of enteroviruses has been associated with the virus stability and the removal of the lipid moiety (pocket factor) from this pocket is vital for its genome release. Capsid binding drugs bind to the HP and displace the pocket factor resulting in capsid stabilization and stopping its genome release (Pevear *et al.* 1989). Hence, there might be a possibility that these natural inhibitors interact with the HP of the virus, resulting in its stabilization. Thus, it was evident that *Salix* bark extracts and *Ganoderma* sp. ferments inhibit the enterovirus infection by clustering and aggregating the virus that leads to its stabilization and prevention of genome release.

5.2.5.2 Enveloped viruses

First, TEM studies were performed to gain insight of the coronavirus morphological changes after treatment with the *Salix* bark extract. The untreated coronavirus looked mostly intact and appeared spherical or elliptical in shape with spike proteins present around the membrane surface. Few broken virus particles were present that looked ruptured, with inside of the virus more darkly stained and having fewer spike proteins compared to the intact particles (V, Fig. 8C). Similar to enteroviruses, the extracts also clustered the enveloped coronaviruses (V, Fig. 8D). However, in the case of treated coronavirus, the envelope membrane of the virions looked a bit distorted, and it seemed like some of the spike proteins had fallen off (V, Fig. 8D). Moreover, more stain was observed inside the virions, indicating presence of broken particles. Thus, TEM studies provided visual evidence of coronavirus structural changes due to extract treatment.

Now it was important to investigate if the clustering and distortion of the enveloped virions caused stabilization or promoted genome release. This was studied by performing sedimentation analysis where the virions were separated into intact and broken particles and the sediment was quantified for the presence of viral RNA. Untreated virus showed high amounts of viral RNA, which was in line with the fact that the untreated virus should contain majority of intact virus particles, that would have pelleted down after separation. For extract treated virus, a significant decline in the viral RNA amount was detected (V, Fig. 10). This indicated that the extract treatment disrupted majority of the virus particles that resulted in its genome release. Thus, the treatment with the bark extract clusters the coronavirus and causes structural changes, which leads to disruption of the virus particles and release of its genome.

Thus, we demonstrated the broad-spectrum antiviral efficacy of both *Salix* bark extracts and *Ganoderma* sp. ferments. The natural antivirals exhibited their efficacy within short duration of less than a minute against both the enterovirus and the coronavirus. The antivirals inhibited the viruses by directly interacting with them. Though, TEM image analysis revealed clustering of both viruses, it indicated presence of more intact and stable particles for enteroviruses whereas, showed more distorted and broken particles for coronaviruses. Thermal assay showed that the genome of the enterovirus was not released when it was treated with either the *Salix* extract or the ferment, confirming their stabilization effect

on the non-enveloped virus. In case of the extract treated coronavirus, the sediment assay revealed disruption of virus particles and loss of viral RNA. The effect of antivirals on enveloped and non-enveloped virus binding and entry would be interesting to study in future. The characterization of bark extracts and ferments is currently ongoing to identify the bioactive compounds responsible for their antiviral nature.

5.3 Polyphenols and polyphenol-functionalized nanoparticles efficiently inhibit enterovirus infection by clustering and stabilization them

Polyphenols Epigallocatechin gallate (EGCG) and Resveratrol (RES) as (i) soluble molecules and (ii) functionalized on surface of gold nanoparticles (AuNPs) were investigated during the study for their antiviral efficacy and their mechanism of action against enteroviruses. Gold nanoparticles (AuNPs) were produced using the green chemistry approach where polyphenols were used as redox agents to decrease the number of potential toxic components present on AuNPs surface. Visualization of the functionalized AuNPs under TEM and dynamic light scattering (DLS) analysis showed that RES-AuNPs were smaller in size compared to EGCG-AuNPs (VII, Fig. 1 C and D). However, the determination of gold concentration revealed RES-AuNPs had three times more gold concentration compared to that of EGCG-AuNPs (VII, Fig. 1 D). Based on the values of gold concentration and diameter of AuNPs, the concentration of the ligands on the surface of AuNPs was estimated to be 5.61 μM and 34.4 μM for EGCG and RES, respectively (VII, Supplementary materials). These ligand concentrations were also determined experimentally using the Ellman test and were found to be similar as the calculated ones.

First, we evaluated whether the selected polyphenolic compounds had any antiviral efficacy. So, we performed an initial screening assay where the enterovirus was treated with the compound for 1 h at 37 °C. 10-fold serial dilutions of each compound were tested against CVB1. Soluble polyphenols as well as polyphenol-functionalized AuNPs were able to block CVB1 infection and none of the compounds showed any cytotoxicity at any of the dilutions tested (VII, Fig. 1 A and B).

5.3.1 Antiviral efficacy studies

After the initial screening assay confirmed the antiviral nature of these compounds, detailed antiviral efficacy studies were performed against different enteroviruses. The antiviral efficacy was reported as 50% effective concentration (EC_{50}), calculated from the regression analysis of the dose-response curves. Both soluble polyphenols and polyphenol-functionalized nanoparticles inhibited the CVB3 infection in a dose-dependent manner (VII, Fig. 2A). Based on EC_{50} values, EGCG was more potent than RES in inhibiting CVB3. In addition, ligands bound

to AuNPs were more effective (67-fold or 26,974-fold improvement) in showing antiviral activity than soluble polyphenols (VII, Table 2). The compounds also protected the cells against other enteroviruses, CVB1 and CVA9 in a dose-dependent manner (VII, Fig. 2 B and C). The EC_{50} values depicted the noteworthy antiviral potency of these compounds against different enteroviruses. Cytotoxicity for all the compounds was also performed and 50% cytotoxic concentration (CC_{50}) was calculated. None of the compounds showed any toxicity on the A549 cells at the effective antiviral concentrations (VII, Fig. 2D). Based on CC_{50} values, neither soluble RES nor its functionalized NP counterpart showed any cytotoxicity (VII, Table 2). However, EGCG showed a slight toxicity at very high concentration (CC_{50} – 2.218 mM). Functionalization of EGCG on AuNPs not only improved its antiviral efficacy but also decreased its cytotoxicity (VII, Table 2). Based on the selectivity index (SI) values, these compounds demonstrate their potential to be further developed as antiviral molecules.

In general, soluble EGCG was more effective than RES against all the enteroviruses tested. This could be since EGCG is a bigger molecule and has more hydroxyl groups to interact with the viruses, making it more efficient in inhibiting them. In an earlier study on Apigenin and Luteolin, the positive correlation between the number of hydroxyl groups and their antiviral activity was shown (Lv *et al.* 2014). Another important trend that was observed, was the many-fold improvement in the antiviral efficacy of ligands when bound on AuNPs, compared to the soluble polyphenols (VII, Table 2). The enhancement in efficacy was exceptionally more for RES compared to EGCG. One plausible explanation could be the increase in solubility of RES when it is bound on NPs surface. RES being a flat molecule, binds to the surface of AuNPs such that their aromatic rings are oriented parallel to the NPs surface (Mandal *et al.* 2011). This binding geometry as well as strong surface curvature in small nanoparticles allows for high number of interactions between the bound RES and viruses. This interplay of solubility, geometry and surface characteristics explains the high antiviral activity of surface bound RES. It was also important to understand if the antiviral efficacy of functionalized AuNPs was due to bound ligands and not because of free ligands present in the solution. This was studied by making pellets of the functionalized AuNPs and testing it for their antiviral activity. The resuspended pellet of functionalized NPs displayed similar antiviral activity as the nanoparticle solution, confirming that antiviral activity was due to bound ligands on AuNPs (VII, Supplementary Fig. 1).

5.3.2 Polyphenols demonstrate long-term antiviral activity

Similar to *Salix* bark extracts, time and temperature studies were performed. So, the virus and compounds were incubated for 6, 24, 48 and 72 h at different temperatures. The antiviral activity of the polyphenols and polyphenol-functionalized AuNPs were retained at the temperatures tested and showed CVB3 inhibition for all the time-points for which untreated virus was showing infectivity (VII, Fig. 3 A and B). We further investigated the effect of compounds at shorter time-points. When the virus was treated with the compounds for only

1 min at 37 °C, the ability of polyphenols to protect the cells from enterovirus infection was already noticeable. It was more evident and statistically significant when the incubation time was increased to 5 min. Moreover, the polyphenols demonstrated their antiviral activity even at 21 °C during this shorter time-point (VII, Fig. 3D). Overall, polyphenolic compounds exhibited long-term antiviral efficacy at various temperatures and efficiently inhibited the infection at shorter time-points also.

There was a slight possibility that a strong dilution of the virus-compound solution might lead to a disconnect between the virus and the compound, resulting in the virus regaining its infectivity. Hence, after 1 h of virus treatment with polyphenol-functionalized AuNPs, the solution was diluted 50 times and incubated at different time-points. The functionalized AuNPs were able to retain their antiviral efficacy even after performing a strong dilution (VII, Fig. 3C), suggesting a strong interaction between the polyphenol functionalized AuNPs and the virus. In addition, soluble polyphenols also showed a similar efficacy when diluted.

5.3.3 Polyphenols cause stabilization of enteroviruses

It was clear from the antiviral efficacy studies that the interactions between the compound and the virus during 1 h incubation was rendering the virus ineffective in causing a successful infection. It was now important to understand whether the compounds acted as inhibitors only during the early steps of the viral infection or did it also exert its antiviral efficacy during other steps of virus lifecycle. Time of addition studies revealed that the polyphenols inhibited the infection only when the virus was incubated with the compound before adding onto the cells. The polyphenols showed no antiviral activity when they were added 1 h post-infection (VII, Fig. 4A). This suggested that polyphenols targeted the attachment and/or entry step of viral infection. A similar mode of action has been reported for other polyphenol molecules as well. Lin and his colleagues revealed in their study that tannins inhibited CVA16 infection by targeting the early steps of viral lifecycle (Lin *et al.* 2018).

The interaction of the polyphenols and the virus could lead to one of two possibilities. (i) polyphenols and functionalized AuNPs might be stabilizing the virus and preventing its opening and genome release; (ii) the interaction of the polyphenols damages or disrupts the capsids and thus the genome is released prematurely from the virions. In order to test the stability of the virus capsid, we first performed a thermal stability assay. When CVB3 was treated with EGCG, a very low fluorescence was recorded, and it remained unchanged throughout the temperature range. This indicated that EGCG stabilized the virion and prevented its genome release (VII, Fig. 4B). The in-depth stabilization effect of polyphenols was studied further using the in-house developed real-time spectroscopy uncoating assay, where SGII and RNAse were used to differentiate between the expanded capsid, the fully opened capsid and the intact capsid of the virions. The untreated virus in the storage buffer showed a low background fluorescence that remained unchanged mostly during the 1 h duration of the experiment,

indicating that the virus was relatively stable in the buffer at 37 °C (VII, Fig. 4C). A similar result has already been obtained in our group (Ruokolainen *et al.* 2019). Treatment of the virus with polyphenol-functionalized AuNPs further decreased the fluorescent signal compared to untreated virus, indicating that the compounds prevented the expansion of the virions, which otherwise happens to some extent at 37 °C in storage buffer (VII, Fig. 4C). Moreover, the fluorescent signal of the treated virus remained the same through the entire duration of the assay, supporting that polyphenol functionalized AuNPs prevented the opening and viral RNA release. A similar outcome was recorded from soluble polyphenols treated viruses as well.

Binding assay was also performed using a metabolically radiolabelled virus to investigate if the polyphenols interfered with the virus binding on the cell surface. Treating the radiolabelled virus with the compound for 1 h, followed by binding them to A549 cells on ice for another 1 h revealed that polyphenols and polyphenol-functionalized AuNPs immensely decreased the virus binding to the cells (VII, Fig. 4D). These results propose the theory that polyphenolic compounds whether in soluble form or functionalized on AuNPs interact directly with the virus during incubation, stabilizing them and thus preventing the virus binding and its genome release.

5.3.4 Polyphenols cause clustering of the virus by binding to multiple sites on the virus surface

To further understand the state of enteroviruses after treatment with the polyphenols, sucrose gradient studies were done using radiolabelled virus. An untreated virus without any incubation produced a typical single peak corresponding to intact viruses (Myllynen *et al.* 2016). However, treating the virus with polyphenols resulted in a complete loss of radioactivity (VII, Fig. 5A). The proposed explanation for this was that the polyphenols might have clustered the virions and formed aggregates that would have either precipitated or adhered on the tube walls. This theory was tested by performing TEM studies and DLS measurements of treated and untreated enteroviruses. Under the TEM, untreated CVA9 appeared mostly as intact virions that are spread homogenously all over the grid. However, large aggregates of virions were visualized when CVA9 was treated with polyphenols for 1 h at 37 °C (VII, Fig. 5B). Strikingly, the virions within the aggregates appeared mostly as intact particles. DLS analysis showed a reproducible peak corresponding to a hydrodynamic diameter of 22 nm for untreated viruses. When EGCG treatment of the virus was done, the DLS recorded the signal only in the size range of 650-1240 nm and virus-associated peak was not observed, confirming the presence of aggregates (VII, Fig. 5C). Thus, TEM studies and DLS analysis supported the idea that polyphenols cause clustering of enteroviruses.

In silico docking studies were carried out to study the polyphenol molecules (ligand) and CVB3 or CVA9 capsid (protein) interactions. A novel in-house algorithm was developed for the purpose of studying these interactions on larger areas around the 2-fold and 3-fold axes of symmetry. Multiple binding

sites were identified from the docking poses of EGCG or RES on the viral capsids 2-fold (VII, Fig. 6) and 3-fold (VII, Fig. 7) axes of symmetry. Analysis of docking result indicated that there were both distinct as well as common binding sites for EGCG and RES, with the strain of the virus also playing a vital role. In addition, formation of multiple hydrogen bonds coupled with hydrophobic interactions were crucial in providing stability during the binding of molecules at multiple sites on the virus surface (VII, Fig. 8). Most of the known capsid binders bind at the hydrophobic pocket of enteroviruses, leading to their stabilization and preventing its genome release (Pevear *et al.* 1989). Docking studies revealed hydrophobic pocket as one of the binding sites for polyphenols. Molecular docking analysis of other polyphenols, such as tannins, has also reported a tendency to bind near the canyon region of enteroviruses, leading to the inhibition of viral binding on cell surface (Lin *et al.* 2018). Of all the docking poses, the majority of them were assigned to the HP, followed by S1, S2, the butcher-Neyts pocket, the pore at the 3-fold axis and the S3. This meant that HP on the virion surface remained the primary attraction site for the molecules to bind. Among all the multiple binding sites, EGCG and RES recorded the most favourable binding energies for HP of CVA9 (VII, Fig. 9). Both compounds recorded poor energies for CVB3 HP, compared to CVA9 and it could be due to the collapsed pocket structure in the Nancy strain of CVB3. Overall, four new binding sites were determined, apart from the known HP and the recently identified pocket by Abdelnabi and co-workers, also referred to as Butcher-Neyts pocket (Abdelnabi *et al.* 2019). Hence, the results of the docking studies fitted the final piece in the jigsaw puzzle of investigating the antiviral mechanism of action of polyphenols.

Thus, polyphenols exhibit phenomenal antiviral efficacy against different enteroviruses. The antiviral efficacy was increased by many folds when polyphenols were functionalized on surface of AuNPs, especially for RES. Also, cytotoxicity of EGCG was reduced when functionalized on NPs. Treatment of the virus with the compounds for only a couple of minutes at room temperature was adequate to inhibit the infection. Studies to investigate their mechanism of action showed that polyphenols and polyphenol-functionalized AuNPs targeted the entry and/or attachment step of viral infection. In addition, treatment of the virus with these compounds led to clustering and stabilization of the virions, restricting the binding of the virus on the cell surface, and eventually preventing the release of viral RNA. Moreover, computational studies identified four novel binding sites of polyphenols against 2- and 3-fold symmetry axes of the virus capsid, in addition to the known HP, and the Butcher-Neyts pocket. Thus, the potent antiviral efficacy of polyphenols was due to its binding at multiple sites on the virus surface, resulting in clustering of virions and its stabilization, and hence preventing its genome release.

6 CONCLUDING REMARKS

The main conclusion of this thesis are:

I Many of the natural extracts screened for their antiviral potential were able to rescue the cells from enterovirus infection. The antiviral potential of these natural extracts are strongly associated with the presence of phenolic compounds as their secondary metabolites.

II *Salix* bark extracts and *Ganoderma* sp. ferments exhibit broad-spectrum antiviral activity against enveloped as well as non-enveloped viruses. A short treatment of the virus (enterovirus and coronavirus) for less than a minute with the natural antivirals was adequate for them to significantly inhibit infection. Direct interaction of the natural antivirals with the viruses, led to their clustering. Treatment of coronavirus with the *Salix* extract, causes disruption of the virion which results in genome release. In case of non-enveloped viruses, treatment with bark extract or ferment causes stabilization of the virus and prevents its genome release.

III Polyphenols and polyphenol-functionalized nanoparticles strongly inhibit different enterovirus serotypes. The antiviral efficacy of polyphenols is enhanced when functionalized on the surface of gold nanoparticles. The compounds bind at multiple sites on the virus surface causing clustering of the virions. Interaction with the compound causes stabilization of the virus, prevents its genome release and its binding on host cell receptor.

Acknowledgements

This work was carried out at the University of Jyväskylä, at the Department of Biological and Environmental Sciences and Nanoscience centre, Division of Cell and Molecular Biology. The thesis was funded by Jane and Aatos Erkko foundation and Business Finland.

I would like to acknowledge all the people associated with my PhD journey. First and foremost, I would like to thank my supervisor, Professor Varpu Marjomäki for her constant support and help during the entire duration of my doctoral work. Her unwavering optimistic nature helped me sail even through the challenging times. I really appreciate the way she took care of all her students during the tough phase of the COVID-19 pandemic. I express my deepest gratitude to her for showing faith in my abilities and providing me the opportunity to grow as a researcher.

Next, I would like to acknowledge the reviewers of my thesis, Docent Kari Airenne and Docent Tytti Vuorinen. Your feedback and invaluable comments have been very helpful. I would also like to thank Professor Urs Greber for accepting the invitation to serve as an opponent for this thesis. In addition, I would also like to acknowledge my thesis committee members Dr. Tanja Lahtinen and Dr. Silke Krol, for their helpful suggestions and productive discussions over the years. Thank you Dr. Silke Krol for also collaborating and sharing your expertise for one of my PhD projects. I would also like to acknowledge Prof. Janne Ihalainen for his mentorship during the start phase of my PhD journey. Furthermore, I would like to make a special mention about our research collaborators, Dr. Riikka Linnakoski, Dr. Tuula Jyske, Dr. Jenni Tienaho and the entire team from LUKE for joining forces with us and sharing their respective expertise on projects associated with my PhD. I would also like to thank all the co-authors in the papers.

Next, I would like to thank all my wonderful colleagues for their help over the years. First, I would like to thank all the people associated with Marjomäki group. I feel blessed to be part of the group where everyone has been very accommodating and considerate, apart from being amazing colleagues. Thank you all for creating an atmosphere within the group where everyone shared their knowledge and supported each other. Thank you, to all the past and current group members for making my PhD journey more memorable. Thank you, Mira and Visa, for all the wonderful discussion over the years, your invaluable guidance and also for all the enjoyable moments inside and outside the lab. It has been my pleasure to get to know both of you and work with you. Both of you have been the best of colleagues that anyone could ask for. You have been very helpful even outside the work premises and I really appreciate both of you for that. I would also like to acknowledge all the trainees and students Orla, Annika, Annitta and Eetu who have been a part of the Marjomäki group over the years and have helped me grow as a responsible researcher. Thank you to past members of the group Paula, Tino, Niko and Ville. Many thanks to the current group members Abhishek, Marjo, Jun, Anni, Laura, Jenni and Suvi. I would like

to acknowledge visiting doctoral research fellow, Helena for creating a vibrant atmosphere during her short visit. Moreover, I would also like to thank Alli, Laura and Petri for their technical expertise and their help with practical things in the lab. Also, thank you to Kati for all the amazing personal and professional conversations over the years. Thank you for organizing exciting and memorable events which helped me distract from tensed situations. I would like to thank Chandan and Lina for always sharing their thoughts on important aspects of PhD work and guiding from their own experience. I have been fortunate enough to know Kati, Chandan and Lina outside of work as friends and thank you for all the fun times.

Next, I would like to thank all my family members and friends. Thank you for your constant support and affection. Thank you, Mom and Dad, for believing in me and giving me the wings to fly. Thank you, Raj, for having my back all these years and for being the best brother anyone could ask for. Thank you to all my uncles and aunts for their constant support, especially Bansari mami. Thank you to all my and Sailee's family members.

In a small city like Jyvaskyla, I wouldn't have imagined making so many friends but thank you to all my friends Bhavesh, Kunal, Vaibhav, Leeni, Ardra, Elan, Praveen, Afra, Jaako, Souvik, Subroto, Nisha, Shahsank, Barani, Asha, Vijay, Shweta, Prasad, Yash, Nidhi, Rahul, Disheet, Anmol, Shriya, Pankaj, Ankit, Sarika, Bhavani, Kartik, Subhash, Ashwini, Manoj, Anju, Ajay, Suvarna, Sheela and Karthik with whom I spent most of my weekends building memories. Thank you for being the ones that I can always rely on and giving me the memories that I will cherish for a lifetime.

Most importantly, a big thank you to my best friend, colleague and wife, Sailee. There are not enough words in the world that can express my deepest gratitude towards you. Without your support, this journey wouldn't have started and got me so far. I cannot thank you enough for standing like a rock besides me and for believing in me all these years.

REFERENCES

Abdelnabi R., Geraets J.A., Ma Y., Mirabelli C., Flatt J.W., Domanska A., Delang L., Jochmans D., Kumar T.A., Jayaprakash V., Sinha B.N., Leyssen P., Butcher S.J. & Neyts J. 2019. A novel druggable interprotomer pocket in the capsid of rhino- and enteroviruses. *PLOS Biology* 17: e3000281.

Ader F., Bouscambert-Duchamp M., Hites M., Peiffer-Smadja N., Poissy J., Belhadi D., Diallo A., Lê M.-P., Peytavin G., Staub T., Greil R., Guedj J., Paiva J.-A., Costagliola D., Yazdanpanah Y., Burdet C., Mentré F., & DisCoVeRy Study Group. 2022. Remdesivir plus standard of care versus standard of care alone for the treatment of patients admitted to hospital with COVID-19 (DisCoVeRy): a phase 3, randomised, controlled, open-label trial. *The Lancet. Infectious Diseases* 22: 209–221.

Andries K., Dewindt B., Snoeks J., Willebrords R., Eemeren K. van, Stokbroekx R. & Janssen P.A. 1992. In vitro activity of pirodavir (R 77975), a substituted phenoxy-pyridazinamine with broad-spectrum antipicornaviral activity. *Antimicrobial Agents and Chemotherapy* 36: 100–107.

Ang W.X., Sarasvathy S., Kuppusamy U.R., Sabaratnam V., Tan S.H., Wong K.T., Perera D. & Ong K.C. 2021. In vitro antiviral activity of medicinal mushroom Ganoderma neo-japonicum Imazeki against enteroviruses that caused hand, foot and mouth disease. *Tropical Biomedicine* 38: 239–247.

Anusiya G., Gowthama Prabu U., Yamini N.V., Sivarajasekar N., Rambabu K., Bharath G. & Banat F. 2021. A review of the therapeutic and biological effects of edible and wild mushrooms. *Bioengineered* 12: 11239–11268.

Assis G.G. de, Murawska-Cialowicz E., Cieszczyk P. & Gasanov E.V. 2020. Respiratory Syndrome Coronavirus Infections: Possible Mechanisms of Neurological Implications—A Systematic Review. *Frontiers in Neurology* 11.

Baggen J., Thibaut H.J., Strating J.R.P.M. & Kuppeveld F.J.M. van. 2018. The life cycle of non-polio enteroviruses and how to target it. *Nature Reviews Microbiology* 16: 368–381.

Barbieri R., Coppo E., Marchese A., Daglia M., Sobarzo-Sánchez E., Nabavi S.F. & Nabavi S.M. 2017. Phytochemicals for human disease: An update on plant-derived compounds antibacterial activity. *Microbiological Research* 196: 44–68.

Bergelson J.M. & Coyne C.B. 2013. Picornavirus entry. *Advances in Experimental Medicine and Biology* 790: 24–41.

Blaising J., Polyak S.J. & Pécheur E.-I. 2014. Arbidol as a broad-spectrum antiviral: An update. *Antiviral Research* 107: 84–94.

Boriskin Y.S., Pécheur E.-I. & Polyak S.J. 2006. Arbidol: a broad-spectrum antiviral that inhibits acute and chronic HCV infection. *Virology Journal* 3: 56.

Bouin A., Gretteau P.-A., Wehbe M., Renois F., N'Guyen Y., Lévêque N., Vu M.N., Tracy S., Chapman N.M., Bruneval P., Fornes P., Semler B.L. &

Andreoletti L. 2019. Enterovirus Persistence in Cardiac Cells of Patients With Idiopathic Dilated Cardiomyopathy Is Linked to 5′ Terminal Genomic RNA-Deleted Viral Populations With Viral-Encoded Proteinase Activities. *Circulation* 139: 2326–2338.

Bushman F.D., McCormick K. & Sherrill-Mix S. 2019. Virus Structures Constrain Transmission Modes. *Nature microbiology* 4: 1778–1780.

Butler M.S., Blaskovich M.A. & Cooper M.A. 2013. Antibiotics in the clinical pipeline in 2013. *The Journal of Antibiotics* 66: 571–591.

Chang K.H., Auvinen P., Hyypiä T. & Stanway* G. 1989. The Nucleotide Sequence of Coxsackievirus A9; Implications for Receptor Binding and Enterovirus Classification. *Journal of General Virology* 70: 3269–3280.

Cheng P.-W., Ng L.-T., Chiang L.-C. & Lin C.-C. 2006. Antiviral effects of saikosaponins on human coronavirus 229E in vitro. *Clinical and Experimental Pharmacology & Physiology* 33: 612–616.

Chiang L.-C., Ng L.-T., Cheng P.-W., Chiang W. & Lin C.-C. 2005. Antiviral activities of extracts and selected pure constituents of Ocimum basilicum. *Clinical and Experimental Pharmacology & Physiology* 32: 811–816.

Chojnacka K., Skrzypczak D., Izydorczyk G., Mikula K., Szopa D. & Witek-Krowiak A. 2021. Antiviral Properties of Polyphenols from Plants. *Foods* 10: 2277.

Christianson D.W. 2008. Unearthing the roots of the terpenome. *Current Opinion in Chemical Biology* 12: 141–150.

Clardy J. & Walsh C. 2004. Lessons from natural molecules. *Nature* 432: 829–837.

Collett M.S., Hincks J.R., Benschop K., Duizer E., Avoort H. van der, Rhoden E., Liu H., Oberste M.S., McKinlay M.A. & Hartford M. 2017. Antiviral Activity of Pocapavir in a Randomized, Blinded, Placebo-Controlled Human Oral Poliovirus Vaccine Challenge Model. *The Journal of Infectious Diseases* 215: 335–343.

Crotty S., Cameron C.E. & Andino R. 2001. RNA virus error catastrophe: Direct molecular test by using ribavirin. *Proceedings of the National Academy of Sciences of the United States of America* 98: 6895–6900.

Cushnie T.P.T. & Lamb A.J. 2011. Recent advances in understanding the antibacterial properties of flavonoids. *International Journal of Antimicrobial Agents* 38: 99–107.

De Palma A.M., Vliegen I., De Clercq E. & Neyts J. 2008. Selective inhibitors of picornavirus replication. *Medicinal Research Reviews* 28: 823–884.

Debing Y., Neyts J. & Delang L. 2015. The future of antivirals: broad-spectrum inhibitors. *Current Opinion in Infectious Diseases* 28: 596–602.

Denaro M., Smeriglio A., Barreca D., De Francesco C., Occhiuto C., Milano G. & Trombetta D. 2020. Antiviral activity of plants and their isolated bioactive compounds: An update. *Phytotherapy research: PTR* 34: 742–768.

Derksen A., Kühn J., Hafezi W., Sendker J., Ehrhardt C., Ludwig S. & Hensel A. 2016. Antiviral activity of hydroalcoholic extract from Eupatorium perfoliatum L. against the attachment of influenza A virus. *Journal of Ethnopharmacology* 188: 144–152.

Doi K., Ikeda M., Hayase N., Moriya K., Morimura N., Maehara H., Tagami S., Fukushima K., Misawa N., Inoue Y., Nakamura H., Takai D., Kurimoto M., Tokunaga K., Yamamoto M., Hirayama I., Horie R., Endo Y., Hiwatashi K., Shikama M., Jubishi D., Kanno Y., Okamoto K., Harada S., Okugawa S., Miyazono K., Seto Y., Inoue J., & the COVID-UTH Study Group. 2020. Nafamostat mesylate treatment in combination with favipiravir for patients critically ill with Covid-19: a case series. *Critical Care* 24: 392.

Doremalen N. van, Bushmaker T., Morris D.H., Holbrook M.G., Gamble A., Williamson B.N., Tamin A., Harcourt J.L., Thornburg N.J., Gerber S.I., Lloyd-Smith J.O., Wit E. de & Munster V.J. 2020. Aerosol and Surface Stability of SARS-CoV-2 as Compared with SARS-CoV-1. *New England Journal of Medicine* 382: 1564–1567.

El-Mekkawy S., Meselhy M.R., Nakamura N., Tezuka Y., Hattori M., Kakiuchi N., Shimotohno K., Kawahata T. & Otake T. 1998. Anti-HIV-1 and anti-HIV-1-protease substances from Ganoderma Lucidum. *Phytochemistry* 49: 1651–1657.

EMA. 2022. COVID-19: EMA recommends conditional marketing authorisation for Paxlovid. *European Medicines Agency*.

Engelenburg F.A.C. van, Terpstra F.G., Schuitemaker H. & Moorer W.R. 2002. The virucidal spectrum of a high concentration alcohol mixture. *Journal of Hospital Infection* 51: 121–125.

Frausto S.D., Lee E. & Tang H. 2013. Cyclophilins as modulators of viral replication. *Viruses* 5: 1684–1701.

Furuta Y., Komeno T. & Nakamura T. 2017. Favipiravir (T-705), a broad spectrum inhibitor of viral RNA polymerase. *Proceedings of the Japan Academy. Series B, Physical and Biological Sciences* 93: 449–463.

Geller C., Varbanov M. & Duval R.E. 2012. Human Coronaviruses: Insights into Environmental Resistance and Its Influence on the Development of New Antiseptic Strategies. *Viruses* 4: 3044–3068.

Goh V.S.L., Mok C.-K. & Chu J.J.H. 2020. Antiviral Natural Products for Arbovirus Infections. *Molecules* 25: 2796.

Guinea M.C., Parellada J., Lacaille-Dubois M.A. & Wagner H. 1994. Biologically active triterpene saponins from Bupleurum fruticosum. *Planta Medica* 60: 163–167.

Hapuarachchi K. 2017. Mycosphere Essays 20: Therapeutic potential of Ganoderma species: Insights into its use as traditional medicine. *Mycosphere* 8: 1653–1694.

Harris K.G. & Coyne C.B. 2014. Death waits for no man – Does it wait for a virus? How Enteroviruses Induce and Control Cell Death. *Cytokine & growth factor reviews* 25: 587–596.

Hoffmann M., Kleine-Weber H., Schroeder S., Krüger N., Herrler T., Erichsen S., Schiergens T.S., Herrler G., Wu N.-H., Nitsche A., Müller M.A., Drosten C. & Pöhlmann S. 2020. SARS-CoV-2 Cell Entry Depends on ACE2 and TMPRSS2 and Is Blocked by a Clinically Proven Protease Inhibitor. *Cell* 181: 271-280.e8.

Hogle J.M., Chow M. & Filman D.J. 1985. Three-dimensional structure of poliovirus at 2.9 A resolution. *Science (New York, N.Y.)* 229: 1358–1365.

Huang C., Wang Y., Li X., Ren L., Zhao J., Hu Y., Zhang L., Fan G., Xu J., Gu X., Cheng Z., Yu T., Xia J., Wei Y., Wu W., Xie X., Yin W., Li H., Liu M., Xiao Y., Gao H., Guo L., Xie J., Wang G., Jiang R., Gao Z., Jin Q., Wang J. & Cao B. 2020. Clinical features of patients infected with 2019 novel coronavirus in Wuhan, China. *The Lancet* 395: 497–506.

Hui D.S., I Azhar E., Madani T.A., Ntoumi F., Kock R., Dar O., Ippolito G., Mchugh T.D., Memish Z.A., Drosten C., Zumla A. & Petersen E. 2020. The continuing 2019-nCoV epidemic threat of novel coronaviruses to global health - The latest 2019 novel coronavirus outbreak in Wuhan, China. *J. Inf. Dis* 91: 264–266.

Ikuta K., Hashimoto K., Kaneko H., Mori S., Ohashi K. & Suzutani T. 2012. Anti-viral and anti-bacterial activities of an extract of blackcurrants (Ribes nigrum L.). *Microbiology and Immunology* 56: 805–809.

Jassim S. a. A. & Naji M.A. 2003. Novel antiviral agents: a medicinal plant perspective. *Journal of Applied Microbiology* 95: 412–427.

Karia R., Gupta I., Khandait H., Yadav A. & Yadav A. 2020. COVID-19 and its Modes of Transmission. *SN Comprehensive Clinical Medicine* 2: 1798–1801.

Karimi A., Majlesi M. & Rafieian-Kopaei M. 2015. Herbal versus synthetic drugs; beliefs and facts. *Journal of Nephropharmacology* 4: 27–30.

Kim Y., Lovell S., Tiew K.-C., Mandadapu S.R., Alliston K.R., Battaile K.P., Groutas W.C. & Chang K.-O. 2012. Broad-Spectrum Antivirals against 3C or 3C-Like Proteases of Picornaviruses, Noroviruses, and Coronaviruses. *Journal of Virology* 86: 11754–11762.

Kim Y., Shivanna V., Narayanan S., Prior A.M., Weerasekara S., Hua D.H., Kankanamalage A.C.G., Groutas W.C. & Chang K.-O. 2015. Broad-Spectrum Inhibitors against 3C-Like Proteases of Feline Coronaviruses and Feline Caliciviruses. *Journal of Virology* 89: 4942–4950.

Knoops K., Kikkert M., Worm S.H.E. van den, Zevenhoven-Dobbe J.C., Meer Y. van der, Koster A.J., Mommaas A.M. & Snijder E.J. 2008. SARS-Coronavirus Replication Is Supported by a Reticulovesicular Network of Modified Endoplasmic Reticulum. *PLOS Biology* 6: e226.

Kramer A., Schwebke I. & Kampf G. 2006. How long do nosocomial pathogens persist on inanimate surfaces? A systematic review. *BMC Infectious Diseases* 6: 130.

Kreutzberger A.J.B., Sanyal A., Ojha R., Pyle J.D., Vapalahti O., Balistreri G. & Kirchhausen T. Synergistic Block of SARS-CoV-2 Infection by Combined Drug Inhibition of the Host Entry Factors PIKfyve Kinase and TMPRSS2 Protease. *Journal of Virology* 95: e00975-21.

Kumar S. & Pandey A.K. 2013. Chemistry and biological activities of flavonoids: an overview. *TheScientificWorldJournal* 2013: 162750.

Kurai D., Saraya T., Ishii H. & Takizawa H. 2013. Virus-induced exacerbations in asthma and COPD. *Frontiers in Microbiology* 4.

Laajala M., Hankaniemi M.M., Määttä J.A.E., Hytönen V.P., Laitinen O.H. & Marjomäki V. 2019. Host Cell Calpains Can Cleave Structural Proteins from the Enterovirus Polyprotein. *Viruses* 11: 1106.

Lai J.K.F., Sam I.-C. & Chan Y.F. 2016. The Autophagic Machinery in Enterovirus Infection. *Viruses* 8: 32.

Lamers M.M., Mykytyn A.Z., Breugem T.I., Wang Y., Wu D.C., Riesebosch S., Doel P.B. van den, Schipper D., Bestebroer T., Wu N.C. & Haagmans B.L. 2021. Human airway cells prevent SARS-CoV-2 multibasic cleavage site cell culture adaptation Marsh M., Meer J.W. van der & Hale B.G. (eds.). *eLife* 10: e66815.

Lau K.-M., Lee K.-M., Koon C.-M., Cheung C.S.-F., Lau C.-P., Ho H.-M., Lee M.Y.-H., Au S.W.-N., Cheng C.H.-K., Lau C.B.-S., Tsui S.K.-W., Wan D.C.-C., Waye M.M.-Y., Wong K.-B., Wong C.-K., Lam C.W.-K., Leung P.-C. & Fung K.-P. 2008. Immunomodulatory and anti-SARS activities of Houttuynia cordata. *Journal of Ethnopharmacology* 118: 79–85.

Lavola A., Maukonen M. & Julkunen-Tiitto R. 2018. Variability in the composition of phenolic compounds in winter-dormant Salix pyrolifolia in relation to plant part and age. *Phytochemistry* 153: 102–110.

Lin L.-T., Hsu W.-C. & Lin C.-C. 2014. Antiviral Natural Products and Herbal Medicines. *Journal of Traditional and Complementary Medicine* 4: 24–35.

Lin C.-J., Liu C.-H., Wang J.Y., Lin C.-C., Li Y.-F., Richardson C.D. & Lin L.-T. 2018. Small molecules targeting coxsackievirus A16 capsid inactivate viral particles and prevent viral binding. *Emerging Microbes & Infections* 7: 1–11.

Linnakoski R., Reshamwala D., Veteli P., Cortina-Escribano M., Vanhanen H. & Marjomäki V. 2018. Antiviral Agents From Fungi: Diversity, Mechanisms and Potential Applications. *Frontiers in Microbiology* 9.

Liu S., Chen R. & Hagedorn C.H. 2015. Tannic Acid Inhibits Hepatitis C Virus Entry into Huh7.5 Cells. *PLOS ONE* 10: e0131358.

Liu Y., Hill M.G., Klose T., Chen Z., Watters K., Bochkov Y.A., Jiang W., Palmenberg A.C. & Rossmann M.G. 2016. Atomic structure of a rhinovirus C, a virus species linked to severe childhood asthma. *Proceedings of the National Academy of Sciences* 113: 8997–9002.

Lu R., Zhao X., Li J., Niu P., Yang B., Wu H., Wang W., Song H., Huang B., Zhu N., Bi Y., Ma X., Zhan F., Wang L., Hu T., Zhou H., Hu Z., Zhou W., Zhao L., Chen J., Meng Y., Wang J., Lin Y., Yuan J., Xie Z., Ma J., Liu W.J., Wang D., Xu W., Holmes E.C., Gao G.F., Wu G., Chen W., Shi W. & Tan W. 2020. Genomic characterisation and epidemiology of 2019 novel coronavirus: implications for virus origins and receptor binding. *The Lancet* 395: 565–574.

Lv X., Qiu M., Chen D., Zheng N., Jin Y. & Wu Z. 2014. Apigenin inhibits enterovirus 71 replication through suppressing viral IRES activity and modulating cellular JNK pathway. *Antiviral Research* 109: 30–41.

Makarov V.A., Braun H., Richter M., Riabova O.B., Kirchmair J., Kazakova E.S., Seidel N., Wutzler P. & Schmidtke M. 2015. Pyrazolopyrimidines: Potent Inhibitors Targeting the Capsid of Rhino- and Enteroviruses. *ChemMedChem* 10: 1629–1634.

Manach C., Scalbert A., Morand C., Rémésy C. & Jiménez L. 2004. Polyphenols: food sources and bioavailability. *The American Journal of Clinical Nutrition* 79: 727–747.

Mandal S., Bonifacio A., Zanuttin F., Sergo V. & Krol S. 2011. Synthesis and multidisciplinary characterization of polyelectrolyte multilayer-coated nanogold with improved stability toward aggregation. *Colloid and Polymer Science* 289: 269–280.

Martikainen M., Salorinne K., Lahtinen T., Malola S., Permi P., Häkkinen H. & Marjomäki V. 2015. Hydrophobic pocket targeting probes for enteroviruses. *Nanoscale* 7: 17457–17467.

Martinez J.P., Sasse F., Brönstrup M., Diez J. & Meyerhans A. 2014. Antiviral drug discovery: broad-spectrum drugs from nature. *Natural Product Reports* 32: 29–48.

Matthews D.A., Dragovich P.S., Webber S.E., Fuhrman S.A., Patick A.K., Zalman L.S., Hendrickson T.F., Love R.A., Prins T.J., Marakovits J.T., Zhou R., Tikhe J., Ford C.E., Meador J.W., Ferre R.A., Brown E.L., Binford S.L., Brothers M.A., DeLisle D.M. & Worland S.T. 1999. Structure-assisted design of mechanism-based irreversible inhibitors of human rhinovirus 3C protease with potent antiviral activity against multiple rhinovirus serotypes. *Proceedings of the National Academy of Sciences of the United States of America* 96: 11000–11007.

Matz J. 2013. Vapendavir significantly improves upper respiratory symptoms of naturally acquired rhinovirus infection in asthmatic adults: Results of a phase 2 clinical trial. *European Respiratory Journal* 42.

Mehta P., McAuley D.F., Brown M., Sanchez E., Tattersall R.S. & Manson J.J. 2020. COVID-19: consider cytokine storm syndromes and immunosuppression. *The Lancet* 395: 1033–1034.

Metsämuuronen S. & Sirén H. 2019. Bioactive phenolic compounds, metabolism and properties: a review on valuable chemical compounds in Scots pine and Norway spruce. *Phytochemistry Reviews* 18: 623–664.

Min B.-S., Nakamura N., Miyashiro H., Bae K.-W. & Hattori M. 1998. Triterpenes from the Spores of Ganoderma lucidum and Their Inhibitory Activity against HIV-1 Protease. *Chemical & Pharmaceutical Bulletin* 46: 1607–1612.

Myllynen M., Kazmertsuk A. & Marjomäki V. 2016. A Novel Open and Infectious Form of Echovirus 1. *Journal of Virology* 90: 6759–6770.

Nekoua M.P., Alidjinou E.K. & Hober D. 2022. Persistent coxsackievirus B infection and pathogenesis of type 1 diabetes mellitus. *Nature Reviews Endocrinology* 18: 503–516.

Newman D.J. & Cragg G.M. 2020. Natural Products as Sources of New Drugs over the Nearly Four Decades from 01/1981 to 09/2019. *Journal of Natural Products* 83: 770–803.

Oberste M.S., Moore D., Anderson B., Pallansch M.A., Pevear D.C. & Collett M.S. 2009. In Vitro Antiviral Activity of V-073 against Polioviruses. *Antimicrobial Agents and Chemotherapy* 53: 4501–4503.

Orhan D.D., Ozçelik B., Ozgen S. & Ergun F. 2010. Antibacterial, antifungal, and antiviral activities of some flavonoids. *Microbiological Research* 165: 496–504.

Owczarek K., Szczepanski A., Milewska A., Baster Z., Rajfur Z., Sarna M. & Pyrc K. 2018. Early events during human coronavirus OC43 entry to the cell. *Scientific Reports* 8: 7124.

Panche A.N., Diwan A.D. & Chandra S.R. 2016. Flavonoids: an overview. *Journal of Nutritional Science* 5: e47.

Patick A.K., Brothers M.A., Maldonado F., Binford S., Maldonado O., Fuhrman S., Petersen A., Smith G.J., Zalman L.S., Burns-Naas L.A. & Tran J.Q. 2005. In Vitro Antiviral Activity and Single-Dose Pharmacokinetics in Humans of a Novel, Orally Bioavailable Inhibitor of Human Rhinovirus 3C Protease. *Antimicrobial Agents and Chemotherapy* 49: 2267–2275.

Pevear D.C., Fancher M.J., Felock P.J., Rossmann M.G., Miller M.S., Diana G., Treasurywala A.M., McKinlay M.A. & Dutko F.J. 1989. Conformational change in the floor of the human rhinovirus canyon blocks adsorption to HeLa cell receptors. *Journal of Virology* 63: 2002–2007.

Pevear D.C., Tull T.M., Seipel M.E. & Groarke J.M. 1999. Activity of Pleconaril against Enteroviruses. *Antimicrobial Agents and Chemotherapy* 43: 2109–2115.

Pfizer's Novel COVID-19 Oral Antiviral Treatment Candidate Reduced Risk of Hospitalization or Death by 89% in Interim Analysis of Phase 2/3 EPIC-HR Study | Pfizer.

Pizzato M., Baraldi C., Boscato Sopetto G., Finozzi D., Gentile C., Gentile M.D., Marconi R., Paladino D., Raoss A., Riedmiller I., Ur Rehman H., Santini A., Succetti V. & Volpini L. 2022. SARS-CoV-2 and the Host Cell: A Tale of Interactions. *Frontiers in Virology* 1.

Puhl A.C., Lane T.R., Urbina F. & Ekins S. 2022. The Need for Speed and Efficiency: A Brief Review of Small Molecule Antivirals for COVID-19. *Frontiers in Drug Discovery* 2.

Ragab T.I.M., Amer H., Mossa A.T., Emam M., Hasaballah A.A. & Helmy W.A. 2018. Anticoagulation, fibrinolytic and the cytotoxic activities of sulfated hemicellulose extracted from rice straw and husk. *Biocatalysis and Agricultural Biotechnology* 15: 86–91.

Rossmann M.G., Bella J., Kolatkar P.R., He Y., Wimmer E., Kuhn R.J. & Baker T.S. 2000. Cell Recognition and Entry by Rhino- and Enteroviruses. *Virology* 269: 239–247.

Ruokolainen V., Domanska A., Laajala M., Pelliccia M., Butcher S.J. & Marjomäki V. 2019. Extracellular Albumin and Endosomal Ions Prime Enterovirus Particles for Uncoating That Can Be Prevented by Fatty Acid Saturation. *Journal of Virology* 93: e00599-19.

Salvati A.L., De Dominicis A., Tait S., Canitano A., Lahm A. & Fiore L. 2004. Mechanism of action at the molecular level of the antiviral drug 3(2H)-isoflavene against type 2 poliovirus. *Antimicrobial Agents and Chemotherapy* 48: 2233–2243.

Sandoni M., Ciardo L., Tamburini C., Boncompagni A., Rossi C., Guidotti I., Garetti E., Lugli L., Iughetti L. & Berardi A. 2022. Enteroviral Infections in the First Three Months of Life. *Pathogens* 11: 60.

Schaar H.M. van der, Dorobantu C.M., Albulescu L., Strating J.R.P.M. & Kuppeveld F.J.M. van. 2016. Fat(al) attraction: Picornaviruses Usurp Lipid Transfer at Membrane Contact Sites to Create Replication Organelles. *Trends in Microbiology* 24: 535–546.

Schirtzinger E.E., Kim Y. & Davis A.S. 2022. Improving human coronavirus OC43 (HCoV-OC43) research comparability in studies using HCoV-OC43 as a surrogate for SARS-CoV-2. *Journal of Virological Methods* 299: 114317.

Schmitt E.K., Moore C.M., Krastel P. & Petersen F. 2011. Natural products as catalysts for innovation: a pharmaceutical industry perspective. *Current Opinion in Chemical Biology* 15: 497–504.

Shang J., Ye G., Shi K., Wan Y., Luo C., Aihara H., Geng Q., Auerbach A. & Li F. 2020. Structural basis of receptor recognition by SARS-CoV-2. *Nature* 581: 221–224.

Simons-Linares C.R., Imam Z. & Chahal P. 2021. Viral-Attributed Acute Pancreatitis: A Systematic Review. *Digestive Diseases and Sciences* 66: 2162–2172.

Singh A.K., Rana H.K. & Pandey A.K. 2019. Fungal-Derived Natural Product: Synthesis, Function, and Applications. In: Yadav A.N., Singh S., Mishra S. & Gupta A. (eds.), *Recent Advancement in White Biotechnology Through Fungi: Volume 2: Perspective for Value-Added Products and Environments*, Springer International Publishing, Cham, pp. 229–248.

Smyth M.S. & Martin J.H. 2002. Picornavirus uncoating. *Molecular Pathology* 55: 214–219.

Theisen L.L., Erdelmeier C.A.J., Spoden G.A., Boukhallouk F., Sausy A., Florin L. & Muller C.P. 2014. Tannins from Hamamelis virginiana Bark Extract: Characterization and Improvement of the Antiviral Efficacy against Influenza A Virus and Human Papillomavirus. *PLOS ONE* 9: e88062.

Thevenin T., Lobert P.E. & Hober D. 2013. Inactivation of Coxsackievirus B4, Feline Calicivirus and Herpes Simplex Virus Type 1: Unexpected Virucidal Effect of a Disinfectant on a Non-Enveloped Virus Applied onto a Surface. *Intervirology* 56: 224–230.

Thomford N.E., Senthebane D.A., Rowe A., Munro D., Seele P., Maroyi A. & Dzobo K. 2018. Natural Products for Drug Discovery in the 21st Century: Innovations for Novel Drug Discovery. *International Journal of Molecular Sciences* 19: E1578.

Tian Y., Liimatainen J., Alanne A.-L., Lindstedt A., Liu P., Sinkkonen J., Kallio H. & Yang B. 2017. Phenolic compounds extracted by acidic aqueous ethanol from berries and leaves of different berry plants. *Food Chemistry* 220: 266–281.

Tijsma A., Franco D., Tucker S., Hilgenfeld R., Froeyen M., Leyssen P. & Neyts J. 2014. The Capsid Binder Vapendavir and the Novel Protease Inhibitor SG85 Inhibit Enterovirus 71 Replication. *Antimicrobial Agents and Chemotherapy* 58: 6990–6992.

Torelli A., Gianchecchi E., Piccirella S., Manenti A., Piccini G., Pastor E.L., Canovi B. & Montomoli E. 2015. Sea buckthorn bud extract displays activity against cell-cultured Influenza virus. *Journal of Preventive Medicine and Hygiene* 56: E51–E56.

Tyśkiewicz K., Konkol M., Kowalski R., Rój E., Warmiński K., Krzyżaniak M., Gil Ł. & Stolarski M.J. 2019. Characterization of bioactive compounds in the biomass of black locust, poplar and willow. *Trees* 33: 1235–1263.

Ulferts R., Linden L. van der, Thibaut H.J., Lanke K.H.W., Leyssen P., Coutard B., De Palma A.M., Canard B., Neyts J. & Kuppeveld F.J.M. van. 2013. Selective Serotonin Reuptake Inhibitor Fluoxetine Inhibits Replication of Human Enteroviruses B and D by Targeting Viral Protein 2C. *Antimicrobial Agents and Chemotherapy* 57: 1952–1956.

Veeresham C. 2012. Natural products derived from plants as a source of drugs. *Journal of Advanced Pharmaceutical Technology & Research* 3: 200–201.

Watts S., Ramstedt M. & Salentinig S. 2021. Ethanol Inactivation of Enveloped Viruses: Structural and Surface Chemistry Insights into Phi6. *The Journal of Physical Chemistry Letters* 12: 9557–9563.

Wilde A.H. de, Zevenhoven-Dobbe J.C., Meer Y. van der, Thiel V., Narayanan K., Makino S., Snijder E.J. & Hemert M.J. van. 2011. Cyclosporin A inhibits the replication of diverse coronaviruses. *The Journal of General Virology* 92: 2542–2548.

Wu J.T., Leung K. & Leung G.M. 2020. Nowcasting and forecasting the potential domestic and international spread of the 2019-nCoV outbreak originating in Wuhan, China: a modelling study. *Lancet (London, England)* 395: 689–697.

Yang Y., Zhang H., Zuo J., Gong X., Yi F., Zhu W. & Li L. 2019. Advances in research on the active constituents and physiological effects of Ganoderma lucidum. *Biomedical Dermatology* 3: 6.

Yi L., Li Z., Yuan K., Qu X., Chen J., Wang G., Zhang H., Luo H., Zhu L., Jiang P., Chen L., Shen Y., Luo M., Zuo G., Hu J., Duan D., Nie Y., Shi X., Wang W., Han Y., Li T., Liu Y., Ding M., Deng H. & Xu X. 2004. Small Molecules Blocking the Entry of Severe Acute Respiratory Syndrome Coronavirus into Host Cells. *Journal of Virology* 78: 11334–11339.

Zhang W., Tao J., Yang X., Yang Z., Zhang L., Liu H., Wu K. & Wu J. 2014a. Antiviral effects of two Ganoderma lucidum triterpenoids against enterovirus 71 infection. *Biochemical and Biophysical Research Communications* 449: 307–312.

Zhang W., Tao J., Yang X., Yang Z., Zhang L., Liu H., Wu K. & Wu J. 2014b. Antiviral effects of two Ganoderma lucidum triterpenoids against enterovirus 71 infection. *Biochemical and Biophysical Research Communications* 449: 307–312.

Zhang S., Tuo J., Huang X., Zhu X., Zhang D., Zhou K., Yuan L., Luo H., Zheng B., Yuen K., Li M., Cao K. & Xu L. 2018. Epidemiology characteristics of human coronaviruses in patients with respiratory infection symptoms and phylogenetic analysis of HCoV-OC43 during 2010-2015 in Guangzhou. *PLOS ONE* 13: e0191789.

Zhou L., Ayeh S.K., Chidambaram V. & Karakousis P.C. 2021. Modes of transmission of SARS-CoV-2 and evidence for preventive behavioral interventions. *BMC Infectious Diseases* 21: 496.

Zhu Q., Bang T.H., Ohnuki K., Sawai T., Sawai K. & Shimizu K. 2015. Inhibition of neuraminidase by Ganoderma triterpenoids and implications for neuraminidase inhibitor design. *Scientific Reports* 5: 13194.

ORIGINAL PAPERS

I

TOXICOLOGICAL AND BIOACTIVITY EVALUATION OF BLACKCURRANT PRESS CAKE, SEA BUCKTHORN LEAVES AND BARK FROM SCOTS PINE AND NORWAY SPRUCE EXTRACTS UNDER A GREEN INTEGRAL APPROACH

by

Nora Pap, Dhanik Reshamwala, Risto Korpinen, Petri Kipeläinen, Marina Fidelis, Marianna M. Furtado, Anderson S. Sant'Ana, Mingchun Wen, Liang Zhang, Jarkko Hellström, Pertti Marnilla, Pirjo Mattila, Tytti Sarjala, Barou Yang, Amanda dos Santos Lima, Luciana Azevedo, Varpu Marjomäki & Daniel Granato 2021

Food and Chemical Toxicology 153: 112284.

Food and Chemical Toxicology 153 (2021) 112284

Contents lists available at ScienceDirect

Food and Chemical Toxicology

journal homepage: www.elsevier.com/locate/foodchemtox

Toxicological and bioactivity evaluation of blackcurrant press cake, sea buckthorn leaves and bark from Scots pine and Norway spruce extracts under a green integrated approach

Nora Pap [a], Dhanik Reshamwala [b], Risto Korpinen [c], Petri Kilpeläinen [c], Marina Fidelis [d], Marianna M. Furtado [e], Anderson S. Sant'Ana [e], Mingchun Wen [f], Liang Zhang [f], Jarkko Hellström [g], Pertti Marnilla [g], Pirjo Mattila [h], Tytti Sarjala [i], Baoru Yang [j], Amanda dos Santos Lima [k], Luciana Azevedo [k], Varpu Marjomäki [b], Daniel Granato [d,*]

[a] Biorefinery and Bioproducts, Natural Resources Institute Finland (Luke), FI-31600, Jokioinen, Finland
[b] Department of Biological and Environmental Science, University of Jyväskylä, Jyväskylä, Finland
[c] Biorefinery and Bioproducts, Natural Resources Institute Finland (Luke), FI-02150, Espoo, Finland
[d] Food Processing and Quality, Natural Resources Institute Finland (Luke), FI-02150, Espoo, Finland
[e] Department of Food Science and Nutrition, Faculty of Food Engineering, University of Campinas, Campinas, SP, Brazil
[f] State Key Laboratory of Tea Plant Biology and Utilization, Anhui Agricultural University, Hefei, 230036, China
[g] Food Processing and Quality, Natural Resources Institute Finland (Luke), FI-31600, Jokioinen, Finland
[h] Food Processing and Quality, Natural Resources Institute Finland (Luke), FI- 20520, Turku, Finland
[i] Biomass Characterization and Properties, Natural Resources Institute Finland (Luke), FI-39700, Parkano, Finland
[j] Food Chemistry and Food Development, Department of Biochemistry, University of Turku, 20014, Turku, Finland
[k] Department of Food, Faculty of Nutrition, Federal University of Alfenas, Rua Gabriel Monteiro da Silva, 714, 37130-000, Alfenas, Brazil

ARTICLE INFO

Handling Editor: Dr. Jose Luis Domingo

Keywords:
Extraction technologies
Bioactive compounds
Circular economy
Industrial by-products
Natural resources
Free radicals

ABSTRACT

Aqueous extracts from blackcurrant press cake (BC), Norway spruce bark (NS), Scots pine bark (SP), and sea buckthorn leaves (SB) were obtained using maceration and pressurized hot water and tested for their bioactivities. Maceration provided the extraction of higher dry matter contents, including total phenolics (TPC), anthocyanins, and condensed tannins, which also impacted higher antioxidant activity. NS and SB extracts presented the highest mean values of TPC and antioxidant activity. Individually, NS extract presented high contents of proanthocyanidins, resveratrol, and some phenolic acids. In contrast, SB contained a high concentration of ellagitannins, ellagic acid, and quercetin, explaining the antioxidant activity and antibacterial effects. SP and BC extracts had the lowest TPC and antioxidant activity. However, BC had strong antiviral efficacy, whereas SP can be considered a potential ingredient to inhibit α-amylase. Except for BC, the other extracts decreased reactive oxygen species (ROS) generation in HCT8 and A549 cells. Extracts did not inhibit the production of TNF-alpha in lipopolysaccharide-stimulated THP-1 macrophages but inhibited the ROS generation during the THP-1 cell respiratory burst. The recovery of antioxidant compounds from these by-products is incentivized for high value-added applications.

1. Introduction

Side streams of berries and woods offer diverse sources of various bioactive compounds. Especially berries are excellent and variable sources of phenolic compounds, such asphenolic acids, flavonoids, and proanthocyanidins (Ovaskainen et al., 2008). Industrial side streams from berry and wood sectors have a huge potential as they may contribute to the improvement of the circular economy, especially if cascade use models are adopted, that is, reusing and recycling products as many times as possible before their final disposal via energy generation or landfilling. In this panorama, in many EU countries, the production of sea buckthorn (SB), Norway spruce (NS), Scots pine (SP), and blackcurrant (BC) is of economic significance as a wide array of products are manufactured – from food ingredients to furniture. The recovery of

* Corresponding author.
E-mail addresses: nora.pap@luke.fi (N. Pap), granatod@gmail.com (D. Granato).

https://doi.org/10.1016/j.fct.2021.112284
Received 21 April 2021; Received in revised form 14 May 2021; Accepted 18 May 2021
Available online 24 May 2021

bioactive compounds from industrial by-products using green approaches would be an alternative for the energetic use of these valuable materials.

Leaves of sea buckthorn (*Hippophaë rhamnoides* L.) are by-products of berry plant cultivation. They have been reported to contain high levels of phenolic compounds, proteins, amino acids, minerals, vitamins, fatty acids, carotenoids, and tocopherols. Further, sea buckthorn leaf extracts are reported to have antibacterial, anti-viral, antitumoral, anti-inflammatory, and antioxidative activities (Ciesarová et al., 2020; Tian et al., 2017). According to Tian et al. (2017), the sea buckthorn leaves contained more polyphenols and showed different phenolic profiles (ellagitannins above 90%) from the corresponding berries.

Blackcurrant (*Ribes nigrum*) pomace is the material that remains after juice pressing containing mainly stems, peels and seeds. According to the recent review by Cortez and de Mejia (2019), BC pomace is still not sufficiently exploited even though it is rich in highly antioxidative polyphenols and other bioactivities that may improve the consumer's overall health. In cell-based studies, BC press cake, which is a rich source of cyanidin and delphinidin rutinoside) enhanced the proliferation of the *Lactobacillus rhamnosus* and showed antimicrobial effects in relation to *Salmonella enterica* and *Streptococcus pneumonia* (Parkar et al., 2014; Ikuta et al., 2012). The antiviral activity of blackcurrant extracts against respiratory syncytial virus (RSV), influenza virus A and B (IFV-A and IFV-B), adenovirus (AdV), and herpes simplex virus type 1 has already been reported (Ikuta et al., 2012).

Scots pine (*Pinus sylvestris*) and Norway spruce (*Picea abies*) are the most common trees in Northern Europe. Bark and knot wood are the most economically available wood residues. The phenolic compounds found in these trees include stilbenes, flavonoids, proanthocyanidins, phenolic acids, and lignans which have demonstrated antioxidant and antibacterial properties (Metsämuuronen and Sirén, 2019; Mäkinen et al., 2020).

The use of polyphenols as bioactive compounds at various business levels has urged scientists to investigate green extraction approaches to achieve eco-friendlier/sustainable, efficient and cost-effective techniques. Because the industrial side streams are still underutilized, there is a clear need to develop sustainable, green, and safe extraction methods to recover value-added compounds from these natural resources. More information about the extract's potential regarding its toxicological safety and *in vitro* bioactivities is required to understand more deeply the health benefits of industrial side-streams of BC, SB, NS, and SP. Thus, the objectives of this study are to characterize the chemical composition and antioxidant, antimicrobial and anti-inflammatory activities of BC, SB, NS, and SP aqueous extracts and their relative toxicological profile (i.e., toxicity) in different human cell lines.

2. Materials and methods

2.1. Chemical reagents

Cyanidin 3-*O*-rutinoside (≥95%), cyanidin 3-*O*-glucoside (≥95%), delphinidin 3-*O*-rutinoside (≥95%), delphinidin 3-*O*-glucoside (≥95%), petunidin 3-*O*-glucoside (≥95%), peonidin 3-*O*-glucoside (≥95%), and procyanidin B2 (>90%) were purchased from Extrasynthese (Lyon, France). Glacial acetic acid and phosphoric acid (85%) were from J. T. Baker (Mallinckrodt Baker Inc., Utrecht, The Netherlands). Folin-Ciocalteu reagent, gallic acid, ferrozine (3- (2-pyridyl) −5,6-di (2-furyl) −1,2,4-triazine-5′,5″ disodium disulfonic acid), ascorbic acid, 2-thiobarbituric acid (TBA), bacterial lipopolysaccharides (LPS), neocuproin (2,9-dimethyl-1,10-fenantroline), sodium carbonate, and 2,4,6-tris(2-pyridyl)-S-triazine (TPTZ), catechin (99%), epicatechin (98%), gallocatechin (98%), and epigallocatechin (95%), gallic acid (98%), ellagic acid (95%), cysteamine (98%), formic acid (98%), dichlorodihydro-fluorescein diacetate (DCFH-DA), 3–4,5 dimethylthiazol-2, 5 diphenyl tetrazolium bromide (MTT), Dulbecco's Modified Eagle's Medium/Nutrient Mixture F-12 Ham (DMEM), heneicosanoic acid, betulinol were acquired from Sigma Aldrich (St. Louis, USA). HPLC grade methanol (≥99.8%), acetonitrile (≥99.8%), ferric chloride hexahydrate, anhydrous sodium acetate, copper sulfate pentahydrate, 1,10 phenanthroline monohydrate, and copper chloride dihydrate were from VWR Chemicals BDH® (Germany). 2,2-Diphenyl-1-picrylhydrazyl radical (DPPH) was purchased from Alfa Aesar (Ward Hill, Massachusetts, USA), while phosphate buffer pH 7.5 and potassium hexacyanoferrate (III) were obtained from Merck (Darmstadt, Germany). The other reagents were of analytical grade. Aqueous solutions were prepared using ultrapure water (Millipore, São Paulo, Brazil). Sodium pyruvate, RPMI 1640-GlutaMAX™ medium, streptomycin, 2-mercaptoethanol, L-glutamine, [+]-D-glucose were obtained from Gibco® Invitrogen™, USA. HEPES was obtained from Fisher Scientific, Göteborg, Sweden. Phorbol-12-myristate-13-acetate, PMA was obtained from Santa Cruz Biotechnology, Santa Cruz, USA. The other reagents were of analytical grade.

2.2. Plant materials

Sea buckthorn leaves var. Raisa (moisture content of 61.1%) were collected in Nurmela, Finland, in September 2016. Freeze-dried Norway spruce bark (moisture content of 3.8%) and fresh Scots pine barks (moisture content of 59.4%) were collected in a wood industry Pietarsaari in March 2020. Industrial blackcurrant press cake (moisture content of 49.6%) was obtained in 2019 from a berry processing company located in East-Finland (Suomussalmi). All samples were standardized concerning the particle size (2 mm) using an industrial mill (Fritsch GmbH, model 15903, Idar-Oberstein, Germany) and extracted within 24 h. It is important to note that the study was conducted without further drying of the raw materials to avoid degradation of bioactive compounds and to eliminate one more operation unit in the process, thus mimicking how the industrial process.

2.3. Extraction technologies

Raw materials were extracted using a classic method (e.g., maceration) compared to pressurized hot water extraction (PHWE). For maceration, 100 g of raw material was extracted with 1000 mL of distilled water, under constant magnetic agitation and temperature monitoring, for 60 min at either 40 °C (blackcurrant press cake) or 50 °C (sea buckthorn leaves, Norway spruce bark, and Scots pine bark). For PHWE, the same temperature and extraction time parameters were used in accelerated solvent extractor (ASE-350, Dionex, Sunnyvale, USA), employing a pressure of 100 bar (98.7 atm) in 2 extraction cycles. Then, extracts were filtered using qualitative paper (Whatman n.1) and directly analyzed. The total solids content, expressed as a percentage of the raw material used in the extraction, was analyzed by weighing 3 mL of the extract and let it dry until constant weight at 105 °C. Part of the liquid extracts was freeze-dried under vacuum at 1200 μL of Hg for 120 h, and the extraction yield, expressed as a percentage, was calculated concerning the raw material used in the procedure. Extractions were performed in two independent replicates.

2.4. Phenolic composition

The total phenolic content (TPC) of extracts was analyzed using the spectrophotometric method based on the Prussian Blue assay, and results were expressed as mg of gallic acid equivalent per 100 g of material (wet basis), mg GAE/100 g or per gram (freeze-dried extracts) (Margraf et al., 2015). Total condensed tannins (CT) were estimated using the spectrophotometric method that employs vanillin in acidic medium (H_2SO_4), and results were expressed as mg of (+)-catechin equivalent per 100 g of material (wet basis), mg CE/100 g or per gram (freeze-dried extracts) (Horszwald and Andlauer, 2011). Total monomeric anthocyanins (TA) of blackcurrant press cake extracts were quantified using the

pH differential method described by Lee et al. (2005), and results were expressed as mg of malvidin-3-glucoside equivalent per 100 g of material (wet basis), mg/100 g. Total flavonoid content was assayed using the aluminum chloride hexahydrate protocol described by Zhishen et al. (1999) and results were expressed as mg CE/g. Analyses were performed in triplicate.

HPLC determination of anthocyanins from BC extract was performed according to the method described by Hellström et al. (2013). Agilent 1100 (Agilent Technologies Inc., Espoo, Finland) HPLC device equipped with diode array detection (DAD) and a Gemini C_{18} column (150 × 4.6 mm, 5 μm) was used and the separation was accomplished with a gradient elution of acetonitrile into 5% formic acid (aq). Peonidin and petunidin rutinoside and coumaroyl derivatives of glucosides of cyanidin and petunidin were quantified as corresponding glucosides. Ellagitannin content was determined after acid hydrolysis, according to Mattila and Kumpulainen (2002). Ellagic and gallic acids were determined using an Inertsil ODS-3 column (150 × 4.0 mm, 3 μm) with a gradient elution of acetonitrile into 50 mmol/L H_3PO_4 (pH 2.5).

Proanthocyanidins in freeze-dried extracts was determined by HPLC after thiolytic degradation, according to Mattila et al. (2018). A Zorbax Eclipse Plus C_{18} column (50 × 2.1 mm, 1.8 μm) was used with a gradient elution of acetonitrile into 0.5% formic acid (v/v) provided by UHPLC device (Agilent 1290 Infinity, Agilent Technologies, Inc., Santa Clara, CA, USA) equipped with diode array (DAD) and fluorescence detection (FLD).

2.5. Monomeric sugar composition

The monomeric sugar composition was determined by gas chromatography-flame ionization (GC-FID) detection via acid methanolysis and derivatization as described by Raitanen et al. (2020). Analyses were conducted in triplicate and results were expressed as mg/g od freeze dried extract.

2.6. Gas chromatography-mass spectra of extracts

The GC-mass spectrometry (MS) screening and quantification of some phenolic compounds (except for anthocyanins, ellagitannins, and proanthocyanidins) was performed on a GC-MS (HP6890-5973 GC-MSD instrument, Hewlett Packard, Palo Alto, CA, USA) using a HP-5 column (Agilent Technologies, Inc., Santa Clara, CA, USA; 30 m × 0.25 mm i.d., film thickness 0.25 μm) according to the methodology and conditions described by Raitanen et al. (2020). Helium was used as carrier gas and the injection was made in splitless mode. Mass spectra were obtained in EI mode (70 eV) and the fragmentation pattern was compared to standards in commercial (NIST14/Wiley11) libraries, as well as the standards in our own MS libraries available at our laboratory. Analyses were conducted in triplicate and results were expressed as mg/g od freeze-dried extract.

2.7. Antioxidant activity (AA)

The ferric reducing antioxidant power (FRAP), the scavenging activity of DPPH radical and the cupric ion reducing antioxidant capacity (CUPRAC) were assayed according to Xu et al. (2021) and results were expressed as mg of ascorbic acid equivalent per 100 g of material (wet basis), mg AAE/100 g. Folin-Ciocalteu reducing capacity was assessed using the methodology described by Margraf et al. (2015), and results expressed as mg GAE/100 g. The Fe^{2+} chelating ability (6–75 mg/L, R^2 = 0.986) was evaluated using ferrozine as the chromogen agent, and results were expressed as mg of disodium ethylenediaminetetraacetic acid (EDTA) per 100 g of material (wet basis), mg EDTAE/100 g) (Santos et al., 2017). Oxygen radical absorbance capacity (ORAC) of the freeze-dried extracts was determined in triplicate according to the methods described by Prior et al. (2003) and results were expressed as Trolox equivalent per gram of freeze-dried extract (μmol TE/g).

The inhibition of lipid oxidation (ILP) of Wistar rat's brain homogenate was assessed using the protocol described by Fidelis et al. (2018), in which 7-month old male wild-type Wistar rats (Envigo Venray, the Netherlands) were used in the experiment. Different concentrations of freeze-dried extracts obtained via maceration were tested (500, 1000, 2000, 3000, and 4000 mg/L) and thiobarbituric acid reactive species (TBARS) were measured at 532 nm using a spectrophotometer. Water was used as the negative control (maximum oxidation), and results were expressed as mg quercetin equivalent per gram of freeze-dried extract (mg QE/g). Approval of the Ethics Committee was obtained at the University of Helsinki.

The hydroxyl radical scavenging capacity of freeze-dried extract was assessed using a modified method initially described by Mukhopadhyay et al. (2016). For 750 μL of diluted sample, 150 μL of the $FeSO_4.7H_2O$ solution at 1 mmol/L and 100 μL of a H_2O_2 solution at 15 mmol/L. After 5 min, 750 μL of 1,10-phenanthroline at 1 mmol/L were added to the test tube and the content was vortexed for 10 s. After 20 min, the absorbance was read at 536 nm and water was used as the negative control and for the blank, H_2O_2 was replaced by water. The hydroxyl radical scavenging capacity was calculated according to Equation 1 and results were compared to a standard curve using gallic acid as the standard (0.75–50 mg/L, $R^2 = 0.995$) and expressed as mg GAE/g:

Hydroxyl radical scavenging capacity (%inhibition) = (Abs_{sample}/Abs_{blank}) x 100 (Eq. 1).

2.8. Antimicrobial effects

2.8.1. Microorganisms and cell suspensions

The microorganisms used were *Pseudomonas aeruginosa* (IAL, 1853), *Staphylococcus aureus* (ATCC 13565), *Staphylococcus epidermidis* (ATCC 12228), grown in Nutrient agar (Kasvi, São Paulo, Brazil) during 24 h at 37 °C for *P. aeruginosa* and 30 °C for *Staphylococcus. Candida albicans* (INCQS 40071) and *Propionibacterium acnes* (INCQS 229) were cultivated in Potato Dextrose Agar (Kasvi, São Paulo, Brazil) (30 °C/48 h) and Blood Agar (Laborclin, Paraná, Brazil) (37 °C/48 h, under anaerobiosis). The concentration of cells in the suspensions were standardized at 0.5 McFarland scale using turbidimeter (MS Tecnopon, Piracicaba, Brazil).

2.8.2. Antimicrobial tests

The antimicrobial activity tests carried out in this study were done as previously proposed (Cleeland and Squires, 1991) using the plate-cavity agar diffusion method (Escher et al., 2018) using 10^6 CFU per mL of each microorganism. Dimethyl sulfoxide (DMSO) was used as a negative control while imipenem (10 μg) was used as a positive control, excluding for *P. acnes* for which Penicillin G (10 IU) was used. All tests were performed twice in triplicate and the results expressed as halo of inhibition (in cm).

The minimum inhibitory concentration was performed according to Siddiqi et al. (2011). The extracts were diluted in DMSO so that the concentration of the stock solution was equal to 1000 μg/mL. Serial dilutions were prepared to obtain 250, 125, 62.5, 31.25, 15.625 μg/mL, respectively. The lowest concentration that did not show microbial growth was considered to be the minimum inhibitory concentration (MIC).

2.9. Inhibition of α-amylase and α-glucosidase

The inhibition of α-amylase and α-glucosidase activities were determined using the protocol outlined by Johnson et al. (2011). Freeze-dried extracts were resuspended in ultrapure water and tested at different concentrations (α-amylase: 1, 5, 10, 15, and 20 mg/mL; α-glucosidase: 10, 25, 50, 100, 200 and 500 μg/mL). For the α-amylase assay, acarbose (1 mmol/L) was used as a positive control. The inhibition of the enzyme activity was expressed in percentage and, when applicable, IC_{50} values (the concentration required to inhibit enzyme

Table 1
Comparison between maceration and pressurized hot water extraction (PHWE) on the extraction yield, dry matter content, bioactive compounds, and antioxidant activity of sea buckthorn leaves, blackcurrant press cake, Scots pine bark, and Norway Spruce bark extracts.

Extraction techniques	Raw materials	Extraction yield (% w/w)	Dry matter (% w/w)	TPC (mg GAE/100 g)	Condensed tannins (mg CE/100 g)	Total anthocyanins (mg/100 g)	CUPRAC (mg AAE/100 g)	Fe^{2+} chelating ability (mg EDTAE/100 g)	DPPH (mg AAE/100 g)	FCRC (mg GAE/100 g)
Maceration	Norway spruce bark	11.59 ± 0.20^{b}	16.09 ± 0.13^{a}	2199±6^{a}	932 ± 61^{a}	ND	34414 ± 353^{a}	ND	2383±5^{b}	5388 ± 73^{a}
	Scots pine bark	2.20 ± 0.16^{e}	2.16 ± 0.04^{f}	488 ± 15^{f}	238 ± 19^{d}	ND	3051 ± 63^{d}	ND	296±3^{f}	509 ± 14^{e}
	Sea buckthorn leaves	12.74 ± 0.35^{a}	11.76 ± 0.10^{b}	2119 ± 31^{b}	218±6^{d}	ND	22992 ± 104^{b}	155 ± 25^{a}	3318 ± 30^{a}	3280 ± 90^{b}
	Blackcurrant press cake	4.90 ± 0.52^{c}	5.37 ± 0.03^{d}	944 ± 10^{e}	632 ± 48^{b}	225.80 ± 12.36^{a}	2409 ± 283^{c}	ND	543±6^{e}	656 ± 21^{d}
PHWE	Norway spruce bark	3.73 ± 0.33^{d}	5.33 ± 0.06^{d}	1173±5^{d}	551 ± 24^{c}	ND	9431 ± 492^{c}	ND	1279 ± 34^{d}	2148 ± 112^{c}
	Scots pine bark	2.18 ± 0.26^{e}	1.72 ± 0.15^{g}	194±6^{h}	51±2^{e}	ND	785 ± 18^{g}	ND	162±3^{g}	325±5^{f}
	Sea buckthorn leaves	10.90 ± 0.23^{b}	10.25 ± 0.10^{c}	1402±8^{c}	86±5^{e}	ND	9829 ± 136^{c}	61 ± 12^{b}	1663 ± 16^{c}	2087 ± 47^{c}
	Blackcurrant press cake	5.37 ± 0.26^{c}	4.65 ± 0.04^{e}	333 ± 13^{g}	510 ± 10^{c}	92.28 ± 0.36^{b}	1821 ± 84^{f}	ND	305±4^{f}	288±3^{f}

Note: Values are expressed as means followed by the standard deviation (n = 3) and are related to the raw materials (wet basis). Different letters in the same column represent statistically different results ($p < 0.05$). TPC = total phenolic content, FCRC = Folin-Ciocalteu reducing capacity, ND = not detected, GAE = gallic acid equivalent, CE = catechin equivalent, AAE = ascorbic acid equivalent, EDTAE = EDTA equivalent.

activity by 50%) were obtained in triplicate.

2.10. Anti-inflammatory activity in THP-1 cells

Kinetic measurements of THP-1 cell respiratory burst (RB) activity were conducted with a microplate reader (Hidex Sense, Turku, Finland) using white 96-well flat-bottom non-treated microtiter plates following the method fully described by Tompa et al. (2011) and LPS at 10 μg/mL was used to trigger ROS generation in the system. The freeze-dried extracts were dissolved in HBSS-buffer (30 mg/mL) and the pH was adjusted to 7.4, whereby different freeze-dried extract concentrations were tested (7–1667 μg/mL). The chemiluminescence (CL) signal was counted and integrated at 0.5 s at 2.33 min intervals for 90 min to obtain kinetic curves. The CL peak (relative light units, rlu) was regarded as the sample's CL value. The efficacies of extracts were expressed as IC_{50} values, i.e., concentrates, which inhibit 50% of the CL emission obtained from cells without extracts in the same plate.

2.10.1. THP-1 cell differentiation and cytokine production

THP-1 cells (2×10^5/mL) were differentiated for 48 h using a 50 ng/mL solution of PMA as described in Alqarni et al. (2019). After the 24 h incubation in PMA free medium, the extracts at different concentrations (7–1667 μg/mL) were added to cells and thereafter LPS (0.5 μg/mL) was added. After additional 24 h incubation, the TNF-α content was measured by ELISA kits (BioLegend® ELISA MAX™ Deluxe Set Human TNF-α, Cat No. 430204, San Diego, USA) according to the manufacturer's instructions. The plates were read at 450 nm and 570 nm and the absorbance readings were corrected by subtracting readings taken at 570 nm.

2.11. Anti-viral activity

Adenocarcinomic human alveolar basal epithelial (A549) cells and Coxsackievirus A9 strain (CVA9; Griggs strain, ATCC) were used in the assays. CVA9 was produced and purified as described before (Ruokolainen et al., 2019). The anti-viral activity was assessed using a cytopathic effect (CPE) Inhibition assay, as described before (Martikainen et al., 2015), and modified from Schmidtke et al. (2001). Cytotoxicity was also evaluated using the CPE inhibition assay, where the compounds (without any virus) were tested for their toxicity on A549 cells. Mock infection was used as a control for the assay.

2.12. Cell viability and proliferation: preliminary toxicological safety assessment

Effects of extracts on THP-1 promonocyte viability was measured as described in Alqarni et al. (2019). Briefly, the THP-1 cells were added into 96-well plates at a density of 1×10^5 cells per well and incubated for 24 h in an incubator (at 37 °C, in 5% CO_2 and 100% RH). After 24 h the buffered (pH 7.4) SP, NS, BC and SB extract solutions were added in final concentrations ranging from 7 to 1667 μg/mL (same as in the TNF-α production test), and the cells were incubated further for 24 h. Only the medium was added in negative control cells, and 2.5% and 5% DMSO was used as a positive control. Resazurin salt solution (0.1 mg/mL) was added at final concentration of 10% (v/v) and cells were incubated further. Fluorescence (544 nm excitation, 595 nm emission) was measured with Hidex Sense fluorometer (Hidex, Turku, Finland) at 6, 8 and 24 h time points. Cell viability was assessed as relative to the mean values of the negative controls.

The cytotoxicity of the extracts (SB, NS, SP, and BC) was evaluated in relation to lung adenocarcinoma epithelial cells (A549), human ileocecal adenocarcinoma cells (HCT8), and normal human lung fibroblast (IMR90). Briefly, cells were seeded into 96-well plates at a density of 6×10^3 cells/well (IMR90) and 1×10^4 cells/well (HCT8, A549). Following the treatment (100, 500, 1000, and 2000 μg/mL) for 48 h, MTT (0.5 mg/mL) was added to each well and incubated for 4 h at 37 °C. The metabolically active cells reduced the MTT to blue formazan crystals, which were dissolved in DMSO and absorbance was measured at 570 nm. The IC_{50} (50% cell viability inhibition), GI_{50} (50% growth inhibition), and LC_{50} (50% cell death) parameters were performed. Moreover, the selectivity index (SI) was calculated by the ratio IC_{50} (IMR90)/IC_{50} (cancer cell lines). Any sample with an SI value higher than 3 will be considered to have high selectivity (Boechat et al., 2014). Intracellular ROS generation was assessed using the DCFH-DA assay. Malignant (A549, HCT8) cells (6×10^4 per well) were treated for 1 h with different concentrations of anthocyanins extracts (100–1000 μg/mL) or 22.5 μmol/L H_2O_2 (positive control) or culture medium (negative control). Following the treatment, H_2O_2 was added at 22.5 μmol/L in the wells, and the fluorescence intensity (λemission = 538 nm and λexcitation = 485 nm) was measured (Escher et al., 2018).

Table 2
Chemical composition of freeze-dried extracts obtained with maceration from sea buckthorn leaves, Norway spruce bark, Scots pine bark, and blackcurrant press cake.

Chemical compounds	Norway spruce bark	Scots pine bark	Sea buckthorn leaves	Blackcurrant press cake
Arabinose (mg/g)	0.43 ± 0.09^{c}	2.03 ± 0.03^{a}	0.44 ± 0.09^{c}	1.58 ± 0.01^{b}
Fructose (mg/g)	75.26 ± 15.29^{d}	111.75 ± 15.36^{c}	138.94 ± 21.53^{b}	221.99 ± 14.61^{a}
Galactose (mg/g)	7.94 ± 1.62^{c}	24.54 ± 0.21^{b}	121.42 ± 8.26^{a}	3.16 ± 0.21^{d}
Galacturonic acid (mg/g)	1.39 ± 0.34^{c}	7.09 ± 0.61^{b}	0.54 ± 0.04^{d}	46.27 ± 2.42^{a}
Glucose (mg/g)	81.58 ± 17.31^{d}	95.13 ± 14.98^{c}	153.43 ± 1.18^{a}	137.93 ± 6.34^{b}
Glucuronic acid (mg/g)	0.52 ± 0.19^{c}	4.63 ± 0.72^{b}	6.41 ± 0.37^{a}	5.36 ± 11.11^{ab}
Mannose (mg/g)	8.34 ± 2.05^{c}	14.61 ± 2.44^{b}	11.03 ± 0.10^{b}	37.82 ± 7.17^{a}
Rhamnose (mg/g)	0.26 ± 0.05^{b}	0.86 ± 0.01^{a}	0.32 ± 0.01^{b}	0.07 ± 0.05^{c}
Xylose (mg/g)	0.30 ± 0.10^{c}	0.87 ± 0.01^{b}	1.70 ± 0.01^{a}	0.61 ± 0.04^{b}
Sucrose (mg/g)	89.58 ± 12.78^{a}	13.25 ± 1.29^{c}	24.04 ± 0.55^{b}	27.47 ± 0.75^{b}
Malic acid (mg/g)	2.70 ± 0.30^{c}	3.70 ± 0.50^{c}	31.70 ± 0.10^{a}	22.00 ± 0.10^{b}
Quercetin (mg/g)	26.20 ± 1.40^{b}	28.40 ± 5.80^{a}	21.10 ± 0.50^{c}	21.10 ± 0.10^{c}
Quinic acid (mg/g)	25.70 ± 2.20^{b}	51.10 ± 2.30^{a}	15.20 ± 0.70^{c}	ND
3,4,5-Trihydroxybenzoic acid (mg/g)	ND	ND	13.90 ± 0.30	ND
Ellagic acid (mg/g)	ND	ND	1.50 ± 0.60	ND
Pinitol (mg/g)	24.80 ± 0.60^{c}	70.60 ± 3.70^{b}	302.70 ± 11.70^{a}	ND
(+)-Catechin (mg/g)	ND	3.00 ± 0.20	ND	ND
Taxifolin (mg/g)	ND	2.60 ± 1.10	ND	ND
4-Hydroxycinnamic acid (mg/g)	2.60 ± 0.10^{a}	ND	ND	0.30 ± 0.10^{b}
3,5,4′-Trihydroxystilbene (mg/g)	0.30 ± 0.10	ND	ND	ND
Neoabietic acid (mg/g)	0.40 ± 0.10	ND	ND	ND
Isorhapontin (mg/g)	2.90 ± 0.30	ND	ND	ND
Astringin (mg/g)	3.00 ± 0.20	ND	ND	ND
Proanthocyanidins (mg/100 g)	4113 ± 39^{c}	8172 ± 210^{b}	9287 ± 711^{a}	1579 ± 42^{d}
Degree of polymerization	7.29 ± 0.61^{b}	4.92 ± 0.06^{c}	2.80 ± 0.07^{d}	25.6 ± 1.3^{a}
Procyanidins (%)	95.9	100	58.7	43.3
Prodelphinidins (%)	4.1	NA	41.3	56.7
Ellagitannins (mg/100 g)	ND	ND	3148 ± 35	ND
Ellagic acid (%)	NA	NA	78	NA
Gallic acid (%)	NA	NA	22	NA
Delphinidin 3-*O*-glucoside (mg/100 g)	ND	ND	ND	736 ± 21
Delphinidin 3-*O*-rutinoside (mg/100 g)	ND	ND	ND	1524 ± 26
Cyanidin 3-*O*-glucoside (mg/100 g)	ND	ND	ND	200 ± 6
Cyanidin 3-*O*-rutinoside (mg/100 g)	ND	ND	ND	1159 ± 15
Petunidin 3-*O*-rutinoside (mg/100 g)	ND	ND	ND	42.4 ± 1.9
Peonidin 3-*O*-rutinoside (mg/100 g)	ND	ND	ND	24.4 ± 1.0
Cyanidin-coumaroyl-glucoside (mg/100 g)	ND	ND	ND	17.3 ± 0.5
Petunidin-coumaroyl-glucoside (mg/100 g)	ND	ND	ND	6.30 ± 0.46

Note: ND = not detected, NA = Not applicable. Different letters in the same line represent different results ($p < 0.05$) between extracts.

2.13. Statistical analysis

A completely randomized experimental design was used in the experiments, in which two extractions were performed and samples were analyzed in triplicate (except for monosaccharides), totaling six results per sample. Experimental data are expressed as means followed by the standard deviation. Comparison between extraction technologies and extracts from different sources was based on one-way analysis of variances (ANOVA) and, when appropriate, the Fisher's test was used to compare the mean values. When two samples are compared, an unpaired Student-*t* test was used. Correlation coefficients between responses were calculated. Probability values below 0.05 were considered to be significant (Granato et al., 2014). The software TIBCO Statistica v. 13.3 (TIBCO Software Ltd, Palo Alto, USA) was used in the analyses.

3. Results and discussion

3.1. Physicochemical properties, phenolic composition (TPC, TA, CT), and antioxidant activity (AA): comparison between maceration and PHWE

In this study, as observed in Table 1, the maceration provided greater extraction of dry matter contents, including total phenolics (TPC), anthocyanins (TA), and condensed tannins (CT), compared to PHWE. The conventional method also provided a higher antioxidant activity for all protocols tested (CUPRAC, Fe^{2+} chelating ability, DPPH, and FCRC). Similarly, a study concerning the effects of different pre-treatment maceration techniques on the content of phenolic compounds, antioxidant capacity, and other chemical properties reported that this procedure improved the extraction of compounds from red grape skin (Wojdyło et al., 2021).

Comparing the raw materials, The NS and SB extracts presented the highest extraction yield, followed by dry matter, mean values of TPC, CUPRAC, DPPH, and FCRC. On the other hand, SP and BC extracts had the lowest mean values of antioxidant activity and TPC among the plant materials studied (Table 1). Michalska et al. (2017) reported similar TPC values for BC (701 mg/100 g). A fractionation study of SB pomace into valuable components using high pressure and enzyme-assisted extraction methods was conducted (Kitrytė et al., 2017). The authors revealed that under pressurized ethanol extraction (10.3 MPa/70 °C/15 min) recovered 158 g/kg (15.8% of extraction yield) of polar constituents from the pomace, indicating similar results to our findings. The results also agree with those reported by Kim et al. (2011) found that the aqueous extract from SB leaves could decrease oxidation products' formation (i.e., peroxides) in a TBA-based test. The extract also had a similar antioxidant activity with vitamin E and BHT. Ma et al. (2019) found that ellagitannins (peduncalagin, stacchyurin, hippophaenin B and C, casuarin, and casuarictin) were the main responsible for the antioxidant activity of SB leaves aqueous extract measured by the 2-deoxyribose assay and metal chelating ability.

3.2. Characterization of the extracts obtained by the most promising extraction process

3.2.1. Carbohydrates, phenolic composition, and antioxidant activity

The maceration process was selected to continue the study, as it was

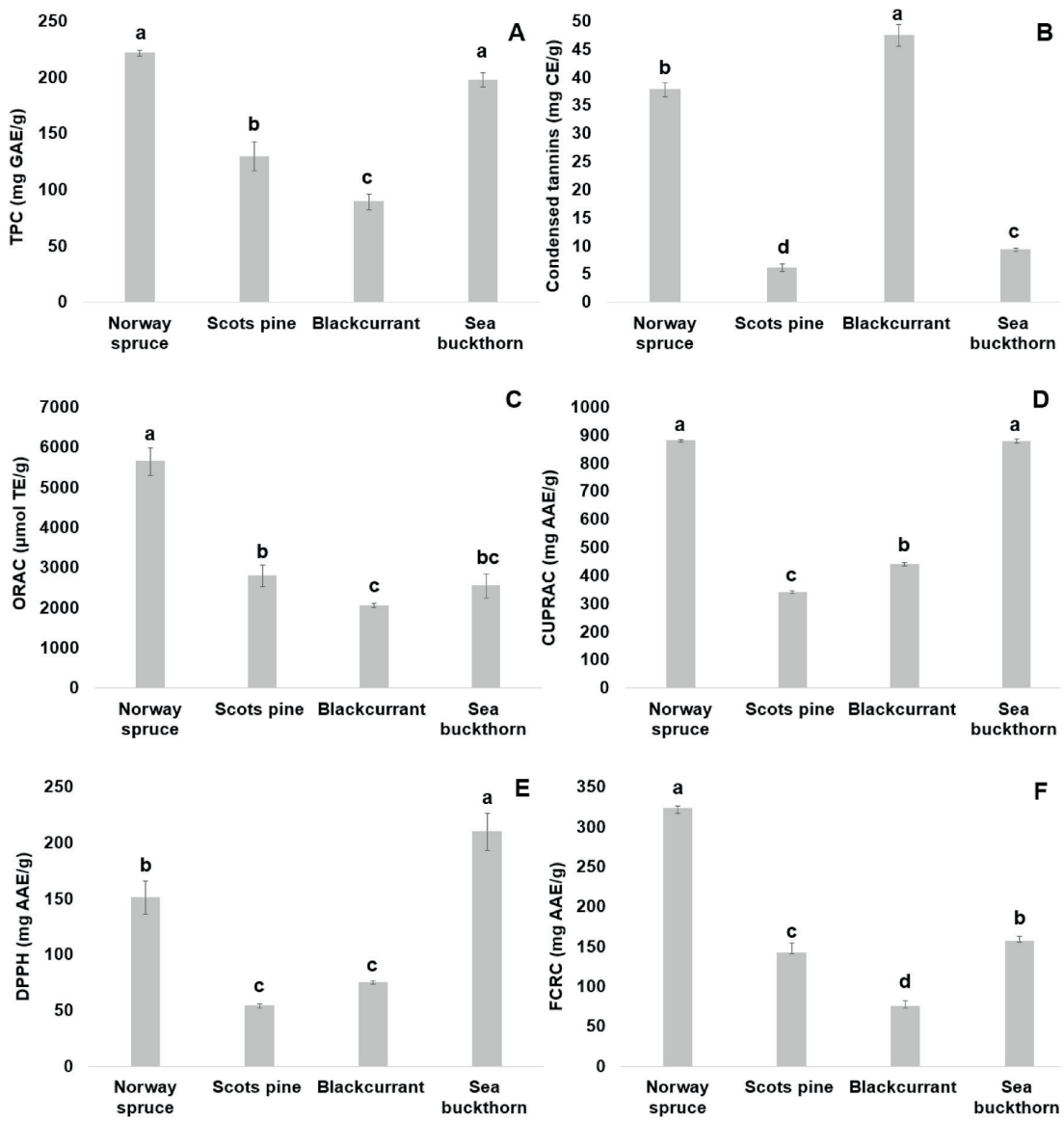

Fig. 1. Total phenolic content (TPC), condensed tannins (B), oxygen radical absorbance capacity (C), cupric ion reducing antioxidant capacity (D), free radical scavenging activity towards DPPH (E), Folin-Ciocalteu reducing capacity, FCRC (F), inhibition of lipid oxidation (ILP) using Wistar rat's brain as substrate (G), inhibition of α-amylase (H) and α-glucosidase (I), ferric reducing antioxidant power, FRAP (J), total flavonoids (K), and scavenging of hydroxyl radical (L) of freeze-dried extracts obtained with maceration from sea buckthorn leaves, Norway spruce bark, Scots pine bark, and blackcurrant press cake. Different letters represent statistically different results at $p < 0.05$. Note: AAE = ascorbic acid equivalent, CE = catechin equivalent, GAE = gallic acid equivalent, QE = quercetin equivalent, TE = Trolox equivalent.

considered the most promising approach. Regarding the carbohydrate composition shown in Table 2, 10 different compounds were identified in the extracts, in which fructose, glucose, sucrose were the most abundant ones. Fig. 1 contains the chemical composition and antioxidant activity of the freeze-dried extracts obtained by maceration. NS and SB freeze-dried extracts presented the highest mean values of TPC (Fig. 1A), CUPRAC (Fig. 1D), DPPH (Fig. 1E), FCRC (Fig. 1F), ILP (Fig. 1G), and scavenging of hydroxyl radical (Fig. 1L). As observed in Table 2, NS freeze-dried extract presented high content of proanthocyanidins, resveratrol, and some phenolic acids while SB freeze-dried extracts contained a high concentration of ellagitannins, proanthocyanidins, ellagic acid, and quercetin, explaining the high mean values for the antioxidant activity. On the contrary, SP and BC freeze-dried extracts had the lowest TPC (Fig. 1A), ORAC (Fig. 1C), DPPH (Fig. 1E), FCRC (Fig. 1F), ILP (Fig. 1G), and scavenging of hydroxyl radical (Fig. 1L). However, BC showed a comparable ($p > 0.05$) antioxidant activity measured by FRAP (Fig. 1J) with NS, while SB showed an intermediate FRAP value. The main chemical compounds found in the BC extract were anthocyanins and proanthocyanidins. Four major anthocyanins (3-rutinosides and 3-glucosides of delphinidin and cyanidin) comprised over 97% of total anthocyanins in BC agreeing with previous studies (Mattila et al., 2016; Wu et al., 2004).

Proanthocyanidins in the SP were essentially procyanidins while in other extracts CTs were mixtures of procyanidins and prodelphinidins in accordance to earlier studies on the same plant species (Gu et al., 2003; Hellström et al., 2009; Matthews et al., 1997). The average degree of

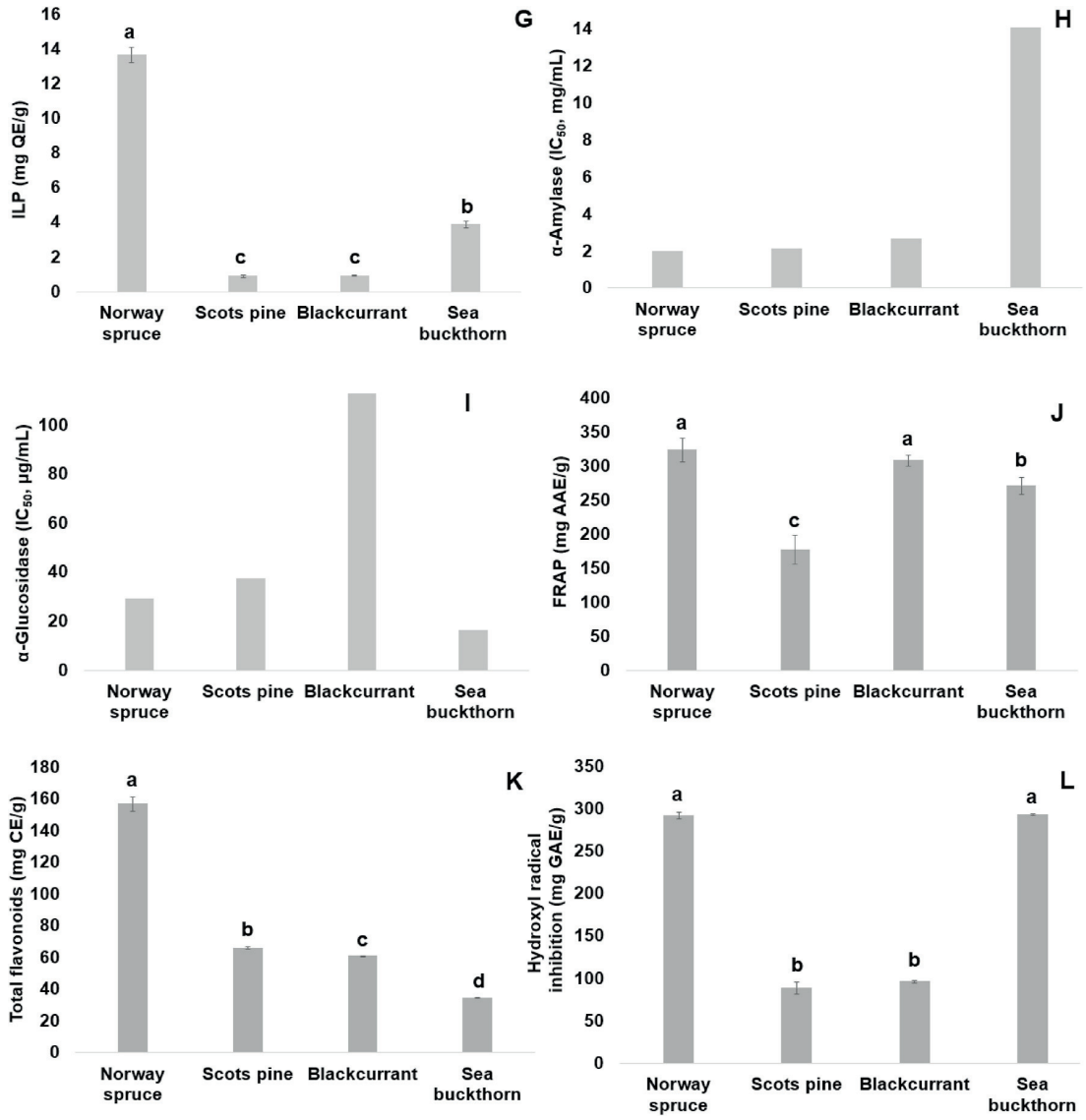

Fig. 1. (*continued*).

polymerization (DP) varied from 4.9 (SB) to 25.6 (BC). Monomeric forms were not analyzed separately, i.e. they were considered as 'terminal units' in thiolysis. Consequently, high content of free monomers, i.e. (epi)catechin and (epi)gallocatechin, would have some decreasing effect on DP. High DP of BC tannins have been reported already before (Gu et al., 2003; Hellström et al., 2009).

Correlation analysis showed an obvious result: the antioxidant capacity measured by different assays was significantly ($p < 0.05$) correlated to TOC, flavonoids, and TCT: DPPH ($r_{TPC} = 1.00$, $r_{flavonoids} = 0.935$), FCRC ($r_{TPC} = 0.847$, $r_{flavonoids} = 0.909$), and FRAP ($r_{TCT} = 0.586$). This result corroborates the findings of previous research on the bioactivity of phenolic-rich extracts (Santos et al., 2017; Margraf et al., 2015).

3.2.2. Antimicrobial activity

The results obtained for the antimicrobial activity test are shown in Table 1 – supplementary material. Among the analyzed extracts, SB showed an antimicrobial potential for some of the tested microorganisms, with the greatest activity obtained for *P. aeruginosa* IAL 1853. BC press cake, NS and SP freeze-dried extracts did not present any antimicrobial activity. These findings indicate SB freeze dried extract may be useful in inhibiting both Gram-negative and Gram-positive microorganisms. Despite this, the MIC assessment indicated that none of the studied extracts were able to inhibit the microorganisms in any of the concentrations evaluated (data not shown).

3.2.3. Inhibition of digestive enzymes

As shown in Fig. 1, all four extracts showed potent inhibition effects on two digestive enzymes at low concentrations. For the α-glucosidase inhibition, the BC freeze-dried extract had the lowest inhibition activity with IC_{50} value ($IC_{50} = 113$ μg/mL), while SB freeze-dried extract had the opposite behavior ($IC_{50} = 16.19$ μg/mL). This result corroborates the findings of Sharma et al. (2011) who observed that streptozotocin-nicotinamide induced type-2 diabetic rats had a significant decrease in blood sugar levels (up to 50%) and an increase of antioxidant activity in blood (up to 200%) after the administration of SB juice. On the contrary, our results do not agree with those obtained by Iizuka et al. (2018), who found that blackcurrant extract (obtained from the pulp) significantly reduced blood glucose concentration and improved glucose tolerance in type 2 diabetic mice, and this result is

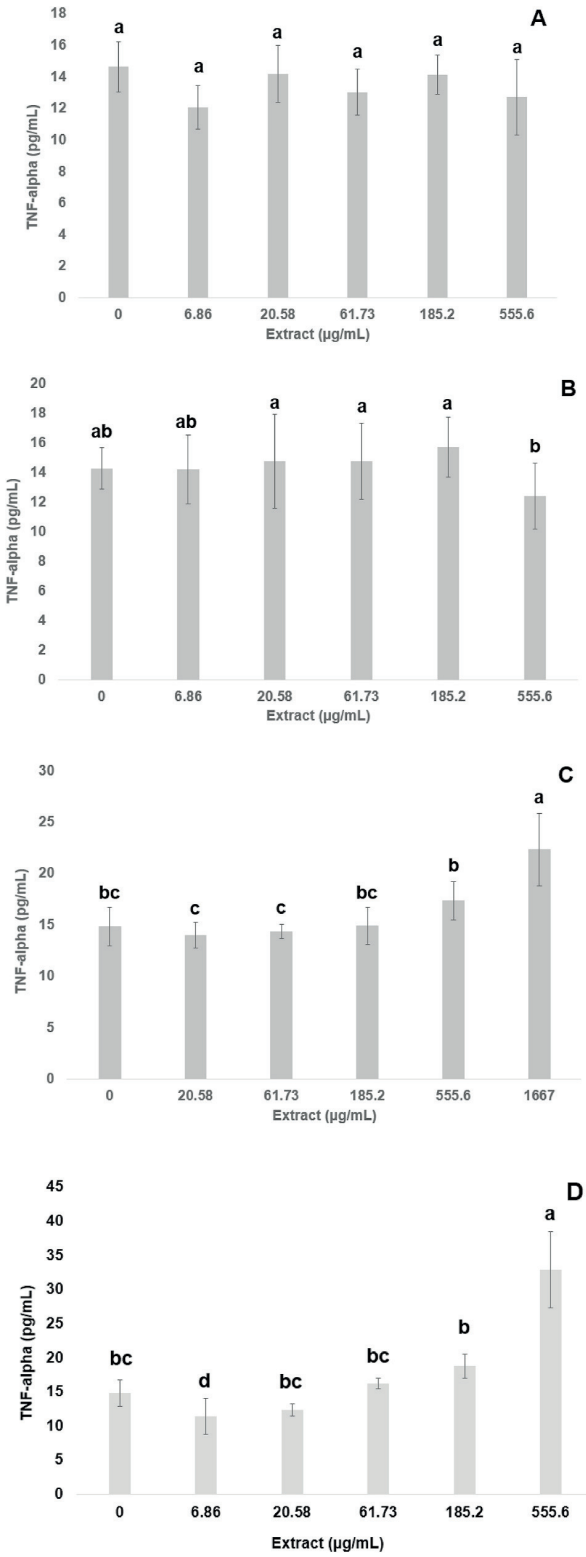

Fig. 2. The effects of freeze-dried extracts from Scots pine bark (A), Norway spruce bark (B), blackcurrant press cake (C), and sea buckthorn leaves (D) on *Escherichia coli* LPS induced TNF-alpha secretion in THP-1 macrophages. Different letters comparing the extracts represent statistically different results ($p < 0.05$).

associated with the levels of anthocyanins, especially delphinidin 3-*O*-rutinoside.

Table 1 indicated that the TPC in SB was much higher than the other extracts, which may explain its inhibition effects on α-glucosidase. On the contrary, for the α-amylase inhibition, SB presented the lowest value (IC_{50} = 14.06 mg/mL) while NS and SP extracts presented the highest and comparable inhibition (IC_{50} = 1.96 and IC_{50} = 2.10 mg/mL, respectively). Herein, the inhibition of α-amylase was correlated ($p < 0.05$) with total condensed tannins ($r = -0.487$) but not with TPC ($r = 0.375$), while the inhibition of α-glucosidase was correlated ($p < 0.05$) with TPC ($r = -0.830$). These results are in line with those obtained by Fidelis et al. (2018), who analyzed an industrial by-product from the juice industry (camu-camu seed coat), rich in ellagitannins. Kim et al. (2011) studied different aqueous and organic extracts of SB and found that quercetin, kaempferol, and isorhamnetin glucosides are responsible for the antioxidant activity and inhibition of α-glucosidase. Therefore, the results suggest that the freeze-dried extracts produced by maceration can be further tested *in vivo* for their antidiabetic potential.

3.2.4. *Anti-inflammatory activity*

Although many published studies have been reporting that phenolic extracts from plants can inhibit pro-inflammatory cytokines, including TNF-alpha from THP-1 macrophages, our extracts did not inhibit LPS stimulated TNF-alpha production. SP had no significant effect on the TNF-alpha activation (Fig. 2A), whereas NS had a slight inhibition effect on the TNF-alpha activation (Fig. 2B). Correlation analysis showed that higher TPC ($r = -0.670$, $p = 0.017$) and flavonoids ($r = -0.662$, $p = 0.019$) were associated with lower TNF-alpha release and higher DPPH and ORAC values ($r = -0.670$, $p = 0.017$ and $r = -0.553$, $p = 0.064$). On the other hand, BC (556 and 1667 μg/mL, Fig. 2C) and SB (62–556 μg/mL, Fig. 2D) extracts increased TNF-alpha activation, thus indicating a pro-inflammatory effect. When administered alone, chlorogenic acid increased TNF-alpha production in THP-1 cells stimulated with LPS, thus supporting the observation that depending on the matrix (i.e., crude extract or isolated compound), phenolic compounds may show ambiguous behavior toward the activation of pro-inflammatory cytokines (Bisht et al., 2020). Regarding the release of TNF-alpha in THP-1 cells challenged with LPS, although, the antioxidant effects observed using multiple chemical assays were not enough to counteract the inflammation response in LPS-challenged THP-1 cells.

Extracts showed a dose-dependent inhibition of reactive oxygen species (ROS) generation during the THP-1 cell respiratory burst (Fig. 3). The mean concentrations that inhibited 50% of ROS production (ID_{50}) were in SP, NS, BC, and SB as follows: 68.7, 57.1, 157.3, and 41.6 μg/mL, respectively. Comparatively, BC extract showed lower efficacy ($p < 0.05$) compared to the other extracts, which corroborated with the AA data. Extracts inhibited the ROS generation almost totally in the highest concentrations, 476 and 1429 μg/mL (Fig. 3). This is of importance since ROS are signaling molecules in the immune system. Interestingly, neither TPC nor flavonoids were significantly correlated ($r<0.30$, $p>0.60$, data not shown) with the decrease of ROS generation in THP-1 cell model. However, the decrease of ROS generation in THP-1 cells was strongly correlated ($p < 0.05$) with CUPRAC ($r = -0.601$) and scavenging of hydroxyl radical ($r = -0.689$), implying that multiple *in vitro* chemical antioxidant assays still can be important tools to explain cell-based anti-inflammatory/antioxidant data (Granato et al., 2018).

For the BC extract, results are in agreement with previous reports: mimicking obesity-associated chronic inflammation using RAW264.7 macrophages stimulated with LPS, Lee and Lee (2019) found that BC powder (0–100 μg/mL) was able decrease IL-1β and IL-6 mRNA, but not TNF-alpha mRNA levels. In a mouse model of obesity, authors verified that when BC powder was administered daily for 22–23 weeks, no changes were observed on the expression of pro-inflammatory genes (IL-1β, IL-6, and TNF-alpha). On the contrary, THP-1 cells treated with LPS and anthocyanin-rich BC extract (5–50 ng/mL) showed a lower activation of TNF-alpha and IL-6, showing that, hypothetically, the

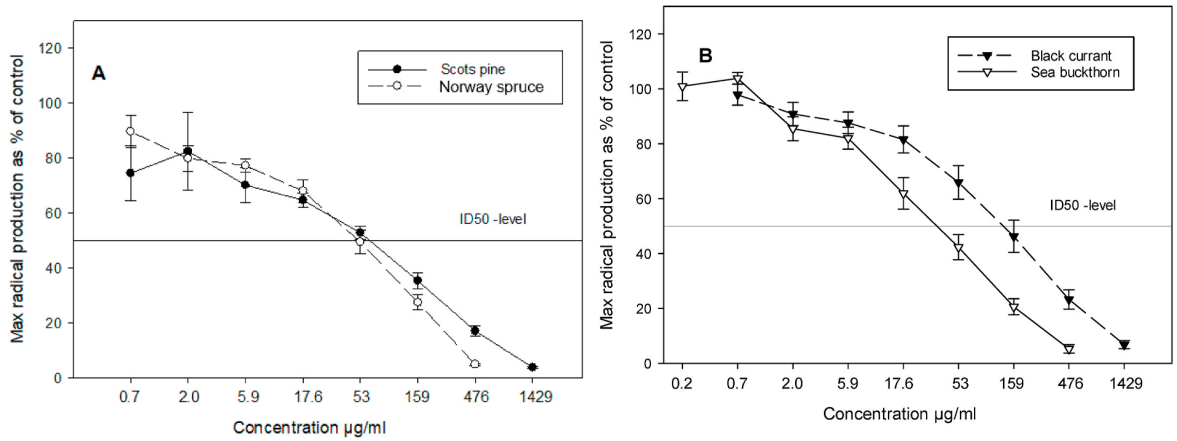

Fig. 3. The effects of extracts on the maximum radical production rate of THP-1 cells during respiratory burst. The cells were primed to an inflammatory state with *Escherichia coli* LPS, and 35 min later, the respiratory burst reaction was induced by human serum-treated yeast cell wall particles. The values are the peroxidase dependent luminol enhanced chemiluminescence reaction maxima presented as percent of that of the controls with no extract. The error bars represent the standard error of the mean (S.E., n = 9). The ID_{50} means the level of 50% inhibition.

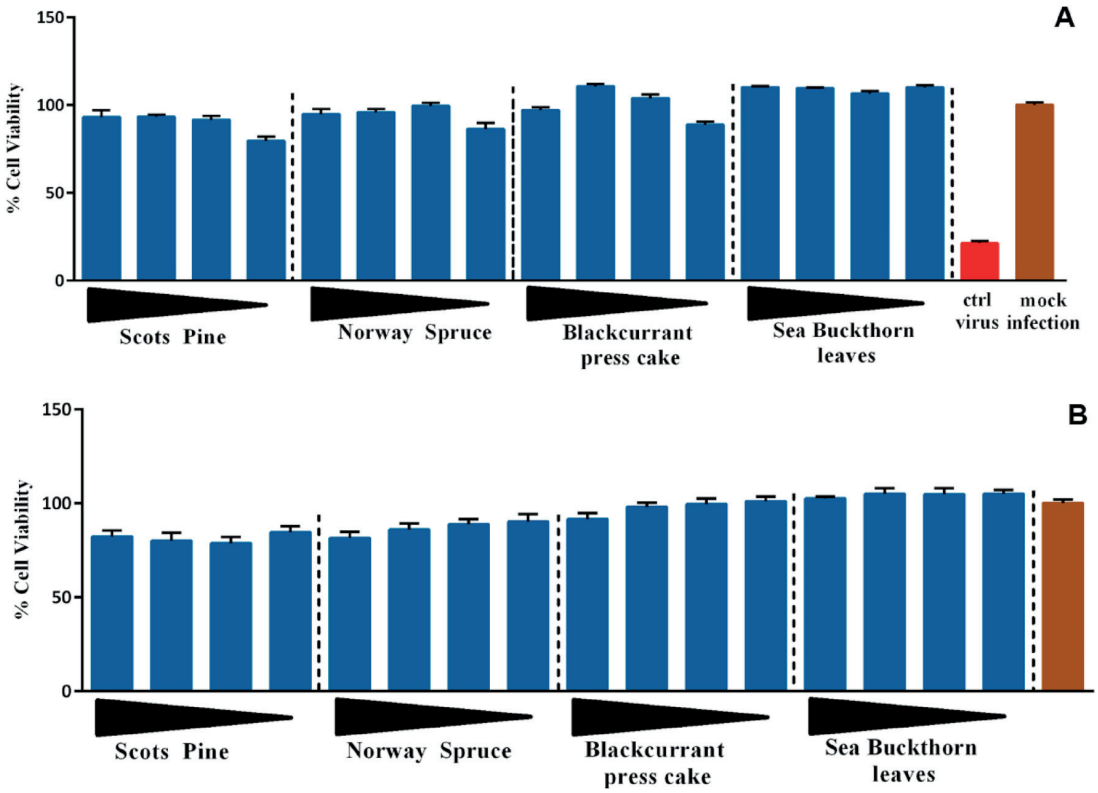

Fig. 4. Antiviral efficacy (A) and cytotoxicity (B) of the different samples at different concentrations (1, 50, 100, and 200 µg/mL) tested on human A549 cells. For the antiviral assessment, CoxsackievirusA9 (2 × 10E7 pfu) was treated with increasing concentrations from the left to the right-hand side (1, 50, 100, and 200 µg/mL).

modulation of pro-inflammatory response in cell models is mostly attributed to the anthocyanins and not by the pool of chemical compounds in crude BC extract (Lyall et al., 2009). For SB, it seems that the anti-inflammatory activity is related to the flavonoids: Jian et al. (2017) treated LPS-stimulated RAW264.7 macrophages with SB extract (12.5–100 µg/mL) and flavonoids downregulated the production and mRNA expression of pro-inflammatory cytokines (TNF-alpha, IL-6, and IL-1β) in a dose-dependent manner. A knot extract of SP rich in lignans (e.g. nortrachelogenin) was tested for its anti-inflammatory effects in murine J774 macrophages. Authors observed that SP extract downregulated the production of nitric oxide, prostaglandin E2, IL-6, and monocyte chemotactic protein-1 in J774 macrophages (Laavola et al., 2017). Similarly, Laavola et al. (2015) compared the anti-inflammatory effects of a knot extract of SP and two stilbenes found in the extract (pinosylvin and monomethylpinosylvin) in a cell-based model (J774 macrophages challenged with LPS). Results showed that the SB extract (up to 100 µg/mL) and the phenolic compounds (up to 100 µM) decreased the release of nitric oxide and IL-6. Similarly, Spilioti et al. (2014) observed that lignans (up to 100 µM) from NS knot were able to downregulate the expression of pro-inflammatory markers

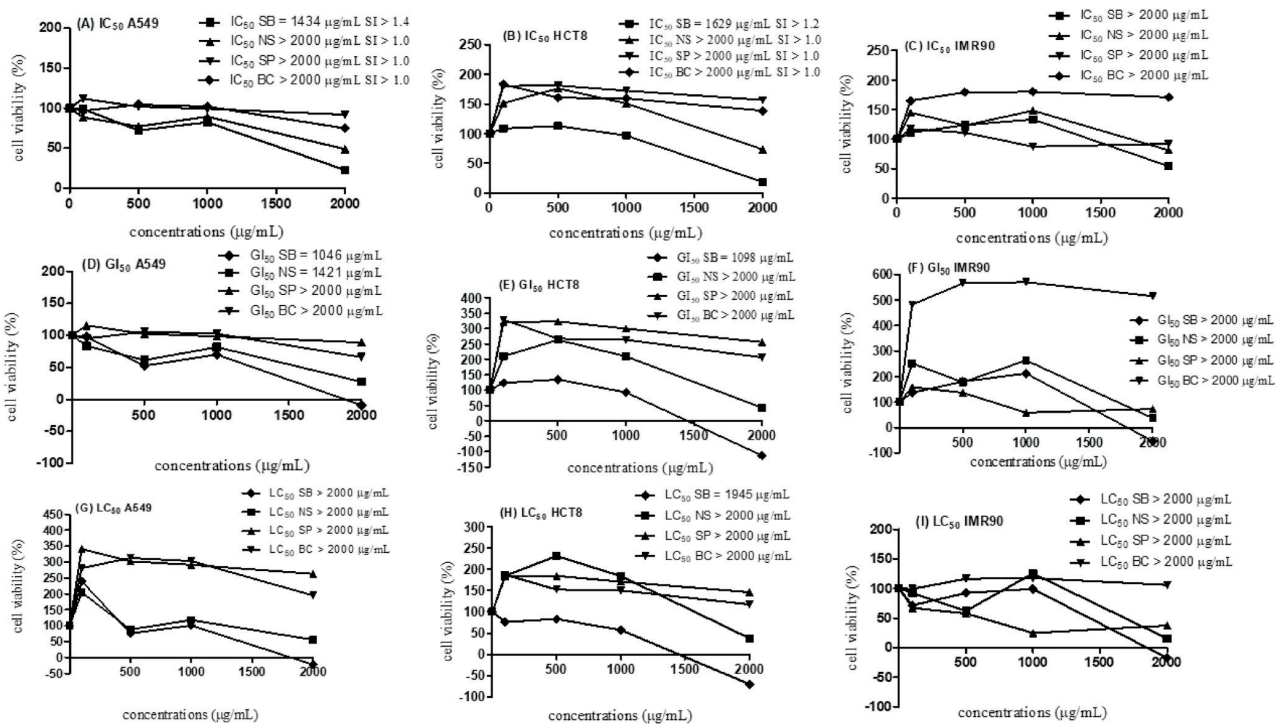

Fig. 5. Cell viability and representative evaluation of the concentration-dependent impact after 48 h exposure to the anthocyanins extracts in A549, HCT8, and IMR90 line cells. (A, B, C): IC_{50}, (D, E, F): GI_{50}, (G, H, I): LC_{50} in A549, HCT8, and IMR90 line cells. Note: SI = selectivity index based on the IC_{50} of the normal cell line (IMR90).

(TNF-alpha, JNK, VCAM-1, ICAM-1, and NF-κβ) in human aortic endothelial cells activated with TNF-alpha.

3.2.5. *Antiviral activity*

Various concentrations of the extracts from NS, SP, SB, and BC were tested for their ability to reduce infectivity in A549 cells (Fig. 4). NS and SP extracts were able to completely rescue the cells against infection at around 10 μg/mL. Those concentrations were also non-cytotoxic, which was evaluated by the CPE assay without virus in the solution. BC showed strong anti-viral efficacy with even lower concentrations and without cytotoxicity in A549 cells in a similar assay. The extracts from SB also showed antiviral potential. In the correlation analyses, both TPC ($r = -0.607$, $p = 0.036$) and flavonoids ($r = -0.538$, $p = 0.071$) seemed to be associated with the antiviral activity. Our results are in-line with those reported by Ikuta et al. (2012) who concluded that BC extract was able to decrease the adsoption and replication of respiratory syncytial virus, influenza virus A and B, adenovirus (AdV), herpes simplex virus type 1, and Haemophilus influenzae type B. Similarly, Torelli et al. (2015) found that an extract from sea buckthorn bud had anti-influenza (H1N1) virus potential *in vitro*.

Antiviral activity of the extracts was tested against the non-enveloped enterovirus coxsackievirus A9. Enteroviruses, and non-enveloped viruses in general, are known to be very stable and to resist alcohol-based solutions much better than viruses with a lipid envelope (Linnakoski et al., 2018). Enteroviruses are very prevalent viruses and cause vast amounts of acute infections around the world. They also contribute to chronic diseases such as atherosclerosis, and asthma, thus causing a substantial economic burden (Hyöty, 2016). Presently, there is a demand for anti-viral molecules that would be non-toxic, certainly less harmful than synthetic and irritable chemicals, which would efficiently and irreversibly compromise viral infectivity. For any viruses, the anti-viral action may be based on either directly acting on the virion, or attacking the cellular proteins needed for virus infection, or on the newly synthesized viral proteins in the cells (Laajala et al., 2020).

3.2.6. *Cell viability and proliferation: preliminary toxicological safety assessment*

All freeze-dried extracts did not show any apparent cytotoxicity in THP-1 cells as the cell viability was higher than 93% at concentrations ranging from 7 to 1667 μg/mL (data not shown). As freeze-dried extracts contain a high content of different chemical compounds, it is important to assess whether their interaction with human cell lines is deleterious. Our results clearly show that freeze-dried aqueous extracts from the four side-streams are not cytotoxic in this cell-based model.

Fig. 5 shows the cytotoxicity evaluation of freeze-dried extracts obtained via maceration. Results show that SB showed a slight decrease in cell viability in cancer cell lines (A549, IC_{50} = 1434 μg/mL; HCT8, IC_{50} = 1629 μg/mL), which suggests that this extract presented better anti-proliferative activity than the other extracts. Moreover, SB was the only extract that presented lethal concentration (LC_{50} = 1945 μg/mL) towards HCT8 cell line. NS showed a decrease in cell growth of A549 cell line, which suggests that this extract demonstrate antiproliferative activity, although it has not reduced cell viability and has not been lethal. On the other hand, the SP and BC extracts exhibited high IC_{50} and IG_{50} values for all the cell lines (>2000 μg/mL), indicating relative safety. Among the cell lines, IMR90 cells have been shown to be more resistant to all extracts, which exhibited high IC_{50} and GI_{50} values (>2000 μg/mL), meaning no cytotoxicity and no cell inhibition. Herein, the malignant cells seemed to be more susceptible to the extracts than the normal cell line indicating a possible therapeutic window as an anti-cancer agent. The SI values (IC_{50} cancer cell/IC_{50} normal cell) ranged from 1.2 to 1.4, meaning that there was no selectivity of the extracts in relation cell lines, once high selectivity is for values higher than 3.

The effects of freeze-dried extracts obtained via maceration were analyzed in relation to the ROS generation in cancer cell lines (A549, HCT8) and results are presented in Fig. 6. The levels of ROS induced by H_2O_2 were higher than the control and similar to the treatment group. in A549 cells, all the extracts exhibited a significant decrease in ROS generation to the same levels of spontaneous generation (negative

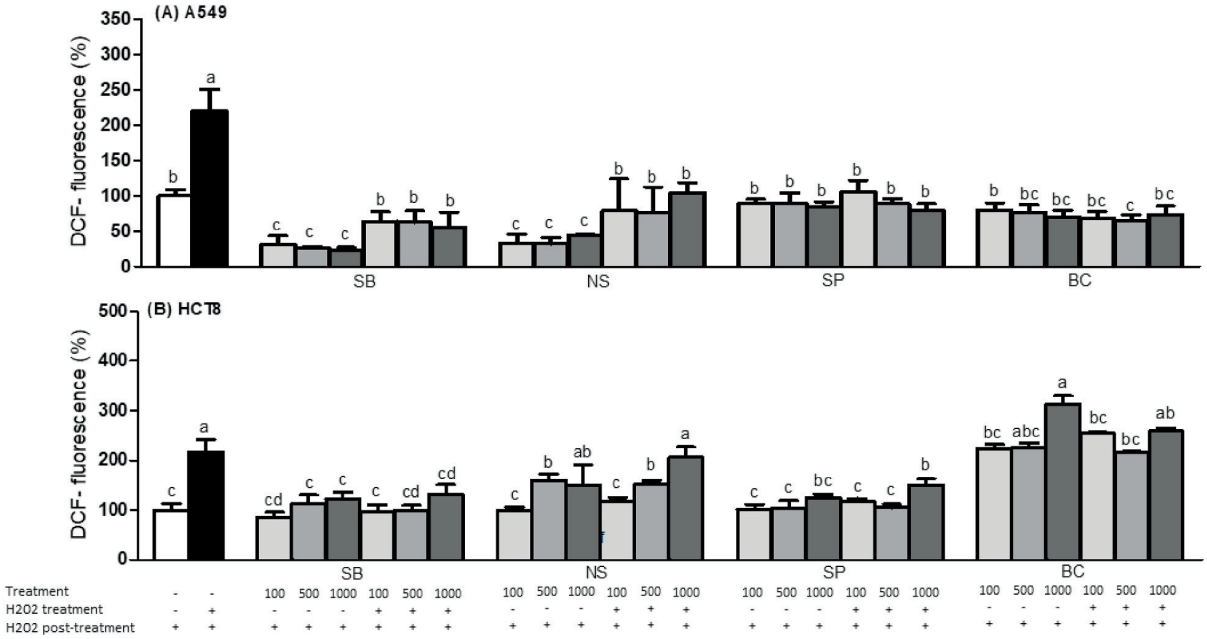

Fig. 6. Results of intracellular ROS measurement in A549, HCT8 cells by spectrofluorimetry. Treatment anthocyanins extracts at 100–1000 μg/mL. Quantitative data are the mean ± standard deviation (n = 4). Different letters represent statistically significant differences ($p < 0.05$).

control), suggesting a protective effect against H_2O_2. Similarly, in HCT8 cells, SB and SP were able to significantly reduce the ROS generation, implying higher cellular antioxidant capacity towards H_2O_2-induced oxidation. According to Kim et al. (2011) and Upadhyay et al. (2010), this antioxidant activity may be associated to isorhamnetin glucosides present in SB aqueous extract. On the contrary, higher BC and NS extract concentrations triggered intracellular ROS generation, which is somehow in-line with the data obtained using THP-1 macrophages. Similar results were found by Olejnik et al. (2018), who showed that the gastrointestinal digested BC extract at 100 μg/mL induced a substantial increase in ROS generation in colon cancer cells.

4. Conclusions

Four different side streams from the food and forestry industries were studied for their cytotoxicity in different human cell lines and their bioactivities. The recovery of bioactive compounds using maceration proved to be the most promising technology to produce extracts with biological activities. Freeze-dried extracts represent a rich source of carbohydrates and polyphenols, expressed toxicity to a cancer cell (HCT8), inhibition effects on digestive enzymes, and reactive oxygen species (ROS) generation during the THP-1 cell respiratory burst. Our results clearly show the aqueous extracts from BC press cake, SB leaves, and bark from NS and SP are suitable candidates for further *in vivo* tests to assess their toxicological profile and bioactivities.

CRediT authorship contribution statement

Nora Pap: Conceptualization, Investigation, Writing – original draft, Funding acquisition, Formal analysis. **Dhanik Reshamwala:** Formal analysis, Writing – original draft. **Risto Korpinen:** Formal analysis, Writing – original draft. **Petri Kilpeläinen:** Formal analysis, Writing – original draft. **Marina Fidelis:** Formal analysis. **Marianna M. Furtado:** Formal analysis, Writing – original draft. **Anderson S. Sant'Ana:** Formal analysis, Writing – original draft. **Mingchun Wen:** Formal analysis, Writing – original draft. **Liang Zhang:** Formal analysis, Writing – original draft. **Jarkko Hellström:** Formal analysis, Writing – original draft. **Pertti Marnilla:** Formal analysis, Writing – original draft. **Pirjo Mattila:** Formal analysis, Writing – original draft. **Tytti Sarjala:** Formal analysis, Writing – original draft. **Baoru Yang:** Writing – review & editing. **Luciana Azevedo:** Formal analysis, Writing – original draft. **Varpu Marjomäki:** Formal analysis, Writing – original draft. **Daniel Granato:** Conceptualization, Methodology, Software, Validation, Investigation, Formal analysis, Resources, Data curation, Writing – original draft, Supervision, Project administration, Funding acquisition.

Declaration of competing interest

The authors declare that they have no known competing financial interests or personal relationships that could have appeared to influence the work reported in this paper.

Acknowledgements

The authors thank Luke for providing funds for this project (Power-Xtract – 41007–00185200). Sant'Ana and Furtado thank the support of Coordenação de Aperfeiçoamento de Pessoal de Nível Superior (Finance Code 001) and Conselho Nacional de Desenvolvimento Científico e Tecnológico (302763/2014-7, and 305804/2017-0).

Appendix A. Supplementary data

Supplementary data to this article can be found online at https://doi.org/10.1016/j.fct.2021.112284.

References

Alqarni, A.M., Dissanayake, T., Nelson, D.J., Parkinson, J.A., Dufton, M.J., Ferro, V.A., Watson, D.G., 2019. Metabolomic profiling of the immune stimulatory effect of eicosenoids on PMA-differentiated THP-1 cells. Vaccines 7 (4), 142.

Bisht, A., Dickens, M., Rutherfurd-Markwick, K., Thota, R., Mutukumira, A.N., Singh, H., 2020. Chlorogenic acid potentiates the anti-inflammatory activity of curcumin in LPS-stimulated THP-1 cells. Nutrients 12, 2706.

Boechat, N., Ferreira, M.D.L.G., Pinheiro, L.C.S., Jesus, A.M.L., Leite, M.M.M., Júnior, C. C.S., Aguiar, A.C.C., De Andrade, I.M., Krettli, A.U., 2014. New compounds hybrids 1H-1,2,3-triazole-quinoline against plasmodium falciparum. Chem. Biol. Drug Des. 84, 325–332.

Ciesarová, Z., Murkovic, M., Cejpek, K., Kreps, F., Tobolková, B., Koplík, R., Belajová, E., Kukurová, K., Daško, Ľ., Panovská, Z., Revenco, D., Burčová, Z., 2020. Why is sea

buckthorn (*Hippophae rhamnoides* L.) so exceptional? A review. Food Res. Int. 133, 109170.
Cleeland, L., Squires, E., 1991. Evaluation of new antimicrobials *in vitro* and experimental animal infections. In: Lorian VMD. Antibiotics in Laboratory Medicine. Baltimore. Williams & Wilkins, pp. 739–788.
Cortez, R.E., de Mejia, E.G., 2019. Blackcurrants (*Ribes nigrum*): a review on chemistry, processing, and health benefits. J. Food Sci. 84, 2387–2401.
Escher, G.B., Santos, J.S., Rosso, N.D., Marques, M.B., Azevedo, L., do Carmo, M.A.V., Daguer, H., Molognoni, L., Prado-Silva, L. do, Sant'Ana, A.S., da Silva, M.C., Granato, D., 2018. Chemical study, antioxidant, anti-hypertensive, and cytotoxic/cytoprotective activities of Centaurea cyanus L. petals aqueous extract. Food Chem. Toxicol. 118, 439–453.
Fidelis, M., Santos, J.S., Escher, G.B., do Carmo, M.A.V., Azevedo, L., da Silva, M.C., Putnik, P., Granato, D., 2018. In vitro antioxidant and antihypertensive compounds from camu-camu (*Myrciaria dubia* McVaugh, Myrtaceae) seed coat: a multivariate structure-activity study. Food Chem. Toxicol. 120, 479–490.
Granato, D., Calado, V.M. de A., Jarvis, B., 2014. Observations on the use of statistical methods in food science and technology. Food Res. Int. 55, 137–149.
Granato, D., et al., 2018. Antioxidant activity, total phenolics and flavonoids contents: should we ban *in vitro* screening methods? Food Chem. 184, 471–475.
Gu, L., Kelm, M.A., Hammerstone, J.F., Beeche, G., Holden, J., Haytowitz, D., Prior, R.L., 2003. Screening of foods containing proanthocyanidins and their structural characterization using LC-MS/MS and thiolytic degradation, 2003 J. Agric. Food Chem. 51, 7513–7521.
Hellström, J.K., Törrönen, A.K., Mattila, P.H., 2009. Proanthocyanidins in common food products of plant origin, 2009 J. Agric. Food Chem. 57, 7899–7906.
Hellström, J., Mattila, P., Karjalainen, R., 2013. Stability of anthocyanins in berry juices stored at different temperatures. J. Food Compos. Anal. 31, 12–19.
Horszwald, A., Andlauer, W., 2011. Characterisation of bioactive compounds in berry juices by traditional photometric and modern microplate methods. J. Berry Res. 1, 189–199.
Hyöty, H., 2016. Viruses in type 1 diabetes. Pediatr. Diabetes 17, 56–64.
Iizuka, Y., Ozeki, A., Tani, T., Tsuda, T., 2018. Blackcurrant extract ameliorates hyperglycemia in type 2 diabetic mice in association with increased basal secretion of Glucagon-Like Peptide-1 and activation of AMP-activated protein kinase. J. Nutr. Sci. Vitaminol. 64 (4), 258–264.
Ikuta, K., Hashimoto, K., Kaneko, H., Mori, S., Ohashi, K., Suzutani, T., 2012 Dec. Anti-viral and anti-bacterial activities of an extract of blackcurrants (*Ribes nigrum* L.). Microbiol. Immunol. 56 (12), 805–809.
Johnson, M.H., Lucius, A., Meyer, T., Gonzalez de Mejia, E., 2011. Cultivar evaluation and effect of fermentation on antioxidant capacity and in vitro inhibition of α-amylase and α-glucosidase by highbush blueberry (*Vaccinium corombosum*). J. Agric. Food Chem. 59, 8923–8930.
Kim, J.-S., Kwon, Y.-S., Sa, Y.-J., Kim, M.-J., 2011. Isolation and identification of sea buckthorn (*Hippophae rhamnoides*) phenolics with antioxidant activity and α-glucosidase inhibitory effect. J. Agric. Food Chem. 59, 138–144.
Kitrytė, V., Povilaitis, D., Kraujalienė, V., Šulniūtė, V., Pukalskas, A., Venskutonis, P.R., 2017. Fractionation of sea buckthorn pomace and seeds into valuable components by using high pressure and enzyme-assisted extraction methods. Lebensm. Wiss. Technol. 85, 534–538.
Laajala, M., Reshamwala, D., Marjomäki, V., 2020. Therapeutic targets for enterovirus infections. Expert Opin. Ther. Targets 24, 745–757.
Laavola, M., Nieminen, R., Leppänen, T., Eckerman, C., Holmbom, B., Moilanen, E., 2015. Pinosylvin and monomethylpinosylvin, constituents of an extract from the knot of Pinus sylvestris, reduce inflammatory gene expression and inflammatory responses *in vivo*. J. Agric. Food Chem. 63 (13), 3445–3453.
Laavola, M., Leppänen, T., Eräsalo, H., Hämäläinen, M., Nieminen, R., Moilanen, E., 2017. Anti-inflammatory effects of nortrachelogenin in murine J774 macrophages and in carrageenan-induced paw edema model in the mouse. Planta Med. 83 (6), 519–526.
Lee, Y., Lee, J.-Y., 2019. Blackcurrant (*Ribes nigrum*) extract exerts an anti-inflammatory action by modulating macrophage phenotypes. Nutrients 11, 975.
Lee, J., Durst, R.W., Wrolstad, R.E., Collaborators, Eisele, T., Giusti, M.M., Hach, J., Hofsommer, H., Koswig, S., Krueger, D.A., Kupina, S., Martin, S.K., Martinsen, B.K., Miller, T.C., Paquette, F., Ryabkova, A., Skrede, G., Trenn, U., Wightman, J.D., 2005. Determination of total monomeric anthocyanin pigment content of fruit juices, beverages, natural colorants, and wines by the pH differential method: collaborative study. J. AOAC Int. 88, 1269–1278.
Linnakoski, R., Reshamwala, D., Veteli, P., Cortina-Escribano, M., Vanhanen, H., Marjomäki, V., 2018. Antiviral agents from fungi: diversity, mechanisms and potential applications. Front. Microbiol. 9, 2325.
Lyall, K.A., Hurst, S.M., Cooney, J., Jensen, D., Lo, K., Hurst, R.D., Stevenson, L.M., 2009. Short-term blackcurrant extract consumption modulates exercise-induced oxidative stress and lipopolysaccharide-stimulated inflammatory responses. Am. J. Physiol. Regul. Integr. Comp. Physiol. 297, R70–R81.
Ma, X., Moilanen, J., Laaksonen, O., Yang, W., Tenhu, E., Yang, B., 2019. Phenolic compounds and antioxidant activities of tea-type infusions processed from sea buckthorn (*Hippophaë rhamnoides*) leaves. Food Chem. 272, 1–11.
Mäkinen, S., Hellström, J., Mäki, M., Korpinen, R., Mattila, P.H., 2020. Bilberry and sea buckthorn leaves and their subcritical water extracts prevent lipid oxidation in meat products. Foods 9 (3), 265.
Margraf, T., Karnopp, A.R., Rosso, N.D., Granato, D., 2015. Comparison between Folin-Ciocalteu and Prussian Blue assays to estimate the total phenolic content of juices and teas using 96-well microplates. J. Food Sci. 80, C2397–C2403.
Martikainen, M., Salorinne, K., Lahtinen, T., Malola, S., Permi, P., Häkkinen, H., Marjomäki, V., 2015. Hydrophobic pocket targeting probe for enteroviruses. Nanoscale 7 (41), 17457–17467.
Matthews, S., Mila, I., Scalbert, A., Donnelly, D.M.X., 1997. Extractable and non-extractable proanthocyanidins in barks. Phytochemistry 45, 405–410.
Mattila, P., Kumpulainen, J., 2002. Determination of free and total phenolic acids in plant-derived foods by HPLC with diode-array detection. J. Agric. Food Chem. 50, 3660–3667.
Mattila, P.H., Hellström, J., Karhu, S., Pihlava, J.-M., Veteläinen, M., 2016. High variability in flavonoid contents and composition between different North-European currant (Ribes spp.) varieties. Food Chem. 204, 14–20.
Mattila, P.H., Pihlava, J.-M., Hellström, J., Nurmi, M., Eurola, M., Mäkinen, S., Jalava, T., Pihlanto, A., 2018. Contents of phytochemicals and antinutritional factors in commercial protein-rich plant products. Food Qual. Saf. 2 (4), 213–219. https://doi.org/10.1093/fqsafe/fyy021.
Metsämuuronen, S., Sirén, H., 2019. Bioactive phenolic compounds, metabolism and properties: a review on valuable chemical compounds in Scots pine and Norway spruce. Phytochem. Rev. 18, 623–664.
Michalska, A., Wojdyło, A., Lech, K., Łysiak, G.P., Figiel, A., 2017. Effect of different drying techniques on physical properties, total polyphenols and antioxidant capacity of blackcurrant pomace powders. Lebensm. Wiss. Technol. 78, 114–121.
Mukhopadhyay, D., Dasgupta, P., Roy, D.S., Palchoudhuri, S., Chatterjee, I., Ali, S., Dastidar, S.G., 2016. A sensitive in vitro spectrophotometric hydrogen peroxide scavenging assay using 1,10 phenanthroline. Free Radic. Antioxidants 6 (1), 124–132.
Olejnik, A., et al., 2018. ROS-modulating anticancer effects of gastrointestinally digested *Ribes nigrum* L. fruit extract in human colon cancer cells. J. Funct. Foods 42, 224–236.
Ovaskainen, M.-L., Törrönen, R., Koponen, J.M., Sinkko, H., Hellström, J., Reinivuo, H., Mattila, P., 2008. Dietary intake and major food sources of polyphenols in Finnish adults. J. Nutr. 138, 562–566.
Parkar, S.G., Redgate, E.L., McGhie, T.K., Hurst, R.D., 2014. In vitro studies of modulation of pathogenic and probiotic bacterial proliferation and adhesion to intestinal cells by blackcurrant juices. J. Funct. Foods 8, 35–44.
Prior, R.L., Hoang, H., Gu, L., Wu, X., Bacchiocca, M., Howard, L., Hampsch-Woodill, M., Huang, D., Ou, B., Jacob, R., 2003. Assays for hydrophilic and lipophilic antioxidant capacity (oxygen radical absorbance capacity ($ORAC_{FL}$)) of plasma and other biological and food samples. J. Agric. Food Chem. 51, 3273–3279.
Raitanen, J.-E., Jarvenpaa, E., Korpinen, R., Makinen, S., Hellstrom, J., Kilpelainen, P., Liimatainen, J., Ora, A., Tupasela, T., Jyske, T., 2020. Tannins of conifer bark as nordic piquancy-sustainable preservative and aroma? Molecules 25, 567.
Ruokolainen, V., Domanska, A., Laajala, M., Pelliccia, M., Butcher, S.J., Marjomäki, V., 2019. Extracellular albumin and endosomal ions prime enterovirus particles for uncoating that can Be prevented by fatty acid saturation. J. Virol. 93.
Santos, J.S., Alvarenga Brizola, V.R., Granato, D., 2017. High-throughput assay comparison and standardization for metal chelating capacity screening: a proposal and application. Food Chem. 214, 515–522.
Schmidtke, M., Schnittler, U., Jahn, B., Dahse, H.M., Stelzner, A., 2001. A rapid assay for evaluation of antiviral activity against coxsackie virus B3, influenza virus A, and herpes simplex virus type 1. J. Virol Methods 95, 133–143.
Sharma, M., Siddique, M.W., Shamim, A.M., Gyanesh, S., Pillai, K.K., 2011. Evaluation of Antidiabetic and antioxidant effects of sea buckthorn (*Hippophae rhamnoides* L.) in streptozotocin-nicotinamide induced diabetic rats. Open Conf. Proc. J. 2, 53–58.
Siddiqi, R., Naz, S., Ahmad, S., Sayeed, S.A., 2011. Antimicrobial activity of the polyphenolic fractions derived from *Grewia asiatica, Eugenia jambolana* and *Carissa carandas*. Int. J. Food Sci. Technol. 46, 250–256.
Spilioti, E., Holmbom, B., Papavassiliou, A.G., Moutsatsou, P., 2014. Lignans 7-hydroxymatairesinol and 7-hydroxymatairesinol 2 exhibit anti-inflammatory activity in human aortic endothelial cells. Mol. Nutr. Food Res. 58 (4), 749–759.
Tian, Y., Liimatainen, J., Alanne, A.-L., Lindstedt, A., Liu, P., Sinkkonen, J., Kallio, H., Yang, B., 2017. Phenolic compounds extracted by acidic aqueous ethanol from berries and leaves of different berry plants. Food Chem. 220, 266–281.
Tompa, G., Laine, A., Pihlanto, A., Korhonen, H., Rogelj, I., Marnilla, P., 2011. Chemiluminescence of non-differentiated THP-1 promonocytes: developing an assay for screening anti-inflammatory milk proteins and peptides. Luminescence 26, 252–258.
Torelli, A., Gianchecchi, E., Piccirella, S., Manenti, A., Piccini, G., Llorente Pastor, E., Canovi, B., Montomoli, E., 2015. Sea buckthorn bud extract displays activity against cell-cultured Influenza virus. J. Prev. Med. Hyg. 56 (2), E51–E66.
Upadhyay, N.K., Kumar, M.S.Y., Gupta, A., 2010. Antioxidant, cytoprotective and antibacterial effects of Sea buckthorn (*Hippophae rhamnoides* L.) leaves. Food Chem. Toxicol. 48 (12), 3443–3448.
Wojdyło, A., Samoticha, J., Chmielewska, J., 2021. Effect of different pre-treatment maceration techniques on the content of phenolic compounds and color of Dornfelder wines elaborated in cold climate. Food Chem. 339, 127888.
Wu, X., Gu, L., Prior, R.L., McKay, S., 2004. Characterization of anthocyanins and proanthocyanidins in some cultivars of *Ribes, aronia*, and *Sambucus* and their antioxidant capacity. J. Agric. Food Chem. 52, 7846–7856.
Xu, Y.-Q., Gao, Y., Granato, D., 2021. Effects of epigallocatechin gallate, epigallocatechin and epicatechin gallate on the chemical and cell-based antioxidant activity, sensory properties, and cytotoxicity of a catechin-free model beverage. Food Chem. 339, 128060.
Zhishen, J., Mengeheng, T., Jianming, W., 1999. The determination of flavonoid contents in mulberry and their scavenging effects on superoxide radicals. Food Chem. 64, 555–559.

II

FROM THE FOREST TO THE PLATE – HEMICELLULOSES, GALACTOGLUCOMANNAN, GLUCURONOXYLAN, AND PHENOLIC-RICH EXTRACTS FROM UNCONVENTIONAL SOURCES AS FUNCTIONAL FOOD INGREDIENTS

by

Daniel Granato, Dhanik Reshamwala, Risto Korpinen, Luciana Azevedo, Mariana Araujo Vieira do Carmo, Thiago Mendanha Cruz, Mariza Boscacci Marques, Mingchun Wen, Liang Zhang, Varpu Marjomäki & Petri Kilpeläinen 2022

Food Chemistry 381: 132284

Food Chemistry 381 (2022) 132284

Contents lists available at ScienceDirect

Food Chemistry

journal homepage: www.elsevier.com/locate/foodchem

From the forest to the plate – Hemicelluloses, galactoglucomannan, glucuronoxylan, and phenolic-rich extracts from unconventional sources as functional food ingredients

Daniel Granato [a,*], Dhanik Reshamwala [b], Risto Korpinen [c,d], Luciana Azevedo [e], Mariana Araújo Vieira do Carmo [e], Thiago Mendanha Cruz [e], Mariza Boscacci Marques [f], Mingchun Wen [g], Liang Zhang [g], Varpu Marjomäki [b], Petri Kilpeläinen [c,*]

[a] Department of Biological Sciences, Faculty of Science and Engineering, University of Limerick, V94 T9PX Limerick, Ireland
[b] Department of Biological and Environmental Science/Nanoscience Center, University of Jyväskylä, Jyväskylä, Finland
[c] Biorefinery and Bioproducts, Production Systems Unit – Natural Resources Institute Finland (Luke), Tietotie 2, FI-02150 Espoo, Finland
[d] Separation Science, LUT School of Engineering Science, LUT University, Yliopistonkatu 34, 53850 Lappeenranta, Finland
[e] Faculty of Nutrition, Federal University of Alfenas, Rua Gabriel Monteiro da Silva, 714, 37130-000 Alfenas, Brazil
[f] Department of Chemistry, State University of Ponta Grossa, Av. Carlos Cavalcanti, 4748, 84030-900 Ponta Grossa, Brazil
[g] State Key Laboratory of Tea Plant Biology and Utilization, Anhui Agricultural University, 230036 Hefei, China

ARTICLE INFO

Keywords:
Forest byproducts
Reactive oxygen species
Cell-based models
Phenolic composition
Galactoglucomannans
Tannins

ABSTRACT

This study aimed to characterise pressurised hot water (PHW) extracts from nonconventional sources of functional carbohydrates and phenolic compounds in terms of antioxidant capacity, antiviral activity, toxicity, and human erythrocytes' protection antidiabetic potential. PHW extracts of Norway spruce bark (E1 + E2) and Birch sawdust (E3 + E4) contained mostly galactoglucomannan and glucuronoxylan. In contrast, samples E5 to E9 PHW extracted from Norway spruce, and Scots pine bark are rich sources of phenolic compounds. Overall, phenolic-rich extracts presented the highest inhibition of α-amylase and α-glucosidase and protection against stable non-enveloped enteroviruses. Additionally, all extracts protected human erythrocytes from hemolysis. Cell-based experiments using human cell lines (IMR90 and A549) showed extracts' non-toxic *in vitro* profile. Considering the relative toxicological safety of extracts from these unconventional sources, functional carbohydrates and polyphenol-rich extracts can be obtained and further used in food models.

1. Introduction

The pharmaceutical and chemical industries look for new natural materials for high value-added applications, such as drugs and cosmetics (Ragab et al., 2018). Plant cell walls are a potential source of pharmacologically active polysaccharides. Cellulose, hemicellulose, and lignin are considered the three major components of lignocellulosic biomass. More precisely, hemicellulose is the second most abundant polysaccharide class in nature, indicating the attractiveness of the exploitation of lignocellulose material as its inexpensive and plentiful natural resource (Đorđević and Antov, 2018). The new trend for extraction of hemicelluloses, galactomannans, and other potentially functional carbohydrates from renewable biomass with low cost and available industrial byproducts that can be used to produce value-added ingredients is promising (Wu et al., 2019).

Forests are essential sources of renewable materials. Forest industries such as pulp mills and sawmills provide pulp and timber used, e.g., in packages and construction. These huge industries also produce important byproducts of wood bark and sawdust mainly combusted for energy. Cascading use (e.g., biorefinery approach) would be preferable to utilise these resources fully. The cascading approach would first extract valuable compounds from either bark or sawdust, utilise extracted biomass in different applications, and finally combust or gasify the remaining matter to energy (Rasi et al., 2019). In this aspect, pressurised hot water extraction (PHWE), which uses non-toxic water and is considered a green extraction method (Teo et al., 2010), can extract compounds from woody materials. Tannins from spruce and pine bark can be extracted at lower temperatures under 100 °C. Spruce bark PHWE

* Corresponding author.
E-mail addresses: Daniel.granato@ul.ie (D. Granato), petri.kilpelainen@luke.fi (P. Kilpeläinen).

https://doi.org/10.1016/j.foodchem.2022.132284
Received 22 November 2021; Received in revised form 26 January 2022; Accepted 26 January 2022
Available online 31 January 2022

Table 1
Chemical antioxidant activity of Norway spruce galactoglucomannan, birch glucuronoxylan, Norway spruce and Scots pine phenolics-rich extracts.

Extracts	Total phenolic content (mg GAE/100 g)	Reducing capacity (mg GAE/100 g)	Cu^{2+} chelating ability (mg EDTAE/100 g)	FRAP (mg AAE/100 g)	DPPH (mg AAE/100 g)
E1 - Norway spruce galactoglucomannan	20889 ± 99^{d}	792 ± 8^{f}	ND	7446 ± 293 ^{h}	9230 ± 21^{c}
E2 - Norway spruce galactoglucomannan (ethanol precipitation)	2310 ± 105 ^{g}	142 ± 3 ^{g}	ND	742 ± 2^{i}	341 ± 7 ^{h}
E3 - Birch glucuronoxylan	18743 ± 41^{e}	1239 ± 4^{e}	414 ± 1 ^{g}	12590 ± 149^{f}	3377 ± 189 ^{g}
E4 - Birch glucuronoxylan (ethanol precipitation)	2250 ± 15 ^{g}	614 ± 6^{f}	ND	1238 ± 6^{i}	3899 ± 56^{f}
E5 - Norway spruce phenolics (crude extract)	45525 ± 393^{c}	5296 ± 333^{d}	1492 ± 2^{b}	23614 ± 253^{d}	9547 ± 150^{d}
E6 - Norway spruce phenolics (partial purification with XAD7HP)	50723 ± 219^{b}	6422 ± 32^{b}	1386 ± 3^{d}	40097 ± 74^{b}	10803 ± 32^{b}
E7 - Norway spruce phenolics (complete purification with XAD7HP)	45590 ± 230^{c}	5904 ± 33^{c}	1475 ± 13^{c}	33729 ± 218^{c}	10439 ± 99^{b}
E8 - Scots pine phenolics (90 °C/60 min)	22187 ± 218^{d}	1312 ± 5^{e}	1348 ± 3^{e}	16695 ± 588^{e}	5235 ± 78^{e}
E9 - Scots pine phenolics (140 °C/60 min)	13332 ± 134^{f}	1249 ± 3^{e}	1294 ± 2^{f}	9488 ± 374 ^{g}	3279 ± 102 ^{g}
E10 – Industrial tannin QS-SOL	83746 ± 2501^{a}	6749 ± 8^{a}	2316 ± 2^{a}	81642 ± 1015^{a}	38565 ± 518^{a}

Note: AAE = ascorbic acid equivalents, EDTAE = EDTA equivalents, GAE = gallic acid equivalents, ND = not detected. Different letters in the same column represent statistically different results ($p < 0.05$).

extract includes condensed tannins, stilbene glucosides, such as astringin, isorhapontin, and piceid. Pine bark PHWE extracts have – condensed tannins and sugars. Hemicelluloses of wood can be extracted at higher extraction temperatures at 160–180 °C. Increasing temperature promotes hydrolysis of hemicellulose and changes the properties of water as a solvent. PHWE extracts of hardwood birch are mainly composed of glucuronoxylans with lignin-derived phenolics (Kilpeläinen et al., 2014). Softwood spruce PHW extracts have mainly galactoglucomannans (GGM). More importantly, on an industrial scale, hemicellulose extracts can be concentrated and purified with ultrafiltration and ethanol precipitation (Bhattarai et al., 2019) or centrifugation (Valoppi et al., 2019).

When it comes to new products, compounds, and crude extracts from industrial byproducts, toxicological safety should continually be assessed to ascertain compliance with international guidelines (Pitkanen et al., 2018). As hemicellulose and other polysaccharides can be used as a thickening and stabilising agent in foods and cosmetics and as ingredients in bio-based films and coatings, it is evident that the application of hemicellulose in different products can be diverse. For this purpose, however, studies that ascertain the toxicological safety and potential bioactivities of the raw material or its extract should be meticulously tested (Li et al., 2019; Ragab et al., 2018).

For instance, cell-based experiments with different human cells have shown that crude extracts from rice straw and husk, radix (*Astragalus radix*) byproducts, bamboo (*Phyllostachys pubescens*) processing byproducts (stems), and many other sources have no deleterious effects on normal human cells (Huang et al., 2017; Li et al., 2019; Ragab et al., 2018). These practical examples indicate that these bioactive-rich extracts can be further tested to develop new technological applications in the chemical, pharma and, possibly, food sectors.

Toxicological safety is essential when new crude extracts and ingredients are developed and their bioactivity. The bioactivity study can be done using different *in vitro* chemical-based and cell-based assays. For instance, Wu et al. (2019) assessed the effects of hemicellulose and lignin fractions of mushroom (*Lentinus edodes*) on their antioxidant activity using the 2,2-diphenyl-1-picrylhydrazyl (DPPH) and 2,2′-azino-bis (3-ethylbenzothiazoline-6-sulfonic acid (ABTS) assays and the scavenging of hydroxyl radical assay. Results showed that the fractions (from 2 to 4%) exerted free-radical scavenging activity in a dose-dependent manner, and the activity was correlated to the hemicellulose content. Similarly, Li et al. (2019) analysed the antitumor and immunomodulatory activities of hemicellulose fractions extracted from radix (*Astragalus radix*) byproducts using a mice model of lung cancer. Fractions could inhibit tumour progression in a dose-dependent manner (50 to 200 mg/kg). Moreover, fractions increased the levels of cytokines IL-2, IL-6, and TNF-α in mice serum together with $CD4^{+}$ T cells, thus indicating an immunomodulatory stimulation in cancer-bearing mice. Pap et al. (2021) assessed the chemical and toxicological profile of macerated spruce and pine bark extract. Especially Norway spruce bark extracts showed antioxidative capacity (oxygen-radical antioxidant capacity, cupric-ion antioxidant capacity, and free radical scavenging activity in relation to DPPH) and antiviral activities against Coxsackievirus A9 (CVA9). Assessing antiviral activity has become very important due to yearly viral infections but more so due to the present pandemic caused by SARS-CoV-2.

Coxsackievirus A9 (CVA9) belongs to the enteroviruses, which are human pathogens, causing vast amounts of acute and chronic infections worldwide (Hyöty, 2016; Marjomäki et al., 2015). These viruses are difficult to decontaminate due to their compact protein shell around the viral genome. Presently, there are no non-toxic but still effective ways to decontaminate surfaces and hands to lower the virus load from our surroundings. Nature-derived compounds contain several potential bioactive agents for their protection, which may fight microbes safely.

Several molecules bearing antioxidant and anti-cancer activities may also show antiviral capabilities. Phenolic compounds, e.g., resveratrol, have been suggested to exert several of these actions (Abba et al., 2015). Therefore, it is also relevant to assess the antiviral activity and antioxidant, anti-carcinogenic, and anti-inflammatory actions of extracts containing different bioactive compounds, mainly extracts obtained from industrial byproducts, such as sawdust and bark materials.

Taken together, it is evident that any technological application in which phenolic or functional carbohydrate-rich fractions are incorporated into product models (i.e., cosmetics or foods) should be carefully and meticulously analysed to guide the industry to develop new potentially functional ingredients. Thus, detailed chemical composition, impurity content, bioactivities, and toxicological safety profile play an essential role during the development period. Following this trend, the main objectives of this study are to characterise extracts from Norway spruce (*Picea abis*) bark and sawdust, birch (*Betula pendula*) sawdust, and Scots pine (*Pinus sylvestris*) bark, rich in polyphenols, hemicellulose, and galactomannans, in terms of antioxidant, antidiabetic, antiviral and anti-inflammatory potential, and their effects on human cell's growth and proliferation. Using industrial byproducts to recover bioactive fractions/extracts would significantly contribute to the bio circular economy concepts and align with the Sustainable Goals of the United Nations – Goal 12 – Sustainable Consumption and Production.

2. Materials and methods

2.1. Chemical reagents and cell cultures

Gallic, ascorbic and chlorogenic acids, (+)-catechin, Folin-

Ciocalteu's phenol reagent, 2,4,6-tris(2-pyridyl)-S-triazine (TPTZ), pyrocatechol violet, fluorescein, ferric chloride hexahydrate, dimethyl sulfoxide (DMSO), 2,2-diphenyl-1-picrylhydrazyl radical (DPPH) were obtained from Thermo Fischer Scientific (Ward Hill, Massachusetts, USA). Potassium hexacyanoferrate (III) was obtained from Merck (Darmstadt, Hesse, Germany). The other chemical reagents were of analytical grade. A549 – lung adenocarcinoma, HepG2 - hepatocellular carcinoma, HCT8 - human ileocecal colorectal adenocarcinoma, and IMR90 – normal human lung fibroblast cell lines were obtained from the Rio de Janeiro cell bank (Rio de Janeiro, São Paulo, Brazil). Milli-Q ultrapure water was used in the experiments.

2.2. Plant materials and extraction procedures

Ten wood hemicellulose and polyphenols samples were extracted from sawdust or bark with hot water. Samples were extracted from Norway spruce (*Picea abies*), birch (*Betula pendula*), or Scots pine (*Pinus sylvestris*), which were collected from sawmills in the centre and southern Finland. Hot water extractions were conducted on a pilot scale using a 300 L extraction system (Kilpeläinen et al., 2014). Sample amount varied from 70 to 100 kg of fresh bark or sawdust depending on the moisture content and sample density. Details of the extractions, treatments and samples are in Table 1 **- SM.**

Sawdust samples were stored in a freezer at −20 °C before extractions and used as such without milling or other pretreatments. Birch and spruce sawdust samples were extracted in flow-through mode with a continuous flow of hot water through the extraction vessel during the whole 60 min extraction time (Table 1**-SM**). Hemicellulose samples from sawdust were concentrated with ultrafiltration (Bhattarai et al., 2019) and spray dried or purified with ethanol precipitation. Ethanol precipitation was used to remove lignin-derived phenols from hemicellulose. Spruce galactoglucomannan containing samples E1 and E2 mainly consisted of carbohydrates (710–780 mg/g). Birch gluclucurunoxylan samples E3 and E4 contained 580 – 690 mg/g of carbohydrates. The composition of carbohydrates, acetyl groups and extractives of the hemicellulose samples is fully described by Mikkonen et al. (2019). For more information, detailed structural characterisation of the typical hot water extracted glucuronoxylan and galactoglucomannan by nuclear magnetic resonance (NMR) and analytical pyrolysis was carried out elsewhere (Lahtinen et al., 2019).

Spruce and pine bark samples were extracted in batch mode, where the bark was placed inside the reactor and kept for the whole extraction time. In both cases, the extract was collected in a 1000 L container after the extraction. Spruce bark extracts were dried under vacuum in a rotary evaporator (E5), or extract was further purified with XAD7HP adsorbent (E6 and E7) and dried. Details of extraction, treatments, and chemical composition can be found (Varila et al., 2020). Briefly, the extract was eluted through an adsorbent to remove simple sugars. The adsorbent then contained polyphenols that were eluted out with ethanol. Samples E5 – E7 mainly consisted of polyphenols (430–760 mg/g) and carbohydrates (170 – 310 mg/g). Pine bark samples E8 - E9 are from two-stage extraction. The first bark was extracted at 90 °C and then at 140 °C. Samples were concentrated and freeze-dried in the laboratory. As a reference, there was an industrial purified tannin sample Tannino QS-SOL from Silvateam, Italy (Sample E10).

2.3. Total phenolics and chemical antioxidant activity

Freeze-dried extracts (100 mg) were dissolved in water (100 mL) and analysed for total phenolic content and *in vitro* antioxidant activity. The total phenolic content was assayed according to a standardised spectrophotometric Folin-Ciocalteu method, and results were expressed as mg of gallic acid equivalents (GAE) per 100 g (Granato et al., 2015). The DPPH free-radical scavenging activity was assayed using a methanolic DPPH solution at 0.10 mmol/L. Results were expressed as mg of ascorbic acid equivalent per 100 g of extract (mg AAE/100 g). The extracts' ferric reducing antioxidant power (FRAP) was assessed under acidic conditions (pH 3.6), and results were expressed as mg AAE/100 g. The reducing power of extracts was evaluated using the Prussian Blue assay, and results were expressed as mg of gallic acid equivalent per 100 g of extract (mg GAE/100 g). The Cu^{2+} chelating ability was evaluated using pyrocatechol violet as the chromogen agent, and results were expressed as mg of disodium ethylenediaminetetraacetic acid (EDTA) per 100 g of extract (mg EDTA/100 g). All these methods were conducted using the experimental conditions described in our previous works (Fidelis et al., 2020; Santos et al., 2018), and analyses were performed in triplicate.

2.4. Cell viability and proliferation tests and cellular antioxidant activity

Cells were cultured in Dulbecco's modified Eagle's medium F12 Ham (DMEM, Sigma, Germany) with 10% FBS and 1% penicillin/streptomycin, at 37 °C under 5% CO_2. To assess the viability of cells in relation to each extract, A549 (human lung cancer cells), HCT8 (human colorectal cancer cell), HepG2 (human liver cancer cell), and IMR90 (lung normal cell) were seeded into 96 well plates with a density of 1×10^4 cells/well. Twenty-four hours later, cells were treated with the extracts at different concentrations (50, 250, 500, 1000 μg/mL) for 48 h. At the end of the incubation period, the cell viability was evaluated by the MTT (3-(4,5-dimethylthiazol-2-yl)-2,5-diphenyl tetrazolium bromide) assay, as described by Zhang et al. (2019).

For the cellular antioxidant activity assay, the DCFH-DA (2',7'-dichlorofluorescein diacetate) was used to detect oxidative products from the cell lines (Li et al., 2020). Briefly, all cell lines (6×10^4 cells/well) were treated for 1 h with the extracts previously diluted in DCFH-DA solution (25 mmol/L) at different concentrations (100, 500, and 1000 μg/mL). Cells were treated with or without 15 μmol/L H_2O_2 to induce reactive oxygen species (ROS) and assess ROS induction caused by the extracts. For the positive control, cells were treated with 15 μmol/L H_2O_2. The cells were only treated with a culture medium for the negative control which was taken to reference the percentage of protection against H_2O_2. Intracellular ROS generation was measured as described by do Carmo et al. (2019) using a spectrophotometer (excitation, 485 nm; emission, 530 nm).

2.5. Antihemolytic activity

Extracts were tested to protect human erythrocytes against mechanical hemolysis following the procedures adopted elsewhere (Fidelis et al., 2020). Extracts were solubilised in phosphate saline buffer (PBS, 5 mmol/L, pH 7.35, with NaCl 0.85% w/v) until 1, 5, and 10 μg GAE/g was achieved. Then, extracts were tested under harsh hypotonic (0.1% w/v NaCl), hypotonic (0.4% w/v NaCl), and isotonic conditions (0.85% w/v NaCl). Ultrapure water was used as the positive control for total hemolysis and quercetin at 5 μg/mL as a negative control for comparison purposes. Analyses were performed in triplicate, and results were expressed as a percentage of hemolysis. The ethics committee approved the biological protocol (CAAE 94830318.1.0000.0105).

2.6. Inhibition of α-amylase and α-glucosidase

The inhibition of α-amylase and α-glucosidase activities of the freeze-dried extracts was determined using the methods proposed elsewhere (Johnson et al., 2011). Extracts were diluted in ultrapure water and tested at different concentrations (α-amylase: 1, 5, 10, 15, and 20 mg/mL; α-glucosidase: 10, 25, 50, 100, 200 and 500 μg/mL). For the α-amylase assay, acarbose (1 mmol/L) was used as a positive control. The inhibition of the enzyme activity was expressed in percentage, and, when applicable, IC_{50} values (the concentration required to inhibit enzyme activity by 50%) were obtained in triplicate.

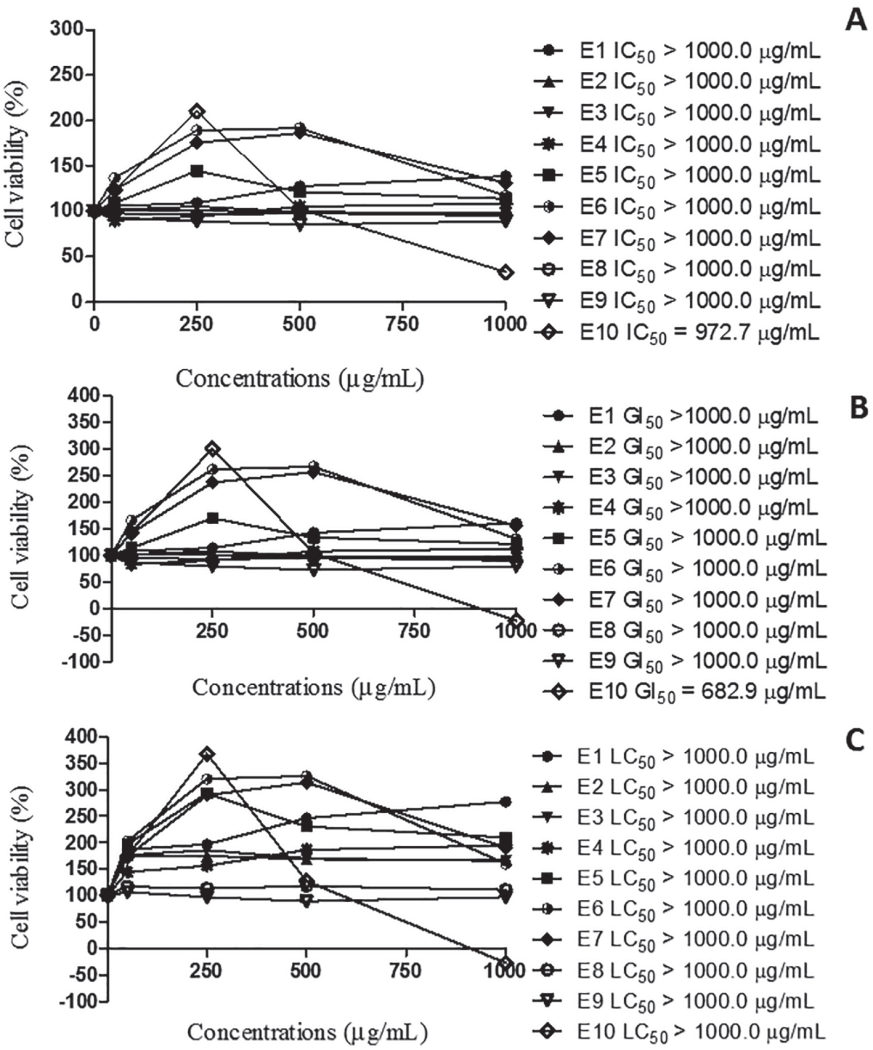

Fig. 1. Cell viability and representative evaluation of the concentration-dependent impact after 48 h exposure of A549 (A, B, C), HepG2 (D, E, F), HCT8 (G, H, I), and IMR90 (J, K, L) cell lines. Values correspond to the IC_{50}, GI_{50}, and LC_{50}. Note: E1 = Norway spruce hemicellulose galactoglucomannan (GGM); E2 = concentrated and ethanol precipitated spruce hemicellulose GGM; E3 = birch hemicellulose xylan; E4 = concentrated and ethanol precipitated xylan; E5 = spruce bark tannin extract; E6 = XAD7HP partially purified spruce bark tannin extract; E7 = XAD7HP completely purified spruce bark tannin extract; E8 = pine bark tannin extract; E9 = pine hemicellulose extract; E10 = Purified industrial tannin. Concentrations are expressed in µg/mL of lyophilized extracts.

2.7. Antiviral effects

Adenocarcinomic human alveolar basal epithelial (A549) cells and Coxsackievirus A9 strain (CVA9; Griggs strain, ATCC) were used in the assays. CVA9 was produced and purified as described before (Ruokolainen et al., 2019). The antiviral activity was assessed using a cytopathic effect (CPE) inhibition assay, modified by Schmidtke et al. (2001). Briefly, A549 cells were plated in 96-well plates at a density of 12,000 cells/well in DMEM supplemented with 10% FBS, 1% GlutaMAX, and 1% penicillin/streptomycin antibiotics. The following day, 2 X 10^8 PFU/mL of CVA9 was pre-incubated with different extracts concentrations for 1 h at 37 °C. The virus-compound mixture was further diluted and added to cells for 24 h incubation at a 5% CO_2 incubator. A similar amount of virus without the extract and mock infection (without the virus and extract) were used as two controls for the experiments. The development of cytopathic effect (CPE) was monitored using light microscopy. For quantification of the CPE, cells were fixed and stained for 10 min with CPE dye (0.03% crystal violet, 2% ethanol, and 36.5% formaldehyde), washed twice with water, and then lysed using a lysis buffer (0.8979 g of sodium citrate and 1 N HCl in 47.5% ethanol) to elute the crystal violet. The absorbance was measured spectrophotometrically at 570 nm using the PerkinElmer VICTOR™ X4 multilabel reader. For the antiviral assay, cytotoxicity was also evaluated using the CPE Inhibition assay, where the compounds (without any virus) were tested for their toxicity on A549 cells for 24 h. Mock infection was used as a control for the assay.

2.8. Statistical analysis

Experimental data are expressed as means ± standard deviation. Multiple comparisons between extractives were performed using one-way analysis of variances (ANOVA) followed by Duncan's multiple range test, considering $p < 0.05$ as significant (Granato, de Araujo Calado, & Jarvis, 2014). Correlation analysis was based on Pearson's correlation coefficient. The software TIBCO Statistica v. 13.3 (TIBCO Software Ltd, Palo Alto, CA, USA) was used in the analyses.

3. Results and discussion

3.1. Total phenolics and antioxidant activity

Table 1 shows that the TPC ranged from 2250 to 83746 mg GAE/100 g, in which samples E5, E6, E7, and E10 presented the highest values. These values corroborate with the data presented by Neiva et al. (2018) and Spinelli et al. (2019). Tannins and stilbenes, phenolic acids, and some flavonoids have already been found from spruce and pine species

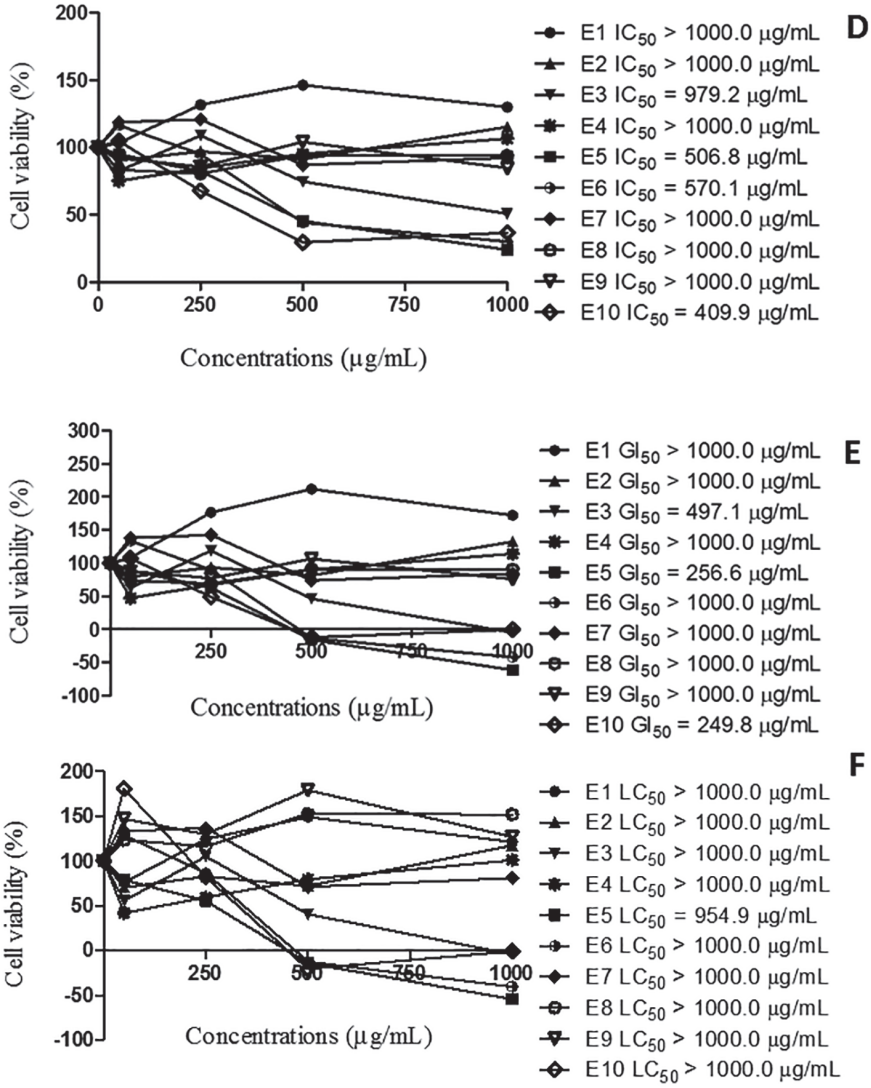

Fig. 1. (*continued*).

(Metsämuuronen and Sirén, 2019; Spinelli et al., 2019; Kim et al., 2020). Regarding the reducing capacity, values ranged from 142 to 6749 mg GAE/100 g, in which phenolic rich-extracts E5, E6, E7, and E10 presented the highest values. FRAP values followed the same trend – phenolic-rich extracts, namely E5 to E8 and E10, gave the highest mean values, while samples E2 and E4, containing carbohydrates, showed the lowest mean values. For the DPPH free radical scavenging activity, the industrial tannin sample, E10, presented the highest antioxidant activity, followed by samples E6/E7, E1, and E5.

Regarding the Cu^{2+} chelating ability, only sample E3 had a chelation effect from the carbohydrate-rich samples. On the contrary, samples E5-E10 had a clear and pronounced copper chelating effect. From all samples, E10 (purified industrial tannin) presented the highest antioxidant activity using all methodologies, while sample E2 (concentrated and ethanol precipitated spruce hemicellulose GGM) had the opposite effect. Correlation analysis showed that the TPC correlated significantly with DPPH ($r = 0.888$; $p = 0.001$), FRAP ($r = 0.966$; $p < 0.001$), Cu^{2+} chelating ability ($r = 0.846$; $p = 0.002$), and slightly correlated with reducing power ($r = 0.626$; $p = 0.053$), which is in-line with previous studies that aimed to correlate the TPC and *in vitro* antioxidant activity assays (Granato et al., 2015; Santos et al., 2018; Fidelis et al., 2020).

Studies reported that aqueous Norway spruce bark extracts (without further purification) obtained with maceration or ultrasound-assisted extraction (UAE) presented a lower TPC ($TPC_{maceration} = 113.5$ mg GAE/g and $TPC_{UAE} = 84.3$ mg GAE/g) than the values observed for samples E5-E7, implying that the purification procedures using resins/adsorbents are effective in eliminating compounds that do not react with Folin-Ciocalteu. Authors also observed that the aqueous spruce extract (0.5 to 10 mg/mL) presented free-radical scavenging activity towards DPPH (maceration = 42.4 to 84.4% inhibition; UAE = 51.5 to 83.4% inhibition). Similarly, Ferreira-Santos et al. (2020) extracted pine (*Pinus pinaster*) bark with ethanolic solutions ranging from 30 to 90% (v/v) (maceration method). They found TPC ranging from 450 to 700 mg GAE/g, FRAP values ranging from 100 to 140 mmol Fe^{2+}/g, and DPPH values ranging from $IC_{50} = 49$ to 100 µg/mL.

Korean red pine (*Pinus densiflora* Sieb. et Zucc.) bark extracted with water showed to be a source of protocatechuic acid, procyanidin B1, catechin, caffeic acid, vanillin, and taxifolin, totalling 44 mg/g of freeze-dried extract (Kim et al., 2020). This phenolic-rich extract showed antihypertensive and antioxidant in Wistar-Kyoto rats.

3.2. Cell viability tests and cellular antioxidant activity

Different concentrations of the extracts (from 50 to 1000 µg/mL) were used to investigate the relative potential of cytotoxicity and growth inhibition against cancer (A549, HCT8, and HepG2) and normal

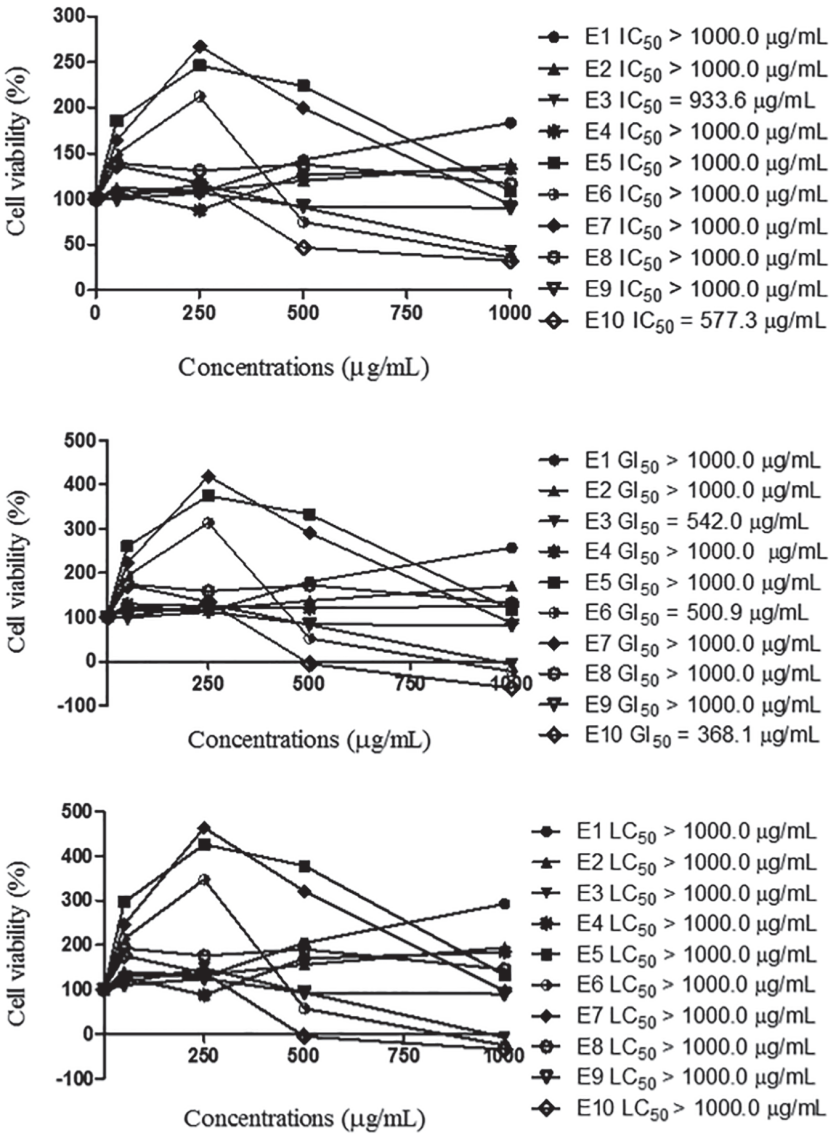

Fig. 1. (*continued*).

(IMR90) cell lines (Fig. 1). In general, the extracts presented non-toxic *in vitro* profiles. For A549 cells, only E10 (pure tannin extract) caused growth inhibition, with a GI_{50} value of 682.9 µg/mL. In contrast, the HepG2 cell line seemed to be more sensitive to the extract effects since E3, E5, E6, and E10 revealed antiproliferative effects (GI_{50} values from 249.8 to 497.1 µg/mL). In comparison, E5 exhibited cytotoxic activity with a lethal concentration (LC_{50}) of 954.9 µg/mL. The GI_{50} values for HCT8 varied between 368.1 and 542 µg/mL for E3, E6, and E10. Considering the normal cell (IMR90), only E9 showed an antiproliferative effect in lower concentrations (GI_{50} = 153 µg/mL), although this sample presented no cytotoxic activity (LC_{50} > 1000 µg/mL). *Lunasia amara* wood extracts, which contained alkaloids and lunacrine in their main chemical composition, showed cytotoxicity (IC_{50} from 71.1 to 412.4 µg/mL) against T47D (human breast cancer cell) and HeLa (cervix adenocarcinoma) cells. Thus, it is possible to infer that the effects of different extracts from woods are highly associated with their chemical composition.

Overall, considering the three cancer cell lines used in the present study, E10 displayed a higher potential in interfering with cell viability, followed by E3. Our results can be of technological importance, as they can be the basis for developing food and cosmetic models.

In a previous work conducted by Coșarcă et al. (2018), Spruce bark extract and beech bark (TPC = 40.2 mg GAE/g) did not show cytotoxicity of A375 (human melanoma), A549 (lung carcinoma), and normal human keratinocytes (HaCaT), implying the extracts show no cytotoxicity at a maximum concentration of 2.5 mg/mL. Similarly, *Pinus pinaster* bark extracts (water and ethanol mixtures) at concentrations up to 1000 µg/mL stimulated the growth of murine fibroblast cells (L929) and embryonic kidney cells (HEK293T) – and inhibited the growth of A549 cancerous cells (Ferreira-Santos et al., 2020).

Concerning the intracellular antioxidant activity data shown in Fig. 2, the extracts presented different results concerning cell viability when distinct cell lines were analysed. Briefly, for HCT8 cells, E1, E3, E5-E10 exhibited pro-oxidant effects, while E2 and E4 protected the cells against H_2O_2 action at 100 µg/mL. For A549 cells, E1-E3, E6, E7, and E10 increased the ROS generation when associated with H_2O_2. In contrast, E8 and E9 exerted antioxidant effects by decreasing ROS generation. Herein, in HepG2 cells, E3 and E4 decreased the ROS levels induced by H_2O_2. Interestingly, the same structural features responsible for the antioxidant activity of phenolic compounds are also related to their pro-oxidant properties, showing a selective behaviour (Fidelis et al., 2020; de Mejia et al., 2010). Moreover, our findings displayed that

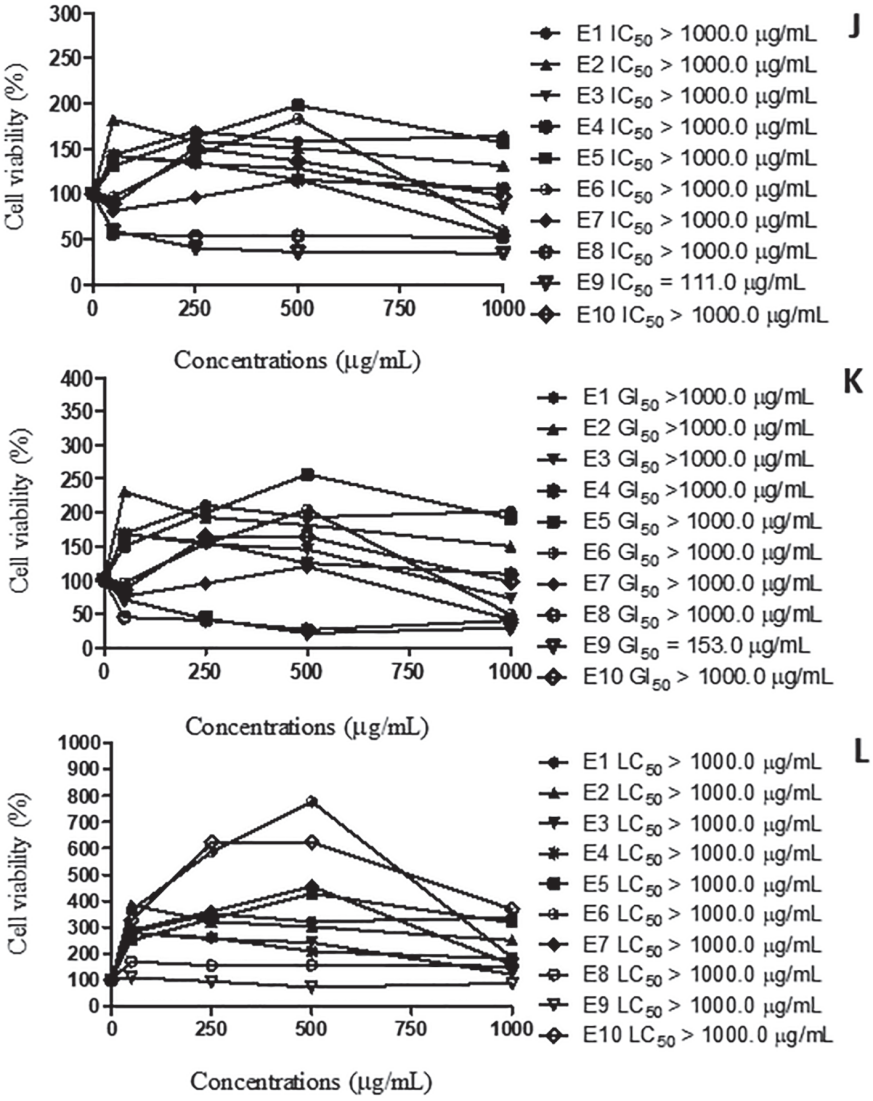

Fig. 1. (*continued*).

the same extract exerted different behaviour acting as an antioxidant or pro-oxidant depending on the cell line. This behaviour could be attributed to the variation in the specific levels of oxygen species that each cell line deals with to maintain its homeostasis, besides peculiarities such as origin, mutations and genetic variability, and microenvironment (Carvalho et al., 2019). This ROS variation strongly impacts cellular metabolism by regulating signalling, proliferation, and differentiation (Harris and DeNicola, 2020). Correlation analysis was performed and we verified that the GI_{50} values of HCT8 and A549 were significantly correlated with the antioxidant activity measured by the DPPH ($r = -0.644$; $p = 0.045$ and $r = -0.944$; $p < 0.001$, respectively), FRAP ($r = -0.721$; $p = 0.019$ and $r = -0.842$; $p = 0.002$, respectively), and TPC ($r = -0.640$; $p = 0.046$ and $r = -0.731$; $p = 0.016$, respectively). No significant correlation ($p > 0.05$) was found between TPC, antioxidant activity, and the GI_{50} values of IMR90 and HepG2 cell lines (data not shown).

Indeed, we remarked that for normal IMR90, extracts did not induce ROS generation, and they were able to reestablish the ROS levels to the same magnitude as that of the negative control. Normal cells adaptations may drive these findings and different results among cell lines in overcoming the damaging effects of ROS through the balanced generation of these species, sufficient antioxidant activity, and cellular repair, which result in low concentrations of ROS, toward to limited cell survival and proliferation (do Carmo et al., 2018).

3.3. Antihemolytic activity

In the isotonic condition ([NaCl] = 0.8% w/v), none of the samples presented hemolytic property (Fig. 3**A**) since these compounds (5 µg GAE/mL) did not cause a significant increase in the hemolysis rate. Contrariwise, the samples significantly ($p \leq 0.05$) decreased the hemolysis rate, presenting efficiency similar to that achieved with quercetin 5 µg/mL, excepting the E3 and E9 samples. E1, E4, and E9 reached the highest protective effect, at this osmotic condition and among the tested concentrations, at 1 µg GAE/Ml (Fig. 3**B**). The maximum erythrocyte protection of the other samples was achieved at 5 µg GAE/mL (E2, E5, E7 and E10) or 10 µg GAE/mL (E3, E6, and E8), thus showing a dose-dependent behaviour.

In the hypotonic condition ([NaCl] = 0.4% w/v), the erythrocytes were osmotically fragilised and, compared to the positive control (PBS), all samples (5 µg GAE/mL) reduced the hemolysis rate significantly ($p \leq 0.05$) (Fig. 3**C**).

Although carbohydrates have already been demonstrated (Escher et al., 2019), anti-hemolytic activity is more commonly attributed to phenolic compounds (Olchowik et al., 2012). In this work, tannin-rich

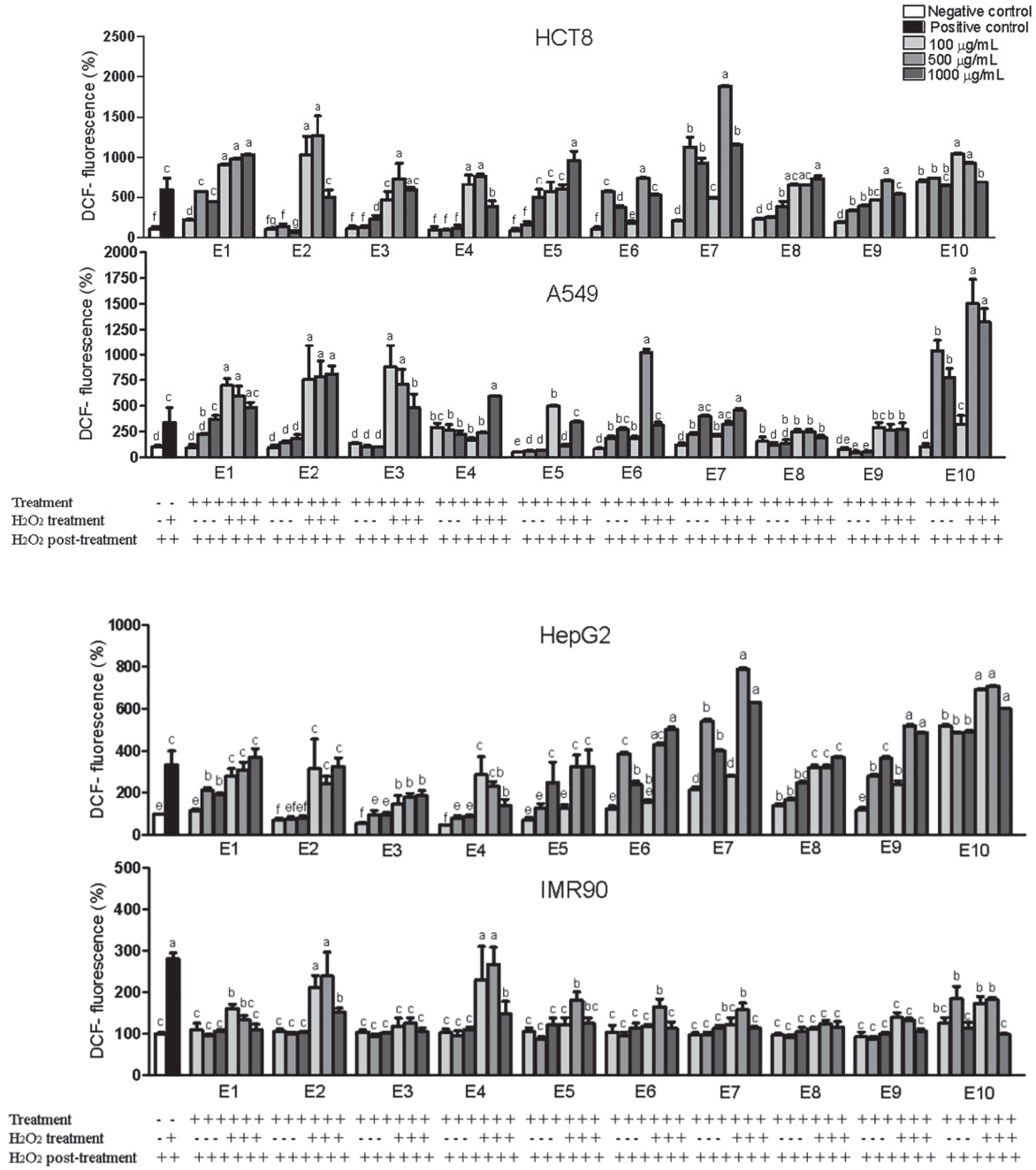

Fig. 2. Results of intracellular ROS measurement in HCT8, A549, HepG2, and IMR90 cell lines. Treatments tested at 10 – 100 μg/mL: E1 = Norway spruce hemicellulose galactoglucomannan (GGM); E2 = concentrated and ethanol precipitated spruce hemicellulose GGM; E3 = birch hemicellulose xylan; E4 = concentrated and ethanol precipitated xylan; E5 = spruce bark tannin extract; E6 = XAD7HP partially purified spruce bark tannin extract; E7 = XAD7HP completely purified spruce bark tannin extract; E8 = pine bark tannin extract; E9 = pine hemicellulose extract; E10 = Purified industrial tannin. Quantitative data are expressed as the mean ± standard deviation and different letters represent statistically different results ($p < 0.05$).

extracts displayed anti-hemolytic efficiency similar to the hemicellulose-rich extracts. This similarity occurs because, although the tannins are phenolic compounds, their rigid structure makes it difficult to penetrate the cell membrane and offer protection (Weber-Lotfi et al., 2002). The antihemolytic effect was already reported for needle spruce extracts (Rasouli et al., 2017), but our paper is the first report involving sawdust and bark extracts. As for wild pine, a previous study indicates the possibility of bark extracts acting as antihemolytic agents (Harris et al., 2008), which was confirmed herein.

Hemolysis rate was not correlated to any of the antioxidant activity assays ($r < 0.500$, $p > 0.340$) and TPC ($r = -0.360$, $p = 0.308$), thus implying that the protective action of human erythrocytes is not only associated with phenolic compounds or functional carbohydrates separately. Two possible hypotheses emerge from the data: carbohydrates, in solution, may form a colloidal system that exerts a physical barrier that impedes hemolysis; phenolic compounds and carbohydrates interact, creating a physicochemical barrier that protects erythrocytes from hemolysis.

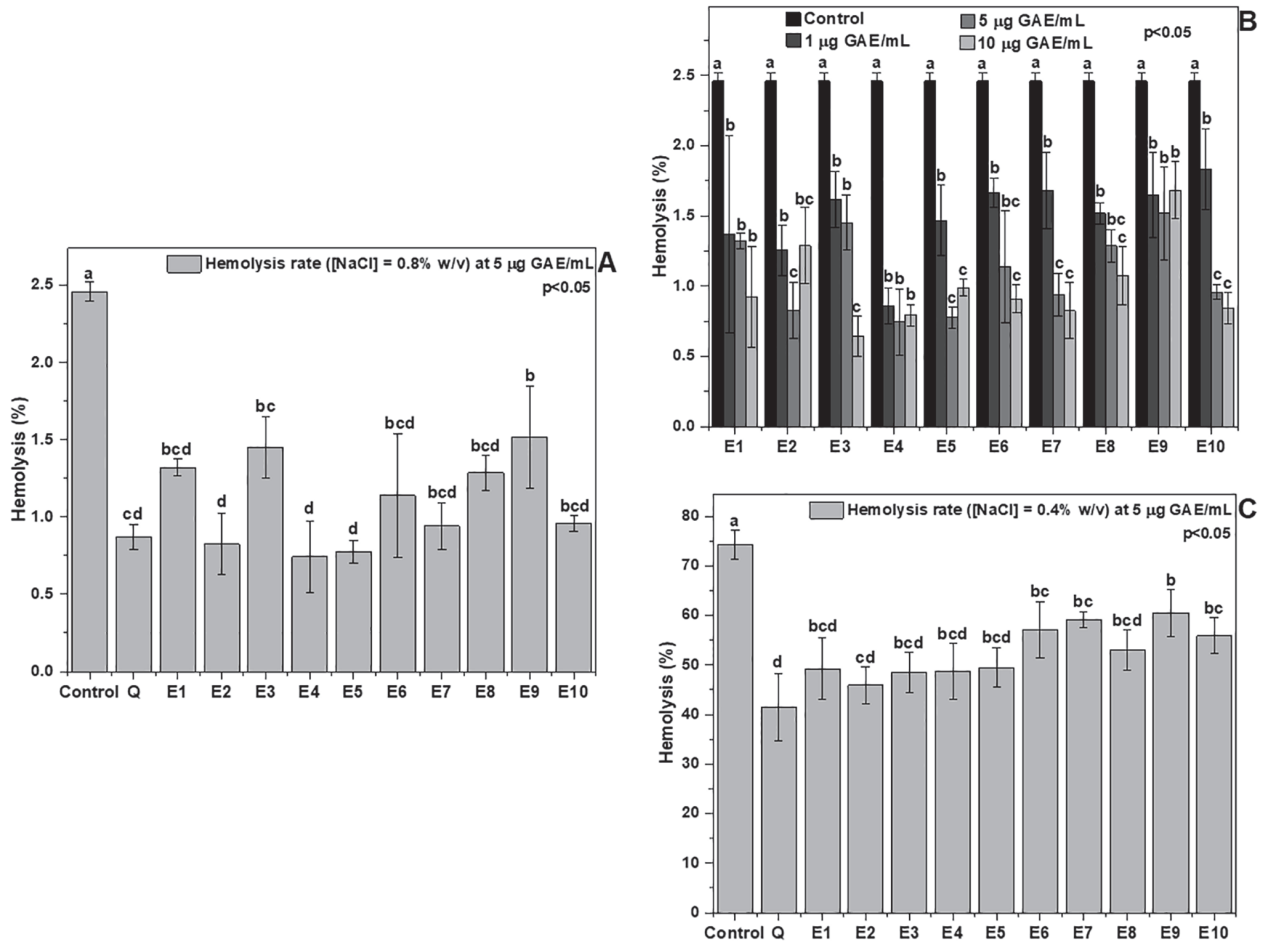

Fig. 3. Antihemolytic behavior of extracts (5 μg/mL) compared to quercetin (5 μg/mL) in different osmolarity conditions: NaCl at 0.8% w/v (E, isotonic condition), NaCl at 0.4% w/v (C, hypotonic condition), and 0.1% w/v (A, harsh hypotonic condition). The dose-dependent effect of the samples in all osmotic conditions is shown in B, D and F. Note: E1 = Norway spruce hemicellulose galactoglucomannan (GGM); E2 = concentrated and ethanol precipitated spruce hemicellulose GGM; E3 = birch hemicellulose xylan; E4 = concentrated and ethanol precipitated xylan; E5 = spruce bark tannin extract; E6 = XAD7HP partially purified spruce bark tannin extract; E7 = XAD7HP completely purified spruce bark tannin extract; E8 = pine bark tannin extract; E9 = pine hemicellulose extract; E10 = Purified industrial tannin. Different letters represent statistically different results ($p < 0.05$).

3.4. Inhibition of α-amylase and α-glucosidase

Regarding the inhibition of α-amylase (Table 2), it is possible to note that samples E1, E2, and E4 presented the highest IC_{50} values (α-amylase: 22 to > 500 mg/mL). In contrast, samples E5 to E7 and E10 gave the opposite behaviour (α-amylase: 0.46 to 2.68 mg/mL). Regarding the inhibition of α-glucosidase, samples E10, E5 to E8 presented the highest enzyme inhibition (IC_{50} values ranging from 6.7 to 137 μg/mL), while samples E2 to E4 gave the lowest enzyme inhibition (IC_{50} values ranging from 1159 to 3821 μg/mL). Sample E10, which corresponds to the phenolic-rich fraction, presented the highest inhibition of the enzymes, proving that phenolic compounds are very active in inhibiting these key enzymes' activity (Harris et al., 2008). Similarly, Ferreira-Santos et al. (2020) extracted *Pinus pinaster* bark with ethanolic solutions ranging from 30 to 90% (v/v). They found that the extract inhibited both α-amylase (IC_{50} ranging from 250 to 537 μg/mL) and α-glucosidase (IC_{50} ranging from 122 to 11,000 μg/mL). Our results corroborate the findings obtained with bark extracts from *Picea glauca* (Jiang et al., 2017) and *Eucalyptus grandis* and *E. urophylla* (Vadivel and Biesalski, 2011).

Recent evidence supports specific non-covalent bonds between different polyphenols (mainly flavonoids and tannins) and carbohydrate polymers via hydrogen bonds and hydrophobic interactions, so it is not surprising that samples E5-E10 showed the highest potential as enzyme inhibitors (Vadivel and Biesalski, 2011). Correlation analysis showed that the inhibition of α-glucosidase (IC_{50}) was significantly associated with TPC ($r = -0.675$, $p = 0.032$), Cu^{2+} chelating ability ($r = -0.723$, $p = 0.018$) and reducing power ($r = -0.868$, $p = 0.001$). Similarly, the inhibition of α-amylase (IC_{50}) was significantly associated with the reducing power ($r = -0.846$, $p = 0.002$) but not with TPC ($r = -0.486$, $p = 0.155$). These results are in-line with those obtained earlier (Deby-Dupont et al., 2005) with extracts of Karanja (*Pongamia pinnata*), rich in phenolics. Extracts with higher TPC presented higher antioxidant activity (FRAP and DPPH) and higher inhibition of α-glucosidase and α-amylase activities.

3.5. Antiviral activity

Herein, the potential of bark extracts was tested for their capability to rescue cells from infection against CVA9, and results are shown in Fig. 4. Samples E1 to E4 are spruce (E1-E2) and birch-derived extracts (E3-E4) enriched in hemicellulose only (E2, E4) or also containing lignin-derived phenols (E1, E3). To our surprise, none of the hemicellulose extracts with or without lignin showed potency to protect against

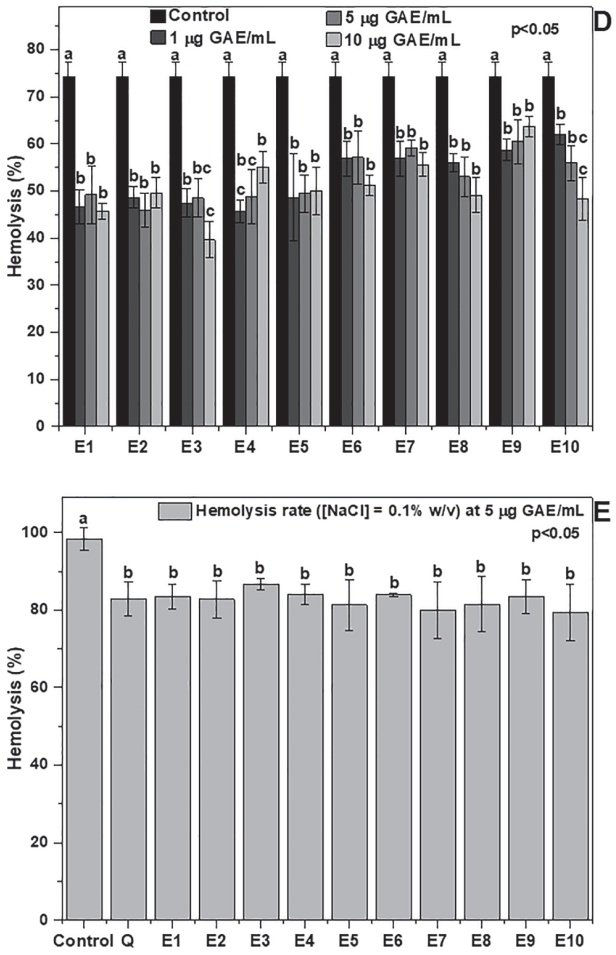

Fig. 3. (*continued*).

Table 2
In vitro antidiabetic potential of Norway spruce galactoglucomannan, birch glucuronoxylan, Norway spruce and Scots pine phenolic-rich extracts.

Samples	α-Glucosidase (IC_{50} μg/mL)	α-Amylase (IC_{50} mg/mL)
E1 - Norway spruce galactoglucomannan	274 ± 12	58.17 ± 6.07
E2 - Norway spruce galactoglucomannan (ethanol precipitation)	3821 ± 931	>500
E3 - Birch glucuronoxylan	1159 ± 172	22.98 ± 2.70
E4 - Birch glucuronoxylan (ethanol precipitation)	3493 ± 881	46.24 ± 6.94
E5 - Norway spruce phenolics (crude extract)	37.39 ± 0.72	2.68 ± 0.05
E6 - Norway spruce phenolics (partial purification with XAD7HP)	18.43 ± 0.96	1.06 ± 0.02
E7 - Norway spruce phenolics (complete purification with XAD7HP)	19.90 ± 4.20	2.27 ± 0.03
E8 - Scots pine phenolics (90 °C/60 min)	137 ± 7	31.46 ± 0.77
E9 - Scots pine phenolics (140 °C/60 min)	381 ± 38	35.19 ± 1.01
E10 – Industrial tannin QS-SOL	6.73 ± 0.45	0.46 ± 0.01

CVA9 infection with used concentrations from 1 to 200 μg/mL. In contrast, all the samples containing tannin fractions, from spruce (E5-E7) and pine (E8 and E9), were very effective against CVA9. Total rescue of cells against viral infection was gained with 50 μg/mL, and even 1 μg/mL showed>50% rescue for most samples. The purified tannin showed somewhat better recovery at 1 μg/mL concentration, altogether confirming that tannins show excellent antiviral efficacy against enterovirus infection. In addition, the charged sugars present in the pine sample E8 showed somewhat better antiviral potential than E9 without the sugars at 1 μg/mL concentration, suggesting that the presence of sugars could be beneficial in some bark preparations. It is noteworthy that none of the tested samples was cytotoxic at used concentrations during 24 h tested in A549 cells.

Correlation analysis showed that the antiviral activity is closely associated with FCRC ($r = 0.709$, $p = 0.032$) and Cu^{2+} chelating ability ($r = 0.916$, $p = 0.001$). The antiviral activity of extracts was significantly correlated to TPC ($r = 0.750$, $p = 0.020$), which implies that phenolic compounds are the main responsible antiviral agents. Another observation should be pondered: the higher the antioxidant activity, the higher the antiviral and anti-inflammatory activity of the extracts from the species studied. This work can be the basis for future works dedicated to isolating specific bioactive compounds or standardising extracts with specific bioactivity.

4. Conclusions

Different extracts from Norway spruce birch sawdust and Scots pine bark were analysed for their bioactive potential. Results showed that the antidiabetic potential, antioxidant activity, in terms of the free-radical scavenging activity, reducing effect, and metal chelation mainly were associated with the total phenolic content of the extracts. None of the

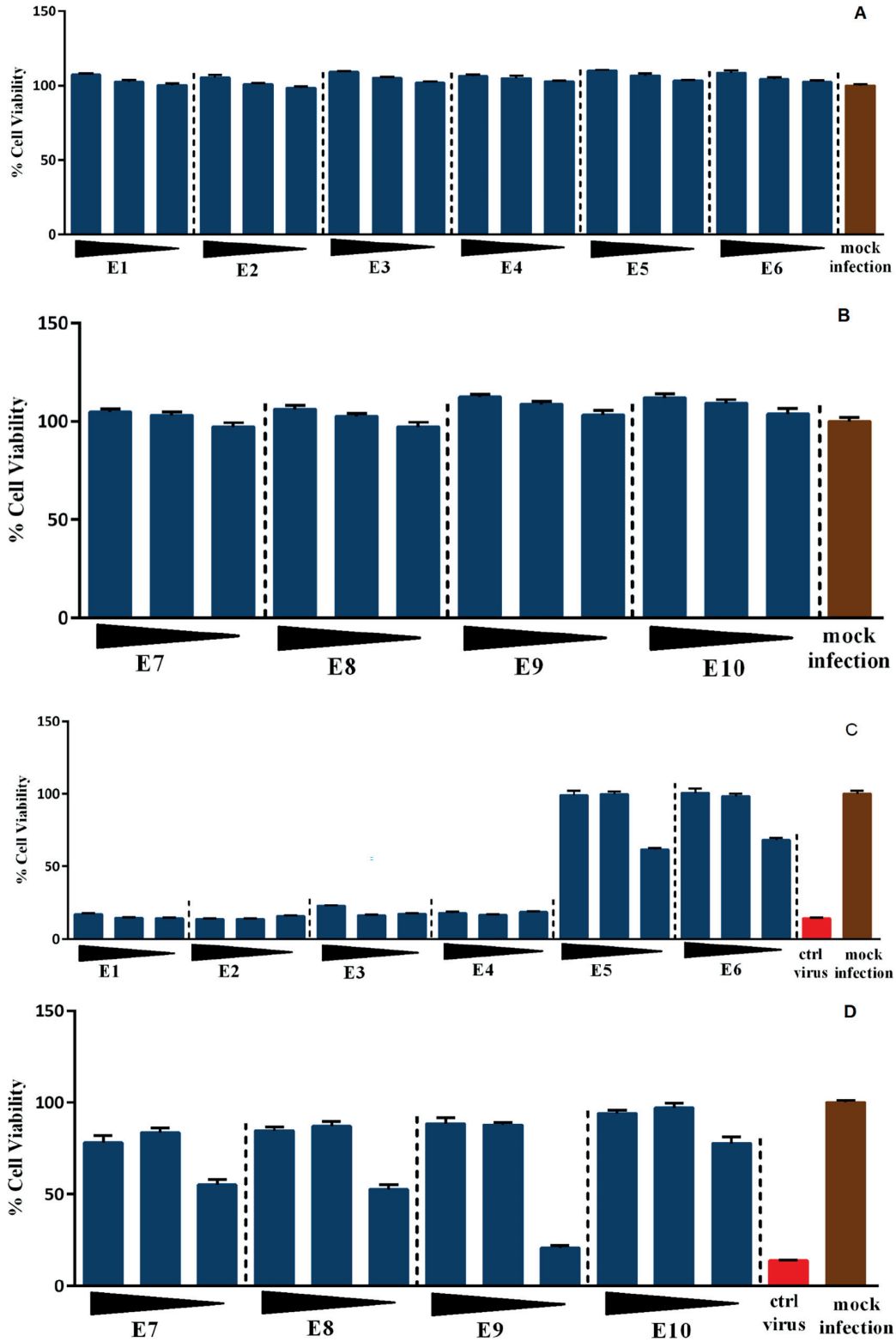

Fig. 4. Cytotoxicity (A, B), and antiviral efficacy (C, D) of the samples E1 - E10 (1, 50 and 200 μg/mL) tested on human A549 cells. For the antiviral assessment, CoxsackievirusA9 (2×10^8 PFU/mL) was treated with increasing concentrations (1, 50 and 200 μg/mL) of E1-E10 samples. Note: E1 = Norway spruce hemicellulose galactoglucomannan (GGM); E2 = concentrated and ethanol precipitated spruce hemicellulose GGM; E3 = birch hemicellulose xylan; E4 = concentrated and ethanol precipitated xylan; E5 = spruce bark tannin extract; E6 = XAD7HP partially purified spruce bark tannin extract; E7 = XAD7HP completely purified spruce bark tannin extract; E8 = pine bark tannin extract; E9 = pine hemicellulose extract; E10 = Purified industrial tannin.

extracts was toxic to normal human IMR90 cells, and the other cell lines observed low (or inexistent) toxicity. On the contrary, pronounced protection of human erythrocytes was observed for all the extracts. Considering the relative toxicological safety of the extracts using different biological assays and human cells, food models, and cosmetic applications using the extracts coming from forest industry byproducts represent a green-based approach to produce new functional ingredients for high value-added applications.

CRediT authorship contribution statement

Daniel Granato: Data curation, Formal analysis, Writing – original draft, Methodology. **Dhanik Reshamwala:** Investigation, Formal analysis, Writing – original draft. **Risto Korpinen:** Investigation, Formal analysis, Writing – original draft. **Luciana Azevedo:** Investigation, Formal analysis, Writing – original draft. **Mariana Araújo Vieira do Carmo:** Investigation, Formal analysis, Writing – original draft. **Thiago Mendanha Cruz:** Investigation, Formal analysis, Writing – original draft. **Mariza Boscacci Marques:** Investigation, Formal analysis, Writing – original draft. **Mingchun Wen:** Investigation, Formal analysis. **Liang Zhang:** Investigation, Formal analysis, Writing – original draft. **Varpu Marjomäki:** Investigation, Formal analysis, Writing – original draft. **Petri Kilpeläinen:** Conceptualization, Methodology, Project administration, Funding acquisition, Writing – original draft.

Declaration of Competing Interest

The authors declare that they have no known competing financial interests or personal relationships that could have appeared to influence the work reported in this paper.

Acknowledgments

The authors thank Natural Resources Institute Finland (Luke) for partially funding this work Project WoodHype (41007-00173600) and Business Finland Co-creation project Antiviral fibres (40699/31/2020) for supporting the antiviral work in the University of Jyväskylä. We also thank SimsBioPro (Luke 41007-00155200) and TanWat (EU/Interreg/Botnia-Atlantica, 20201484) projects for providing samples for the experiments.

Appendix A. Supplementary data

Supplementary data to this article can be found online at https://doi.org/10.1016/j.foodchem.2022.132284.

References

Abba, Y., Hassim, H., Hamzah, H., & Noordin, M. M. (2015). Antiviral activity of resveratrol against human and animal viruses. *Advances in Virology, 2015*, 1–7. https://doi.org/10.1155/2015/184241

Bhattarai, M., Pitkänen, L., Kitunen, V., Korpinen, R., Ilvesniemi, H., Kilpeläinen, P. O., … Mikkonen, K. S. (2019). Functionality of spruce galactoglucomannans in oil-in-water emulsions. *Food Hydrocolloids, 86*, 154–161. https://doi.org/10.1016/j.foodhyd.2018.03.020

Carvalho, T. M. A., Cardoso, H. J., Figueira, M. I., Vaz, C. V., & Socorro, S. (2019). The peculiarities of cancer cell metabolism: A route to metastasization and a target for therapy. *European Journal of Medical Chemistry, 171*, 343–363. https://doi.org/10.1016/j.ejmech.2019.03.053

Coșarcă, S.-L., Moacă, E.-A., Tanase, C., Muntean, D. L., Pavel, I. Z., & Dehelean, C. A. (2018). Spruce and beech bark aqueous extracts: Source of polyphenols, tannins and antioxidants correlated to *in vitro* antitumor potential on two different cell lines. *Wood Science and Technology, 53*(2), 313–333. https://doi.org/10.1007/s00226-018-1071-5

Deby-Dupont, G., Mouithys-Mickalad, A., Serteyn, D., Lamy, M., & Deby, C. (2005). Resveratrol and curcumin reduce the respiratory burst of Chlamydia-Primed THP-1 cells. *Biochemical and Biophysical Research Communications, 333*(1), 21–27. https://doi.org/10.1016/j.bbrc.2005.05.073

Carmo, M. A. V. D., Fidelis, M., Pressete, C. G., Marques, M. J., Castro-Gamero, A. M., Myoda, T., … Azevedo, L. (2019). Hydroalcoholic *Myrciaria dubia* (Camu-Camu) seed extracts prevent chromosome damage and act as antioxidant and cytotoxic agents. *Food Research International, 125*, 108551. https://doi.org/10.1016/j.foodres.2019.108551

Đorđević, T., & Antov, M. (2018). The influence of hydrothermal extraction conditions on recovery and properties of hemicellulose from wheat chaff – A modelling approach. *Biomass and Bioenergy, 119*, 246–252. https://doi.org/10.1016/j.biombioe.2018.09.030

Escher, G. B., Borges, L. C. C., Santos, J. S., Cruz, T. M., Marques, M. B., do Carmo, M. A. V., Azevedo, L., Furtado, M. M., Sant'Ana, A. S., Wen, M., Zhang, L., Granato, D., 2019. From the Field to the Pot: Phytochemical and Functional Analyses of *Calendula officinalis* L. Flower for Incorporation in an Organic Yogurt. Antioxidants. 8 (11), 559. Doi: 10.3390/antiox8110559.

Ferreira-Santos, P., Genisheva, Z., Botelho, C., Santos, J., Ramos, C., Teixeira, J. A., & Rocha, C. M. R. (2020). Unravelling the biological potential of *Pinus pinaster* bark extracts. *Antioxidants., 9*(4), 334. https://doi.org/10.3390/antiox9040334

Fidelis, M., do Carmo, M. A. V., da Cruz, T. M., Azevedo, L., Myoda, T., Miranda Furtado, M., … Granato, D. (2020). Camu-Camu seed (*Myrciaria dubia*) - From side stream to an antioxidant, antihyperglycemic, antiproliferative, antimicrobial, antihemolytic, anti-inflammatory, and antihypertensive ingredient. *Food Chemistry, 310*, 125909. https://doi.org/10.1016/j.foodchem.2019.125909

de Mejia, E. G., Song, Y. S., Heck, C. I., & Ramirez-Mares, M. (2010). Yerba mate tea (*Ilex paraguariensis*): Phenolics, antioxidant capacity and *in vitro* inhibition of colon cancer cell proliferation. *Journal of Functional Foods, 2*(1), 23–34. https://doi.org/10.1016/j.jff.2009.12.003

Granato, D., Koot, A., Schnitzler, E., & van Ruth, S. M. (2015). Authentication of geographical origin and crop system of grape juices by phenolic compounds and antioxidant activity using chemometrics. *Journal of Food Science, 80*(3), C584–C593. https://doi.org/10.1111/jfds.2015.80.issue-310.1111/1750-3841.12794

Granato, D., Calado, V. M. A., & Jarvis, B. (2014). Observations on the use of statistical methods in food science and technology. *Food Research International, 55*, 137–149.

Harris, C. S., Lambert, J., Saleem, A., Coonishish, J., Martineau, L. C., Cuerrier, A., … Bennett, S. A. L. (2008). Antidiabetic activity of extracts from needle, bark, and cone of *Picea Glauca*.: Organ-specific protection from glucose toxicity and glucose deprivation. *Pharmaceutical Biology, 46*(1-2), 126–134. https://doi.org/10.1080/13880200701735080

Harris, I. S., & DeNicola, G. M. (2020). The complex interplay between antioxidants and ROS in cancer. *Trends in Cell Biology, 30*(6), 440–451. https://doi.org/10.1016/j.tcb.2020.03.002

Huang, J.-Q., Qi, R.-T., Pang, M.-R., Liu, C., Li, G.-y., & Zhang, Y. (2017). Isolation, chemical characterization, and immunomodulatory activity of naturally acetylated hemicelluloses from bamboo shavings. *J. Zhejiang Univ.-SCI.B, 18*(2), 138–151. https://doi.org/10.1631/jzus.B1500274

Hyöty, H. (2016). Viruses in Type 1 Diabetes. *Pediatric Diabetes., 17*(S22), 56–64. https://doi.org/10.1111/pedi.12370

Jiang, P., Xiong, J., Wang, F., Grace, M. H., Lila, M. A., & Xu, R. (2017). α -Amylase and α-Glucosidase Inhibitory Activities of Phenolic Extracts from Eucalyptus Grandis × E. Urophylla Bark. *Journal of Chemistry, 2017*, 1–7. https://doi.org/10.1155/2017/8516964

Johnson, M. H., Lucius, A., Meyer, T., & de Mejia, E. G. (2011). Cultivar evaluation and effect of fermentation on antioxidant capacity and *in vitro* inhibition of α-amylase and α-glucosidase by highbush blueberry (*Vaccinium corombosum*). *Journal of Agriculture and Food Chemistry, 59*(16), 8923–8930. https://doi.org/10.1021/jf201720z

Kilpeläinen, P. O., Hautala, S. S., Byman, O. O., Tanner, L. J., Korpinen, R. I., Lillandt, M.-K.-J., … Ilvesniemi, H. S. (2014). Pressurized hot water flow-through extraction system scale up from the laboratory to the pilot scale. *Greem Chemistry, 16*(6), 3186–3194. https://doi.org/10.1039/C4GC00274A

Kim, K. J., Hwang, E.-S., Kim, M.-J., Park, J.-H., & Kim, D.-O. (2020). Antihypertensive effects of polyphenolic extract from korean red pine (*Pinus densiflora* Sieb. et Zucc.) bark in spontaneously hypertensive rats. *Antioxidants., 9*(4), 333. https://doi.org/10.3390/antiox9040333

Lahtinen, M. H., Valoppi, F., Juntti, V., Heikkinen, S., Kilpeläinen, P. O., Maina, N. H., & Mikkonen, K. S. (2019). Lignin-rich PHWE hemicellulose extracts responsible for extended emulsion stabilization. *Frontiers in Chemistry, 7*, 1–18. https://doi.org/10.3389/fchem.2019.00871

Li, K.e., Li, S., Wang, D.i., Li, X., Wu, X., Liu, X., … Du, Y. (2019). Extraction, characterization, antitumor and immunological activities of hemicellulose polysaccharide from *Astragalus radix* herb residue. *Molecules, 24*(20), 3644. https://doi.org/10.3390/molecules24203644

Li, W., Li, D., Kuang, H., Feng, X., Ai, W., Wang, Y., … Fan, R. (2020). Berberine Increases Glucose Uptake and Intracellular ROS Levels by Promoting Sirtuin 3 Ubiquitination. *Biomedicine & Pharmacotherapy, 121*, 109563. https://doi.org/10.1016/j.biopha.2019.109563

Marjomäki, V., Turkki, P., & Huttunen, M. (2015). Infectious Entry Pathway of Enterovirus B Species. *Viruses, 7*, 6387–6399. https://doi.org/10.3390/v7122945

Metsämuuronen, S., & Sirén, H. (2019). Bioactive Phenolic Compounds, Metabolism and Properties: A Review on Valuable Chemical Compounds in Scots Pine and Norway Spruce. *Phytochemistry Reviews, 18*(3), 623–664. https://doi.org/10.1007/s11101-019-09630-2

Mikkonen, K. S., Kirjoranta, S., Xu, C., Hemming, J., Pranovich, A., Bhattarai, M., … Willför, S. (2019). Environmentally-Compatible Alkyd Paints Stabilized by Wood Hemicelluloses. *Industrial Crops and Products, 133*, 212–220. https://doi.org/10.1016/j.indcrop.2019.03.017

Neiva, D. M., Araújo, S., Gominho, J., Carneiro, A.d. C., Pereira, H., & Lightfoot, D. A. (2018). An Integrated Characterization of *Picea abies* Industrial Bark Regarding Chemical Composition, Thermal Properties and Polar Extracts Activity. *PLoS ONE, 13*(11), e0208270. https://doi.org/10.1371/journal.pone.0208270

Olchowik, E., Lotkowski, K., Mavlyanov, S., Abdullajanova, N., Ionov, M., Bryszewska, M., & Zamaraeva, M. (2012). Stabilization of Erythrocytes against Oxidative and Hypotonic Stress by Tannins Isolated from Sumac Leaves *(Rhus typhina* L.) and Grape Seeds (*Vitis vinifera* L.). *Cellular & Molecular Biology Letters, 17* (3), 333–348. https://doi.org/10.2478/s11658-012-0014-7

Pap, N., Reshamwala, D., Korpinen, R., Kilpeläinen, P., Fidelis, M., Furtado, M. M., … Granato, D. (2021). Toxicological and bioactivity evaluation of blackcurrant press cake, sea buckthorn leaves and bark from Scots pine and Norway spruce extracts under a green integrated approach. *Food and Chemical Toxicology, 153*, 112284. https://doi.org/10.1016/j.fct.2021.112284

Pitkänen, L., Heinonen, M., & Mikkonen, K. S. (2018). Safety considerations of plant polysaccharides for food use: A case study on phenolic-rich softwood galactoglucomannan extract. *Food & Function, 9*(4), 1931–1943. https://doi.org/10.1039/C7FO01425B

Ragab, T. I. M., Amer, H., Mossa, A. T., Emam, M., Hasaballah, A. A., & Helmy, W. A. (2018). Anticoagulation, Fibrinolytic and the Cytotoxic Activities of Sulfated Hemicellulose Extracted from Rice Straw and Husk. *Biocatalysis and Agricultural Biotechnology, 15*, 86–91. https://doi.org/10.1016/j.bcab.2018.05.010

Rasi, S., Kilpeläinen, P., Rasa, K., Korpinen, R., Raitanen, J.-E., Vainio, M., … Jyske, T. (2019). Cascade Processing of Softwood Bark with Hot Water Extraction, Pyrolysis and Anaerobic Digestion. *Bioresource Technology, 292*, 121893. https://doi.org/10.1016/j.biortech.2019.121893

Rasouli, H., Hosseini-Ghazvini, S.-M.-B., Adibi, H., & Khodarahmi, R. (2017). Differential α-Amylase/α-Glucosidase Inhibitory Activities of Plant-Derived Phenolic Compounds: A Virtual Screening Perspective for the Treatment of Obesity and Diabetes. *Food & Function, 8*(5), 1942–1954. https://doi.org/10.1039/c7fo00220c

Ruokolainen, V., Domanska, A., Laajala, M., Pelliccia, M., Butcher, S. J., Marjomäki, V., & López, S. (2019). Extracellular Albumin and Endosomal Ions Prime Enterovirus Particles for Uncoating That Can Be Prevented by Fatty Acid Saturation. *Journal of Virology, 93*(17). https://doi.org/10.1128/JVI.00599-19

Santos, J. S., Deolindo, C. T. P., Hoffmann, J. F., Chaves, F. C., do Prado-Silva, L., Sant'Ana, A. S., … Granato, D. (2018). Optimized *Camellia sinensis* var. *sinensis*, *Ilex paraguariensis*, and *Aspalathus linearis* blend presents high antioxidant and antiproliferative activities in a beverage model. *Food Chemistry, 254*, 348–358. https://doi.org/10.1016/j.foodchem.2018.02.021

Schmidtke, M., Schnittler, U., Jahn, B., Dahse, H.-M., & Stelzner, A. (2001). A Rapid Assay for Evaluation of Antiviral Activity against Coxsackie Virus B3, Influenza Virus A, and Herpes Simplex Virus Type 1. *Journal of Virological Methods, 95*(1), 133–143. https://doi.org/10.1016/S0166-0934(01)00305-6

Spinelli, S., Costa, C., Conte, A., La Porta, N., Padalino, L., & Nobile, M. A. D. (2019). Bioactive Compounds from Norway Spruce Bark: Comparison Among Sustainable Extraction Techniques for Potential Food Applications. *Foods, 8*, 524. https://doi.org/10.3390/foods8110524

Teo, C. C., Tan, S. N., Yong, J. W. H., Hew, C. S., & Ong, E. S. (2010). Pressurized hot water extraction (PHWE). *Journal of Chromatography A, 1217*(16), 2484–2494. https://doi.org/10.1016/j.chroma.2009.12.050

Vadivel, V., & Biesalski, H. K. (2011). Contribution of phenolic compounds to the antioxidant potential and type II diabetes related enzyme inhibition properties of *Pongamia pinnata l.* Pierre seeds. *Process Biochemistry, 46*(10), 1973–1980. https://doi.org/10.1016/j.procbio.2011.07.007

Valoppi, F., Lahtinen, M. H., Bhattarai, M., Kirjoranta, S. J., Juntti, V. K., Peltonen, L. J., … Mikkonen, K. S. (2019). Centrifugal fractionation of softwood extracts improves the biorefinery workflow and yields functional emulsifiers. *Greem Chemistry, 21*(17), 4691–4705. https://doi.org/10.1039/C9GC02007A

Varila, T., Brännström, H., Kilpeläinen, P., Hellström, J., Romar, H., Nurmi, J., & Lassi, U. (2020). From Norway Spruce Bark to Carbon Foams: Characterization, and Applications. *Bioresources, 15*(2), 3651–3666.

do Carmo, M. A. V., Pressete, C. G., Marques, M. J., Granato, D., & Azevedo, L. (2018). Polyphenols as Potential Antiproliferative Agents: Scientific Trends. *Current Opinion in Food Science, 24*, 26–35. https://doi.org/10.1016/j.cofs.2018.10.013

Weber-Lotfi, F., Guillemaut, P., Poirey, R., Schmitz, M., & Dietrich, A. (2002). Biochemical and Molecular Studies on Declining and Decline-Resistant Spruce in the North-East of France. *Environmental Science and Pollution Research, 9*(2), 122–129. https://doi.org/10.1007/BF02987459

Wu, F., Jia, X., Yin, L., Cheng, Y., Miao, Y., & Zhang, X. (2019). The effect of hemicellulose and lignin on properties of polysaccharides in lentinus edodes and their antioxidant evaluation. *Molecules, 24*, 1834. https://doi.org/10.3390/molecules24091834

Zhang, L., Santos, J. S., Cruz, T. M., Marques, M. B., do Carmo, M. A. V., Azevedo, L., … Granato, D. (2019). Multivariate effects of Chinese keemun black tea grades (Camellia sinensis var. sinensis) on the phenolic composition, antioxidant, antihemolytic and cytotoxic/cytoprotection activities. *Food Research International, 125*, 108516. https://doi.org/10.1016/j.foodres.2019.108516

III

FIELD-GROWN AND IN VITRO PROPAGATED ROUND-LEAVED SUNDEW (*DROSERA ROTUNDIFOLIA* L.) SHOW DIFFERENCES IN METABOLIC PROFILES AND BIOLOGICAL ACTIVITIES

by

Jenni Tienaho, Dhanik Reshamwala, Maarit Karonen, Niko Silvan, Leila Korpela, Varpu Marjomäki & Tytti Sarjala 2021

Molecules 26, 3581

molecules

MDPI

Article

Field-Grown and In Vitro Propagated Round-Leaved Sundew (*Drosera rotundifolia* L.) Show Differences in Metabolic Profiles and Biological Activities

Jenni Tienaho [1,*], Dhanik Reshamwala [2], Maarit Karonen [3], Niko Silvan [1], Leila Korpela [4], Varpu Marjomäki [2] and Tytti Sarjala [1]

[1] Biomass Characterization and Properties Group, Production Systems Unit, Natural Resources Institute Finland, Latokartanonkaari 9, FI-00791 Helsinki, Finland; niko.silvan@luke.fi (N.S.); tytti.sarjala@luke.fi (T.S.)
[2] Department of Biological and Environmental Science, University of Jyväskylä, Seminaarinkatu 15, FI-40014 Jyväskylä, Finland; dhanik.d.reshamwala@jyu.fi (D.R.); varpu.s.marjomaki@jyu.fi (V.M.)
[3] Natural Chemistry Research Group, University of Turku, FI-20014 Turku, Finland; maarit.karonen@utu.fi
[4] Forest Health and Biodiversity Group, Natural Resources Unit, Natural Resources Institute Finland, FI-00791 Helsinki, Finland; leila.korpela@luke.fi
* Correspondence: jenni.tienaho@luke.fi; Tel.: +358-29-532-4986

Abstract: *Drosera rotundifolia* L. is a carnivorous plant used in traditional medicine for its therapeutic properties. Because of its small size, its collection in nature is laborious and different cultivation methods have been studied to ensure availability. However, only a few studies exist where the lab-grown sundew tissue and field-grown sundew would have been compared in their functionality or metabolic profiles. In this study, the antioxidant and antiviral activities of lab-grown and field-grown sundew extracts and their metabolic profiles are examined. The effect of drying methods on the chromatographic profile of the extracts is also shown. Antioxidant activity was significantly higher (5–6 times) in field-grown sundew but antiviral activity against enterovirus strains coxsackievirus A9 and B3 was similar in higher extract concentrations (cell viability ca. 90%). Metabolic profiles showed that the majority of the identified compounds were the same but field-grown sundew contained higher numbers and amounts of secondary metabolites. Freeze-drying, herbal dryer, and oven or room temperature drying of the extract significantly decreased the metabolite content from −72% up to −100%. Freezing was the best option to preserve the metabolic composition of the sundew extract. In conclusion, when accurately handled, the lab-grown sundew possesses promising antiviral properties, but the secondary metabolite content needs to be higher for it to be considered as a good alternative for the field-grown sundew.

Keywords: *Drosera rotundifolia*; antioxidants; antiviral properties; phenolic compounds; secondary metabolites

Citation: Tienaho, J.; Reshamwala, D.; Karonen, M.; Silvan, N.; Korpela, L.; Marjomäki, V.; Sarjala, T. Field-Grown and In Vitro Propagated Round-Leaved Sundew (*Drosera rotundifolia* L.) Show Differences in Metabolic Profiles and Biological Activities. *Molecules* **2021**, *26*, 3581. https://doi.org/10.3390/molecules26123581

Academic Editor: Enrique Barrajon

Received: 18 May 2021
Accepted: 9 June 2021
Published: 11 June 2021

1. Introduction

Round-leaved sundews (*Drosera rotundifolia* L.) are small carnivorous plants growing in Northern peatlands and other nutrient-poor soils [1,2]. They secrete sugary glowing mucilage into the hairs covering their leaves and feed on the attracted insects, which get caught on the sticky liquid and are then enzymatically dissolved [1,3]. *D. rotundifolia* is used in traditional medicine, where its ability to relieve coughs and pulmonary diseases has been acknowledged for centuries [2–4]. The therapeutic activities have mainly been associated with two compound groups: flavonoids and naphthoquinones. For example, the anti-inflammatory [5] and antimicrobial [6–8] activities of *D. rotundifolia* have been established and the drug Droserae Herba, which is traditionally produced from the dried aerial parts of the plant, is accepted in various pharmacopeias of the world [3,4]. Some naphthoquinones and flavonoids, which are important secondary metabolites of *Drosera* have also been considered antiviral [9,10]. In addition, *Drosera* has in some cases been identified with

antioxidant activity and iron-chelating properties [11]. The secondary metabolites of *Drosera* can for example be of use in the pharmaceutical, cosmetics, and food industry [12]. The round-leaved sundew is not endangered in Finland [13], but the collection of small-sized plants from natural stands is laborious and therefore cultivation methods [2,14] and in vitro propagation [2,12,15] have been studied to achieve better availability of the valuable plant material. The chemical composition and functional properties may vary in sundew plants depending on the growth conditions and site [16]. Therefore, the potential differences in the properties of field-grown and in vitro propagated plant material should be studied. In an earlier study, we demonstrated that antibacterial activity was significantly higher in field-grown *D. rotundifolia* ethanol extract in comparison to the propagated sundew extracts [8]. However, only a few studies exist where the functional properties and metabolic profiles of propagated and field-grown sundews are compared.

In this study, we investigate and compare the antioxidant (oxygen radical absorbance capacity (ORAC), ferric reducing antioxidant power (FRAP), H_2O_2 scavenging) and antiviral (enteroviruses CVA9 and CVB3) activities of both propagated and field-grown sundew, and describe the differences in their metabolic profiles using UPLC-DAD-ESI-QOrbitrap-MS/MS. We also describe the effects of different handling techniques, such as the drying of the extracts, on their chromatographic profile.

2. Results and Discussion

2.1. Growth of the Laboratory Propagated Sundew Tissue

The laboratory propagated sundew tissues grew well on the $\frac{1}{2}$ MS medium. The fresh weight of the tissues increased 250% in six weeks when growing on Petri dishes (⦰14 cm) and 470% when growing in 125 mL pots (Figure 1). No significant difference was observed between the final biomass levels from the pots or Petri dishes (p-value = 0.605), whereas significance was established between the initial and final biomass levels of the pots and Petri dishes (both with p-values < 0.001). This suggests that by selecting the growth conditions it is possible to optimize and significantly improve the yield of sundew tissue production. The morphological features of the propagated tissue showed the development of green leaf structures without red color or a proper stem (Figure 2A), thus lacking the typical look of sundew plants grown in a natural environment (Figure 2B).

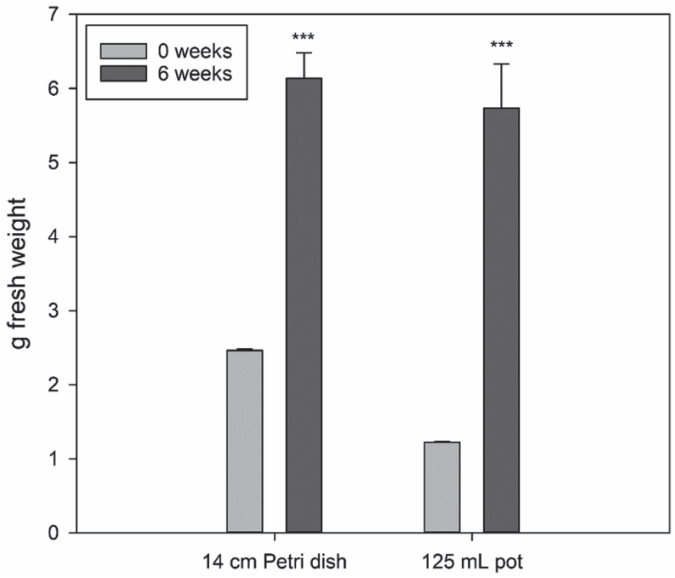

Figure 1. Yield (g fresh weight, mean ± stdev, n = 6) of the total propagated sundew tissue in six weeks on $\frac{1}{2}$ MS medium on Petri dishes and 125 mL pots. A one-way ANOVA test was used to assess the statistical significance of differences between 0 weeks and 6 weeks (*** = $p < 0.001$). No significant difference was observed between Petri dish and pot-grown biomass after 6 weeks.

The growth potential of propagated sundew tissue was promising, showing an increase of over 400% in fresh weight within six weeks. This could probably be further optimized, because only one growth medium was used here.

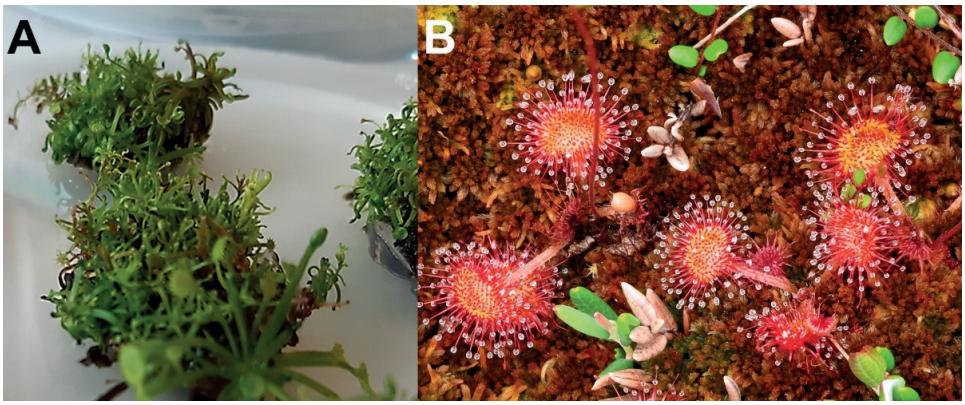

Figure 2. The sundew plants used in this study: (**A**) The in vitro propagation of *D. rotundifolia* on a Petri dish (photo: Tytti Sarjala) and (**B**) sundew growing wild on *Sphagnum* moss (photo: Hannu Nousiainen). The sundew cultivations in pots were morphologically alike to the tissue in figure (**A**).

2.2. Antiviral Activity

The antiviral potential of the round-leaved sundew was determined against non-enveloped enteroviruses CVB3 and CVA9 in our assays. Enteroviruses are responsible for numerous acute and chronic infections globally [17,18]. Compared with enveloped viruses, these non-enveloped viruses are quite stable and resistant to disinfectants [19]. Chemical-based disinfectants have other limitations in terms of their toxicity and being hazardous to health. Here, we tested various concentrations (10%, 5%, 1%, and 0.1%, *v/v*) of field-grown and in vitro propagated/lab-grown sundew to assess their ability to rescue A549 cells from CVA9 and CVB3 infections. Interestingly, both the field and lab-grown round-leaved sundews were able to protect cells from both virus serotypes. The extracts were more effective against CVA9 compared with CVB3 (Figure 3A,B). In addition, the field-grown sundews showed antiviral activity even at lower concentrations, suggesting that it was better at reducing virus infectivity compared with the lab-grown sundews. It is likely that this phenomenon is affected by the metabolic profile of the extracts. For example, Lin et al. [20] found that polyphenols, such as tannins are effective against coxsackieviruses. None of the concentrations tested were cytotoxic (Figure 3C), which was evaluated using CPE Inhibition assay. Based on our findings, the extracts are acting directly on the virus capsid as they showed good antiviral activity when the virus was pre-treated with them for 1 h at +37 °C. In the future, it would be interesting to study, the actual antiviral mechanism of these extracts.

2.3. Antioxidant Activity

Both ORAC and FRAP assays showed that field-grown sundew plants possessed much higher antioxidant properties in comparison with the lab-grown propagated biomass (Figure 4). Significant differences for the ORAC values were observed between the lab *Drosera* and Lehtolamminneva mire sundew (p-value < 0.001) and Kivineva mire sundew (p-value < 0.001). The difference between the two field-grown sundews was also significant (p-value = 0.014). A similar observation was made for the FRAP data, where one-way analysis of variance (ANOVA) gave p-values < 0.001 between the lab *Drosera* results and results for the two mires, whereas the difference between Lehtolamminneva mire and Kivineva mire results was insignificant (p-value = 0.96). H_2O_2 scavenging assay showed very low H_2O_2 inhibition % (3.1–3.5%) for all the samples and no differences between the field-grown or lab-grown *Drosera* were found. Changes in the growth conditions (light,

nutrients, natural peatland environment) of the propagated tissue did not result in any improvement of the antioxidant properties measured as FRAP. Exposing the propagated sundew tissue for two days to ambient daylight in summer affected the tissue by decreasing FRAP activity by 12% from 18.5 ± 1.0 to 16.3 ± 0.8 µmol Fe(II) eq. per 1 g. A decrease in the nutrient content of the growth medium in comparison with the $\frac{1}{2}$ MS medium at a 30% nutrient level or water squeezed from *Sphagnum* moss also decreased the FRAP activity of the tissue from 42.7 ± 6.8 to 19.1 ± 4.7, 21.9 ± 3.4 µmol Fe(II) eq. per 1 g, respectively. Furthermore, the propagated sundew tissue did not survive in a natural environment on a peatland when transplanted there for two weeks.

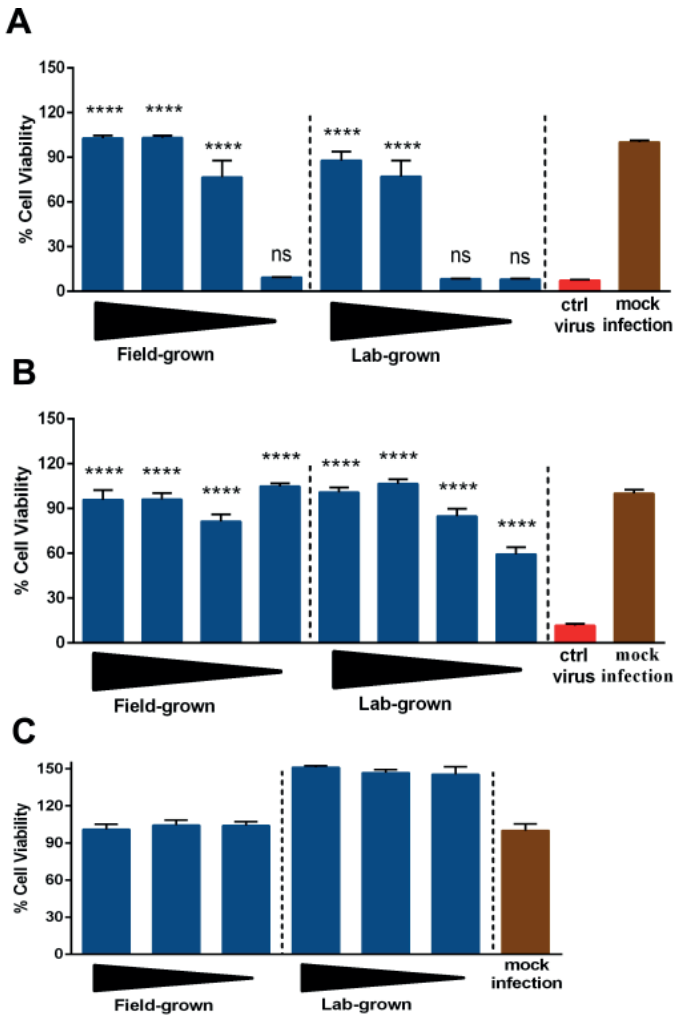

Figure 3. The antiviral efficacy of round-leaved sundew against (**A**) CVA9 and (**B**) CVB3 and its (**C**) cytotoxicity at decreasing concentrations (10%, 5%, and 1% *v/v*) tested on human A549 cells. For the antiviral assessment, CVA9 (2×10^6 PFU/mL) and CVB3 (2×10^5 PFU/mL) were treated with decreasing concentrations (10%, 5%, 1%, and 0.1%, *v/v*) of the round-leaved sundew. Average value + standard errors of mean (SEM) are shown. One-way ANOVA followed by Bonferroni test were used to assess the statistical significance of differences between the virus control and test samples (**** = $p < 0.0001$; ns = non-significant).

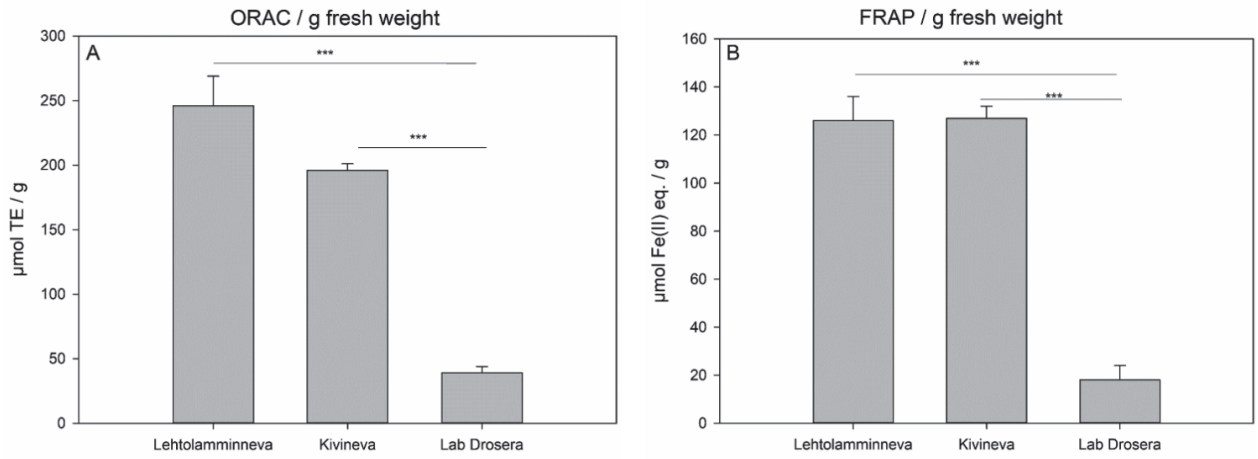

Figure 4. (**A**) ORAC and (**B**) FRAP activities (mean ± standard deviation, $n = 3$) of *D. rotundifolia* plants collected from Lehtolamminneva mire and Kivineva mire and lab-grown propagated *D. rotundifolia* biomass (Lab Drosera). TE = Trolox (vitamin E derivative) equivalent. One-way ANOVA test was used to assess the statistical significance of differences between Lab Drosera and mire grown samples (*** = $p < 0.001$).

2.4. Stability under Different Drying Methods

HPLC analysis revealed that the compound contents of sundew tissue extract were not stable under drying treatments. The peak area, for example, at a retention time of 26 min in the HPLC gram decreased when compared with the sample of the frozen tissue extract (−20 °C) (100%) to 28%, 15%, 10%, and 0% in the extract of sundew after freeze-drying, room temperature (+20 °C), herbal-dryer (+45 °C), and oven drying (+105 °C), respectively (Figure 5). Identical amounts of the same extract with no variation in the compound content were used for all the handling and drying methods.

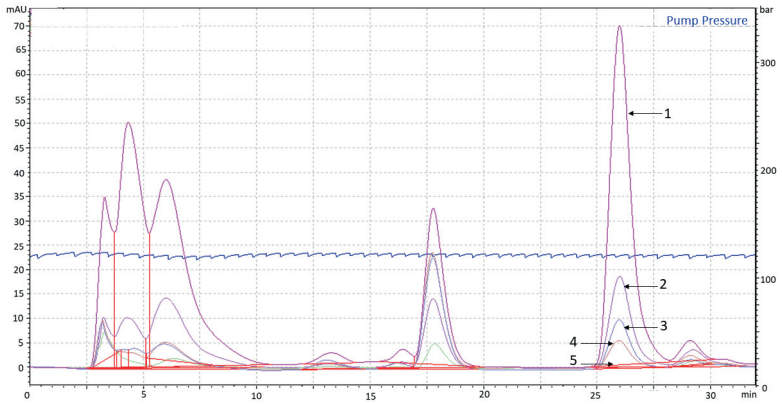

Figure 5. HPLC grams of differently dried sundew tissue extract. The drying treatments of the overlaid HPLC grams are marked as follows: (1) frozen (−20 °C), (2) freeze-drying (43 h), (3) room temperature (43 h), (4) herbal-dryer (+45 °C, 27 h), and (5) oven (+105 °C, 24 h).

2.5. Metabolite Profiles

The metabolite profiles of field-grown and propagated sundews were investigated from untreated extracts using UPLC-DAD-ESI-QOrbitrap-MS/MS and the results for the field-grown sundews are shown in Table 1 and for lab-grown propagated tissues in Table 2. In addition to the metabolites shown in the tables, saccharides and small organic acids were eluting with very early retention times (RT) in both sundew types (Figure 6). The lab-grown sundew extract also indicated the presence of arginine, which was not found in the field-grown extract. Most of the identified metabolites were similar in the lab and field-grown

extracts but also differences were observed. For instance, 14 compounds were found in both extracts, but ten compounds could only be found in the field-grown sundew extract and six in the lab-grown extract. The lab-grown extract contained an isomer of a coumaric acid glycoside eluting at total ion chromatogram (TIC) with a retention time (RT) of 3.04 min, two unknown compounds at RT 3.24 min, hyperoside eluting also at RT 4.09 min, syringetin glycoside eluting at RT 5.24 min, and spinatoside eluting at RT 5.55 min, which were not observed in the field-grown sundew extract. Field-grown sundew extract contained digalloyl glycose at RT 2.49 min, dihydromyricetin at RT 3.32 min, hexahydroxyflavone glycoside at RT 3.72 min, tetrahydroxyflavone at RT 3.83 min, an unknown compound at RT 3.86 min, kaempferol-galloyl-glycoside at RT 4.42 min, quercetin glycoside at RT 4.68 min, methyl ellagic acid at RT 4.79 min, quercetin glycoside gallate at RT 5.25 min, and quercetin at RT 5.37 min. Because the drying methods compromise the metabolic profile and compound stability, the extracts were considerably dilute, which seemed to slightly affect the shape and maxima of UV spectra (Figure 6). Tuominen [21], Zehl et al. [22], Braunberger et al. [23], Jia et al. [24], and Marczak et al. [25] all verify the identification of compounds based on their retention time, elution order, exact masses, and/or characteristic MS/MS fragments.

Table 1. Metabolic profile of the field-grown *Drosera rotundifolia*. Identified based on literature [21–25].

#	RT_{TIC}	RT_{UV}	Compound	UV λ_{max} (nm) *	Exact Mass Detected	Exact Mass Calculated	Characteristic MS/MS Values	Peak Area **
1	0.59	-	Quinic acid	-	192.06188	192.06339	111, 129, 173	***
2	1.29	1.25	Monogalloyl glucose (β-)	216, 278	332.07366	332.07435	125, 151, 169, 211, 271	601 ± 190
3	2.49	2.46	Digalloyl glycose	226, 273	484.08492	484.08531	125, 151, 169, 211, 271, 331	205 ± 79
4	2.57	2.55	Coumaric acid glycoside	296	326.10021	326.10017	163	164 ± 36
5	3.01	2.98	Methyljuglone diglycoside	232, 298	514.16805	514.16865	188, 351	98 ± 26
6	3.32	3.29	Dihydromyricetin	232, 269, 298	320.05257	320.05322	71, 97, 109, 139, 153, 165, 183	125 ± 38
7	3.39	3.34	Ellagic acid glycoside	253, 361	464.05901	464.05910	172, 216, 244, 284, 301	661 ± 155
8	3.66	3.63	Myricetin-glycoside	208, 225, 257, 357	480.08949	480.09040	179, 271, 316	1154 ± 294
9	3.72	3.67	Hexahydroxyflavone-galloyl-glycoside	200, 226, 265, 298, 359	632.10042	632.10136	109, 137, 151, 179, 317, 479	664 ± 155
10	3.83	3.80	Tetrahydroxyflavone	264	286.04711	286.04774	121, 137,165	118 ± 32
11	3.86	3.84	Unknown	235, 272, 278	348.08403	348.08452	329	27 ± 5
12	3.93	3.90	Ellagic acid	200, 254, 368	302.00557	302.00627	257, 271, 299	4390 ± 1041
13	4.04	4.01	Hyperoside	215, 255, 356	464.09474	464.09548	255, 271, 300, 301	8357 ± 2151
14	4.11	4.08	Galloylhyperoside	226, 264, 257	616.10542	616.10644	151, 301, 463	19,141 ± 4914
15	4.28	4.25	Methyljuglone glycoside	228, 309, 327, 342	352.11540	352.11582	189	1601 ± 353
16	4.33	4.31	Dimethylellagic acid glycoside	246, 370	492.08986	492.09040	270, 298, 313, 328, 476	1271 ± 333
17	4.42	4.39	Kaempferol-galloyl-glycoside	265, 346	600.11073	600.11153	125, 151, 169, 285, 313	349 ± 80
18	4.68	4.64	Quercetin glycoside	254, 357	464.0949	464.09548	107, 151, 179, 255, 271, 300, 301	359 ± 74

Table 1. *Cont.*

#	RT_{TIC}	RT_{UV}	Compound	UV λ_{max} (nm) *	Exact Mass Detected	Exact Mass Calculated	Characteristic MS/MS Values	Peak Area **
19	4.79	4.76	Methylellagic acid	250, 373	316.02181	316.02192	300	152 ± 41
20	4.92	4.89	Hydroxybenzoylhyperin	256, 358	584.11659	584.11661	107, 151, 179, 255, 271, 301, 463	194 ± 46
21	5.17	5.14	Methyljuglone	216, 226, 317, 333, 349,428	190.06185	190.06300	115, 130, 145, 161, 171, 174, 188	-
22	5.25	5.22	Quercetin glycoside gallate	257, 290, 298, 348	616.10603	616.10644	189, 299, 507	464 ± 95
23	5.37	5.34	Quercetin	255, 371	302.04225	302.04266	107, 151, 179	480 ± 120
24	5.70	5.67	Dimethylellagic acid	247, 377	330.03716	330.03757	299, 314	981 ± 249

* The extracts were dilute, which can influence the maxima observed. ** Peak areas were integrated from the photodiode array data at 280 nm and are averages from the three extract replicates; error is calculated from the standard deviations. The peak areas are shown for the peaks with a signal/noise ratio >2. - means that the signal/noise ratio for the compound was <2 and the peak area has not been determined. *** The compound cannot be detected by photodiode array detection.

Table 2. Metabolic profile of the lab-grown propagated *Drosera rotundifolia*. Identified based on literature [21–25].

#	RT_{TIC}	RT_{UV}	Compound	UV λ_{max} (nm) *	Exact Mass Detected	Exact Mass Calculated	Characteristic MS/MS Values	Peak Area **
1	0.59	-	Quinic acid	-	192.06188	192.06339	-	***
2	1.28	1.24	Monogalloyl glucose (β-)	213, 275	332.07436	332.07435	125, 151, 169, 211, 271	281 ± 9
3	2.57	2.55	Coumaric acid glycoside	295	326.10030	326.10017	163	250 ± 7
4	3.04	3.01	Methyljuglone diglycoside Coumaric acid glycoside isomer	275, 317	514.16817 326.09993	514.16865 326.10017	188, 351 117, 145, 163, 187	146 ± 13
5	3.24	3.21	Two co-eluting unknowns	238, 271	482.10536 370.12584	482.10605 370.12639	57, 125, 151, 179, 193, 283, 463 59, 71, 85, 101, 143, 159, 171, 189, 207	113 ± 2
6	3.41	3.35	Ellagic acid glycoside	253, 361	464.05901	464.05910	132, 145, 172, 216, 244, 284, 301	189 ± 17
7	3.66	3.63	Myricetin-glycoside	255, 305, 311, 349, 356	480.08949	480.09040	124, 151, 179, 271, 287, 316	166 ± 5
8	3.95	3.92	Ellagic acid	254, 369	302.00594	302.00627	257, 271, 299	1305 ± 90
9	4.04	4.01	Hyperoside	253, 357	464.09459	464.09548	107, 151, 179, 255, 271, 300, 301	557 ± 27
10	4.09	4.06 4.08	Galloylhyperoside Hyperoside	255, 349 256, 358	616.1058 5464.09480	616.10644 464.09548	107, 151, 179, 255, 271, 300, 301	158 ± 32
11	4.28	4.25	Methyljuglone glycoside	228, 309, 327, 342	352.11537	352.11582	189	179 ± 132
12	4.35	4.32	Dimethylellagic acid glycoside	246, 370	492.08943	492.09040	270, 298, 313, 328, 476	1435 ± 184
13	4.92	-	Hydroxybenzoylhyperin	-	584.11775	584.11661	151, 179, 215, 243, 271, 287, 301, 316	-
14	5.17	5.14	Methyljuglone	251, 349, 428	190.06183	190.06300	115, 130, 145, 161, 171, 174, 188	-

Table 2. *Cont.*

#	RT_{TIC}	RT_{UV}	Compound	UV λ_{max} (nm) *	Exact Mass Detected	Exact Mass Calculated	Characteristic MS/MS Values	Peak Area **
15	5.24	5.22	Syringetin glycoside	251, 290	508.12154	508.12170	125, 151, 179, 217, 275, 285, 303, 345, 447, 465	37 ± 3
16	5.55	5.52	Spinatoside	257	522.10103	522.10096	185, 229, 257, 285, 300, 313, 328, 343, 491, 506	-
17	5.70	5.67	Dimethylellagic acid	247, 374	330.03703	330.03757	299, 314	379 ± 38

* The extracts were dilute, which can influence the maxima observed. ** Peak areas were integrated from the photodiode array data at 280 nm and are averages from three extract replicates; error is calculated from the standard deviations. The peak areas are shown for the peaks with a signal/noise ratio >2. - means that the signal/noise ratio for the compound was <2 and the peak area has not been determined. *** The compound cannot be detected by photodiode array detection.

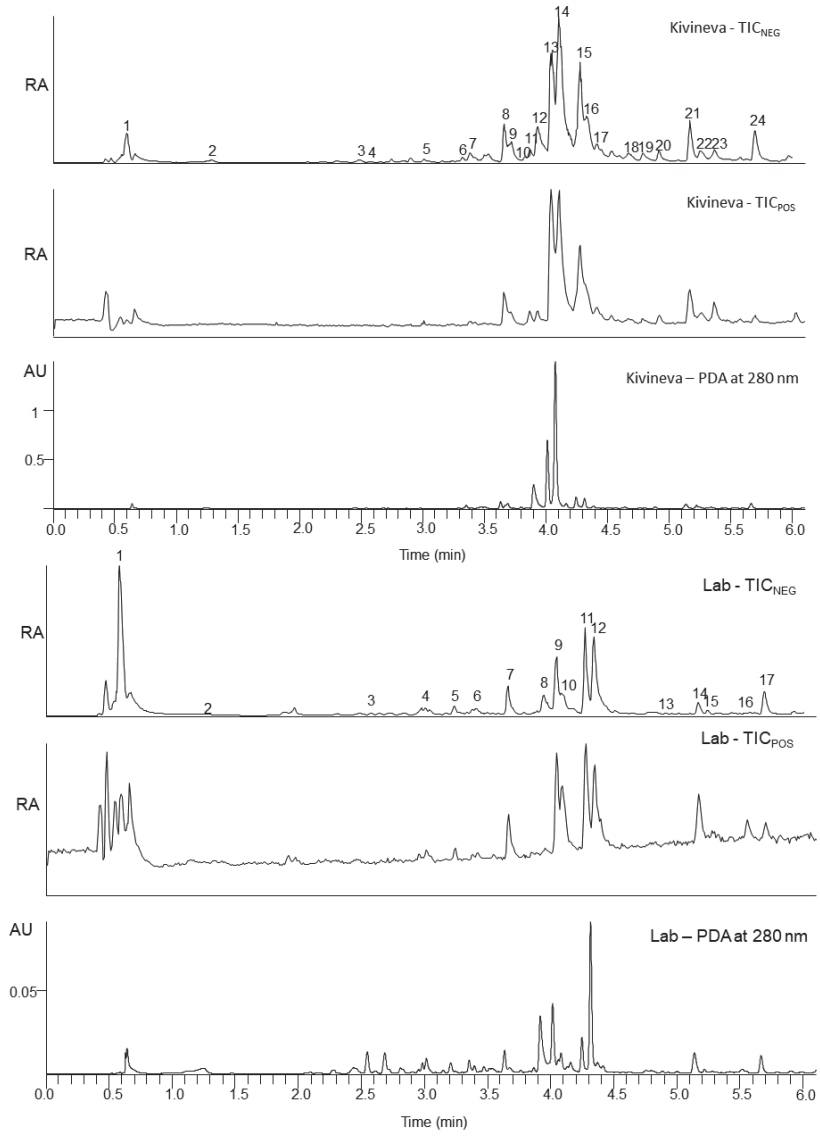

Figure 6. The total ion chromatograms (TIC) in positive and negative ionization and photodiode array (PDA) chromatogram at 280 nm for field-grown sundew (Kivineva mire) on the top and lab-grown propagated sundew (Lab) on the bottom.

In Figure 7, 12 compounds found in both extracts are shown. The majority of the compounds are flavonoids, ellagic acid derivatives, or naphthoquinones. Two methylju-glone glycosides are not shown because the methyl group can be attached to the C-7 (7-methyljuglone) or to C-2 (plumbagin).

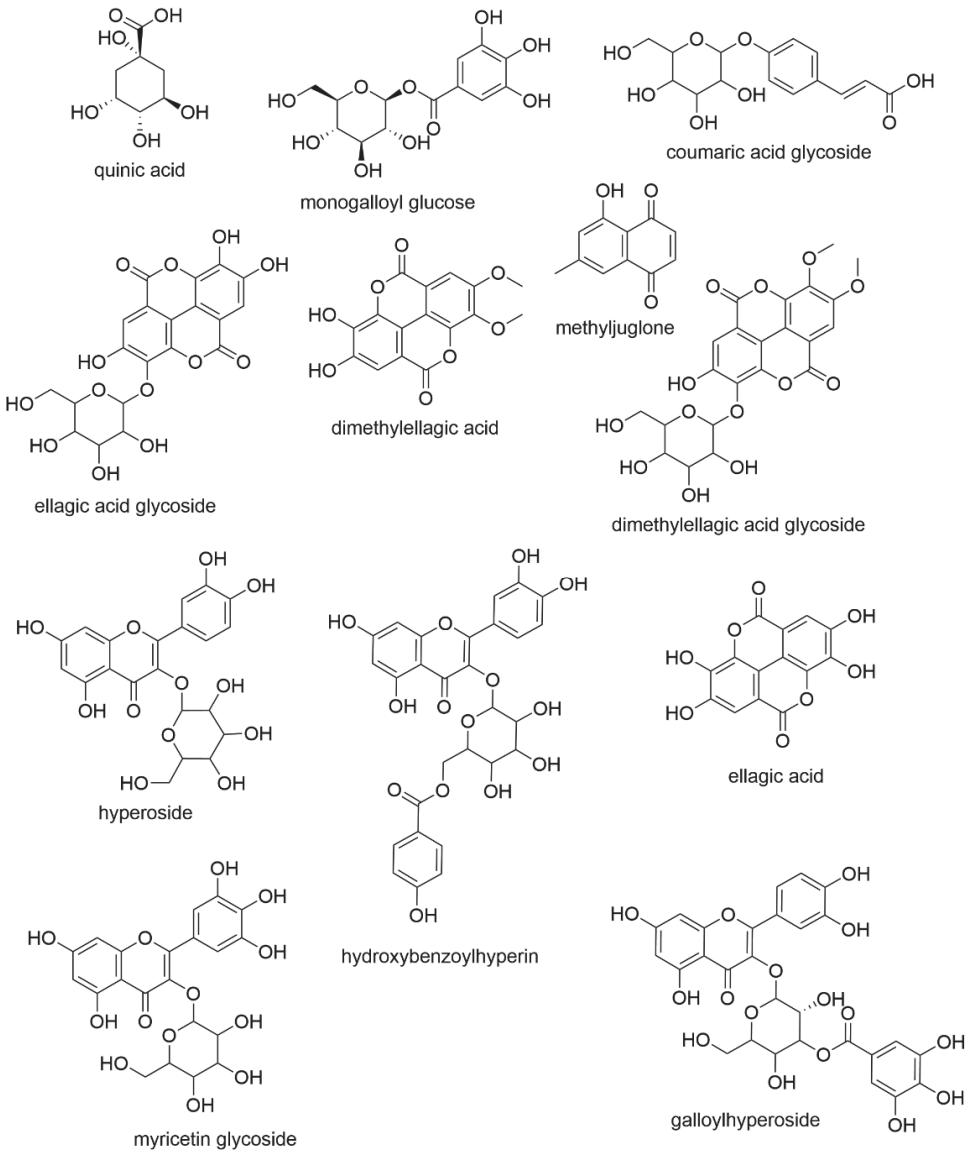

Figure 7. The compounds identified in both field-grown and lab-grown sundew ethanol extracts apart from two methyljuglone glycosides. The positions of the galloyl, benzoyl, and hexose groups are only indicative and could be any free OH-group in the structure.

Quinic acid is a cyclic polyol that has widely been found in plants. Monogalloyl glucose consists of gallic acid and glucose. Hydrolysable tannins (HTs) are a structurally complex group of plant secondary metabolites, which can be divided into three subclasses: simple gallic acid derivatives, gallotannins, and ellagitannins [26]. HTs contain various interesting bioactive properties including antioxidant, antibacterial, antiviral, and anti-cancer activity [27,28]. As well as gallic acid and ellagic acid, coumaric acid is another phenolic acid and is very common in plants. Phenolic acids have been reported with antioxidant, antimicrobial, and antitumor properties [29]. Flavonoids are an important group of secondary metabolites and plant polyphenols, which are, e.g., responsible for

the pigmentation of plants. While flavonoids are not a uniform group, they commonly contain antioxidant, anti-inflammatory, antimicrobial, and antiviral activities [10,30]. Both field-grown and lab-grown extracts contained flavonoids; however, the field-grown sundew was observed to contain significantly higher amounts, which may explain the large difference in the coloration of the field-grown and lab-grown sundew (Figure 2). Of the compounds that were observed from each sundew extract only coumaric acid glycoside and dimethyl ellagic acid glycoside were observed in higher amounts from the lab extract. Naphthoquinones have generally been considered responsible for many of the therapeutic activities in sundew, and they also seem to be more abundant in the field-grown extract. In particular, 7-methyljuglone has been concluded to have antibacterial, antifungal, antiviral, anticancer, and anti-inflammatory properties [31] and it has been observed in Finnish *D. rotundifolia* [16]. While methyljuglone diglycoside has a higher peak area in lab-grown sundew extract, there are two co-eluting compounds, which affect the determined value.

Antioxidants are of use in the food processing industry as preservatives and more recently as active films for packaging and as edible coatings [32]. However, it is important to note that the dosages and possible toxicological effects must be studied in detail before higher consumption of plant materials [32]. Material availability of the field-grown sundew is an issue the needs to be solved before wider use can be considered. The low antioxidant properties of the propagated sundew tissues are related to their chemical characteristics as they contain a lower amount and number of simple phenolics and polyphenols than the field-grown sundews. The modest antioxidant potential of the in vitro grown tissue is a challenge that restrains the potential of further development of the propagation technique unless an appropriate method to improve it is developed. One interesting method to potentially increase the antioxidant activity of the propagated sundew tissue could be a drastic reduction of the mineral content in the growing media. Jadczak et al. [15] found that when the mineral content of the growing media was reduced by 75%, the sundew plants produced the greatest number of long roots, had the highest weight, and were able to produce red coloration in the glandular tentacles. Thus, as the plant would be morphologically more like the field-grown sundew, it could potentially include more phenolic compounds, which are often rich in color and well known for their antioxidant potential. On the other hand, it was fascinating that the propagated sundews showed almost equally high antiviral effects against enterovirus strains CVA9 and CVB3 in high concentrations. With smaller concentrations, the field-grown sundew was more effective, which corresponds with the observation that it contains more effective plant polyphenols. Tannins and other polyphenols have indeed been previously identified with antiviral activities. For example, Lin et al. [20] found that tannins chebulagic acid and punicalagin significantly reduced the coxsackievirus infectivity by both inactivating cell-free viral particles and inhibiting viral binding. In another study by Du et al. [33], resveratrol-loaded nanoparticles were successful in inhibiting enterovirus replication and protecting rhabdosarcoma cells in vitro.

In conclusion, freezing is the best way to maintain the metabolite profile of the sundew extracts, while drying methods compromise the extract profile stability. Antioxidant activity was higher in field-grown extracts and in relation to the secondary metabolite content of the extracts. In higher concentrations, both lab-grown and field-grown extracts are effective against enteroviruses, but the field-grown sundew extract is more effective in smaller concentrations. To increase the antioxidant (this study) and antibacterial [8] activity, the polyphenolic secondary metabolite content of the lab-grown extracts should be increased significantly for it to be considered an effective alternative to the field-grown round-leaved sundew.

3. Materials and Methods

3.1. Sundew Material, Growth, and Extraction

Sundews grown on peatlands in western Finland and in vitro propagated sundews in a laboratory environment were used in this study. Round-leaved sundew plants

(*Drosera rotundifolia*) were collected (26 June 2018) from two peatlands (Lehtolamminneva, 62°6.01′ E 22°57.22′ and Kivineva N 61°57.77′ E 23°23.98′) in Western Finland and stored in a freezer (−20 °C) until extracted and tested.

The in vitro propagated sundew biomass was grown at room temperature (22–25 °C) under continuous fluorescent room light. Seeds of field-grown *D. rotundifolia* were surface sterilized by placing them within folded filter paper and soaking the package first in 70% ethanol for ca. 30 s, followed by 5% sodium hypochlorite for 10–15 min, and rinsing three times in sterile distilled H_2O. The surface-sterilized seeds were placed on ⌀9 cm Petri dishes with a modified half-strength Murashige-Skoog (MS) [34] growing media. The plates contained 2.2 g/L of MS basal medium, 0.039 mg/L $FeSO_4 \cdot 7H_2O$, 100 mg/L myoinositol, 0.1 mg/L benzyl aminopurine, 0.05 mg/L 1-naphthalene acetic acid, 30 g/L sucrose, and 6.5 g/L of agar. The pH was adjusted to 5.8. Inoculated plates were sealed with parafilm and incubated at room temperature. During the germination, the light cycle was 16 h of light and 8 h of darkness, but, after germination, they were grown under continuous room light (fluorescent lamp). To grow the plant tissue continuously it was repeatedly divided under sterile conditions onto a new $\frac{1}{2}$ MS agar medium without the addition of benzyl aminopurine or 1-naphthalene acetic acid.

For the antioxidant assays, the sundew samples were extracted by grinding 1.0 g fresh weight of plant biomass per 7.0 mL of 99.5% ethanol and incubating the extract in test tubes for one hour by mixing the vials with using a vortex several times during the extraction. The ethanol extract was stored in freeze (−20 °C) until analyzed.

Propagated sundew tissues were weighed before and after transferring to a new medium to define the growth rate under laboratory conditions. The amount of sundew yield at laboratory scale on ⌀14 cm Petri dishes and 125 mL pots were compared by starting the growth with 4–8 pieces of 0.3 g sundew tissues and weighing the yield after 6 weeks growth on six Petri dishes and six pots. Furthermore, to study whether natural daylight in summer would affect the antioxidant properties of the propagated sundew tissues, Petri dishes with sundew tissues were moved outside for two days under ambient daylight (day temperature +20 °C), and extracted for the FRAP testing after that. The effect of nutrient availability of the growing medium on the FRAP activity of the propagated sundew tissue was tested by decreasing the nutrient content to 30% of the normal (1/2 MS) and by replacing all the nutrients with soil water squeezed from *Sphagnum* moss collected from the natural peatland site. The propagated tissue was also moved to a natural peatland just beside naturally grown sundew plants for two weeks to monitor the survival in the natural environment.

3.2. The Effects of the Drying of the Plant Material on the Properties of the Extract

To elucidate the effect of different drying methods on the properties of sundew plant material the extracts of differently dried sundew tissues were compared with HPLC. Extract of the frozen (–20 °C) sundew tissue was compared with extracts from sundews dried at room temperature (43 h), herbal-dryer (+45 °C, 27 h), freeze-dryer (sample kept frozen, 43 h), or oven dried (+105 °C, 24 h).

3.3. Antioxidant Activity

3.3.1. FRAP (Ferric Reducing Antioxidant Power)

Ferric reducing antioxidant power (FRAP) assay is based on single-electron transfer and measures the ability of an antioxidant to reduce ferric (FeIII) to ferrous (FeII) ion [35]. Samples, with three technical replicates in a 96-well format, were used in the assay as described by Vaario et al. [36]. The samples were mixed with 20 mM $FeCl_3 \cdot 6H_2O$ and 10 mM 2,4,6-tris (2-pyridyl)-s-triazine (TPTZ) (both from Sigma-Aldrich Chemie GmbH, Steinheim, Germany) in 300 mM acetate buffer pH 3.6. The absorbance was measured at 594 nm with a fluorescence microplate reader (Varioskan Flash, Thermo Scientific) after the formation of the ferrous-tripyridyltriazine complex in the reaction mixture. $FeSO_4 \cdot 7H_2O$ (Sigma-Aldrich Chemie GmbH, Steinheim, Germany) was used as a standard compound

and L(+)-ascorbic acid (150 μM and 800 μM) (VWR Chemicals) as a control and the results are expressed as μmol Fe(II) equivalents per 100 g.

3.3.2. ORAC (Oxygen Radical Absorbance Capacity)

Oxygen Radical Absorbance Capacity (ORAC) assay is based on hydrogen atom transfer and measures the reduction in fluorescence signal caused by the oxidative dissociation of fluorescein in the presence of peroxyl radicals (R-O-O•) [37,38]. The inhibition of the fluorescein breakdown indicates the antioxidant's protective ability. The assay was carried out as described by Vaario et al. [36], with two technical replicates, by mixing the sample in 0.075 M phosphate buffer pH 7.5 (Merck) with 8.16×10^{-5} mM fluorescein and 2,2′-Azobis(2-methylpropionamidine) dihydrochloride (both from Sigma-Aldrich Chemie GmbH, Steinheim, Germany). Trolox (vitamin E analog, (±)-6-Hydroxy-2,5,7,8-tetramethylchromane-2-carboxylic acid) (Sigma-Aldrich Chemie GmbH, Steinheim, Germany) was used as a standard compound and the results are expressed as Trolox equivalents (μmol TE per 100 g).

3.3.3. H_2O_2 Scavenging

The hydrogen peroxide (H_2O_2) scavenging activity was determined using a method modified from Hazra et al. [39] and Jiang et al. [40]. The assay was carried out according to Vaario et al. [36]. An aliquot of 2 mM H_2O_2 (Merck KGaA, Darmstadt, Germany) was added to the reaction mixture with the sample and a mixture containing 2.56 mM ammonium ferrous (II) sulfate (BDH Prolabo) in 0.25 mM H_2SO_4 (Merck KGaA) and 27.8 μM xylenol orange disodium salt (Sigma-Aldrich Chemie GmbH, Steinheim, Germany) in 4.4 mM sorbitol (D(-)-sorbitol, AppliChem GmbH). After 30 min incubation, the absorbance of violet-colored ferric-xylenol orange complexes at 560 nm was measured. The assay measures the ability of the sample to scavenge H_2O_2 and prevent the oxidation of Fe(II) to Fe(III), which is indicated by the formation of a ferric–xylenol orange complex. The inhibition of the oxidation is expressed as an inhibition % of the reaction and the samples with 100% inhibition activity will remain yellowish. Sodium pyruvate (Sigma-Aldrich) was used as a reference compound.

3.4. Antiviral Properties

Adenocarcinomic human alveolar basal epithelial (A549) cells, coxsackievirus B3 (CVB3; Nancy strain, ATCC), and coxsackievirus A9 (CVA9; Griggs strain, ATCC) were used in the assay. CVA9 and CVB3 were produced and purified as previously described [17,41]. The antiviral activity of the round-leaved sundews (field-grown and in vitro propagated) against CVB3 and CVA9 was determined using a cytopathic effect (CPE) inhibition assay, modified from Schmidtke et al. [42]. Briefly, A549 cells were cultured in 96-well flat-bottomed microtiter plates (VWR International) at a density of 12,000 cells/well in DMEM supplemented with 10% FBS, 1% GlutaMAX, and 1% penicillin/streptomycin antibiotics for 24 h at +37 °C. The following day, CVB3 and CVA9 with a virus titer of 2×10^5 PFU/mL and 2×10^6 PFU/mL respectively, were pre-treated with different concentrations of field-grown and lab-grown sundews (10%, 5%, 1%, and 0.1%, *v/v*) for 1 h at +37 °C. The virus-compound mixture was further diluted and added to cells for 48 h incubation in a humidified 5% CO_2 incubator at +37 °C, to attain MOI of 0.1 and 1 for CVB3 and CVA9, respectively. Virus control (the absence of the compound) and mock infection (the absence of the virus and compound) were used as two controls in the assay. The development of CPE was monitored using light microscopy. After 48 h incubation, cells were washed twice with PBS, before fixing and staining them for 10 min using CPE dye (0.03% crystal violet, 2% ethanol, and 36.5% formaldehyde). Following the staining, cells were washed twice with water and later lysed using a lysis buffer (0.8979 g of sodium citrate and 1M HCl in 47.5% ethanol) to elute the crystal violet. The absorbance of the viable cells was measured spectrophotometrically at 570 nm using the PerkinElmer VICTOR^{TM} X4 multilabel reader. The samples were tested in replicates of nine and the controls in replicates of six. The cytotoxicity of the round-leaved

sundews (field-grown and in vitro propagated) at different concentrations (10%, 5%, and 1%, *v/v*) on A549 cells for 24 h was also assessed using CPE Inhibition assay, where a mock infection was used as a control for the experiment.

3.5. Stability Analysis by HPLC-DAD

The ethanol extracts of sundew were analyzed with HPLC-DAD (Shimadzu Prominence Liquid Chromatograph system, Shimadzu, Kioto, Japan) with LC-20AP pumps, degasser, autosampler, column oven (+25 °C), and a Prominence Photodiode array SPD-M20A detector (Shimadzu, USA). The HPLC separation was performed in a Waters XBridge C18 reverse-phase column (4.6 × 150 mm, 5 µm) (Waters Corporation, Milford, MA, USA), using (A) H_2O-phosphoric acid (100:0.1 *v/v*): (B) Methanol (LiChrosolv®, Merck KGaA, Germany) gradient elution A:B (0.01 min 65:35; 4.00 min 55:45; 7.00 min 50:50; 14.00 min 50:50; 25.00 min 45:55; 31.00 min 65:35; 32.00 min 65:35 stop) at a flow rate of 0.8 mL/min. The UV absorption of the eluates was monitored using the DAD at 254 nm. The injection volume of the extract solution was 10 µL.

3.6. Metabolic Profiling by UPLC-DAD-MS/MS

The qualitative and quantitative UPLC-DAD-ESI-TQ-MS/MS analyses were performed according to Engström et al. [43,44]. The ultrahigh-resolution mass spectrometric analyses were performed using a UPLC-DAD-ESI-QOrbitrap-MS/MS consisting of an Acquity UPLC system (Waters Corp., Milford, MA, USA) coupled with a quadrupole-Orbitrap mass spectrometer (QExactiveTM, Thermo Fisher Scientific GmbH, Bremen, Germany). The column and chromatographic conditions were the same as in the UPLC-DAD-ESI-TQ-MS/MS analyses. Negative and positive ionizations were used in the heated ESI source. In negative ionization, the spray voltage was set at −3.0 kV, sheath gas (N_2) flow rate at 60, auxiliary gas (N_2) flow rate at 20, sweep gas flow rate at 0, capillary temperature at +380 °C, S-lens RF level at 60, and in-source collision-induced dissociation (CID) at 30 eV. The parameters were similar in positive ionization, except the spray voltage was set at 3.80 kV. Full-scan MS analyses with a resolution of 140,000 were performed both in the negative and positive ion mode. The mass range of orbitrap was *m/z* 150–2250 and the automatic gain control (AGC) target 3×10^6. MS/MS analyses, namely, dd-MS2 (TopN), were performed in the negative ion mode and the parameters were the following: for full MS, resolution 35,000 and AGC target 3×10^6, and for TopN 3, stepped normalized collision energies 30, 50, and 80 eV, resolution 17,500 and AGC target 1×10^5. The calibration was performed using Pierce ESI Negative Ion Calibration Solution and Pierce ESI Positive Ion Calibration Solution (Thermo Fischer Scientific Inc., Waltham, MA, USA). The data was processed with Thermo Xcalibur Qual Browser software (Version 3.0.63, Thermo Fisher Scientific Inc., Waltham, MA, USA).

3.7. Statistical Methods

The differences between the mean values were assessed using a one-way analysis of variance (ANOVA). Statistical analyzes were performed with the IBM SPSS statistics software package (v. 27.0) (IBM, Armonk, NY, USA), except for the antiviral data, which was analyzed using GraphPad PRISM 5 (GraphPad Software, San Diego, CA, USA).

4. Conclusions

Round-leaved sundew (*Drosera rotundifolia*) is a small plant, which has been used to treat pulmonary diseases and coughs. It owes its therapeutic properties to secondary metabolites, namely, naphthoquinones and flavonoids. Because of the small size of the plant, it is laborious to obtain the required amounts from natural stands to meet the needs of pharmaceutical, food, and cosmetics industries, which need high amounts of safe and broadly acting bioactive secondary metabolites. Therefore, different cultivation methods, such as in vitro propagation, have been of interest. In this study, we compared the in vitro propagated sundew tissue with the field-grown plant material for their antioxidant and

antiviral properties, as well as their metabolic profiles. Field-grown sundew showed significantly higher antioxidant potential whereas the antiviral properties were similar in higher concentrations. Field-grown sundew also contained higher amounts and numbers of potentially effective secondary metabolites in its metabolic profile. We also showed that different drying methods significantly decrease the metabolic composition of the sundew extract and that only freezing could maintain the metabolic profile. Before the in vitro propagated sundew tissue can be considered as an effective alternative to field-grown sundew, the secondary metabolite content and bioactive potential of the in vitro propagated tissue needs to be increased. One possible topic for future studies could be a more significant reduction in the mineral content of the growth media.

Author Contributions: Conceptualization, J.T., N.S., L.K., V.M. and T.S.; Data curation, J.T., D.R., M.K., V.M. and T.S.; Formal analysis, J.T., D.R. and M.K.; Funding acquisition, J.T., N.S., L.K., V.M. and T.S.; Investigation, J.T., D.R., M.K., V.M. and T.S.; Methodology, J.T., D.R., M.K., V.M. and T.S.; Project administration, L.K. and T.S.; Resources, M.K., N.S., L.K., V.M. and T.S.; Supervision, M.K., L.K., V.M. and T.S.; Validation, M.K., V.M. and T.S.; Visualization, J.T., D.R. and T.S.; Writing—original draft, J.T. and T.S.; Writing—review and editing, J.T., D.R., M.K., N.S., L.K., V.M. and T.S. All authors have read and agreed to the published version of the manuscript.

Funding: This research was funded by The European Agricultural Fund for Rural Development: Liaison Entre Actions de Développement de l'Économie Rurale (LEADER) for project Innoherb—new business opportunities from mire herbs in Pohjois-Satakunta, Western Finland (https://www.luke.fi/en/projektit/innoherb/, accesses on 18 April 2021). In addition, antiviral activities were examined under the Business Finland corona-co-creation funded project 'Antiviral fibers—pilot with extracts from Finnish forests [grant: 40699/31/2020]. This study was also funded by Luke's strategic research funding and J. Tienaho received a personal grant from 'Suoviljelysyhdistys ry'.

Institutional Review Board Statement: Not applicable.

Informed Consent Statement: Not applicable.

Data Availability Statement: The data presented in this study are available on request from the corresponding author.

Acknowledgments: We thank Hannu Nousiainen for the picture (Figure 2B) of round-leaved sundew at *Sphagnum* peatland and Ilari Kuukkanen and Anne Koivuniemi for their kind help in the metabolomic profiling. Anneli Käenmäki, Eeva Pihlajaviita, and Hanna Leppälammi are acknowledged for their proficient help with laboratory-grown sundew, extractions, antioxidant analyses, and HPLC runs. We also thank Noora Tienaho for their kind help with the statistical analysis.

Conflicts of Interest: The authors declare no conflict of interest. The funders had no role in the design of the study; in the collection, analyses, or interpretation of data; in the writing of the manuscript, or in the decision to publish the results.

Sample Availability: The sundew extracts and standards used in the UPLC-DAD-ESI-TQ-MS/MS analyses are not available from the authors.

References

1. Matušíková, I.; Salaj, J.; Moravčíková, J.; Mlynarova, L.; Nap, J.P.; Libantova, J. Tentacles of *in vitro*-grown round-leaf sundew (*Drosera rotundifolia* L.) show induction of chitinase activity upon mimicking the presence of prey. *Planta* **2005**, *222*, 1020–1027. [CrossRef]
2. Baranyai, B.; Joosten, H. Biology, ecology, use, conservation and cultivation of round-leaved sundew (*Drosera rotundifolia* L.): A review. *Mires Peat* **2016**, *18*, 1–28. [CrossRef]
3. Baranyai, B.; Bäcker, C.; Reich, C.; Lindequist, U. The production of 7-methyljuglone, plumbagin and quercetin in wild and cultivated *Drosera rotundifolia* and *Drosera intermedia*. *Mires Peat* **2016**, *18*, 1–8. [CrossRef]
4. Egan, P.A.; van der Kooy, F. Phytochemistry of the carnivorous sundew genus *Drosera* (Droseraceae)–future perspectives and ethnopharmacological relevance. *Chem. Biodivers* **2013**, *10*, 1774–1790. [CrossRef]
5. Paper, D.H.; Karall, E.; Kremser, M.; Krenn, L. Comparison of the anti-inflammatory effects of *Drosera rotundifolia* and *Drosera madagascariensis* in the HET-CAM assay. *Phytother. Res.* **2005**, *19*, 323–326. [CrossRef]
6. Kačániová, M.; Ďurechová, D.; Vuković, N.; Kántor, A.; Petrová, J.; Hleba, L.; Vatľák, A. Antimicrobial activity of *Drosera rotundifolia* L. *J. Anim. Sci. Biotechnol.* **2015**, *47*, 366–369. [CrossRef]

7. Durechová, D.; Kacániová, M.; Terentjeva, M.; Petrová, J.; Hleba, L.; Kata, I. Antibacterial activity of *Drosera rotundifolia* L. against gram-positive and gram-negative bacteria. *J. Microbiol. Biotechnol. Food Sci.* **2016**, *5*, 20. [CrossRef]
8. Poikulainen, E.; Tienaho, J.; Sarjala, T.; Santala, V. A panel of bioluminescent whole-cell bacterial biosensors for the screening for new antibacterial substances from natural extracts. *J. Microbiol. Methods* **2020**, *178*, 106083. [CrossRef]
9. Lieberherr, C.; Zhang, G.; Grafen, A.; Singethan, K.; Kendl, S.; Vogt, V.; Maier, J.; Bringmann, G.; Schneider-Schaulies, J. The plant-derived naphthoquinone Droserone inhibits in vitro measles virus infection. *Planta Med.* **2017**, *83*, 232–238. [CrossRef] [PubMed]
10. Lalani, S.; Poh, C.L. Flavonoids as antiviral agents for Enterovirus A71 (EV-A71). *Viruses* **2020**, *12*, 184. [CrossRef]
11. Ghate, N.B.; Chaudhuri, D.; Das, A.; Panja, S.; Mandal, N. An antioxidant extract of the insectivorous plant *Drosera burmannii* Vahl. alleviates iron-induced oxidative stress and hepatic injury in mice. *PLoS ONE* **2015**, *10*, e0128221. [CrossRef]
12. Banasiuk, R.; Kawiak, A.; Królicka, A. In vitro cultures of carnivorous plants from the *Drosera* and *Dionaea* genus for the production of biologically active secondary metabolites. *BioTechnologia* **2012**, *93*, 87–96. [CrossRef]
13. Hämet-Ahti, L.; Suominen, J.; Ulvinen, T.; Uotila, P. (Eds.) *Retkeilykasvio (Field Flora of Finland)*; Finnish Museums of Natural History; Botanical Museum: Helsinki, Finland, 1998.
14. Galambosi, B.; Galambosi, Z.; Repcák, M. Growth, yield and secondary metabolite production of *Drosera* species cultivated in peat beds in Finland. *Suo* **2000**, *51*, 47–57.
15. Jadczak, P.; Kulpa, D.; Zbrojewska, A. In Vitro Micropropagation of *Drosera rotundifolia*. *World Sci. News* **2017**, *66*, 75–85.
16. Kämäräinen, T.; Uusitalo, J.; Jalonen, J.; Laine, K.; Hohtola, A. Regional and habitat differences in 7-methyljuglone content of Finnish *Drosera rotundifolia*. *Phytochemistry* **2003**, *63*, 309–314. [CrossRef]
17. Ruokolainen, V.; Domanska, A.; Laajala, M.; Pelliccia, M.; Butcher, S.J.; Marjomäki, V. Extracellular albumin and endosomal ions prime enterovirus particles for uncoating that can be prevented by fatty acid saturation. *J. Virol.* **2019**, *93*. [CrossRef] [PubMed]
18. Hyöty, H. Viruses in type 1 diabetes. *Pediatr. Diabetes* **2016**, *17*, 56–64. [CrossRef]
19. Linnakoski, R.; Reshamwala, D.; Veteli, P.; Cortina-Escribano, M.; Vanhanen, H.; Marjomäki, V. Antiviral agents from fungi: Diversity, mechanisms and potential applications. *Front. Microbiol.* **2018**, *9*, 2325. [CrossRef] [PubMed]
20. Lin, C.J.; Liu, C.H.; Wang, J.Y.; Lin, C.C.; Li, Y.F.; Richardson, C.D.; Lin, L.T. Small molecules targeting coxsackievirus A16 capsid inactivate viral particles and prevent viral binding. *Emerg. Microbes Infect.* **2018**, *7*, 1–11. [CrossRef]
21. Tuominen, A. Tannins and Other Polyphenols in *Geranium sylvaticum*: Identification, Intraplant Distribution and Biological Activity. Ph.D. Thesis, University of Turku, Turku, Finland, 2017.
22. Zehl, M.; Braunberger, C.; Conrad, J.; Crnogorac, M.; Krasteva, S.; Vogler, B.; Beifuss, U.; Krenn, L. Identification and quantification of flavonoids and ellagic acid derivatives in therapeutically important *Drosera* species by LC–DAD, LC–NMR, NMR, and LC–MS. *Anal. Bioanal. Chem.* **2011**, *400*, 2565–2576. [CrossRef]
23. Braunberger, C.; Zehl, M.; Conrad, J.; Fischer, S.; Adhami, H.R.; Beifuss, U.; Krenn, L. LC–NMR, NMR, and LC–MS identification and LC–DAD quantification of flavonoids and ellagic acid derivatives in *Drosera peltata*. *J. Chromatogr. B* **2013**, *932*, 111–116. [CrossRef]
24. Jia, X.; Luo, H.; Xu, M.; Zhai, M.; Guo, Z.; Qiao, Y.; Wang, L. Dynamic changes in phenolics and antioxidant capacity during pecan (*Carya illinoinensis*) kernel ripening and its phenolics profiles. *Molecules* **2018**, *23*, 435. [CrossRef]
25. Marczak, Ł.; Kawiak, A.; Łojkowska, E.; Stobiecki, M. Secondary metabolites in in vitro cultured plants of the genus *Drosera*. *Phytochem. Anal.* **2005**, *16*, 143–149. [CrossRef] [PubMed]
26. Salminen, J.P.; Karonen, M. Chemical ecology of tannins and other phenolics: We need a change in approach. *Funct. Ecol.* **2011**, *25*, 325–338. [CrossRef]
27. Landete, J.M. Ellagitannins, ellagic acid and their derived metabolites: A review about source, metabolism, functions and health. *Food Res. Int.* **2011**, *44*, 1150–1160. [CrossRef]
28. Yang, B.; Liu, P. Composition and biological activities of hydrolyzable tannins of fruits of *Phyllanthus emblica*. *J. Agric. Food Chem.* **2014**, *62*, 529–541. [CrossRef]
29. Heleno, S.A.; Martins, A.; Queiroz, M.J.R.; Ferreira, I.C. Bioactivity of phenolic acids: Metabolites versus parent compounds: A review. *Food Chem.* **2015**, *173*, 501–513. [CrossRef] [PubMed]
30. Karak, P. Biological activities of flavonoids: An overview. *Int. J. Pharm. Sci. Res.* **2019**, *10*, 1567–1574. [CrossRef]
31. Mbaveng, A.T.; Kuete, V. Review of the chemistry and pharmacology of 7-methyljugulone. *Afr. Health Sci.* **2014**, *14*, 201–205. [CrossRef]
32. Lourenço, S.C.; Moldão-Martins, M.; Alves, V.D. Antioxidants of natural plant origins: From sources to food industry applications. *Molecules* **2019**, *24*, 4132. [CrossRef]
33. Du, N.; Li, X.H.; Bao, W.G.; Wang, B.; Xu, G.; Wang, F. Resveratrol-loaded nanoparticles inhibit enterovirus 71 replication through the oxidative stress-mediated ERS/autophagy pathway. *Int. J. Mol. Med.* **2019**, *44*, 737–749. [CrossRef]
34. Murashige, T.; Skoog, F. A revised medium for rapid growth and bioassays with tobacco tissue cultures. *Physiol. Plant.* **1962**, *15*, 473–497. [CrossRef]
35. Benzie, I.F.; Strain, J.J. The ferric reducing ability of plasma (FRAP) as a measure of "antioxidant power": The FRAP assay. *Anal. Biochem.* **1996**, *239*, 70–76. [CrossRef]

36. Vaario, L.-M.; Asamizu, S.; Sarjala, T.; Matsushita, N.; Onaka, H.; Xia, Y.; Kurokochi, H.; Morinaga, S.-I.; Huang, J.; Zhang, S.; et al. Bioactive properties of Streptomyces may affect the dominance of *Tricholoma matsutake* in shiro. *Symbiosis* **2020**, *81*, 1–13. [CrossRef]
37. Huang, D.; Ou, B.; Hampsch-Woodill, M.; Flanagan, J.A.; Prior, R.L. High-throughput assay of oxygen radical absorbance capacity (ORAC) using a multichannel liquid handling system coupled with a microplate fluorescence reader in 96-well format. *J. Argic. Food Chem.* **2002**, *50*, 4437–4444. [CrossRef]
38. Prior, R.L.; Hoang, H.; Gu, L.; Wu, X.; Bacchiocca, M.; Howard, L.; Hampsch-Woodill, M.; Huang, D.; Ou, B.; Jacob, R. Assays for hydrophilic and lipophilic antioxidant capacity (oxygen radical absorbance capacity (ORAC(FL)) of plasma and other biological and food samples. *J. Argic. Food Chem.* **2003**, *51*, 3273–3279. [CrossRef] [PubMed]
39. Hazra, B.; Biswas, S.; Mandal, N. Antioxidant and free radical scavenging activity of *Spondias pinnata*. *BMC Complement. Altern. Med.* **2008**, *8*, 63. [CrossRef] [PubMed]
40. Jiang, Z.-Y.; Woollard, A.C.; Wolff, S.P. Hydrogen peroxide production during experimental protein glycation. *FEBS Lett.* **1990**, *268*, 69–71. [CrossRef]
41. Myllynen, M.; Kazmertsuk, A.; Marjomäki, V. A novel open and infectious form of echovirus 1. *J. Virol* **2016**, *90*, 6759–6770. [CrossRef]
42. Schmidtke, M.; Schnittler, U.; Jahn, B.; Dahse, H.M.; Stelzner, A. A rapid assay for evaluation of antiviral activity against coxsackie virus B3, influenza virus A, and herpes simplex virus type 1. *J. Virol. Methods* **2001**, *95*, 133–143. [CrossRef]
43. Engström, M.T.; Pälijärvi, M.; Fryganas, C.; Grabber, J.H.; Mueller-Harvey, I.; Salminen, J.P. Rapid qualitative and quantitative analyses of proanthocyanidin oligomers and polymers by UPLC-MS/MS. *J. Agric. Food Chem.* **2014**, *62*, 3390–3399. [CrossRef] [PubMed]
44. Engström, M.T.; Pälijärvi, M.; Salminen, J.P. Rapid fingerprint analysis of plant extracts for ellagitannins, gallic acid, and quinic acid derivatives and quercetin-, kaempferol-and myricetin-based flavonol glycosides by UPLC-QqQ-MS/MS. *J. Agric. Food Chem.* **2015**, *63*, 4068–4079. [CrossRef] [PubMed]

IV

SALIX SPP. BARK HOT WATER EXTRACTS SHOW ANTIVIRAL, ANTIBACTERIAL, AND ANTIOXIDANT ACTIVITIES-THE BIOACTIVE PROPERTIES OF 16 CLONES

by

Jenni Tienaho, Dhanik Reshamwala, Tytti Sarjala , Petri Kilpeläinen, Jaana Liimatainen, Jinze Dou, Anneli Viherä-Aarnio, Riikka Linnakoski, Varpu Marjomäki & Tuula Jyske 2021

Frontiers in Bioengineering and Biotechnology 9: 797939

frontiers in Bioengineering and Biotechnology

ORIGINAL RESEARCH
published: 16 December 2021
doi: 10.3389/fbioe.2021.797939

Salix spp. Bark Hot Water Extracts Show Antiviral, Antibacterial, and Antioxidant Activities—The Bioactive Properties of 16 Clones

Jenni Tienaho[1]*, *Dhanik Reshamwala*[2], *Tytti Sarjala*[1], *Petri Kilpeläinen*[1], *Jaana Liimatainen*[1], *Jinze Dou*[3], *Anneli Viherä-Aarnio*[1], *Riikka Linnakoski*[4], *Varpu Marjomäki*[2] and *Tuula Jyske*[1]

[1]Production Systems, Natural Resources Institute Finland (Luke), Helsinki, Finland, [2]Department of Biological and Environmental Science, Nanoscience Center, University of Jyväskylä, Jyväskylä, Finland, [3]Department of Bioproducts and Biosystems, School of Chemical Engineering, Aalto University, Espoo, Finland, [4]Natural Resources, Natural Resources Institute Finland (Luke), Helsinki, Finland

OPEN ACCESS

Edited by:
Caoxing Huang,
Nanjing Forestry University, China

Reviewed by:
Chuan-Ling Si,
Tianjin University of Science and Technology, China
Hayssam M. Ali,
King Saud University, Saudi Arabia

***Correspondence:**
Jenni Tienaho
jenni.tienaho@luke.fi

Specialty section:
This article was submitted to Bioprocess Engineering, a section of the journal Frontiers in Bioengineering and Biotechnology

Received: 19 October 2021
Accepted: 15 November 2021
Published: 16 December 2021

Citation:
Tienaho J, Reshamwala D, Sarjala T, Kilpeläinen P, Liimatainen J, Dou J, Viherä-Aarnio A, Linnakoski R, Marjomäki V and Jyske T (2021) Salix spp. Bark Hot Water Extracts Show Antiviral, Antibacterial, and Antioxidant Activities—The Bioactive Properties of 16 Clones. Front. Bioeng. Biotechnol. 9:797939. doi: 10.3389/fbioe.2021.797939

Earlier studies have shown that the bark of *Salix* L. species (Salicaceae family) is rich in extractives, such as diverse bioactive phenolic compounds. However, we lack knowledge on the bioactive properties of the bark of willow species and clones adapted to the harsh climate conditions of the cool temperate zone. Therefore, the present study aimed to obtain information on the functional profiles of northern willow clones for the use of value-added bioactive solutions. Of the 16 willow clones studied here, 12 were examples of widely distributed native Finnish willow species, including dark-leaved willow (*S. myrsinifolia* Salisb.) and tea-leaved willow (*S. phylicifolia* L.) (3 + 4 clones, respectively) and their natural and artificial hybrids (3 + 2 clones, respectively). The four remaining clones were commercial willow varieties from the Swedish willow breeding program. Hot water extraction of bark under mild conditions was carried out. Bioactivity assays were used to screen antiviral, antibacterial, antifungal, yeasticidal, and antioxidant activities, as well as the total phenolic content of the extracts. Additionally, we introduce a fast and less labor-intensive steam-debarking method for *Salix* spp. feedstocks. Clonal variation was observed in the antioxidant properties of the bark extracts of the 16 *Salix* spp. clones. High antiviral activity against a non-enveloped enterovirus, coxsackievirus A9, was found, with no marked differences in efficacy between the native clones. All the clones also showed antibacterial activity against *Staphylococcus aureus* and *Escherichia coli*, whereas no antifungal (*Aspergillus brasiliensis*) or yeasticidal (*Candida albicans*) efficacy was detected. When grouping the clone extract results into *Salix myrsinifolia*, *Salix phylicifolia*, native hybrid, artificial hybrid, and commercial clones, there was a significant difference in the activities between *S. phylicifolia* clone extracts and commercial clone extracts in the favor of *S. phylicifolia* in the antibacterial and antioxidant tests. In some antioxidant tests, *S. phylicifolia* clone extracts were also significantly more active than artificial clone extracts. Additionally, *S. myrsinifolia* clone extracts showed significantly higher activities in some antioxidant tests than commercial clone extracts and artificial clone extracts. Nevertheless, the bark extracts of native Finnish willow clones showed high bioactivity. The obtained knowledge paves the way towards

developing high value-added biochemicals and other functional solutions based on willow biorefinery approaches.

Keywords: antimicrobial, antioxidant, antiviral, bark, debarking, *Salix* spp., water-extracts

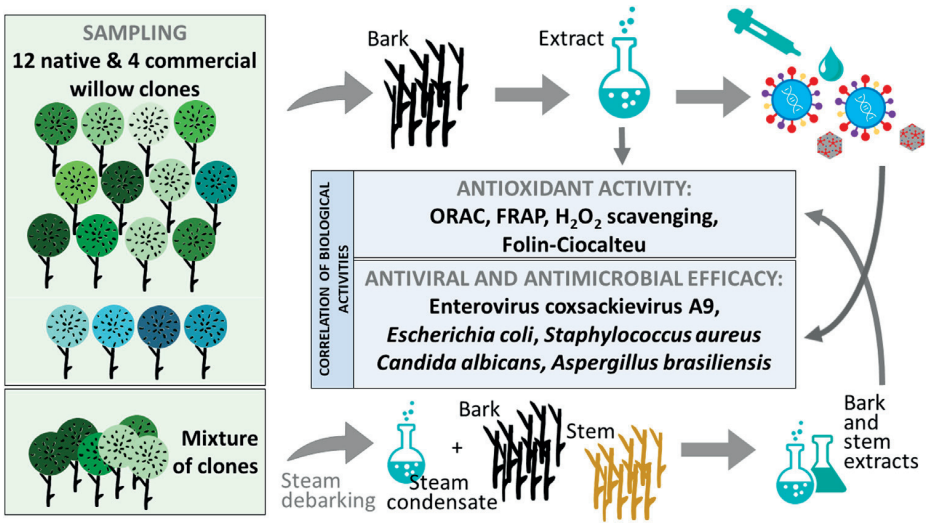

GRAPHICAL ABSTRACT |

1 INTRODUCTION

Willows (genus *Salix* L.) correspond to approximately 450 species of deciduous trees and shrubs, which are mostly found in moist soils of the Northern Hemisphere (Christenhusz et al., 2017). In general, the major components of willows' biomass are cellulose, hemicellulose, and lignin, while various minor constituents include flavonoids and other polyphenols (Yan et al., 2021). Willow leaves and bark have long been known as herbal medicines because of their ability to relieve fever and aches. These properties have been attributed to compounds identified from willow species, such as salicinoids and various polyphenols. Salicinoids (syn. salicylates) are phenolic glucosides, which are derivatives of salicyl alcohol, and are commonly found at high levels in the bark and leaves of willows. Most of the salicinoids are signature compounds of *Salix* and *Populus* L. species, and over 20 individual salicinoids have been characterized. Whereas salicylic acid is a ubiquitous plant hormone. Salicin is the simplest and most common salicinoid compound; however, it is often found at low quantities depending on the willow hybrid. Other salicinoids in willows are formed by the esterification of one or more hydroxyl groups of salicin with organic acids, such as benzoic acid in populin and 1-hydroxy-6-oxocyclohex-2-en-1-carboxylic acid in salicortin (Boeckler et al., 2011; Julkunen-Tiitto and Virjamo, 2017). Other small phenolic glycosides common in willow bark are picein, a glucoside of hydroxyacetophenone, salidroside, a glucoside of phenylethanoid, and derivatives of cinnamic alcohols such as triandrin and vimalin (Julkunen-Tiitto, 1985; Kammerer et al., 2005; Dou et al., 2018). Proanthocyanidins up to 20% of bark dry weight (Heiska et al., 2007) and several flavonoids belonging to flavan-3-ols, flavonols, flavanones, and chalcones have also been characterized. A comprehensive review of the phytochemistry and pharmacological activities of *Salix* spp. was recently published by Tawfeek et al. (2021).

Salicinoids of willow bark can decompose into salicylic acid, which has been found to possess anti-inflammatory and antiviral properties (Singh et al., 2004; Wood, 2015). Highly purified proanthocyanidin fractions of *Salix* spp. extract have also been reported to have antiviral and antibacterial activities (Quosdorf et al., 2017). Overall, proanthocyanidins, or condensed tannins, have been characterized by many biological effects, including antioxidant, antibacterial, antitumor, anticancer, neuroprotective, hypoglycemic, and lipid-lowering activities with a comprehensive positive impact on gastrointestinal health (Yan et al., 2021). Saracila et al. (2018) observed that by feeding the bark extract of *Salix alba* L. to broilers, the number of pathogenic bacteria (Enterobacteriaceae, *Escherichia coli*) on the cecal microbial population decreased while the number of beneficial lactobacilli increased. Three *Salix* spp. bark extracts were also found to have bactericidal effects against *Staphylococcus aureus*, with no significant differences between these species (Ramos et al., 2019). Polyphenols from *Salix tetrasperma* Roxb. stem bark extract were also found to be effective in inhibiting the quorum sensing and virulence of *Pseudomonas*

aeruginosa (Mostafa et al., 2020). Malterud et al. (1985) showed that the flavonoid composition from *Salix caprea* L. wood was able to inhibit rot producing wood-destroying fungi *Caniophora puteana*, *Sporotrichum pulverulentum*, and *Trichoderma viride*. Furthermore, willow bark extracts are known to have strong antioxidant and radical scavenging properties (Durak and Gawlik-Dziki, 2014; Bounaama et al., 2016; Ramos et al., 2019). Pharmacological studies have revealed interesting aspects of antitumor and anticancer therapy, including the discovery of a novel cyclodimeric salicinoid, miyabeacin, from *Salix miyabeana* Seemen. and *Salix dasyclados* Wimm. (El-Shemy et al., 2007; Ward et al., 2020). Willow extracts can also be used to relieve pain, inflammation, and fever in a wide variety of conditions with minor adverse effects (Chrubasik et al., 2000; Vlachojannis et al., 2009; Shara and Stohs, 2015). As only mild cytotoxicity has been discovered in willow bark extracts, willows are a promising biomass for various health applications (Ramos et al., 2019). However, because of the vast number of different willow species and their widespread ability to form hybrids, as well as recently identified compounds (e.g., Wu et al., 2016; Noleto-Dias et al., 2018; Noleto-Dias et al. 2019; Noleto-Dias et al. 2020; Ward et al., 2020), there is still much to explore regarding *Salix* spp. and their metabolites.

The biomass of fast-growing willows is recognized as a suitable raw material for biorefineries (Parajuli et al., 2015). Willows can be grown in low-quality agricultural land that cannot be used for food production, thereby reducing competition between food and biomass production (Krzyżaniak et al., 2016). Also, short-rotation woody crop management is less energy consuming than that required for food crops (Djomo et al., 2011). In addition to its potential as a lignocellulosic option for biofuels and bioenergy, willows can be exploited as a renewable source of biochemicals (Brereton et al., 2017). To fully utilize willows' biomass, both bark and stem wood must be separately valorized (Dou et al., 2016). Carbonized willow bark and wood can be used in supercapacitors (Phiri et al., 2019; Hobisch et al., 2020) and fiber composites (Dou et al., 2019). The cascading use of biomass would be preferential. Isolated biomass fractions should be used as reusable products as much as possible and, finally, after a cycle of reasonable use, compounds and materials should be used as energy after their combustion or anaerobic digestion. For example, the polyphenol containing fraction can be extracted first with hot water, and then the remaining material could be pyrolyzed and anaerobically gasified (Rasi et al., 2019) or used in the production of biochar by slow pyrolysis technology (Rasa et al., 2021). Hot water extraction has been shown to be able to achieve the maximal extract yield from willow bark at 80°C for 20 min (Dou et al., 2018).

Extensive characterization and quantification have been conducted on the components of pharmaceutical preparations from *Salix* spp. (Kammerer et al., 2005) and willow species' phytochemicals extracted from the bark (Julkunen-Tiitto, 1985; Heiska et al., 2007; Lavola et al., 2018), leaves (Ikonen et al., 2002; Lavola et al., 2018), and whole twigs/biomass (Julkunen-Tiitto, 1985; Brereton et al., 2017). Willow bark is one of the most bioactive compound-rich plant parts (Lavola et al., 2018; Tyśkiewicz et al., 2019), but leaves are also a promising source of polyphenols and antioxidants (Piatczak et al., 2020). However, the content of bark phytochemicals is known to vary among *Salix* spp. (Julkunen-Tiitto, 1985) because of seasonal and environmental factors (Förster et al., 2008), as well as among genotypes and developmental stages of the plant (Lavola et al., 2018). Although the variation of phytochemicals between *Salix* spp. genotypes is mainly quantitative, there can be large differences in compound composition between species and hybrids, which could be a result of the effortless hybridization of *Salix* spp. (Julkunen-Tiitto and Virjamo, 2017). Nevertheless, we lack knowledge on the bark bioactive properties of willow species and/or clones that are well adapted to the northern areas of the cool temperate zone. Therefore, the present study focused on the bark extracts of Finnish willows by screening their antioxidant, antiviral, antibacterial, and antifungal properties.

First, we screened the bioactive properties, i.e., the antioxidant, antiviral (enterovirus strain coxsackievirus A9), antibacterial [*E. coli* (Gram-negative) and *S. aureus* (Gram-positive)], antifungal (*Aspergillus brasiliensis*), and yeasticidal (*Candida albicans*) activities of 16 aqueous bark extracts to the potential of willow materials for various biochemicals and functional products. Additionally, we tested steam-debarking at the 300-L scale as a potentially less-laborious debarking method for northern cultivated willows. We hypothesized that (1) the bark extracts of native willows of local origin have higher biological activity than those of commercial willows due to higher resource allocation to secondary metabolites in native willows; (2) between-species variation in the biological activity of bark extracts offsets the variation among clones; (3) the biological activities of bark extracts are highly intercorrelated; for example, antiviral efficacy can be predicted by the total phenolic content and antibacterial power; (4) individual compounds do not explain the biological activities of crude bark extracts but the extract antioxidant activity and efficacies against viruses and bacteria are due to the synergistic effects of several compounds together—to challenge this pure commercial compounds were also tested; (5) when grouping the clones into *S. phylicifolia*, *S. myrsinifolia*, native hybrid, artificial hybrid, and commercial clones, significant differences can be detected; and (6) when compared to conventional debarking methods, steam-aided debarking is an efficient and less laborious process resulting in *Salix* spp. products with high bioactive potential.

2 MATERIALS AND METHODS

2.1 *Salix* spp. Sample Collection

The study materials consisted of 16 willow clones. Of these, 12 clones originated from two common and widely distributed native willow species, dark-leaved willow (*S. myrsinifolia* Salisb.) and tea-leaved willow (*S. phylicifolia* L.) (Väre et al., 2021), as well as from their natural and artificial hybrids. The other four clones were commercial willow varieties from the Swedish willow breeding program (**Table 1**). Herbarium specimens of the native materials were collected, the identification of the willow species was verified, and the plant specimens were deposited at the Finnish Museum of Natural History, Botanical Museum (H).

TABLE 1 | Willow clones used for the screening of biological activities.

Sample number	Clone	Species	Type
1	E6682	*S. myrsinifolia*	Native
2	E6771	*S. myrsinifolia*	Native
3	E6948	*S. myrsinifolia*	Native
4	E6666	*S. phylicifolia*	Native
5	K2191	*S. phylicifolia*	Native
6	K2218	*S. phylicifolia*	Native
7	K2277	*S. phylicifolia*	Native
8	K2183	*S. myrsinifolia* × *phylicifolia*	Native hybrid
9	K2269	*S. myrsinifolia* × *phylicifolia*	Native hybrid
10	K2341	*S. myrsinifolia* × *phylicifolia*	Native hybrid
11	V7545	(K2183 *S. myrs.* × *phyl.*) × S15136 *S. gmelinii*[a]	Artificial hybrid
12	V7546	(K2183 *S. myrs.* × *phyl.*) × P6011 *S. gmelinii*[a]	Artificial hybrid
13	Scherenee		Commercial clone
14	Tordis		Commercial clone
15	Tora		Commercial clone
16	Klara		Commercial clone

[a]Salix gmelinii *Pall. is former* S. dasyclados *Wimm. (Väre et al., 2021).*

The native willow clones and artificial hybrids (sample numbers 1–12) were rooted in 20-cm-long cuttings in polystyrene containers (TA913) in a greenhouse at the Haapastensyrjä field station (N60°43′0.01″ E24°26′60.00″), Natural Resources Institute Finland, in the spring of 2017. The growing medium used was a mixture of 2/3 Kekkilä FPM 420 F6 HS *Sphagnum* peat and 1/3 perlite (size 2–6 mm). The containerized plants were moved to the nursery of the Piikkiö field station (N60°25′29.32″ E22°30′57.64″), Natural Resources Institute Finland, in June 2017, where they were grown for the next 2 years. The plants were watered and fertilized according to the normal nursery practices. On May 7, 2019, the 2-year-old willow plants were cut down and the harvested shoots of each clone were packed separately in plastic bags and immediately frozen at –20°C. The harvested willow coppice varied between 1 and 1.5 m in length and 0.5–2 cm diameter at the base.

Commercial willow clones (sample numbers 13–16) were grown by Carbons Finland Ltd. in a peat field at Aitomäki, Kouvola south-eastern Finland (N60°52′0.01″ E26°41′60.00″) from 2016 to March 2019, when the 3-year-old coppice was cut down on March 30 and taken for the study. The 3-m-long sample shoots were cut to shorter, ca. 40-cm-long, pieces and frozen (–20°C) until further treatment.

Two shoots of each willow clone were debarked 50 cm from the base and pooled. The bark was cut into small pieces, frozen at –80°C, and finally freeze-dried. The freeze-dried material was ground with a Moulinex grinder to 1- to 2-mm pieces and kept frozen at –80°C until water extraction.

In addition, *Salix* Klara for the 2-L stirring reactor extraction was provided by Carbons Finland Ltd. from the same growth environment and site, except from spring 2017 to 2020. The willow banks were partly cut down in spring 2018 and 2019 and, for the present study, were cut and gathered on October 24, 2020. The material was then debarked and immediately placed in a freezer (–20°C). The bark was ground with a Kamas cutting mill with a 2-cm sieve.

The material for the pilot-scale bark removal by steaming was collected from a willow clone bank growing at the Piikkiö field station, Finland. The clone bank was established in the summer of 2007. Part of it was cut down in 2013, and all the clones were cut down again on April 4–5, 2019. Material for the steaming experiment was collected as two sample lots, the first containing a mixture of five 6-year-old *Salix purpurea* L. clones. The second sample included a 12-year-old mixture of five *Salix daphnoides* Vill. clones, one *S. purpurea* clone, and two unknown clones. Finally, these two samples were combined, and a bulk sample was used for the steam debarking experiment to ensure the material availability for testing the suitability of the method in general. Detailed information about the samples and their origin can be found in the **Supplementary Appendix Table SA1**.

2.2 *Salix* spp. Clone Extractions

Salix spp. samples were freeze-dried before the extraction. Bark was extracted using an ASE-350 accelerated solvent extractor (Dionex, Sunnyvale, CA, United States). The bark sample (1 g) was placed in a stainless-steel extraction vessel (22 ml). The sample was then extracted three times for 15 min with hot water (1:66, w/v) at 90°C, and the extract was stored at –20°C before further analyses.

2.2.1 *Salix* Klara 2-L Stirring Reactor Extractions

Klara bark was extracted using a 2-L stirring reactor (Polyclave, Büchi, Switzerland). The fresh willow bark sample (358 g, corresponding to 150 g dry weight) was placed in the reactor and extracted in a 1:10 bark dry weight/water ratio. The extraction temperature was 80°C, and there was constant stirring (60 rpm) during the 60-min extraction. Solids were separated by collecting liquid through a 50-µm sintered metal filter at the bottom of the reactor. The extract was cooled to room temperature using a heat exchanger. In total, four extractions were carried out under the same conditions, and the average measured total dissolved solids of the extracts was 13.7 ± 0.2 wt% of the dry weight of the original bark. After extraction, the bark extracts were combined into one sample. The extract was

FIGURE 1 | Original willow samples **(A)**, combined willow sticks in reactor **(B)**, and steam-treated bark and woody material **(C)**.

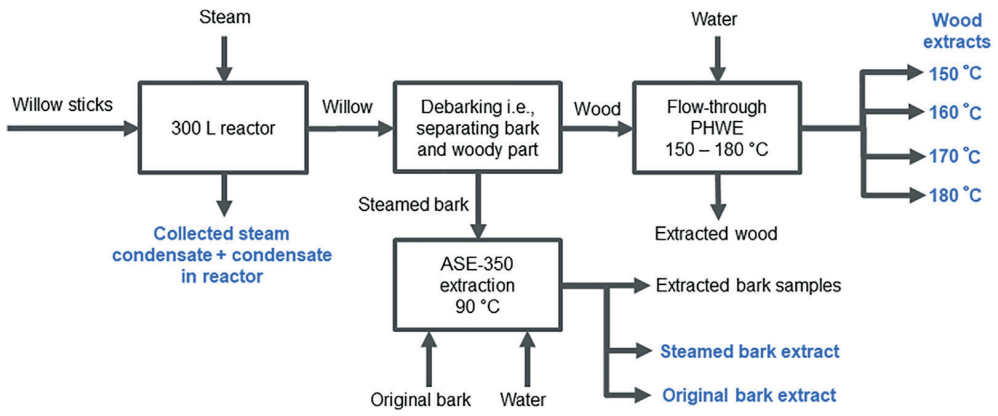

FIGURE 2 | Willow steam treatment, debarking, and extractions. Willow steam treatment condensate, original willow bark ASE-350 extract, and steam-treated bark ASE-350 extract contained polyphenols. Carbohydrates were extracted from woody samples at temperatures from 150 to 180°C after debarking. Collected samples are indicated with blue color.

concentrated using a rotary evaporator at 60°C, freeze-dried, and the dried extract was ground into powder with a mortar and pestle.

2.2.2 Willow Steam Debarking and Extractions

A batch of the combined samples of willow sticks was first steam-treated in a 300-L reactor to remove bark (**Figure 1**). Samples of steam-treated bark and wood were then extracted at small scale to isolate polyphenol- and carbohydrate-containing fractions. Bark samples were extracted in hot water (90°C) with ASE-350 to isolate polyphenols and wood samples were extracted with a pressurized hot water flow-through extraction system with a 50-ml extraction vessel at 150–180°C to extract carbohydrates. Details of the flow-through extraction system can be found in Kilpeläinen et al. (2014).

Fresh willow sticks (42.2 ± 0.2 kg) were loaded inside the 300-L extraction system that was used in the experiments (Kilpeläinen et al., 2014). For steam collection, 30 L of water was weighed into a tub, and steam was directed to water in the tub with a hose from the extraction system. The temperature inside the vessel was measured during the treatment. Continuous steam flow of 1.6 kg/min (214°C) was passed into the vessel containing willow samples for 20 min. The temperature inside the reactor increased to 100°C after 5–6 min. After 7.5 min, steam started to come out of the vessel, and it was collected into the water-filled tub. When steaming ended after 20 min, the temperature increased to 130°C and the pressure increased to 1.7 bar with a fully open exhaust line.

Steam (3.6 ± 0.2 kg) was collected by the steam collection tub. The condensate was removed *via* the reactor's drain valve and weighed (19.2 ± 0.2 kg). The steam-treated willow sticks could be

easily debarked by hand, as the bark was barely attached to the wood. Samples of the steam condensates, steam-treated bark, and wood were collected and frozen (–20°C) before further analysis.

After the willow steam treatment, the woody material was extracted with a pressurized hot water flow-through system (Kilpeläinen et al., 2012) to isolate fractions with the willow hemicelluloses. Pressurized hot water flow-through extraction has been used to extract hemicelluloses from woody materials (Kilpeläinen et al., 2012; Kilpeläinen et al., 2014). Before extraction, the sample was pre-steamed at 100°C to prevent water channeling through the sample during extraction. Samples (10 g o.d.) were extracted at 150–180°C with a flow rate of 4 ml/min for 60 min. The extract was collected, diluted to 250 ml, and stored in a freezer (–20°C) before analysis.

Steamed bark was extracted with hot water using ASE-350 under the same conditions as the *Salix* spp. clones. Willow samples and treatment techniques used are shown in **Figure 2**.

2.3 Commercial Substances and Samples

Commercial substances were used as references in the antibacterial and antiviral measurements. Salicin and picein (purity >98%) were purchased from Merck Life Science Oy. Salicylic acid (purity >99%) was obtained from VWR Chemicals and triandrin (purity 85%) was obtained from Molport EU. Additionally, Salixin Organic Powder (48^{TM}) and Salixin Organic Extract (800NP^{TM}) were supplied by Søren Fisker (Salixin A/S) and Pia Wikström (OY CELEGO AB) and were tested for their antibacterial and antiviral efficacy along with the reference substances.

2.4 Bioactive Efficacy

2.4.1 Antioxidant Properties

The antioxidant properties of the *Salix* spp. clone bark extracts were tested using the oxygen radical absorbance capacity (ORAC) assay, ferric reducing antioxidant power (FRAP), H_2O_2 scavenging test, and Folin-Ciocalteu assay for total phenolic content. All antioxidant assays were carried out using a Varioskan Flash multimode reader (Thermo Scientific) in a 96-well format. The tests covered different antioxidant mechanisms: hydrogen atom transfer (ORAC), single electron transfer (FRAP), and radical scavenging (H_2O_2 scavenging). All tests were performed using internal standards with which the sample results were compared.

Oxygen Radical Absorbance Capacity

This assay is based on hydrogen atom transfer (HAT) and measures the reduction in fluorescence signal caused by the oxidative dissociation of fluorescein in the presence of peroxyl radicals (R-O-O•) (Huang et al., 2002; Prior et al., 2003). The inhibition of fluorescein breakdown indicates the antioxidant's protective ability. The experimental setup is described in detail by Tienaho et al. (2020). Briefly, the assay was carried out using four dilutions of each sample, with two technical replicates, by mixing the sample in 0.075 M phosphate buffer pH 7.5 (Merck) with 8.16 × 10^{-5} mM fluorescein (Sigma-Aldrich Chemie GmbH, Steinheim, Germany) and 2,2′-azobis(2-methylpropionamidine) dihydrochloride (Sigma-Aldrich Chemie GmbH, Steinheim, Germany). Trolox (vitamin E analog) ((±)-6-Hydroxy-2,5,7,8-tetramethylchromane-2-carboxylic acid) (Sigma-Aldrich Chemie GmbH, Steinheim, Germany) was used as the standard, and the results are expressed as Trolox equivalents (μmol TE per 100 g).

Ferric Reducing Antioxidant Power

This assay is based on single electron transfer (SET) and measures the ability of an antioxidant to reduce ferric (Fe^{III}) to ferrous (Fe^{II}) ions (Benzie and Strain, 1996). The test protocol was described by Tienaho et al. (2021). In brief, a series of four dilutions of each sample, with three technical replicates, in a 96-well format were used in the assay. The samples were mixed with 20 mM $FeCl_3$•$6H_2O$ (Sigma-Aldrich Chemie GmbH, Steinheim, Germany) and 10 mM 2,4,6-tris-(2-pyridyl)-s-triazine (TPTZ) (Sigma-Aldrich Chemie GmbH, Steinheim, Germany) in 300 mM acetate buffer (pH 3.6). The absorbance was measured at 594 nm with a microplate fluorescence reader (Varioskan Flash, Thermo Scientific) after the formation of the ferrous-tripyridyltriazine complex in the reaction mixture. $FeSO_4$•$7H_2O$ (Sigma-Aldrich Chemie GmbH, Steinheim, Germany) was used as the standard and L(+)-ascorbic acid (150 and 800 μM) (VWR Chemicals) as the control. The results are expressed as μmol/L Fe(II) equivalents.

The Hydrogen Peroxide (H_2O_2) Scavenging

Activity was determined using a method modified from Hazra et al. (2008) and Jiang et al. (1990). The experimental setup has been described in detail by Tienaho et al. (2020). In brief, an aliquot of 2 mM H_2O_2 (Merck KGaA, Darmstadt, Germany) was added to the reaction mixture with the sample and a mixture containing 2.56 mM ammonium ferrous (II) sulfate (BDH Prolabo) in 0.25 mM H_2SO_4 (Merck KGaA) and 27.8 μM xylenol orange disodium salt (Sigma-Aldrich Chemie GmbH, Steinheim, Germany) in 4.4 mM sorbitol (D(-)-sorbitol, AppliChem GmbH). After 30 min of incubation, the absorbance of violet-colored ferric-xylenol orange complexes at 560 nm was measured. The assay measures the ability of the sample to scavenge H_2O_2 and prevent the oxidation of Fe(II) to Fe(III), which is indicated by the formation of the ferric-xylenol orange complex. The inhibition of oxidation is expressed as the inhibition (%) of the reaction, and the samples with 100% inhibition activity will remain yellowish. Sodium pyruvate (Sigma-Aldrich) was used as a reference compound.

Folin-Ciocalteu Assay

The Folin-Ciocalteu method (Singleton and Rossi, 1965; Singleton et al., 1999; Ainsworth and Gillespie, 2007) was used to analyze the total phenolic content, which is known to reflect antioxidant capacity. The test protocol was described by Tienaho et al. (2021). In brief, the samples were mixed with Folin-Ciocalteu reagent (Merck KGaA, Darmstadt, Germany) and 20% Na_2CO_3 (Merck KGaA, Darmstadt, Germany), and absorbance was measured at 750 nm with gallic acid (Sigma-Aldrich Chemie GmbH, Steinheim, Germany) as a reference compound. The results are expressed as gallic acid equivalents per gram (GAE/g).

2.4.2 Antibacterial Properties

Two constitutively light-emitting bacterial biosensor strains, *E. coli* K12 + pcGLS11 and *S. aureus* RN4220 + pAT19,

described by Vesterlund et al. (2004), were used in the present study. Bacterial cultivation and stocks were grown as previously described (Välimaa et al., 2020). Briefly, the bacteria were stored at –80°C and cultivated for approximately 16 h at 30°C (*E. coli*) and 37°C (*S. aureus*) on lysogeny agar (LA) plates (tryptone 10 g/L; yeast extract 5 g/L; NaCl 10 g/L; and agar 15 g/L). The LA plates were supplemented with 10% (v/v) sterile filtered phosphate buffer (PB) (1 M, pH 7.0) and 100 μg/ml of ampicillin (*E. coli*) or 5 μg/ml erythromycin (*S. aureus*). Biosensor stocks were prepared by inoculating a single colony of bacteria in lysogeny broth supplemented with 10% (v/v) of sterile filtered PB 1 M (pH 7.0), 100 μg/ml ampicillin (*E. coli*), or 5 μg/ml erythromycin (*S. aureus*). Stocks were cultivated for approximately 16 h at 300 rpm shaking at 30°C (*E. coli*) and 37°C (*S. aureus*). Extractions of all the willow clones in **Table 1** were diluted in double-distilled water to achieve a 5% v/v concentration per microplate well. Ethanol 35% per microplate well was used as a positive control, and double-distilled water was used as a negative control. The reference substances, picein, triandrin, salicin, salicylic acid, and Salixin Organic Powder were diluted in double-distilled water to achieve concentrations of 250 μg/ml and 125 μg/ml per microplate well, whereas Salixin Organic Extract was used in 2.5% and 1.25% v/v per microplate well. Aliquots of 50 μl of samples and controls were pipetted in triplicate into opaque white polystyrene microplates, and 50 μl of bacterial culture was pipetted into the same wells. The luminescence was then measured using a Varioskan Flash Multilabel device (Thermo Scientific) once every 5 min for 95 min at room temperature, and the plate was briefly shaken before every measurement. The results are expressed as relative light units (RLUs) drawn at a time point of 40 min of measurement. Error bars represent the standard deviations between the sample triplicates.

2.4.3 Antiviral Activity

Enterovirus coxsackievirus A9 (CVA9; Griggs strain, ATCC) was used to assess the antiviral efficacy of the *Salix* spp. clone extracts. CVA9 was produced and purified using a sucrose gradient, as previously described (Ruokolainen et al., 2019). Pretreatment of CVA9 [2×10^6 plaque-forming unit (PFU) per ml] was performed with different amounts of *Salix* spp. extract (0.1%, 1%, and 10% v/v). After 1 h incubation at 37°C, the virus-*Salix* spp. mix was diluted 10-fold in 10% Dulbecco's Modified Eagle Medium (DMEM). The mixture was added to the lung carcinoma cell line A549 (ATCC) containing 96-well plates with 12,000 cells/well density, plated on the previous day. After 48 h, the wells were washed twice with phosphate-buffered saline (PBS) and stained with crystal violet solution (0.03% crystal violet, 2% ethanol, and 36.5% formaldehyde) for 10 min, as described previously (Ruokolainen et al., 2019). The color was left in the wells because the remaining surviving cells were dissolved in a homogenization solution (0.8979 g of sodium citrate and 1 N HCl in 47.5% ethanol). The absorbance was measured spectrophotometrically at 570 nm using a PerkinElmer VICTOR^{TM} X4 multilabel reader. Cytotoxicity of the *Salix* spp. preparations was evaluated using the crystal violet solution mentioned above (Ruokolainen et al., 2019).

2.4.4 Antifungal Activity

Quantitative suspension tests for the evaluation of basic fungicidal and basic yeasticidal activity of the *Salix* spp. samples were performed according to DIN EN 1275 (2006) and European Standard (2006). The fungicidal activity was evaluated using *A. brasiliensis* (strain ATCC 16404) and the yeasticidal activity using *C. albicans* (ATCC 10231) as a test organism. The microorganism suspension used ranged between 1.5×10^7 colony forming units (CFU)/ml to 5.0×10^7 CFU/ml for *A. brasiliensis* and *C. albicans*. For both organisms, the choice of the test method was the dilution-neutralization method using Tween80 + lecithin (30 g/L polysorbate 80 and lecithin 3 g/L) as a neutralizer. Sterile double-distilled water was used as the diluent during the test. The test concentrations for the samples Salixin Organic Extract 800NP, Salixin Organic Powder, and Klara (2-L scale sample P-16) were 10, 2.5, 1.25, 0.625, 0.3125, 0.156, 0.078, and 0.039 mg/ml. Unlike that described for EN 1275, in some cases, total test volume of 5 ml was used in the experiments instead of 10 ml. The contact time and test temperature were 15 min (±10 s) and 20°C (±1°C), respectively. In addition, the following higher test concentrations were evaluated for the samples: Klara P-16 100 mg/ml, Salixin Organic Powder 100 mg/ml, Salixin Organic Extract 100%, 50%, 25%, 10%, and 5% (v/v), and lyophilized Salixin Organic Extract 50% and 100%.

The number of viable spores was assessed on malt extract agar (four replicates). Plates were incubated for 42–48 h at 30°C, *A. brasiliensis* for a further 20–24 h, and viable spores were determined by counting the colonies (colony counts less than 300 CFU/plate). The reduction in viability is the ratio N/N0, where N0 is the number of CFU/ml in the fungal spore test suspension and N is the number of CFU/ml after the test procedure for the fungicidal activity of the product. The sample is fungicidal or yeasticidal if it produces at least a 10^4 reduction in the number of viable vegetative yeast cells and mold spores under conditions defined by EN 1275 (2006).

2.5 Statistical Methods

Relationships among *Salix* spp. clone extract bioactivities were evaluated by Pearson's correlation coefficients (in absolute values), and the differences between mean values were assessed using a two-tailed *t*-test with a significance level of 0.05 (n = 16 for ORAC, FRAP, and Folin-Ciocalteu tests; n = 17 for the *E. coli*, *S. aureus*, and Enterovirus test). Statistical differences between the grouped clones were determined by one-way ANOVA and Tukey post-hoc test, where results were determined to be statistically significantly different if p-values were below 0.05. All statistical analyses were performed using IBM SPSS Statistics (v. 26.0) (IBM, Armonk, NY, United States).

3 RESULTS

3.1 Antioxidant Properties

The steam treatment results in **Figure 3** show that the highest antioxidant potential and phenolic content (Folin-Ciocalteu) were found in the original willow bark ASE-350 extract. The steamed bark extract also showed elevated antioxidant activity, while the different hot water flow-through extracted wood

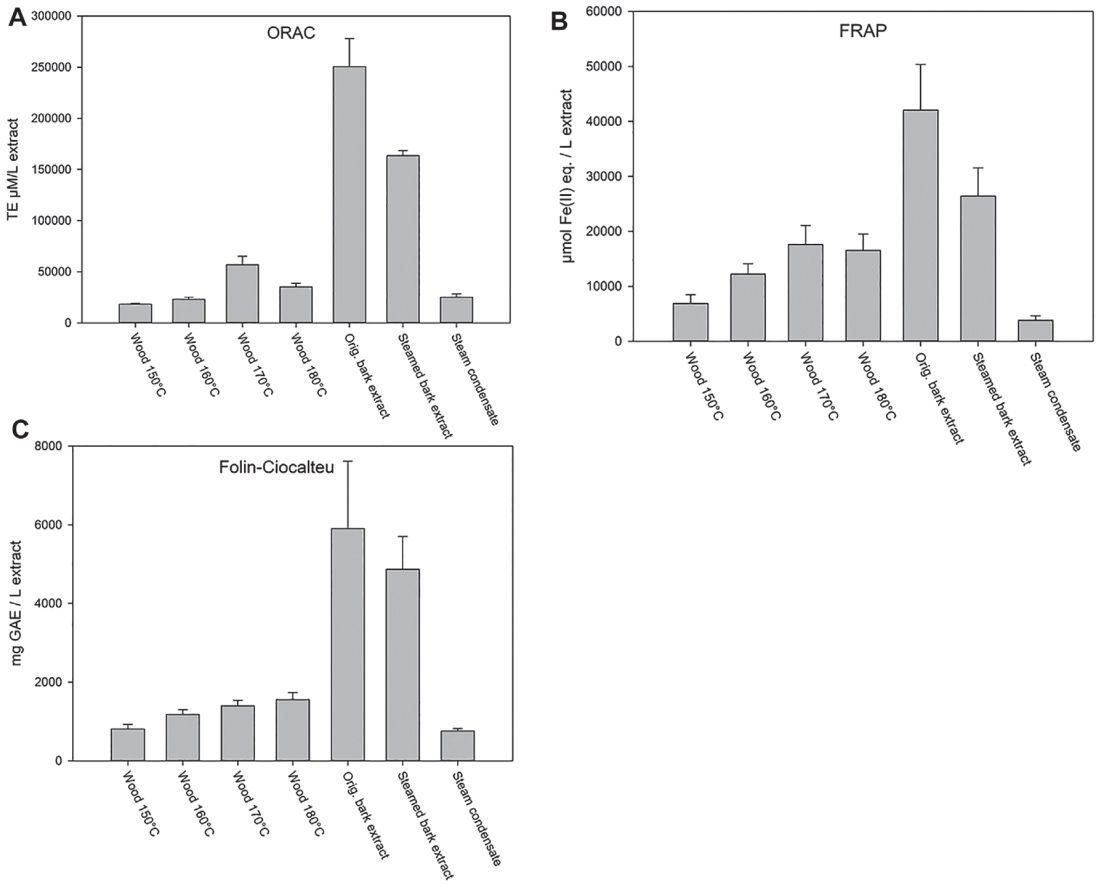

FIGURE 3 | ORAC **(A)** and FRAP **(B)** activities, and total phenolic content (Folin-Ciocalteu) **(C)** of willow wood after debarking extracted at different temperatures (150, 160, 170, and 180°C) and bark extracts (original bark extract, steam-treated bark extract, and steam condensate). Error bars present the standard deviations of the sample triplicates in a microplate. ORAC test results are expressed as Trolox equivalents (TE), FRAP results are expressed as ferrous ion equivalents (Fe(II) eq.), and Folin-Ciocalteu test results are expressed as gallic acid equivalents (GAE).

samples at temperatures of 150–180°C, high in carbohydrates and hemicelluloses, showed much lower antioxidant potential. Reductions in both antioxidant activities (FRAP and ORAC) and total phenolic content were observed when compared to that of original bark extract (**Figure 3**), indicating that some phytochemicals are leached away. In addition, steam condensate showed some activity, which further supported the partial loss of compounds.

The *Salix* spp. clone extract results (**Figure 4**) showed that the highest ORAC activity (µmol TE/100 g) was obtained with clone number 5, while clones 3, 6, and 10 also showed high ORAC activity. Clone extract 6 showed the highest FRAP efficiency, while clone extracts 3, 4, and 5 also showed high activity. All clone extracts except 7, 13, 15, and 16 showed high activity in the hydrogen peroxide scavenging test. The highest total phenolic content was found in the clone extract 6. Commercial clone extracts 13, 15, and 16 showed very low hydrogen peroxide scavenging activity (**Figure 4D**).

When grouping the clone extract antioxidant results into *S. myrsinifolia* (clones 1–3), *S. phylicifolia* (4–7), native hybrid (8–10), artificial hybrid (11–12), and commercial clones (13–16), there was a significant difference between the groups as determined by one-way ANOVA [ORAC: $F(4,11) = 4.012$, $p = 0.030$; FRAP: $F(4,11) = 10.102$, $p = 0.001$; Folin-Ciocalteu: $F(4,11) = 7.552$, $p = 0.004$; and H_2O_2 scavenging with clones 7 and 14 emitted: $F(4,9) = 14065.006$, $p < 0.001$]. A Tukey post-hoc test revealed that *S. phylicifolia* clone extracts showed significantly higher activity in the ORAC test than the commercial clone extracts ($p = 0.045$) (**Figure 5A**), and significantly higher FRAP activity than the artificial hybrid extracts ($p = 0.003$) and commercial clone extracts ($p = 0.002$) (**Figure 5B**). In addition, *S. myrsinifolia* clone extracts showed significantly higher FRAP activity than the artificial hybrid extracts ($p = 0.036$) and commercial clone extracts ($p = 0.041$) (**Figure 5B**). *S. phylicifolia* clone extracts also showed statistically significantly higher total phenolic compound capacity in the Folin-Ciocalteu test than artificial hybrid extracts ($p = 0.009$) and commercial clone extracts ($p = 0.006$). In the H_2O_2 scavenging test, clone 7 gave inconsistently lower results than the other *S. phylicifolia* clone extracts, and clone 14 gave inconsistently high results when

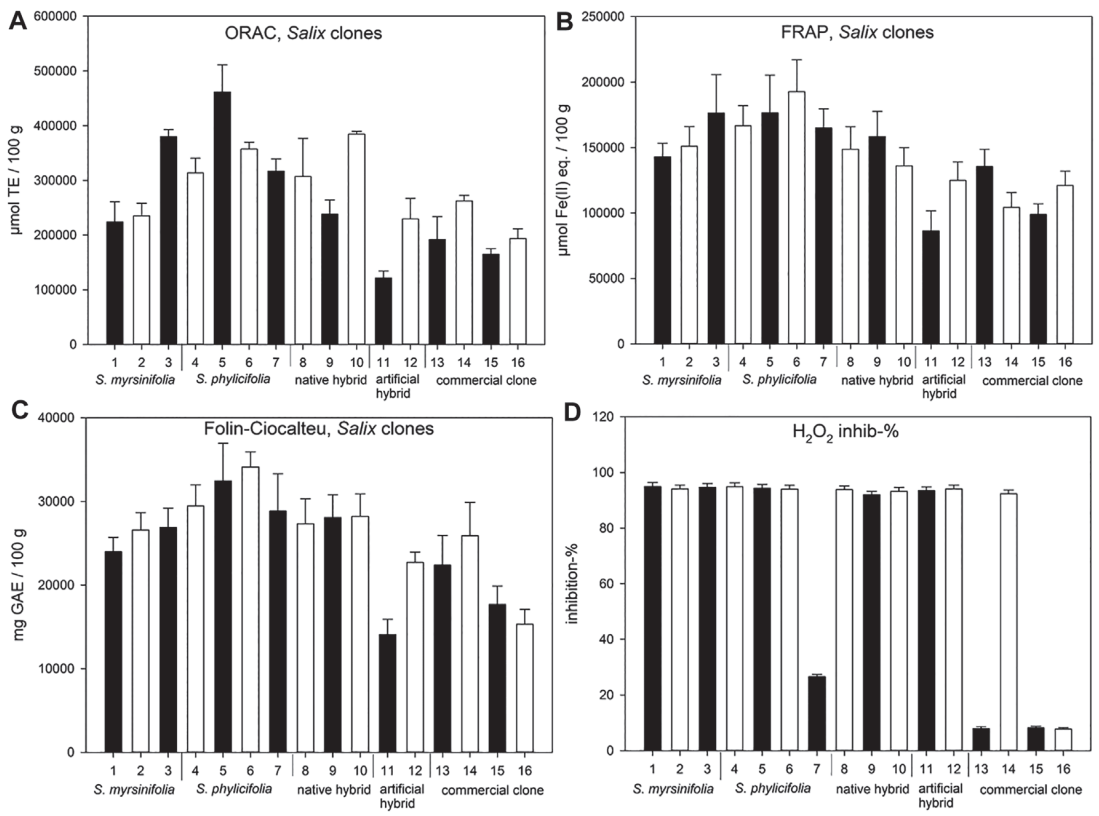

FIGURE 4 | ORAC **(A)**, FRAP **(B)**, and H_2O_2 scavenging **(D)** activities, as well as total phenolic content (Folin-Ciocalteu) **(C)** of the *Salix* spp. clone extracts. Error bars present the standard deviations of the sample triplicates in a microplate. The clones are numbered 1–16 (see **Table 1**) and 13–16 are commercial clones. ORAC test results are expressed as Trolox equivalents (TE), FRAP results are expressed as ferrous ion equivalents (Fe(II) eq.), Folin-Ciocalteu test results are expressed as gallic acid equivalents (GAE), and hydrogen peroxide scavenging test results are expressed as the percentage of H_2O_2 inhibition.

compared to the other commercial clone extracts. In dioecious plant species such as *Salix* spp., gender can be the reason for clonal differences in growth and wood quality, as shown by Hou et al. (2017). In this case, gender may not explain the differences in the activity, because all of the commercial clones included, also clone 14, were known to be female. However, when the outlier clones 7 and 14 were removed from the groups, *S. myrsinifolia* ($p < 0.001$), *S. phylicifolia* ($p < 0.001$), native hybrid ($p < 0.001$), and artificial hybrid ($p < 0.001$) clone extracts showed significantly higher antioxidant activity in the H_2O_2 scavenging test than commercial clone extracts (Figure 5D). In addition, *S. myrsinifolia* clone extracts showed significantly higher activity ($p = 0.049$) than native clone extracts (**Figure 5D**).

3.2 Biosensor Analysis and Antibacterial Activity

The antibacterial activity was evaluated using recombinant constituently bioluminescent strains of the leading bacterial pathogens of healthcare-associated infections and bacteremia: *E. coli* and *S. aureus* (Poolman and Anderson, 2018). The results are shown in **Figure 6**. Tienaho et al. (2015) showed that when using whole-cell bacterial biosensors, the empirical conditions could take from 10 to 15 min of incubation to stabilize. As shown in **Figure 6**, all the *Salix* spp. clone extracts had antibacterial activity, as evidenced by the lower RLU values than the negative control (water) with both bacterial strains after 10 min of incubation. The lower RLU values imply an inhibition of bacterial luminescence production and, thus, interference with bacterial metabolism. The highest inhibition effect after 40 min incubation was achieved by clone extract 4 in *E. coli* and clone extract 10 in *S. aureus*. However, the differences between the clones were small, with the exceptions of commercial clone extracts 14–16 and clone extract number 14, which had a somewhat lower effect on *E. coli* and *S. aureus*, respectively. For both bacterial strains, all the clone extracts exhibited stronger antibacterial activity than the control substances, salicin, salicylic acid, picein, and triandrin. The lowest inhibition seemed to be achieved with the 2-L stirring reactor extracted clone 16 (P-16); however, it still had lower luminescence production (in RLU) than the water control. The commercial reference substances showed lower antibacterial activity against both bacterial strains, except for the Salixin Organic Extract, which was equally active as the willow clone extracts with *E. coli* and showed almost as high antibacterial activity as ethanol (35%) with *S.*

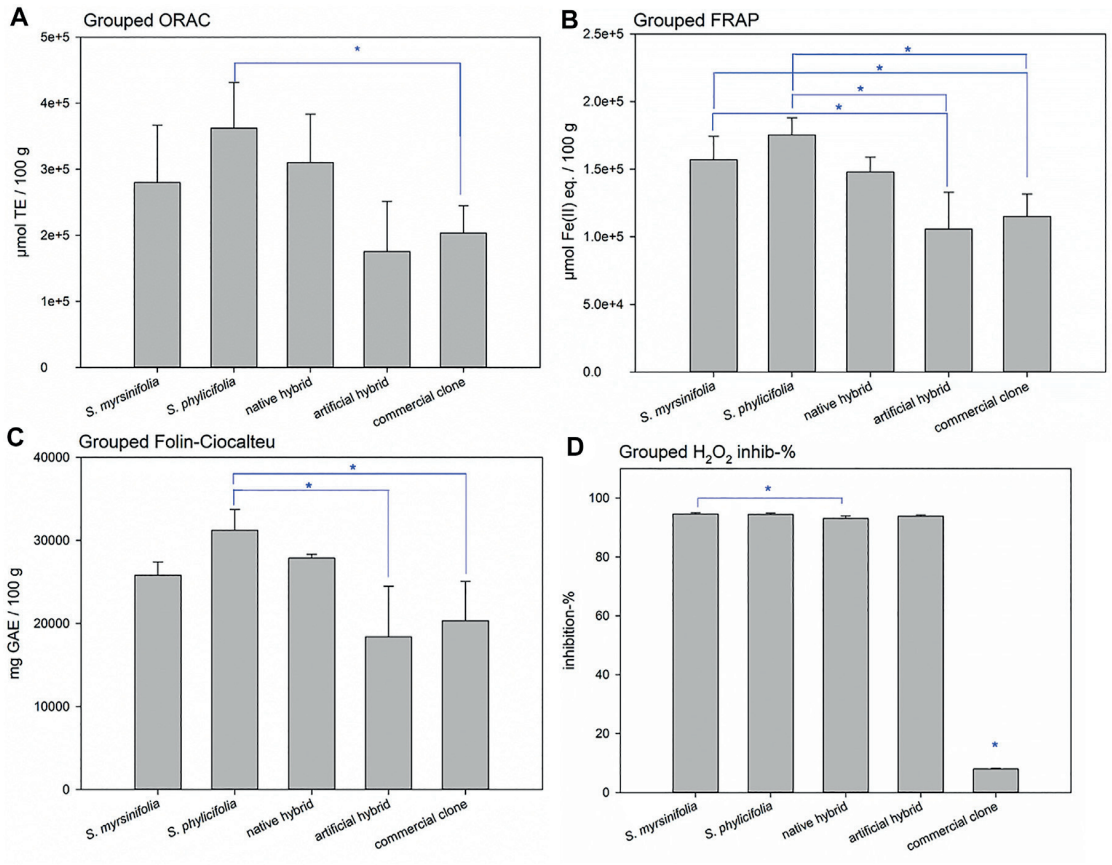

FIGURE 5 | Grouped ORAC **(A)**, FRAP **(B)**, and H_2O_2 scavenging **(D)** activities, as well as total phenolic content (Folin-Ciocalteu) **(C)** of the *Salix* spp. clone extracts. Error bars show the standard deviation between the grouped clones. Significant differences are indicated with a blue asterisk. ORAC test results are expressed as Trolox equivalents (TE), FRAP results are expressed as ferrous ion equivalents (Fe(II) eq.), Folin-Ciocalteu test results are expressed as gallic acid equivalents (GAE), and hydrogen peroxide scavenging test results are expressed as the percentage of H_2O_2 inhibition.

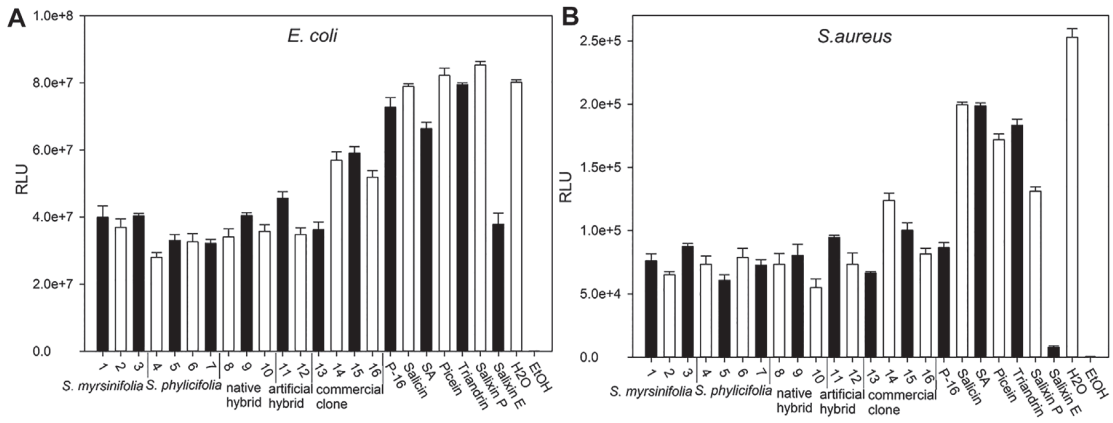

FIGURE 6 | The bacterial biosensor results. Efficacy against *E. coli* **(A)** and *S. aureus* **(B)** after 40 min incubation time. The *Salix* spp. clones **(Table 1)** of 5% v/v concentration per a microplate well are indicated with numbers 1–16. P-16 = 2-L scale clone 16; commercial substances Salixin P = Salixin Organic Powder 48^{TM} (250 µg/ml) and Salixin E = Salixin Organic Extract 800NP^{TM} (1.25% v/v); SA = salicylic acid (250 µg/ml). Results obtained for salicin, triandrin, and picein are also shown at the concentration of 250 µg/ml per microplate well. Error bars indicate the standard deviation between the sample triplicates in the microplate. Lower RLU values indicate stronger antibacterial activity.

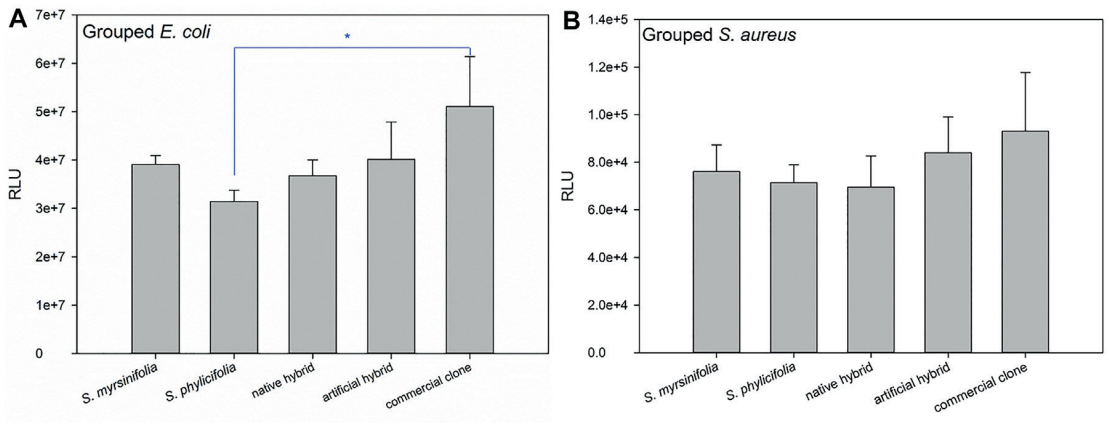

FIGURE 7 | The grouped antibacterial results against *E. coli* **(A)** and *S. aureus* **(B)**. Error bars show the standard deviation between the grouped clones. Significant differences are indicated with a blue asterisk.

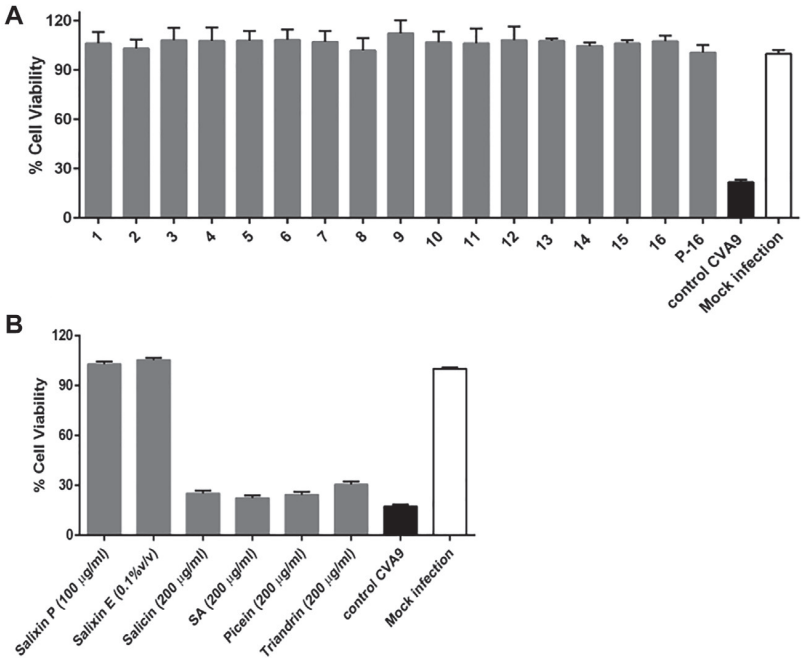

FIGURE 8 | Testing the antiviral activity of **(A)** *Salix* spp. extracts (0.1% v/v) and **(B)** reference compounds (salicin, salicylic acid, picein, and triandrin) and Salixin Organic Powder and Extract against CVA9 using CPE inhibition assay. Virus control and test samples are normalized against a mock infection. The results are mean of two independent experiments with $n = 3$. The average values + standard errors of mean (SEM) are shown. P-16 = 2-L scale clone 16; Salixin P = Salixin Organic Powder 48™; Salixin E = Salixin Organic Extract 800NP™; SA = salicylic acid.

aureus. However, Salixin Organic Extract was considerably darker than the other samples, and this could have an effect on light reduction. The disadvantages of this method have been minimized by using small concentrations of dark-colored samples to reduce the effect of color and by repeating the measurement three times to ensure comparability between measurements (Tienaho, 2020).

When grouping the clone extract results into *S. myrsinifolia* (clones 1–3), *S. phylicifolia* (4–7), native hybrid (8–10), artificial hybrid (11–12), and commercial clones (13–16), there was a significant difference between the groups as determined by one-way ANOVA in the *E. coli* biosensor results [$F(4,9) = 5.266$, $p = 0.013$], whereas the differences in the *S. aureus* results were statistically insignificant (**Figure 7B**). A Tukey post-hoc test revealed that *S. phylicifolia* clone extracts had significantly higher antibacterial activity against *E. coli* than the commercial clone extracts ($p = 0.007$) (**Figure 7A**). Other results were statistically similar.

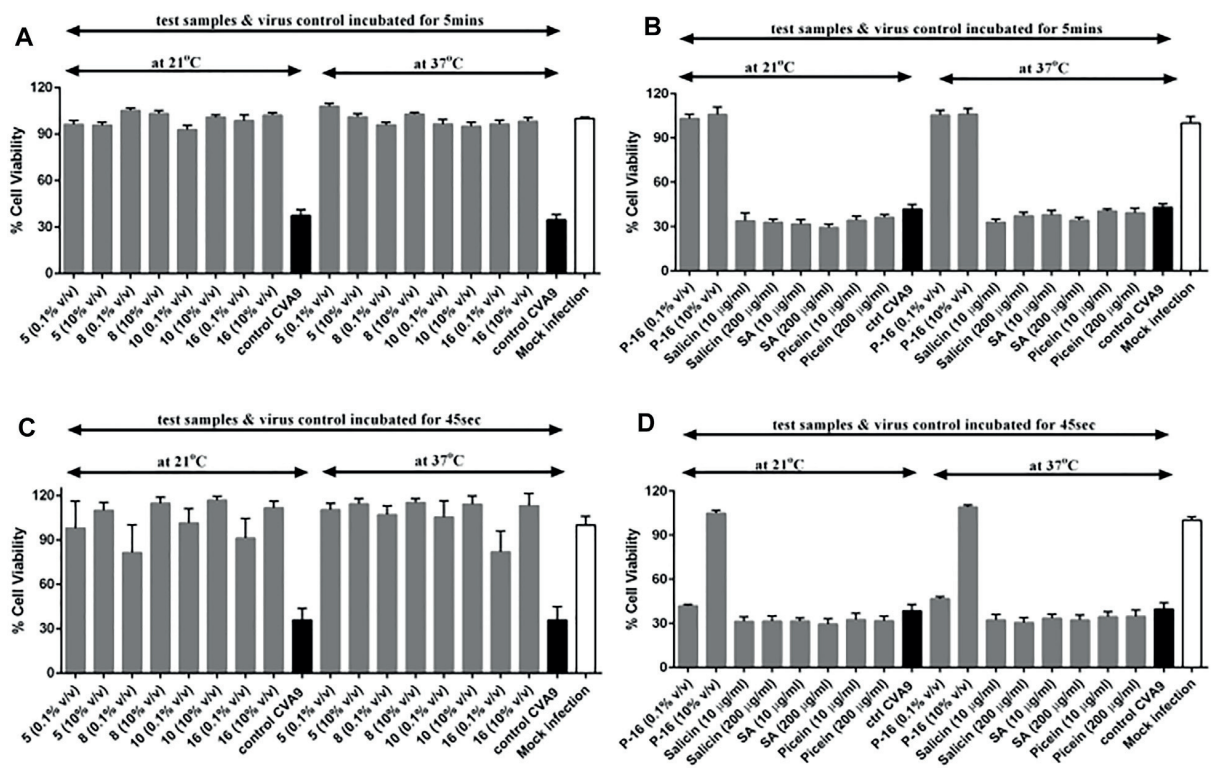

FIGURE 9 | Effect of time and temperature on the antiviral activity of selected *Salix* spp. extracts and reference compounds using CPE inhibition assay. *Salix* spp.-virus mix was incubated at 37°C and 21°C for **(A, B)** 5 min and **(C, D)** 45 s. Virus control and test samples are normalized against a mock infection. The results are mean of two independent experiments, with $n = 3$. The average values + standard errors of mean (SEM) are shown. P-16 = 2-L scale clone 16; SA = salicylic acid.

3.3 Antiviral Activity

The antiviral activity was evaluated using the highly stable non-enveloped enterovirus CVA9. There are more than 100 serotypes of enteroviruses with very similar structures and functions (Marjomäki et al., 2015). To date, there are no clinically approved antivirals against enteroviruses or any non-toxic natural compounds that can safely disinfect enteroviruses or other non-enveloped viruses from surfaces. Here, the tested *Salix* spp. preparations proved to be very efficient against CVA9 (**Figure 8A**). Pre-incubation of the virus with *Salix* spp. extracts fully rescued the A549 cells from infection, proving that the extracts directly bound to the capsid. *Salix* spp. samples did not show any cytotoxicity (data not shown). We also tested Salixin Organic Extract and Powder along with the reference compounds (salicin, salicylic acid, picein, and triandrin). Similar to *Salix* spp. samples, Salixin Organic Powder and Extract also showed antiviral activity and protected the cells against CVA9 infection, whereas none of the reference compounds were effective in stopping the viral infection (**Figure 8B**).

To study the impact of time and temperature on the antiviral activity of *Salix* spp. extracts in further detail, we incubated selected *Salix* spp. samples with CVA9 for a shorter time interval (5 min) and at lower temperatures (21°C vs. 37°C). The selected *Salix* spp. extracts retained their antiviral efficacy even at room temperature (21 °C) and were able to stop CVA9 infection within 5 min of incubation at both temperatures tested (**Figures 9A,B**). None of the reference compounds tested showed antiviral activity (**Figure 9B**). We tested an even shorter incubation time (45 s) to further determine the efficacy of the *Salix* spp. extracts. Interestingly, this short pre-treatment with the *Salix* spp. extracts was sufficient for the samples to exert their antiviral efficacy and protect the cells from CVA9 infection (**Figures 9C,D**). However, the 2-L stirring reactor extracted clone 16, sample P-16, did not show antiviral activity at lower concentrations (0.1% v/v) when incubated with CVA9 for 45 s at 21°C or 37°C. Nevertheless, it completely protected the cells when tested at higher concentrations (10% v/v) (**Figure 9D**). These results indicate that the *Salix* spp. extracts can effectively block CVA9 infection within a few seconds of interacting with the virus at room temperature by acting directly on the virus capsid.

When grouping the clone extract results from **Figure 8** into *S. myrsinifolia* (clones 1–3), *S. phylicifolia* (4–7), native hybrid (8–10), artificial hybrid (11–12), and commercial clones (13–16), there were no statistical differences between the groups as determined by one-way ANOVA [$F(4,11) = 0.276$, $p = 0.887$].

3.4 Antifungal Activity

The tested concentrations of Salix extract Klara (the 2-L scale sample) and Salixin Organic Extract and Powder were not

effective against fungi (*A. brasiliensis*) and yeast (*C. albicans*). A reduction in viability higher than 4 log units, as required by the EN 1275 norms to qualify the product with fungicidal or yeasticidal efficiency, was not detected. However, higher concentrations of the commercial Salixin Organic Extract (50 and 100% v/v) showed minor inhibition against both *C. albicans* and *A. brasiliensis*.

4 DISCUSSION

In the present study, we introduced a steam debarking method, which loosens the bark and allows its efficient removal; therefore, this method has the potential to decrease the costs of willow debarking. However, our results showed that some antioxidant activity was lost in the steam-treated bark samples. The original bark extract had higher polyphenol content and antioxidant capacity than the steam-treated bark extract, indicating that some phytochemicals were leached away in the process. One of the major constituents of various biomasses is lignin, which has been found to possess anti-inflammatory and antioxidant activities, and it has been found to degrade at high temperatures (Gu et al., 2021; Wang et al., 2021; Zheng et al., 2021). However, the steam-treatment temperatures did not rise above 180°C, and the decomposition of lignin, which is rather slow, has been considered to start at temperatures over 180°C (Nassar and MacKay, 1984; Brebu and Vasile, 2010). In the hydrothermal steam treatment of *Populus deltoides* (W. Bartram ex Marshall, Salicaceae), lignin content was only slightly decreased (Bobleter, 1994). Therefore, it is more likely that the degradation of other extractives, such as salicinoid or polyphenol structures, caused the decrease in the antioxidant capacity after steam treatment, especially if salicinoid structures were unstable (Julkunen-Tiitto and Sorsa, 2001; Ruuhola and Julkunen-Tiitto, 2003). Additionally, a substantial degradation of acetyl groups in hemicellulose can be expected at the temperature of 180°C (Steinbach et al., 2017). Antioxidant activity has been reported at least for xylo-oligosaccharide (hemicellulose model compounds) (Wu et al., 2019) and corn bran hemicellulose fragments (Ohta et al., 1994). However, without further structural characterization, any certainty is difficult to accomplish, and this poses a great opportunity for subsequential experimental studies.

All the tested concentrations of *Salix* spp. extracts and the commercial Salixin Organic Extract and Powder were effective against the non-enveloped CVA9. Enteroviruses such as CVA9 cause many acute and chronic infections on a yearly basis (Marjomäki et al., 2015). To the best of our knowledge, no previous studies have investigated the effectiveness of willow extracts directly against non-enveloped enteroviruses. However, effectiveness of natural compounds found in *Salix* spp. has been established for viruses sealed with lipid envelopes. For example, a review by Grienke et al. (2012) covered several studies performed between 2000 and 2011 on natural products specifically targeting the viral surface protein neuraminidase of influenza virus. They showed that the majority of the active natural products with the desired activity belonged to flavonoids, while (oligo)stilbenes, coumarins, and diarylheptanoids exhibited lower activity (Grienke et al., 2012). Liu et al. (2008) found that the activity for flavonoids was highest in aurones followed by flavon(ol)es, isoflavones, and flavanon(ol)es and flavan(ol)es, in this order, and that the C4′-OH, C7-OH, C4-O double bond, and C2-C3 double bond functionalities were essential for the inhibitory activity of these compounds.

Here, we showed that salicin, picein, salicylic acid, and triandrin were not responsible for the antibacterial and antiviral activities detected, at least not alone. *Salix* spp. clone extracts are highly antibacterial even at low concentrations and show similar luminescence light reduction as the bark extracts from Norway spruce [*Picea abies* (L.) H. Karst] found in Välimaa et al. (2020). Salicinoids are not present in spruce, and they are unstable and prone to decomposition especially with higher molecular masses (Julkunen-Tiitto and Sorsa, 2001; Ruuhola and Julkunen-Tiitto, 2003). This could indicate that other secondary metabolites, such as tannins, could affect bactericidal efficacy. In addition, none of the reference compounds showed antiviral activity against non-enveloped CVA9. This indicated that the presence of bioactive compounds other than the reference compounds tested here (e.g., picein and triandrin) is responsible for the antiviral activity of the *Salix* spp. extracts (cf. Dou et al., 2021). One interesting option for future studies is the tannins, which are likely to be found in the willow bark water extracts and have recently been associated with antiviral efficacies (e.g., Vilhelmova-Ilieva et al., 2019; Fraga-Corral et al., 2021). Contradictory results and hypotheses exist on whether polyphenols influence the overall bioactive efficacy of willow extracts (Khayyal et al., 2005; Nahrstedt et al., 2007; Antoniadou et al., 2021). Therefore, more research is needed to achieve any certainty regarding their effects on the bioactivities of willow extracts. However, extracts containing a mixture of willow compounds could also have synergistic effects. Similar observations were made by Shara and Stohs (2015), who concluded that the typical effective dosage of aspirin is twice that of salicin needed in willow bark extract, probably because of the presence of beneficial polyphenols and flavonoids in the bark extract.

The results obtained in the present study demonstrate the excellent antiviral, antioxidant, and antibacterial effects of *Salix* spp. bark extracts. Pearson's linear correlation coefficient absolute values (**Table 2**) indicated either a strong or moderate relationship between *E. coli* and *S. aureus* antibacterial test results (60%) for the *Salix* clones, both bacteria with enterovirus results (*E. coli* vs. entero: 67%; *S. aureus* vs. entero: 28%), ORAC and FRAP values (76%), ORAC and total phenol content (84%), FRAP and total phenol content (85%), and *E. coli* and FRAP test results (75%). A strong relationship was obtained between *E. coli* and ORAC test values (61%), *E. coli* and total phenol results (67%), *S. aureus* and ORAC values (41%), and *S. aureus* and FRAP values (53%). A moderate relationship was obtained for *S. aureus* and total phenol content (38%) and for enterovirus results and FRAP values (47%) as well as enterovirus and total phenol content results (45%), and enterovirus and ORAC results (36%).

TABLE 2 | Pearson's correlation coefficients for the different bioactivity tests. Values 0.70–0.99 indicate a very strong relationship, values 0.40–0.69 indicate a strong relationship, values 0.30–0.39 indicate a mediocre relationship, values 0.20–0.29 indicate a weak relationship, and values 0.01–0.19 indicate no or negligible relationship. The upper part of the matrix indicates the *p*-values for the data determined by a two-tailed *t*-test ($n = 16$ for ORAC, FRAP, and Phenols tests, $n = 17$ for the *E. coli*, *S. aureus*, and Enterovirus test). Most of the *p*-values are below 0.05, which indicates significant differences.

	ORAC	*E. coli*	FRAP	Phenols	*S. aureus*	Enterovirus
ORAC	**1**	<0.05	<0.001	<0.001	0.113	0.167
E. coli	0.61	**1**	<0.001	<0.05	<0.05	<0.05
FRAP	0.76	0.75	**1**	<0.001	<0.05	0.065
Phenols	0.84	0.67	0.85	**1**	0.146	<0.01
S. aureus	0.41	0.60	0.53	0.38	**1**	0.28
Enterovirus	0.36	0.67	0.47	0.45	0.28	**1**

Fungal infections and fungal resistance to currently available antifungal drugs are increasing globally. Fungal infections, as well as their prevention and treatment, also remain largely understudied compared to other infectious diseases (Brown et al., 2012). Novel and safe antifungal drugs and agents are needed for currently less common fungi, such as the recently reported Zygomycetes causing rare and life-threatening mucormycosis infection in patients with COVID-19 (do Monte Junior et al., 2020). For long, Amphotericin B was the only antifungal medication available, and only during the past three decades has a wider spectrum of antifungal agents (e.g., triazoles and echninocandin antifungals) become available (Spanakis et al., 2006). Promising antifungal compounds, including phenolic compounds, have been found in plants (Arif et al., 2008). To the best of our knowledge, no previous studies have investigated the efficacy of willow extracts against fungi and yeasts. Unfortunately, the *Salix* spp. bark extracts tested here showed no antifungal or yeasticidal activity. The only sample with putative mild activity was the commercial Salixin Organic Extract, which showed a minor inhibition of both *C. albicans* and *A. brasiliensis* when considerably concentrated.

The bioactivities of the domestic (1–12) and commercial clone extracts (13–16) were surprisingly similar despite the differences in harvesting time, age, and growing conditions of these two groups. However, the grouped commercial clone extracts showed significantly lower antioxidant (in ORAC and FRAP) and antimicrobial (*E. coli*) activities, as well as lower total phenolic capacity (Folin-Ciocalteu), than *S. phylicifolia*. In the H_2O_2 scavenging tests, the commercial clones showed significantly lower activities than all the other groups, and the FRAP test evidenced lower activity than that of *S. myrsinifolia*. The native clones had already reached the stage of vegetative bud burst, whereas the commercial clones had no visible signs of vegetative growth, indicating that they were in a state of dormancy (Saska and Kuzovkina 2010). According to Förster et al. (2008), the number of secondary metabolites in the bark of willow clones decreased during the vegetative season from March to July. The domestic clones were 1 year younger than the commercial clones. Nissinen et al. (2018) found only a minor decrease in the stem phenolic concentrations of *S. myrsinifolia* during a 7-year study period. Instead, Tahvanainen et al. (1985a) showed a significantly higher concentration of phenolic glycosides in juvenile willow twigs than in mature twigs. In the present study, the domestic clones grew in small polystyrene containers and restricted conditions, which could have resulted in higher amounts of polyphenolic defense and resistance compounds. According to Paunonen et al. (2009), polythene mulching and fertilization increased the yield of foliar salicylates because of the enhanced leaf biomass, but not the salicylate concentration in *S. myrsinifolia* clones. Furthermore, they noted that the yields and concentrations of leaf phenolics seemed to be more influenced by the clone than by the cultivation method. According to Glynn et al. (2004), drought treatment did not affect the foliar phenolic concentrations of willow genotypes.

Small differences were observed in the antibacterial tests, where commercial clones 14–16 seemed to have a somewhat lower effect in *E. coli* and commercial clone 14 seemed to have a lower effect in *S. aureus*. The commercial clones 13, 15, and 16 also showed almost no H_2O_2 scavenging activity in the antioxidant tests. The total phenol content and the composition of phenolic compounds vary widely among willow species, and the composition of leaf phenolic glycosides is species-specific (Julkunen-Tiitto, 1986). *S. myrsinifolia* (former *Salix nigricans* Sm.) clearly differed from other native species in terms of high phenolic glycoside content in leaves, mostly due to salicortin (Tahvanainen et al., 1985b), and so did the introduced species *S. dasyclados*. According to Julkunen-Tiitto (1986), *S. phylicifolia* leaves contained the highest total phenolic content among the 15 Salicaceae species studied, with more than 15% of dry weight, whereas *S. myrsinifolia* leaves had the lowest total phenolic content. In the present study, four clones (clones 4–7) with the highest total phenol content in the bark extracts were identified as *S. phylicifolia*. In contrast, *S. myrsinifolia* bark and leaves were characterized by higher amounts of phenolic glycosides such as salicylates (Julkunen-Tiitto, 1985, 1986), whereas the low content of phenolic glycosides was typical of *S. phylicifolia* and *S. viminalis* L. The latter is the main species in the ancestry of the commercial clones examined here, showing slightly lower antibacterial effects. Clonal variation exists within species; for example, Paunonen et al. (2009) showed highly variable responses of *S. myrsinifolia* clones to fertilization and mulching treatments, and thus to the yield of foliar phenolics, and they concluded that willow cultivation for the herbal industry should be based on correct clone selection.

Bark extracts of *S. myrsinifolia* × *phylicifolia* hybrids (clones 8–10) did not statistically differ from other native clones in terms of bioactivity, except in the H_2O_2 scavenging antioxidant test, when clones 7 and 14 were removed. There was also a statistically

significant difference between the higher inhibition-% values of *S. myrsinifolia* clone extracts compared to native hybrid extract values (p = 0.049). According to Julkunen-Tiitto (1986), these native hybrids resemble *S. phylicifolia* on the basis of total phenolics in leaves, but *S. myrsinifolia* by their foliar glycosidic composition (Julkunen-Tiitto, 1986). In Hallgren et al. (2003), F1-hybrids of *S. caprea* L. and *S. repens* L. were intermediate between their parental species in terms of foliar secondary metabolites and herbivore resistance but increased hybridization decreased this resistance. In the present study, clones 11 and 12 were hybrids of three species from controlled crossings, i.e., female (*S. myrsinifolia* × *phylicifolia*) × male *S. dasyclados*. In particular, the bark extract of clone 11 showed a somewhat lower total phenolic content and weaker antibacterial activity than the bark extracts of native species. In fact, all commercial clones are also outcomes of multiple crossings between different willow species, with *S. viminalis* being the most used ancestor, and characterized by low content of phenolic glycosides (Julkunen-Tiitto, 1985, 1986). Thus, both of these reasons may explain the significantly lower antibacterial effects of the commercial clones. Another possible cause of the difference in the activities of artificial hybrids and commercial clones could be the difference in the bioactive polyphenol compound composition or quantity, which would be interesting to study in the future. Further interesting questions arise, whether the beneficial antioxidant and antimicrobial activities and total phenolic capacity of *S. phylicifolia* could be increased by intraspecific crossings, or whether they are inevitably decreased by repeated species hybridization when, for instance, breeding for higher yield.

This study verified the antimicrobial potential of the willow bark biomass extracts. Antimicrobial and antiviral protection are required for a variety of industrial applications. For example, it has been estimated that by the year 2027, the antimicrobial packaging market would globally reach the value of 13.28 billion pounds (VMR Verified Market Research, 2020). It is noteworthy that viruses such as noroviruses, which cause the nasty outbreaks of stomach infection, are non-enveloped viruses such as the enterovirus CVA9 studied here. Non-enveloped viruses are much more difficult to decontaminate than enveloped viruses because of the tight protein package around the virus genome instead of the lipid envelope, which is more vulnerable to breakage. In addition to noroviruses, enteroviruses transmit easily through surfaces and cause acute and chronic infections. Currently, there are no effective and safe antivirals that directly act on virus particles. *Salix* spp. extracts offer a safe and affordable solution to combat these stable viruses. Antiviral and antimicrobial compounds from renewable willow could also replace products that may not be readily biodegradable.

For obtaining valuable phenolic compounds from willow bark, one of the limiting factors has been laborious debarking. In the present study, we showed that steaming can be used for fast and efficient debarking, while only some antioxidant potential is lost in the process. Thus, this method has potential at industrial scale.

In the European Union, plantations of short rotation coppice (SRC) willows have been established in the past, primarily for energy use purposes. Willows could offer advantages over mainstream commercial conifers owing to their fast growth and high productivity. SRC willows may also provide environmental benefits in terms of carbon sequestration when grown on marginal land, such as abandoned agricultural land or peatland (Rytter et al., 2015). For well-managed willows growing at the underappreciated peatland, the annual yield can reach up to >12.3 oven dry ton (odt)/ha, which exceeds about 8%–30% of the yield obtained with the domestic natural forest species (i.e., birch and grey alder) on the same land (Hytönen and Saarsalmi, 2009). In Finland, bioenergy-targeted projects in the 1980s produced knowledge on the hybridization, cultivation, and management of SRC willows for energy use. High biomass yields are achievable if cultivation is based on well-adapted, selected clones, and biotic and abiotic damages are avoided (Volk et al., 2004; Verwijst et al., 2013). This knowledge is a valuable foundation for creating willow biorefinery approaches for high added value. The comprehensive and optimized utilization of willow lignocellulosic biomass will promote sustainability and carbon neutrality, but requires further research, for example, on the life-cycle assessment of the production and processing value chain (cf. Rasi et al., 2019).

In conclusion, the present study provides novel information on the antioxidant, antibacterial, and antiviral properties of polyphenolic bark extracts of SRC willows well adapted to the Finnish growing environment, by using scalable green extraction techniques. We found that all the tested concentrations of *Salix* spp. extracts were effective against the non-enveloped enterovirus CVA9 as well as *E. coli* and *S. aureus* strains. However, there seemed to be more variation between the clones in their antioxidant activities determined by ORAC, FRAP, and H_2O_2 scavenging abilities. No marked efficacy was detected in the antifungal or yeasticidal tests. When clone extracts were grouped, *S. phylicifolia* clones showed the most promising antioxidant and antibacterial activities with significant differences when compared to commercial and artificial clones. This can partly be caused by the effect of stronger hybridization; however, more studies are needed to examine the possible effects of compound composition and content of the extracts. We also showed that salicin, picein, salicylic acid, and triandrin are not responsible for the antibacterial and antiviral activities detected here, at least not alone. Instead, other compounds of interest, such as polyphenols, or synergistic effects between the compounds, are likely to cause the detected efficacies. We also demonstrated for the first time that steam debarking is a promising, less-laborious method for the efficient separation of bark from wood (harvested in the spring season), with only minor effects on the antioxidant properties of bark. This method promotes the cascade use of willow biomass, where the debarked wood can be used for other purposes. Our findings will potentially lead to scientific breakthroughs given that the studied crude extracts with promising mixtures of components are highly effective against the stable non-enveloped viruses that cause nasty acute and chronic infections. Further investigations and development of such antiviral solutions for enveloped viruses are topics for our next studies. Biochemicals obtained from tree bark biomass and side products of biorefinery approaches have potential for various

applications (e.g., health promotion, cosmetics, pharmaceuticals, packaging, coatings, other functional materials, and surfaces). Willow, as a short-rotation coppice species with a fast growth rate and high yield on marginal lands, presents a promising alternative for the currently most common commercial tree species in Finland.

DATA AVAILABILITY STATEMENT

The original contributions presented in the study are included in the article/**Supplementary Material**. Further inquiries can be directed to the corresponding author.

AUTHOR CONTRIBUTIONS

Conceptualization: AV-A, PK, TJ, and VM; Data curation: DR, JL, JT, PK, RL, and TS; Formal analysis: AV-A, DR, JD, JT, PK, and RL; Funding acquisition and Resources: TJ and VM; Investigation: DR, JD, JT, and PK; Methodology: JD, JT, PK, RL, TS, and VM; Project administration and Supervision: TJ and VM; Validation: AV-A, DR, JT, PK, RL, and TS; Visualization: DR, JT, PK, and TS; Writing—original draft: AV-A, DR, JL, JT, PK, RL, TJ, and VM; Writing—review and editing: all authors.

FUNDING

This work was supported by Business Finland corona-co-creation funding for the project Antiviral Fibers—pilot with extracts from Finnish forests (grant: 40699/31/2020). This study was also funded by the Natural Resources Institute Finland's strategic research funding to the projects "More, faster, higher quality: potential of short-rotation aspen and willow biomass for novel products in bioeconomy" (AspenWill) and "Added value potential of new and under-utilized fibre sources in Finnish value networks of green bioeconomy: prefeasibility, prototyping, and market acceptance" (VALUEPOT). In addition, Academy of Finland has supported this study *via* the project "Antivirals from Forest Biomasses: Structure, Function, and Applicability" (grant: 342250). Work was also funded by Jane and Aatos Erkko Foundation: Novel probes for discovering antivirals.

ACKNOWLEDGMENTS

We thank Elvi Pääkkönen, Esa Ek, Pauli Karppinen, Kalle Kaipanen, Carita Karenius, Katri Leino, Tuija Hytönen, Hanna Leppälammi, Anneli Käenmäki, and Eeva Pihlajaviita for skillful laboratory and field work. Markku Suutari (Carbons Finland Oy) is acknowledged for providing the research with Swedish commercial willow materials. Senior Curator Henry Väre is warmly acknowledged for the help with the willow identifications. The authors also thank Janne Kaseva for proficient help with the statistical analysis.

SUPPLEMENTARY MATERIAL

The Supplementary Material for this article can be found online at: https://www.frontiersin.org/articles/10.3389/fbioe.2021.797939/full#supplementary-material

REFERENCES

Ainsworth, E. A., and Gillespie, K. M. (2007). Estimation of Total Phenolic Content and Other Oxidation Substrates in Plant Tissues Using Folin-Ciocalteu Reagent. *Nat. Protoc.* 2, 875–877. doi:10.1038/nprot.2007.102

Antoniadou, K., Herz, C., Le, N. P. K., Mittermeier-Kleßinger, V. K., Förster, N., Zander, M., et al. (2021). Identification of Salicylates in Willow Bark (*Salix* Cortex) for Targeting Peripheral Inflammation. *Ijms* 22, 11138. doi:10.3390/ijms222011138

Arif, T., Bhosale, J. D., Kumar, N., Mandal, T. K., Bendre, R. S., Lavekar, G. S., et al. (2009). Natural Products - Antifungal Agents Derived from Plants. *J. Asian Nat. Prod. Res.* 11, 621–638. doi:10.1080/10286020902942350

Benzie, I. F. F., and Strain, J. J. (1996). The Ferric Reducing Ability of Plasma (FRAP) as a Measure of "Antioxidant Power": The FRAP Assay. *Anal. Biochem.* 239, 70–76. doi:10.1006/abio.1996.0292

Bobleter, O. (1994). Hydrothermal Degradation of Polymers Derived from Plants. *Prog. Polym. Sci.* 19, 797–841. doi:10.1016/0079-6700(94)90033-7

Boeckler, G. A., Gershenzon, J., and Unsicker, S. B. (2011). Phenolic Glycosides of the Salicaceae and Their Role as Anti-herbivore Defenses. *Phytochemistry* 72, 1497–1509. doi:10.1016/j.phytochem.2011.01.038

Bounaama, A., Enayat, S., Ceyhan, M. S., Moulahoum, H., Djerdjouri, B., and Banerjee, S. (2016). Ethanolic Extract of Bark fromSalix aegyptiacaAmeliorates 1,2-Dimethylhydrazine-Induced Colon Carcinogenesis in Mice by Reducing Oxidative Stress. *Nutr. Cancer* 68, 495–506. doi:10.1080/01635581.2016.1152379

Brebu, M., and Vasile, C. (2010). Thermal Degradation of Lignin—A Review. *Cellul. Chem. Technol.* 44, 353.

Brereton, N. J. B., Berthod, N., Lafleur, B., Pedneault, K., Pitre, F. E., and Labrecque, M. (2017). Extractable Phenolic Yield Variation in Five Cultivars of Mature Short Rotation Coppice Willow from Four Plantations in Quebec. *Ind. Crops Prod.* 97, 525–535. doi:10.1016/j.indcrop.2016.12.049

Brown, G. D., Denning, D. W., and Levitz, S. M. (2012). Tackling Human Fungal Infections. *Science* 336, 647. doi:10.1126/science.1222236

Christenhusz, M. J. M., Fay, M. F., and Chase, M. W. (2017). *Plants of the World*. KewChina: Kew Publishing Royal Botanic GardensThe University of Chicago Press.

Chrubasik, S., Eisenberg, E., Balan, E., Weinberger, T., Luzzati, R., and Conradt, C. (2000). Treatment of Low Back Pain Exacerbations with Willow Bark Extract: a Randomized Double-Blind Study. *Am. J. Med.* 109, 9–14. doi:10.1016/S0002-9343(00)00442-3

DIN EN 1275 (2006). *Chemical Disinfectants and Antiseptics - Quantitative Suspension Test for the Evaluation of Basic Fungicidal or Basic Yeasticidal Activity of Chemical Disinfectants and Antiseptics - Test Method and Requirements*. (phase 1).

Djomo, S. N., Kasmioui, O. E., and Ceulemans, R. (2011). Energy and Greenhouse Gas Balance of Bioenergy Production from poplar and Willow: a Review. *Glob. Change Biol. Bioenergy* 3, 181–197. doi:10.1111/j.1757-1707.2010.01073.x

Dou, J., Galvis, L., Holopainen-Mantila, U., Reza, M., Tamminen, T., and Vuorinen, T. (2016). Morphology and Overall Chemical Characterization of Willow (*Salix* sp.) Inner Bark and Wood: Toward Controlled Deconstruction of Willow Biomass. *ACS Sustainable Chem. Eng.* 4, 3871–3876. doi:10.1021/acssuschemeng.6b00641

Dou, J., Heinonen, J., Vuorinen, T., Xu, C., and Sainio, T. (2021). Chromatographic Recovery and Purification of Natural Phytochemicals from Underappreciated

Willow Bark Water Extracts. *Separation Purif. Technology* 261, 118247. doi:10.1016/j.seppur.2020.118247

Dou, J., Paltakari, J., Johansson, L.-S., and Vuorinen, T. (2019). Novel Insight into the Separation and Composite Utilization of Sclerenchyma Fiber Bundles of Willow Bark. *ACS Sustainable Chem. Eng.* 7, 2964–2970. doi:10.1021/acssuschemeng.8b04001

Dou, J., Xu, W., Koivisto, J. J., Mobley, J. K., Padmakshan, D., Kögler, M., et al. (2018). Characteristics of Hot Water Extracts from the Bark of Cultivated Willow (*Salix* sp.). *ACS Sustainable Chem. Eng.* 6, 5566–5573. doi:10.1021/acssuschemeng.8b00498

Durak, A., and Gawlik-Dziki, U. (2014). The Study of Interactions between Active Compounds of Coffee and Willow (Salixsp.) Bark Water Extract. *Biomed. Res. Int.* 2014, 1–11. doi:10.1155/2014/386953

El-Shemy, H. A., Aboul-Enein, A. M., Aboul-Enein, K. M., and Fujita, K. (2007). Willow Leaves' Extracts Contain Anti-tumor Agents Effective against Three Cell Types. *PLoS One* 2 (1), e178. doi:10.1371/journal.pone.0000178

Förster, N., Ulrichs, C., Zander, M., Kätzel, R., and Mewis, I. (2008). Influence of the Season on the Salicylate and Phenolic Glycoside Contents in the Bark of *Salix Daphnoides, Salix Pentandra*, and *Salix Purpurea*. *J. Appl. Bot. Food Qual.* 82, 99–102.

Fraga-Corral, M., Otero, P., Echave, J., Garcia-Oliveira, P., Carpena, M., Jarboui, A., et al. (2021). By-Products of Agri-Food Industry as Tannin-Rich Sources: A Review of Tannins' Biological Activities and Their Potential for Valorization. *Foods* 10, 137. doi:10.3390/foods10010137

Glynn, C., Rönnberg-Wästljung, A.-C., Julkunen-Tiitto, R., and Weih, M. (2004). Willow Genotype, but Not Drought Treatment, Affects Foliar Phenolic Concentrations and Leaf-Beetle Resistance. *Entomologia Experimentalis et Applicata* 113, 1–14. doi:10.1111/j.0013-8703.2004.00199.x

Grienke, U., Schmidtke, M., von Grafenstein, S., Kirchmair, J., Liedl, K. R., and Rollinger, J. M. (2012). Influenza Neuraminidase: a Druggable Target for Natural Products. *Nat. Prod. Rep.* 29, 11–36. doi:10.1039/C1NP00053E

Gu, J., Guo, M., Zheng, L., Yin, X., Zhou, L., Fan, D., et al. (2021). Protective Effects of Lignin-Carbohydrate Complexes from Wheat Stalk against Bisphenol a Neurotoxicity in Zebrafish via Oxidative Stress. *Antioxidants* 10, 1640. doi:10.3390/antiox10101640

Hallgren, P., Ikonen, A., Hjalten, J., and Roininen, H. (2003). Inheritance Patterns of Phenolics in F1, F2, and Back-Cross Hybrids of willows: Implications for Herbivore Responses to Hybrid Plants. *J. Chem. Ecol.* 29, 1143–1158. doi:10.1023/A:1023829506473

Hazra, B., Biswas, S., and Mandal, N. (2008). Antioxidant and Free Radical Scavenging Activity of *Spondias Pinnata*. *BMC Complement. Altern. Med.* 8, 63. doi:10.1186/1472-6882-8-63

Heiska, S., Tikkanen, O.-P., Rousi, M., and Julkunen-Tiitto, R. (2007). Bark Salicylates and Condensed Tannins Reduce Vole Browsing Amongst Cultivated Dark-Leaved willows (*Salix Myrsinifolia*). *Chemoecology* 17, 245–253. doi:10.1007/s00049-007-0385-9

Hobisch, M. A., Phiri, J., Dou, J., Gane, P., Vuorinen, T., Bauer, W., et al. (2020). Willow Bark for Sustainable Energy Storage Systems. *Materials* 13, 1016. doi:10.3390/ma13041016

Hou, J., Guo, Z., Liu, H., and Yin, T. (2017). Gender Effects on Salix Suchowensis Growth and wood Properties as Revealed by a Full-Sib Pedigree. *Can. J. Plant Sci.* 97, 594–600. doi:10.1139/cjps-2016-0153

Huang, D., Ou, B., Hampsch-Woodill, M., Flanagan, J. A., and Prior, R. L. (2002). High-throughput Assay of Oxygen Radical Absorbance Capacity (ORAC) Using a Multichannel Liquid Handling System Coupled with a Microplate Fluorescence Reader in 96-well Format. *J. Agric. Food Chem.* 50, 4437–4444. doi:10.1021/jf0201529

H. Väre, J. Saarinen, A. Kurtto, and L. Hämet-Ahti (Editors) (2021). *Suomen Puu-Ja Pensaskasvio [Woody Flora of Finland]*. third ed. (Helsinki: Publications of the Finnish Dendrological Society), 10.

Hytönen, J., and Saarsalmi, A. (2009). Long-term Biomass Production and Nutrient Uptake of Birch, Alder and Willow Plantations on Cut-Away Peatland. *Biomass and Bioenergy* 33, 1197–1211. doi:10.1016/j.biombioe.2009.05.014

Ikonen, A., Tahvanainen, J., and Roininen, H. (2002). Phenolic Secondary Compounds as Determinants of the Host Plant Preferences of the Leaf Beetle *Agelastica Alni*. *Chemoecology* 12, 125–131. doi:10.1007/s00012-002-8337-2

Jiang, Z.-Y., Woollard, A. C. S., and Wolff, S. P. (1990). Hydrogen Peroxide Production during Experimental Protein Glycation. *FEBS Lett.* 268, 69–71. doi:10.1016/0014-5793(90)80974-N

Julkunen-Tiitto, R. (1986). A Chemotaxonomic Survey of Phenolics in Leaves of Northern Salicaceae Species. *Phytochemistry* 25, 663–667. doi:10.1016/0031-9422(86)88020-7

Julkunen-Tiitto, R. (1985). Chemotaxonomical Screening of Phenolic Glycosides in Northern Willow Twigs by Capillary Gas Chromatography. *J. Chromatogr. A* 324, 129–139. doi:10.1016/S0021-9673(01)81312-1

Julkunen-Tiitto, R., and Sorsa, S. (2001). Testing the Effect of Drying Methods on Willow Flavonoids, Tannins and Salicylates. *J. Chem. Ecol.* 27, 779–789. doi:10.1023/A:1010358120482

Julkunen-Tiitto, R., and Virjamo, V. (2017). "Biosynthesis and Roles of Salicaceae Salicylates," in *Plant Specialized Metabolism: Genomics, Biochemistry, and Biological Functions*. Editors G. Arimura and M. Maffei (Boca Raton: CRC Press), 65–83.

Kammerer, B., Kahlich, R., Biegert, C., Gleiter, C. H., and Heide, L. (2005). HPLC-MS/MS Analysis of Willow Bark Extracts Contained in Pharmaceutical Preparations. *Phytochem. Anal.* 16, 470–478. doi:10.1002/pca.873

Khayyal, M., El-Ghazaly, M., Abdallah, D., Okpanyi, S., Kelber, O., and Weiser, D. (2005). Mechanisms Involved in the Anti-inflammatory Effect of a Standardized Willow Bark Extract. *Arzneimittelforschung* 55, 677–687. doi:10.1055/s-0031-1296917

Kilpeläinen, P., Leppänen, K., Spetz, P., Kitunen, V., Ilvesniemi, H., Pranovich, A., et al. (2012). BIOREFINERY. Pressurised Hot Water Extraction of Acetylated Xylan from Birch Sawdust. *Pulp Pap. Res. J.* 27, 680–688. doi:10.3183/npprj-2012-27-04-p680-688

Kilpeläinen, P. O., Hautala, S. S., Byman, O. O., Tanner, L. J., Korpinen, R. I., Lillandt, M. K.-J., et al. (2014). Pressurized Hot Water Flow-Through Extraction System Scale up from the Laboratory to the Pilot Scale. *Green. Chem.* 16, 3186–3194. doi:10.1039/C4GC00274A

Krzyżaniak, M., Stolarski, M. J., Szczukowski, S., and Tworkowski, J. (2016). Life Cycle Assessment of New Willow Cultivars Grown as Feedstock for Integrated Biorefineries. *Bioenerg. Res.* 9, 224–238. doi:10.1007/s12155-015-9681-3

Lavola, A., Maukonen, M., and Julkunen-Tiitto, R. (2018). Variability in the Composition of Phenolic Compounds in winter-dormant *Salix Pyrolifolia* in Relation to Plant Part and Age. *Phytochemistry* 153, 102–110. doi:10.1016/j.phytochem.2018.05.021

Liu, A.-L., Wang, H.-D., Lee, S. M., Wang, Y.-T., and Du, G.-H. (2008). Structure-activity Relationship of Flavonoids as Influenza Virus Neuraminidase Inhibitors and Their *In Vitro* Anti-viral Activities. *Bioorg. Med. Chem.* 16, 7141–7147. doi:10.1016/j.bmc.2008.06.049

Malterud, K. E., Bremnes, T. E., Faegri, A., Moe, T., Dugstad, E. K. S., Anthonsen, T., et al. (1985). Flavonoids from the wood of *Salix Caprea* as Inhibitors of wood-destroying Fungi. *J. Nat. Prod.* 48, 559–563. doi:10.1021/np50040a007

Marjomäki, V., Turkki, P., and Huttunen, M. (2015). Infectious Entry Pathway of Enterovirus B Species. *Viruses* 7, 6387–6399. doi:10.3390/v7122945

Monte Junior, E. S. d., Santos, M. E. L. d., Ribeiro, I. B., Luz, G. d. O., Baba, E. R., Hirsch, B. S., et al. (2020). Rare and Fatal Gastrointestinal Mucormycosis (Zygomycosis) in a COVID-19 Patient: a Case Report. *Clin. Endosc.* 53, 746–749. doi:10.5946/ce.2020.180

Mostafa, I., Abbas, H. A., Ashour, M. L., Yasri, A., El-Shazly, A. M., Wink, M., et al. (2020). Polyphenols from *Salix Tetrasperma* Impair Virulence and Inhibit Quorum Sensing of *Pseudomonas aeruginosa*. *Molecules* 25, 1341. doi:10.3390/molecules25061341

Nahrstedt, A., Schmidt, M., Jäggi, R., Metz, J., and Khayyal, M. T. (2007). Willow Bark Extract: the Contribution of Polyphenols to the Overall Effect. *Wien. Med. Wochenschr.* 157, 348–351. doi:10.1007/s10354-007-0437-3

Nassar, M. M., and MacKay, G. D. M. (1984). Mechanism of thermal Decomposition of Lignin. *Wood Fiber Sci.* 16, 441–453.

Nissinen, K., Virjamo, V., Mehtätalo, L., Lavola, A., Valtonen, A., Nybakken, L., et al. (2018). A Seven-Year Study of Phenolic Concentrations of the Dioecious *Salix Myrsinifolia*. *J. Chem. Ecol.* 44, 416–430. doi:10.1007/s10886-018-0942-4

Noleto-Dias, C., Harflett, C., Beale, M. H., and Ward, J. L. (2020). Sulfated Flavanones and Dihydroflavonols from Willow. *Phytochemistry Lett.* 35, 88–93. doi:10.1016/j.phytol.2019.11.008

Noleto-Dias, C., Ward, J. L., Bellisai, A., Lomax, C., and Beale, M. H. (2018). Salicin-7-sulfate: A New Salicinoid from Willow and Implications for Herbal Medicine. *Fitoterapia* 127, 166–172. doi:10.1016/j.fitote.2018.02.009

Noleto-Dias, C., Wu, Y., Bellisai, A., Macalpine, W., Beale, M., and Ward, J. (2019). Phenylalkanoid Glycosides (Non-salicinoids) from Wood Chips of Salix Triandra × Dasyclados Hybrid Willow. *Molecules* 24, 1152. doi:10.3390/molecules24061152

Ohta, T., Yamasaki, S., Egashira, Y., and Sanada, H. (1994). Antioxidative Activity of Corn Bran Hemicellulose Fragments. *J. Agric. Food Chem.* 42, 653–656. doi:10.1021/jf00039a010

Parajuli, R., Knudsen, M. T., and Dalgaard, T. (2015). Multi-criteria Assessment of Yellow, green, and Woody Biomasses: Pre-screening of Potential Biomasses as Feedstocks for Biorefineries. *Biofuels, Bioprod. Bioref.* 9, 545–566. doi:10.1002/bbb.1567

Paunonen, R., Julkunen-Tiitto, R., Tegelberg, R., Rousi, M., and Heiska, S. (2009). Salicylate and Biomass Yield, and Leaf Phenolics of Dark-Leaved Willow (Salix Myrsinifolia Salisb.) Clones under Different Cultivation Methods after the Second Cultivation Cycle. *Ind. Crops Prod.* 29, 261–268. doi:10.1016/j.indcrop.2008.05.009

Phiri, J., Dou, J., Vuorinen, T., Gane, P. A. C., and Maloney, T. C. (2019). Highly Porous Willow Wood-Derived Activated Carbon for High-Performance Supercapacitor Electrodes. *ACS Omega* 4, 18108–18117. doi:10.1021/acsomega.9b01977

Piątczak, E., Dybowska, M., Płuciennik, E., Kośla, K., Kolniak-Ostek, J., and Kalinowska-Lis, U. (2020). Identification and Accumulation of Phenolic Compounds in the Leaves and Bark of *Salix alba* (L.) and Their Biological Potential. *Biomolecules* 10, 1391. doi:10.3390/biom10101391

Poolman, J. T., and Anderson, A. S. (2018). Escherichia coliandStaphylococcus Aureus: Leading Bacterial Pathogens of Healthcare Associated Infections and Bacteremia in Older-Age Populations. *Expert Rev. Vaccin.* 17, 607–618. doi:10.1080/14760584.2018.1488590

Prior, R. L., Hoang, H., Gu, L., Wu, X., Bacchiocca, M., Howard, L., et al. (2003). Assays for Hydrophilic and Lipophilic Antioxidant Capacity (Oxygen Radical Absorbance Capacity (ORACFL)) of Plasma and Other Biological and Food Samples. *J. Agric. Food Chem.* 51, 3273–3279. doi:10.1021/jf0262256

Quosdorf, S., Schuetz, A., and Kolodziej, H. (2017). Different Inhibitory Potencies of Oseltamivir Carboxylate, Zanamivir, and Several Tannins on Bacterial and Viral Neuraminidases as Assessed in a Cell-free Fluorescence-Based Enzyme Inhibition Assay. *Molecules* 22, 1989. doi:10.3390/molecules22111989

Ramos, P. A. B., Moreirinha, C., Silva, S., Costa, E. M., Veiga, M., Coscueta, E., et al. (2019). The Health-Promoting Potential of *Salix* Spp. Bark Polar Extracts: Key Insights on Phenolic Composition and *In Vitro* Bioactivity and Biocompatibility. *Antioxidants* 8, 609. doi:10.3390/antiox8120609

Rasa, K., Viherä-Aarnio, A., Rytkönen, P., Hyväluoma, J., Kaseva, J., Suhonen, H., et al. (2021). Quantitative Analysis of Feedstock Structural Properties Can Help to Produce Willow Biochar with Homogenous Pore System. *Ind. Crops Prod.* 166, 113475. doi:10.1016/j.indcrop.2021.113475

Rasi, S., Kilpeläinen, P., Rasa, K., Korpinen, R., Raitanen, J.-E., Vainio, M., et al. (2019). Cascade Processing of Softwood Bark with Hot Water Extraction, Pyrolysis and Anaerobic Digestion. *Bioresour. Technology* 292, 121893. doi:10.1016/j.biortech.2019.121893

Ruokolainen, V., Domanska, A., Laajala, M., Pelliccia, M., Butcher, S. J., and Marjomäki, V. (2019). Extracellular Albumin and Endosomal Ions Prime Enterovirus Particles for Uncoating that Can Be Prevented by Fatty Acid Saturation. *J. Virol.* 93, e00599–19. doi:10.1128/JVI.00599-19

Ruuhola, T., and Julkunen-Tiitto, R. (2003). Trade-off between Synthesis of Salicylates and Growth of Micropropagated *Salix Pentandra*. *J. Chem. Ecol.* 29, 1565–1588. doi:10.1023/A:1024266612585

Rytter, R.-M., Rytter, L., and Högbom, L. (2015). Carbon Sequestration in Willow (*Salix* spp.) Plantations on Former Arable Land Estimated by Repeated Field Sampling and C Budget Calculation. *Biomass and Bioenergy* 83, 483–492. doi:10.1016/j.biombioe.2015.10.009

Saracila, M., Tabuc, C., Panaite, T. D., Papuc, C. P., Olteanu, M., and Criste, R. D. (2018). Effect of the Dietary Willow Bark Extract (Salix Alba) on the Caecal Microbial Population of Broilers (14-28 Days) Reared at 32°C. *Life Agriculture" Conf. Proc.* 1 (1), 155–161. doi:10.2478/alife-2018-0023

Saska, M. M., and Kuzovkina, Y. A. (2010). Phenological Stages of Willow (*Salix*). *Ann. Appl. Biol.* 156, 431–437. doi:10.1111/j.1744-7348.2010.00400.x

Shara, M., and Stohs, S. J. (2015). Efficacy and Safety of White Willow Bark (Salix alba) Extracts. *Phytother. Res.* 29, 1112–1116. doi:10.1002/ptr.5377

Singh, D. P., Moore, C. A., Gilliland, A., and Carr, J. P. (2004). Activation of Multiple Antiviral Defence Mechanisms by Salicylic Acid. *Mol. Plant Pathol.* 5, 57–63. doi:10.1111/j.1364-3703.2004.00203.x

Singleton, V. L., Orthofer, R., and Lamuela-Raventós, R. M. (1999). [14] Analysis of Total Phenols and Other Oxidation Substrates and Antioxidants by Means of Folin-Ciocalteu Reagent. *Meth. Enzymol.* 299, 152–178. doi:10.1016/S0076-6879(99)99017-1

Singleton, V. L., and Rossi, J. A., Jr. (1965). Colorimetry of Total Phenolics with Phosphomolybdic-Phosphotungstic Acid Reagents. *Am. J. Enol. Vitic.* 16, 144–158. doi:10.2307/3006717

Spanakis, E. K., Aperis, G., and Mylonakis, E. (2006). Reviews of Anti-infective Agents: New Agents for the Treatment of Fungal Infections: Clinical Efficacy and Gaps in Coverage. *Clin. Infect. Dis.* 43, 1060–1068. doi:10.1086/507891

Steinbach, D., Kruse, A., and Sauer, J. (2017). Pretreatment Technologies of Lignocellulosic Biomass in Water in View of Furfural and 5-hydroxymethylfurfural Production- A Review. *Biomass Conv. Bioref.* 7, 247–274. doi:10.1007/s13399-017-0243-0

Tahvanainen, J., Helle, E., Julkunen-Tiitto, R., and Lavola, A. (1985a). Phenolic Compounds of Willow Bark as Deterrents against Feeding by Mountain Hare. *Oecologia* 65, 319–323. doi:10.1007/bf00378905

Tahvanainen, J., Julkunen-Tiitto, R., Kettunen, J., and Lavola, A. (1985b). Phenolic Glycosides Govern the Food Selection Pattern of Willow Feeding Leaf Beetles. *Oecologia* 67, 52–56. doi:10.1007/bf00378451

Tawfeek, N., Mahmoud, M. F., Hamdan, D. I., Sobeh, M., Farrag, N., Wink, M., et al. (2021). Phytochemistry, Pharmacology and Medicinal Uses of Plants of the Genus Salix: An Updated Review. *Front. Pharmacol.* 12, 50. doi:10.3389/fphar.2021.593856

Tienaho, J., Karonen, M., Muilu-Mäkelä, R., Kaseva, J., De Pedro, N., Vicente, F., et al. (2020). Bioactive Properties of the Aqueous Extracts of Endophytic Fungi Associated with Scots Pine (*Pinus Sylvestris*) Roots. *Planta Med.* 86, 1009–1024. doi:10.1055/a-1185-4437

Tienaho, J., Sarjala, T., Franzén, R., and Karp, M. (2015). Method with High-Throughput Screening Potential for Antioxidative Substances Using *Escherichia coli* Biosensor katG′:lux. *J. Microbiol. Methods* 118, 78–80. doi:10.1016/j.mimet.2015.08.018

Tienaho, J., Silvan, N., Muilu-Mäkelä, R., Kilpeläinen, P., Poikulainen, E., and Sarjala, T. (2021). Ultraviolet Absorbance of *Sphagnum Magellanicum, S. Fallax* and *S. Fuscum* Extracts with Seasonal and Species-specific Variation. *Photochem. Photobiol. Sci.* 20, 379–389. doi:10.1007/s43630-021-00026-w

Tienaho, J. (2020). Utilizing Nordic Forest Plant and Fungi Extracts: Bioactivity Assessment with Bacterial Whole-Cell Biosensors. Academic dissertation. . https://trepo.tuni.fi/handle/10024/120296.

Tyśkiewicz, K., Konkol, M., Kowalski, R., Rój, E., Warmiński, K., Krzyżaniak, M., et al. (2019). Characterization of Bioactive Compounds in the Biomass of Black Locust, poplar and Willow. *Trees* 33, 1235–1263. doi:10.1007/s00468-019-01837-2

Välimaa, A.-L., Raitanen, J.-E., Tienaho, J., Sarjala, T., Nakayama, E., Korpinen, R., et al. (2020). Enhancement of Norway spruce Bark Side-Streams: Modification of Bioactive and Protective Properties of Stilbenoid-Rich Extracts by UVA-Irradiation. *Ind. Crops Prod.* 145, 112150. doi:10.1016/j.indcrop.2020.112150

Verwijst, T., Lundkvist, A., Edelfeldt, S., and Albertsso, J. (2013). "Development of Sustainable Willow Short Rotation Forestry in Northern Europe," in *Biomass Now–Sustainable Growth and Use*. Editor M. D. Matovic (London: IntechOpen), 479–502. doi:10.5772/55072

Vesterlund, S., Paltta, J., Lauková, A., Karp, M., and Ouwehand, A. C. (2004). Rapid Screening Method for the Detection of Antimicrobial Substances. *J. Microbiol. Methods* 57, 23–31. doi:10.101/j.mimet.2003.11.01410.1016/j.mimet.2003.11.014

Vilhelmova-Ilieva, N., S. Galabov, A., and Mileva, M. (2019). "Tannins as Antiviral Agents," in *Tannins-Structural Properties, Biological Properties and Current Knowledge*. Editor A. Aires (London: IntechOpen Limited). doi:10.5772/intechopen.86490

Vlachojannis, J. E., Cameron, M., and Chrubasik, S. (2009). A Systematic Review on the Effectiveness of Willow Bark for Musculoskeletal Pain. *Phytother. Res.* 23, 897–900. doi:10.1002/ptr.2747

VMR, Verified Market Research (2020). Global Antimicrobial Packaging Market. https://www.verifiedmarketresearch.com/product/antimicrobial-packaging-market/(accessed May 19, 2021).

Volk, T. A., Verwijst, T., Tharakan, P. J., Abrahamson, L. P., and White, E. H. (2004). Growing Fuel: a Sustainability Assessment of Willow Biomass Crops. *Front. Ecol. Environ.* 2, 411–418. doi:10.1890/1540-9295(2004)002[0411:gfasao]2.0.co;2

Wang, R., Zheng, L., Xu, Q., Xu, L., Wang, D., Li, J., et al. (2021). Unveiling the Structural Properties of Water-Soluble Lignin from Gramineous Biomass by Autohydrolysis and its Functionality as a Bioactivator (Anti-inflammatory and Antioxidative). *Int. J. Biol. Macromolecules* 191, 1087–1095. doi:10.1016/j.ijbiomac.2021.09.124

Ward, J. L., Wu, Y., Harflett, C., Onafuye, H., Corol, D., Lomax, C., et al. (2020). Miyabeacin: A New Cyclodimer Presents a Potential Role for Willow in Cancer Therapy. *Sci. Rep.* 10, 6477. doi:10.1038/s41598-020-63349-1

Wood, J. N. (2015). From Plant Extract to Molecular Panacea: a Commentary on Stone (1763) 'An Account of the success of the Bark of the Willow in the Cure of the Agues'. *Phil. Trans. R. Soc. B* 370, 20140317. doi:10.1098/rstb.2014.0317

Wu, F., Jia, X., Yin, L., Cheng, Y., Miao, Y., and Zhang, X. (2019). The Effect of Hemicellulose and Lignin on Properties of Polysaccharides in *Lentinus Edodes* and Their Antioxidant Evaluation. *Molecules* 24, 1834. doi:10.3390/molecules24091834

Wu, Y., Dobermann, D., Beale, M. H., and Ward, J. L. (2016). Acutifoliside, a Novel Benzoic Acid Glycoside from *Salix Acutifolia*. *Nat. Product. Res.* 30, 1731–1739. doi:10.1080/14786419.2015.1137571

Yan, B., Chen, Z. S., Hu, Y., and Yong, Q. (2021). Insight in the Recent Application of Polyphenols from Biomass. *Front. Bioeng. Biotechnol.* 9. doi:10.3389/fbioe.2021.753898

Zheng, L., Lu, G., Pei, W., Yan, W., Li, Y., Zhang, L., et al. (2021). Understanding the Relationship between the Structural Properties of Lignin and Their Biological Activities. *Int. J. Biol. Macromolecules* 190, 291–300. doi:10.1016/j.ijbiomac.2021.08.168

Conflict of Interest: The authors declare that the research was conducted in the absence of any commercial or financial relationships that could be construed as a potential conflict of interest.

Publisher's Note: All claims expressed in this article are solely those of the authors and do not necessarily represent those of their affiliated organizations, or those of the publisher, the editors, and the reviewers. Any product that may be evaluated in this article, or claim that may be made by its manufacturer, is not guaranteed or endorsed by the publisher.

V

WILLOW (*SALIX* SPP.) BARK HOT WATER EXTRACTS SHOW ANTIVIRAL ACTIVITY FOR BOTH ENVELOPED CORONAVIRUSES AND NON-ENVELOPED ENTEROVIRUSES

by

Dhanik Reshamwala, Sailee Shroff, Jenni Tienaho, Jaana Liimatainen, Mira Laajala, Petri Kilpeläinen, Anneli Viherä-Aarnio, Tuula Jyske & Varpu Marjomäki 2022

Manuscript

Request a copy from author.

VI

SELECTED STRAINS OF *GANODERMA* SP. FROM FINNISH FORESTS HAVE EXCELLENT BROADLY ACTING ANTIVIRAL PROPERTIES

by

Dhanik Reshamwala, Riikka Linnakoski, Sailee Shroff, Mira Laajala, Andrea Civra, Rachele Francese, Pyry Veteli, Marta Cortina-Escribano, Jaana Liimatainen, Jenni Tienaho, Tytti Sarjala, David Lembo, Henri Vanhanen & Varpu Marjomäki 2022

Manuscript

Request a copy from author.

VII

POLYPHENOLS EPIGALLOCATECHIN GALLATE AND RESVERATROL, AND POLYPHENOL-FUNCTIONALIZED NANOPARTICLES PREVENT ENTEROVIRUS INFECTION THROUGH CLUSTERING AND STABILIZATION OF THE VIRUSES

by

Dhanik Reshamwala, Sailee Shroff, Olivier Sheikh Amamuddy, Valentino Laquitana, Nunzi Denora, Antonella Zacheo, Vili Lampinen, Vesa P. Hytonen, Özlem Tastan Bishop, Silke Krol & Varpu Marjomäki 2021

Pharmaceutics 13:1182.

pharmaceutics

MDPI

Article

Polyphenols Epigallocatechin Gallate and Resveratrol, and Polyphenol-Functionalized Nanoparticles Prevent Enterovirus Infection through Clustering and Stabilization of the Viruses

Dhanik Reshamwala [1,†], Sailee Shroff [1,†], Olivier Sheik Amamuddy [2], Valentino Laquintana [3], Nunzio Denora [3], Antonella Zacheo [4], Vili Lampinen [5], Vesa P. Hytonen [5,6], Özlem Tastan Bishop [2], Silke Krol [7,‡] and Varpu Marjomäki [1,*,‡]

1 Department of Biological and Environmental Science/Nanoscience Center, University of Jyväskylä, 40014 Jyväskylä, Finland; dhanik.d.reshamwala@jyu.fi (D.R.); sailee.s.shroff@jyu.fi (S.S.)
2 Research Unit in Bioinformatics (RUBi), Department of Biochemistry and Microbiology, Rhodes University, Makhanda 6140, South Africa; oliserand@gmail.com (O.S.A.); o.tastanbishop@ru.ac.za (Ö.T.B.)
3 Department of Pharmacy–Pharmaceutical Sciences, University of Bari "Aldo Morro", 70125 Bari, Italy; valentino.laquintana@uniba.it (V.L.); nunzio.denora@uniba.it (N.D.)
4 Laboratory for Nanotechnology, IRCCS Istituto Tumori "Giovanni Paolo II", 70124 Bari, Italy; antonellazacheo@gmail.com
5 Faculty of Medicine and Health Technology, Tampere University, 33520 Tampere, Finland; vili.lampinen@tuni.fi (V.L.); vesa.hytonen@tuni.fi (V.P.H.)
6 Fimlab Laboratories, 33520 Tampere, Finland
7 Laboratory for Personalized Medicine, National Institute of Gastroenterology, "S. de Bellis" Research Hospital, 70013 Castellana Grotte, Italy; silke.krol@aol.com
* Correspondence: varpu.s.marjomaki@jyu.fi; Tel.: +358-405634422
† These authors contributed equally to this work.
‡ These authors contributed equally to this work.

Abstract: To efficiently lower virus infectivity and combat virus epidemics or pandemics, it is important to discover broadly acting antivirals. Here, we investigated two naturally occurring polyphenols, Epigallocatechin gallate (EGCG) and Resveratrol (RES), and polyphenol-functionalized nanoparticles for their antiviral efficacy. Concentrations in the low micromolar range permanently inhibited the infectivity of high doses of enteroviruses (10^7 PFU/mL). Sucrose gradient separation of radiolabeled viruses, dynamic light scattering, transmission electron microscopic imaging and an in-house developed real-time fluorescence assay revealed that polyphenols prevented infection mainly through clustering of the virions into very stable assemblies. Clustering and stabilization were not compromised even in dilute virus solutions or after diluting the polyphenols-clustered virions by 50-fold. In addition, the polyphenols lowered virus binding on cells. In silico docking experiments of these molecules against 2- and 3-fold symmetry axes of the capsid, using an algorithm developed for this study, discovered five binding sites for polyphenols, out of which three were novel binding sites. Our results altogether suggest that polyphenols exert their antiviral effect through binding to multiple sites on the virion surface, leading to aggregation of the virions and preventing RNA release and reducing cell surface binding.

Keywords: polyphenols; functionalized gold nanoparticles; antiviral efficacy; enteroviruses; stabilization

check for updates

Citation: Reshamwala, D.; Shroff, S.; Sheik Amamuddy, O.; Laquintana, V.; Denora, N.; Zacheo, A.; Lampinen, V.; Hytonen, V.P.; Tastan Bishop, Ö.; Krol, S.; et al. Polyphenols Epigallocatechin Gallate and Resveratrol, and Polyphenol-Functionalized Nanoparticles Prevent Enterovirus Infection through Clustering and Stabilization of the Viruses. *Pharmaceutics* **2021**, *13*, 1182. https://doi.org/10.3390/pharmaceutics13081182

Academic Editor: Hyun-ouk Kim

Received: 29 June 2021
Accepted: 28 July 2021
Published: 31 July 2021

1. Introduction

The gold standard in viral disease management is prevention, which is vaccination. Pandemics with new viruses remind us that the development and approval of vaccines takes time. Moreover, vaccines are not 100% efficient, and especially elderly people and immunocompromised individuals may not generate sufficient protection against infectious

agents. Therefore, powerful broadly acting antivirals with a more general inhibitory mechanism of action are required.

Non-enveloped enteroviruses are very stable and stay infective on surfaces and in the environment for long periods. Their entry is mostly via the gastro-intestinal tract, but also through the upper respiratory system. They cause a high number of acute infections such as flu, aseptic meningitis and myocarditis, but also contribute to chronic diseases such as dilated cardiomyopathy, asthma or type I diabetes [1]. For enteroviruses, no approved antivirals exist, and there are vaccines available only against poliovirus and EV71 [1]. Therefore, it is necessary to reduce the viral load on the surfaces and in the environment and prevent infection in the primary infection sites. An optimal solution to tackle virus infection would be a drug that directly kills virus infectivity and additionally prevents the virus from entering cells.

Nature provides a large variety of potential antimicrobials and antivirals. Those may be of endophyte origin, secreted by the symbiotic fungi or bacteria living in plants [2]. One example is Resveratrol (3,5,4′-trihydroxy-trans-stilbene), which is a polyphenol, non-flavonoid compound and is produced by plants in response to cellular damage or pathogen attacks [3]. Resveratrol (RES) is found in strongly pigmented vegetables and fruits such as the skin of grapes, blueberries and peanuts, and it has strong bioactive potential [3–5]. Like RES, flavonoids are polyphenols found as secondary metabolites in vegetables, fruits, nuts, red wine and tea. They share great similarity in structure to RES and great promise to be used as antivirals [6–8].

In the present study, EGCG and RES were tested for their antiviral efficacy, and the mechanisms of action was elucidated against the stable non-enveloped enterovirus B group viruses. While RES is considered completely non-toxic [9], high amounts of free EGCG show in vitro hepatotoxic effects, and in particular in cases in vivo [10,11]. Therefore, here, free polyphenols as well as polyphenols functionalized onto gold nanoparticles (AuNPs) were studied for their antiviral efficiency, as binding polyphenols to AuNPs can reduce toxicity. The effect of reduced toxicity by nanoparticle binding has been shown previously for molecules with a known hepatotoxic profile [12]. AuNPs were synthesized by green chemistry using the polyphenols as redox agents to further reduce the toxic components in the preparations. AuNPs synthesized using green chemistry have been previously reported to act as antivirals [13].

In this work, we show that both RES and EGCG have a direct and long-lived antiviral effect through binding to multiple sites on the virus particles, preventing the virus from opening, reducing the binding to the cell surface and inducing clustering of the virions.

2. Materials and Methods

2.1. Cells

Human alveolar basal epithelial adenocarcinoma (A549) cells and Green Monkey Kidney (GMK) cells were obtained from American type culture collection (ATCC, Manassas, VA, USA). The A549 and GMK cell lines were propagated in Dulbecco's Modified Eagle Medium (DMEM) (Gibco, Paisley, UK) and Eagle's Minimum Essential Medium (MEM) (Gibco, Paisley, UK) respectively, supplemented with 10% Fetal Bovine Serum (FBS, Gibco, Paisley, UK), 1% L-GlutaMAX (Gibco, Paisley, UK) and 1% antibiotics (penicillin/streptomycin) (Gibco, Paisley, UK) in a humidified 5% CO_2 incubator at 37 °C.

2.2. Viruses

Coxsackievirus B3 (CVB3; Nancy strain), Coxsackie virus B1 (CVB1, CONN 5 strain) and Coxsackievirus A9 strain (CVA9; Griggs strain), obtained from ATCC, were produced and purified as described before [14–16], with the only exception of adding 0.1% (*v*/*v*) TWEEN® 80 (Sigma-Aldrich, Steinheim, Germany) during the freeze–thaw cycle.

2.3. Polyphenols

Epigallocatechin gallate (EGCG) and Resveratrol (RES) were purchased from Sigma-Aldrich (Munich, Germany). EGCG was dissolved in water and Resveratrol in 0.02 M NaOH. Stock concentrations of EGCG and RES were 6.5 mM (3 mg/mL) and 8.8 mM (2 mg/mL) respectively, and were stored at −20 °C.

2.4. Nanoparticle Preparations

The green chemistry approach using the polyphenolic compounds as redox agents was chosen to reduce the number of potentially toxic molecules present on the surface of the gold nanoparticles (AuNPs). These polyphenols are supposed to form a stable and stabilizing layer on the AuNPs, as it was observed for citrate AuNPs shown by Mandal et al. [17]. For the preparation of RES-coated gold nanoparticles (RES-AuNPs), we used a modified protocol by Sanna et al. [18]. In brief, 20.8 mg of $HAuCl_4 \cdot 3\ H_2O$ (Sigma-Aldrich, Milan Italy) was dissolved in 12 mL of bi-distilled water on ice. Next, an ice-cold light-yellow solution of 3.0 mg of RES in 1.5 mL of 0.02 M NaOH solution was quickly added under vortexing. Under continuous vortexing, the temperature of the solution was slowly raised to room temperature (RT). Immediately after RES addition, the solution became brownish, after 10 min reddish, and after vortexing at 500 rpm for 1 h, the color turned into wine red. Unbound RES was removed by a series of washing (first wash: 0.02 M NaOH; second wash: H_2O) and centrifugation steps (2 × 14,000 rpm, 20 min at 4 °C to remove NaOH; 1 × 12,000 rpm, 20 min at 4 °C to remove H_2O), and the pellet was finally resuspended in water. The centrifugation was carried out by a Microfuge 40R with a Fiberlite F21-48 x2 Fixed Angle Rotor, 45°, R_{max} 97 mm (ThermoFisher, Rome, Italy). The final gold concentration was 5.3 mg/mL, as determined by ICP-MS. The concentration of RES in the stock solution was calculated (Supplementary Material) to be 34.4 μM.

For the preparation of EGCG-AuNPs, 5.9 mg of EGCG was dissolved in 15 mL of bi-distilled water and cooled on ice. An ice-cold solution of 12.9 mg of $HAuCl_4 \cdot 3\ H_2O$ in 2 mL of H_2O was added quickly and mixed by shaking on ice for another 10 min. After the color changed from bright yellow to red within 1 min, the temperature of the solution was slowly increased to RT for 2 h under continuous vortexing at 500 rpm. The excess EGCG was removed by a series of washing and centrifugation steps (2× centrifugation at 14,000 rpm for 20 min at 4 °C addition of ddH_2O, 1× centrifugation at 12,000 rpm for 20 min at 4 °C). The deep red pellet was resuspended in water. The final gold concentration was 1.64 mg/mL, as determined by ICP-MS. The concentration of EGCG in the stock solution was calculated (Supplementary Material) to be 5.61 μM.

Quantitative Analysis of EGCG and RES Bound to the AuNP Surface

The amount of EGCG and RES present on the surface of the gold nanoparticles was estimated indirectly by the substitution with L-cysteine. The thiol group of the cysteine binds stronger to the gold than the aromatic ring system of polyphenols, and therefore will replace it. The colorimetric method finally determines the remaining free thiol groups of the L-cysteine, assuming a complete substitution of the polyphenols by cysteine [19]. The residual-free thiol groups of L-cysteine in solution after polyphenol exchange on the nanoparticle surface were quantified photometrically using Ellman's reagent (5,5′-dithio-bis (2-nitrobenzoic acid)). The amount of polyphenols was then calculated considering a 1:1 ratio of replacement (1 cysteine replaces 1 polyphenol).

For its determination, a fresh stock solution of 1 mg of cysteine in 1 mL of 0.5 M phosphate buffer, pH 8.0, was diluted to a final concentration in L-cysteine of 102 mM. 100 μL of this solution was mixed with different volumes of EGCG-AuNPs or RES-AuNPs stock solution (ranging from 10 to 100 μL) and 0.5 M phosphate buffer solution at pH 8.0 to reach a final solution volume of 500 μL. This was mixed with 500 mL of Ellman's reagent solution (3 mg dissolved in 10 mL of 0.5 M phosphate buffer, pH 8.0). The resulting mixture was incubated in the dark and at room temperature for 2 h. After this time, the samples were centrifuged at 13,000 rpm for 5 min (Mikro 22 R, Hettich Zentrifugen, Germany) and

100 µL of each sample was transferred into a microplate reader (PerkinElmer VICTOR X3 Multilabel) to measure absorbance at 450 nm. The amount of thiol groups was estimated from a standard curve of L-cysteine.

2.5. Dynamic Light Scattering Measurements

For dynamic light scattering (DLS) measurements, CVA9 virus samples were diluted in PBS from a stock solution (5×10^{10} PFU/mL) to 2×10^{9}, 2×10^{8}, 5×10^{7} and 2×10^{7} PFU/mL. EGCG was added to each of these dilutions such that its final concentration was 6.5 µM. Experimental virus controls with the same dilutions but without the EGCG were also prepared. Both the control virus and EGCG-treated virus were incubated for 1 h at 37 °C. Post-incubation, the virus/virus cluster size distribution was measured by DLS at 25 °C with the Zetasizer Nano ZS instrument (Malvern Instruments, Malvern, UK). The attenuator was set by the system according to scattering intensity of the sample and set measurement position at 3 mm. As controls, we measured both EGCG and PBS buffer alone. As expected, no particles were observed in the controls.

2.6. Antiviral Activity Assay

The antiviral activity of the polyphenols against species B enteroviruses was determined using a cytopathic effect (CPE) inhibition assay, modified from Schmidtke et al. [20]. Briefly, A549 cells were cultured for 24 h at 37 °C in 96-well flat-bottomed microtiter plate (Sarstedt, Numbrecht, Germany) at a density of 12,000 cells/well in 100 µL of DMEM supplemented with 10% FBS, 1% GlutaMAX and 1% penicillin/streptomycin antibiotics. The following day, each of the viruses (2×10^{7} PFU/mL for CVB3 and CVB1 and 2×10^{8} PFU/mL for CVA9) were pre-incubated with the compounds for 1 h at 37 °C. The virus–compound mixture was further diluted 10 times with DMEM to obtain a final MOI of 10 for CVB3 and CVB1 and 100 for CVA9. This mix was then added to cells for 24 h in a humidified 5% CO_2 incubator at 37 °C. A virus without the compound was used as a positive control and a mock infection without the virus and compound as a negative control for the experiments. The development of a cytopathic effect (CPE) was monitored using light microscopy. The next day, the cells were fixed and stained for 10 min with CPE dye (0.03% crystal violet, 2% ethanol and 36.5% formaldehyde) after washing twice with PBS. After two washes with water, the stained viable cells were lysed using a lysis buffer (0.8979 g of sodium citrate and 1N HCl in 47.5% ethanol) to elute the crystal violet. Then, the absorbance was measured spectrophotometrically at 570 nm using the VICTOR^{TM} X4 multilabel reader (PerkinElmer, Turku, Finland). This assay was performed twice independently for each of the virus–compound concentrations.

2.7. Cytotixicity Assay

Cytotoxicity studies were performed using the CPE inhibition assay by adding the compounds (without any virus) to A549 cells. Mock infection was used as a negative control. This assay was performed twice independently.

2.8. Time of Addition Studies

Time of addition studies were performed using the CPE inhibition assay. Briefly, A549 cells were cultured for 24 h in 96-well flat-bottomed microtiter plate at a density of 12,000 cells/well in 100 µL of DMEM supplemented with 10% FBS, 1% GlutaMAX and 1% penicillin/streptomycin antibiotics. On the subsequent day, cells were infected with CVB3 (MOI 10) for 1 h at 37 °C. Afterwards, excess virus was removed by repeated washing. Then, fresh media (supplemented with 10% FBS, 1% GlutaMAX and 1% penicillin/streptomycin) containing EGCG (65 µM) and RES (880 µM) were added, and cells were incubated for 24 h. Virus control (without the compounds), compound control (without virus) and mock infection were used as controls for the studies. This assay was performed twice independently for each of the virus–compound concentrations, with 5 technical replicates in each experiment.

2.9. Radioactive Labeling of CVA9

The radioactive virus was produced in confluent monolayers of GMK cells, which were washed and incubated with PBS for 15 min at 37 °C and infected with CVA9 (Griggs strain; ATCC) diluted in low-methionine-cysteine medium (MP Biomedicals, Illkrich, France) supplemented with 1% FBS and 1% Glutamax. After 3 h of infection, 40 µCi/mL of radioactive [^{35}S] methionine/cysteine (PerkinElmer, Boston, MA, USA) diluted in low-methionine-cysteine medium supplemented with 1% FBS was added to the cells, and virus replication was allowed to proceed for 24 h at 37 °C. After three freeze–thaw cycles, the supernatant was cleared by pelleting at 2500× *g* for 10 min. TWEEN® 80 (0.1% *v/v*) was added to the pellet and incubated on ice for 30 min. Post-incubation, centrifugation was performed for 10 min with 4000× *g* at 4 °C. The collected supernatant was added on a 2 mL sucrose cushion (40%). The cushions were ultracentrifuged with an SW-41 rotor at 151,263× *g* for 2.5 h (4 °C). All the liquid up until the cushion and first 500 µL fraction from the top were discarded, and the next 3 × 500 µL fractions were collected, which were pelleted with a 70Ti rotor at 90,140× *g* for 2 h at 4 °C. The concentrated virus was then layered on top of the 10 mL sucrose gradient (5–20%) and ultracentrifuged with a SW-41 rotor at 151,263× *g* for 2 h (4 °C). Fractions (500 µL) were collected from the top to the bottom of the cushion and small samples from each fraction were mixed with a scintillation cocktail UltimaGold™ (PerkinElmer, Waltham, MA, USA) for counting the radioactivity (counts per minute) using a Tri-Carb® 2910TR liquid scintillation analyzer (PerkinElmer, Downers Grove, IL, USA). The 160S-containing fractions were pooled and used for the experiments (7000 CPM/µL; 1.4 × 10^9 PFU/mL).

2.10. Gradient Assay

Metabolically labeled CVA9 (70,000 CPM corresponding to 1.4 × 10^8 PFU/mL) was pre-treated with EGCG (6.5 µM) and RES (1.8 mM) for 1 h at 37 °C. A virus control (without the compounds but the same treatment) and fresh virus (without the polyphenols and without treatment) were used as positive controls for the assay. The test and control samples were further diluted 10 times using a buffer, PBS-$MgCl_2$ (PBS containing 2 mM $MgCl_2$). The samples were then layered over 10 mL sucrose (5–20%) gradients and ultracentrifuged with a SW-41 rotor at 151,263× *g* (average g value) for 2 h (4 °C) using the SW-41 rotor. Gradients were fractionated from top to bottom (500 µL fractions) and mixed with a scintillation cocktail for counting the radioactivity using a PerkinElmer Tri-Carb® 2910TR liquid scintillation analyzer.

2.11. Real-Time Fluorescence Uncoating Assay

The real-time fluorescence uncoating assay has been previously described for measuring uncoating of enteroviruses at 37 °C [16,21]. The assay is based on the fluorescence emitted by SYBR Green II (SGII) when bound to viral genomic RNA. The experiment was carried out in a 96-well plate with a total reaction volume of 100 µL. Each well contained 0.5 µg of Coxsackievirus B3, 10× SGII (Life Technologies, Eugene, OR, USA) diluted in double-distilled water (ddH_2O), polyphenol-functionalized nanoparticles EGCG-AuNPs (Au concentration 16.4 µg/mL, ligand concentration 5.61 × 10^{-2} µM) and RES-AuNPs (Au concentration 53 µg/mL, ligand concentration 3.44 × 10^{-1} µM) in storage buffer PBS-$MgCl_2$ and opening buffer (20 mM NaCl, 6 mM KH_2PO_4, 12 mM K_2HPO_4 and 0.01% faf-BSA). We had two experimental controls: one was a virus in the storage buffer and the other contained a virus in the opening buffer. The samples were prepared on ice to prevent any effect of temperature on uncoating. Additionally, we had controls to exclude fluorescence quenching/enhancement from other molecules in the reaction mix. RNAse at a final concentration of 10 µg/mL was used to distinguish between the fluorescence originating from porous intermediate virions (allowing entry of SGII inside) and the RNA in solution. The fluorescence was recorded every 15 min for an hour at 37 °C using the PerkinElmer Multilabel Reader Victor X4 installed with a F485 lamp filter, F535 emission filter and a counting time of 1 s.

2.12. Particle Stability Thermal Release Assay (PaSTRy)

The PaSTRy assay was performed as described before [22]. The experiment was carried out in thin-walled PCR plates (Agilent, Amstelveen, Netherlands). A reaction mixture containing 0.5 µg of Coxsackievirus B3 and EGCG (65 µM) in storage buffer or opening buffer was preincubated for 1 h at 37 °C and 5% CO_2. Post-incubation, 10× SGII (Invitrogen) in ddH_2O was added to the reaction mix, and a final volume of 50 µL was aliquoted into the thin-walled PCR plates. The thermal cycler (BioRad C100, Helsinki, Finland) recorded the fluorescence in quadruple from 20 to 90 °C with 0.5 °C intervals. The fluorescence data output was extracted from the BioRad CFX manager (2.1 software, accessed on 10 October 2020) and processed in Microsoft Excel (2016). The melt curve was obtained by plotting the relative fluorescence units (RFU) values versus temperature. The melting temperature (Tm) was determined from the melt peak, which was plotted using the derivative of the RFU as a function of temperature (d(RFU)/dT).

2.13. Transmission Electron Microscopy

A reaction mixture containing the CVA9 (1.6×10^{10} PFU/mL), polyphenols (EGCG, 650 µM; RES, 880 µM), polyphenol-functionalized nanoparticles EGCG-AuNPs (Au concentration 164 µg/mL, ligand concentration 5.61×10^{-1} µM) and RES-AuNPs (Au concentration 530 µg/mL, ligand concentration 3.44 µM) in buffer (PBS-$MgCl_2$) was incubated for 1 h at 37 °C and 5% CO_2. During the incubation, the Formvar-coated copper grids were glow-discharged using the EMS/SC7620 Mini sputter coater (Electron Microscopy Sciences, Hatfield, PA, USA). Post-incubation, 5 µL of the reaction mixture was pipetted on the glow-discharged grids for 20 s and then blotted away using Whatman paper. To negatively stain the sample, 5 µL of 1% (*w*/*v*) Phosphotungstic acid (PTA in water, pH adjusted to neutrality) (Sigma-Aldrich, Shinagawa-ku, Japan) or 2% (*w*/*v*) Uranyl acetate (Electron Microscopy Sciences, Hatfield, PA, USA) was pipetted on grids and incubated for 30 s, and blotted away using Whatman paper. The samples were visualized in a JEOL JEM-1400 transmission electron microscope (JEOl, Tokyo, Japan). The diameter of functionalized gold nanoparticles from the images taken using the TEM was measured by automated counting using the BioImageXD software (www.bioimagexd.net, accessed on 16 January 2021).

2.14. Radioactive Binding Assay

A549 cells were cultured for 24 h in 96-well flat-bottomed microtiter plates at a density of 12,000 cells/well in 100 µL of DMEM supplemented with 10% FBS, 1% GlutaMAX and 1% penicillin/streptomycin antibiotics. On day 2, ^{35}SMet/Cys-CVA9 (28,000 CPM corresponding to 1.38×10^8 PFU/mL) was pre-treated with the polyphenols and polyphenol-functionalized nanoparticles EGCG (65 µM), RES (880 µM), EGCG-AuNPs (Au concentration 16.4 µg/mL, ligand concentration 5.61×10^{-2} µM) and RES-AuNPs (Au concentration 53 µg/mL, ligand concentration 3.44×10^{-1} µM) in buffer (PBS-$MgCl_2$), and incubated at 37 °C for 1 h. Virus control without the compound was also prepared and incubated. Post-incubation, the sample tubes were placed on ice and 1% DMEM was added to make the final volume reach 100 µL. Following this, the samples with DMEM were added to the cells. Then, the 96-well plate was kept on ice while rocking for 1 h to ensure uniform binding of the virus on the cell surface. Next, the media was aspirated from each well and three washes with ice-cold PBS were performed to remove any unbound virus from the cell surface. To detach the cells, 150 µL of 1% Triton was added to the wells and incubated for 30 min. The entire liquid was transferred to a tube containing 4 mL of scintillation cocktail UltimaGold™ and measured using the Tri-Carb® 2910TR liquid scintillation analyzer.

2.15. Dilution and Temperature Assays

Dilution and temperature assays were performed using the CPE inhibition assay. For the dilution assay, CVB3 (4.4×10^8 PFU/mL), polyphenol-functionalized nanoparticles EGCG-AuNPs (Au concentration 164 µg/mL, ligand concentration 5.61×10^{-1} µM) and RES-AuNPs (Au concentration 530 µg/mL, ligand concentration 3.44 µM) in buffer (PBS-

$MgCl_2$) were incubated at 37 °C for 1 h. An experimental virus control (without the compounds) and fresh virus control (without the compounds and without any incubation) were used as two controls for the assay. Post-incubation, each of the test samples and the experimental virus control were divided equally into two tubes, one was diluted 50 times using a buffer (PBS-$MgCl_2$) and the other part was stored at −20 °C (as an undiluted sample). The diluted samples were incubated over 72 h at 37 °C, such that equal fractions from them were collected at regular time-intervals (1, 6, 24, 48 and 72 h) and stored at −20 °C. At the end of 72 h, all the diluted and undiluted samples were further diluted with DMEM and added onto the cells, to obtain a final MOI of 15. On the subsequent day, the plates were stained for CPE as explained before.

When testing the effect of temperatures, two approaches were used. One with longer and the other with shorter times of incubation. For testing the longer periods of incubation, CVB3 (4.4×10^8 PFU/mL) was pre-treated with EGCG (650 μM), RES (880 μM), EGCG-AuNPs (Au concentration 164 μg/mL, ligand concentration 5.61×10^{-1} μM) and RES-AuNPs (Au concentration 530 μg/mL, ligand concentration 3.44 μM) in buffer (PBS-$MgCl_2$) at RT (21 °C), 8 and 37 °C for 72 h. An experimental virus control (without the compounds) and fresh virus control (without the compounds and without any incubation) were used as two controls for the assay. Test samples and the experimental virus control were collected after incubating at the above-mentioned temperatures for 6, 24, 48 and 72 h and stored at −20 °C. After 72 h, all the samples were further diluted with DMEM and added to the cells, to obtain a final MOI of 15. On the subsequent day, the plates were stained for CPE, as explained before. In case of shorter incubation times, CVA9 (2×10^7 PFU/mL) was pre-treated with EGCG (6.5 μM) at 21 or 37 °C for 1 min, 5 min and 1 h and then added to the cells.

2.16. Blind Docking of Polyphenolic Compounds against CVA9 and CVB3

2.16.1. The Experimental Design

For the in silico docking experiment, the polyphenols Epigallocatechin gallate (EGCG) and Resveratrol (RES) were to be blindly docked over large external surfaces of the viral capsids of CVA9 and CVB3. Due to the overly large surfaces to be scanned, the capsids were segmented into relatively large grid boxes centered around their fold axes (2, 3 and 5) of rotational symmetry. This strategy was used in order to obtain overlapping segments spanning as much of the viral capsid surfaces as possible.

2.16.2. Ligand Preparation

The molecular structures of the polyphenolic compounds, Epigallocatechin gallate (Drug Bank ID: DB03823) and Resveratrol (Drug Bank ID: DB02709), were reconstituted and protonated from their SMILE strings using the RDKit library. The MGLTools software [23] was then used to assign Gasteiger partial charges and merge non-polar hydrogen atoms.

2.16.3. Capsid Preparation

Full capsids for the CVA9 Griggs strain (PDB ID: 1D4M) [24] and CVB3 Nancy strain (PDB ID: 6GZV) [25] were reconstituted from their first biological assemblies using the PyMOL software. While the CVA9 capsid was already protonated, the PDB2PQR tool was used to protonate the CVB3 capsid to pH 7. However, as this altered the chain labels and segment identifiers, an in-house Python script (capsidockprep.py) was designed to restore these labels. In order to screen the maximum outer surface area from the capsid, the grid box center was placed at each individual capsid fold axis of rotational symmetry, with the box y-z plane being perpendicular to the axis of rotation and partially embedded within the capsid. In order to do so, centroids (x, y and z coordinates measured in angstroms) for each of the fold axes were selected, before shifting the box along the *x*-axis by 10 Å to the right. Internally, before shifting, the capsid centroid is centered at the origin (0, 0, 0) prior to rotating the capsid centroid position vector to be along the *x*-axis. For simplicity, the PDB2PQR tool is wrapped within an in-house Python script to enable protonation when

the "ph" parameter is set. Similar to AutoDock Vina, a grid interval size of 0.375 Å is used. The "gridsize" parameter is specified in grid points. The grid parameters for all of the fold axes are provided in Table 1. The AutoDock Vina plugin from PyMOL was used to visualize the effects of shifting and grid sizing.

Table 1. Parameters for grid placement along the fold capsid fold axes.

Strain	Fold Axis	Centroid (Å)	Grid Size (in Grid Points)	Shift along x Axis (Å)
CVA9	2	−75.446, 105.465, −13.389	40 × 100 × 100	10
	3	−103.647, 73.405, 5.830	40 × 120 × 120	10
	5	−44.878, 108.985, 50.228	90 × 180 × 180	10
CVB3	2	118.389, 223.579, 288.589	40 × 100 × 100	10
	3	110.197, 256.603, 256.603	40 × 120 × 120	10
	5	183.400, 251.025, 292.820	90 × 180 × 180	10

The preprocessing by the in-house Python script greatly reduced the number of atoms by including protein chains belonging to any atom within the grid box, whilst keeping chain labels and segment IDs. Due to the high number of atoms required to capture the complete protomers in their protonated form for the 5-fold axis (beyond the limit of the PDB format), the experiment was focused around the 2- and 3-fold axes of rotation symmetry. As performed for the ligands, charges were assigned, and non-polar hydrogen atoms were merged using MGLTools.

2.16.4. Capsid Ligand Docking

QuickVina-W [26] was used for docking the polyphenolic compounds, with a grid center of (0, 0, 0) and grid dimensions as defined in Table 1. The runs were performed at an exhaustiveness of 1000 with 24 cores per job, using GNU Parallel [27] at the Centre for High-Performance Computing (CHPC). A maximum of 20 top ligand binding poses were retained in each case run.

2.16.5. Analysis of Docking Results

The Arpeggio tool [28] was then used to estimate the protein–ligand interactions around a subset of the complex trimmed at a maximum radius of 14 Å around the ligand atoms. An in-house Python script (without any external library dependency) was used to extract this subset, retaining the chain label and segment ID. Hydrogen bonding, hydrophobic interactions and the binding energy scores were then used to characterize ligand binding. The distributions of these measurements across the entire docking experiment were arranged according to the strains and the detected binding sites. In order to differentiate the binding sites from existing ones, both the canonical hydrophobic pocket [24] and the VP1-VP3 druggable interprotomer pocket (the Butcher Neyts' pocket) from Abdelnabi and co-workers [25] were carefully mapped on all 3D structures, as their compositions and locations were not identical in each strain. In the case of the hydrophobic pocket, the PyVOL plugin [29] in PyMOL was used, specifying VP1 as the search space and a minimal pocket volume of 400 Å, in addition to the default parameters. The minimum volume had been determined beforehand using the palmitic acid-contacting residues (any protein atom within 4 Å of each ligand atom) from a 3D structure of the CVB3 Woodruff strain (PDB ID: 1COV) [30] to guide the cavity search. In the case of the interprotomer pocket, the PROMALS3D web server [31] was used to align the VP1 sequences and correct for any misaligned residue positions using 3D structural information. The ligand-interacting residues (binding the benzene sulfonamide derivative) from CVB3 (6GZV) identified by PDB were used as a reference in a sequence alignment with the CVA9 (1D4M) strain to obtain homologous positions for the latter [32]. No correction was needed for VP3 residues of the interprotomer surface, as the alignment contained no gaps. Unless specified otherwise, residues have been numbered according to the respective crystal structures.

2.17. Statistical Analysis

Statistical analysis was performed using GraphPad Prism 6 (GraphPad Software, San Diego, CA, USA). Data are presented as mean ± standard error (SEM). The 50% effective concentrations (EC_{50}) and 50% cytotoxic concentrations (CC_{50}) were calculated by regression analysis of the dose–response curves generated from the experimental data using the software. Statistical significance was calculated by performing one-way/two-way ANOVA followed by the Bonferroni test (* $p < 0.05$, ** $p < 0.01$, *** $p < 0.001$ and **** $p < 0.0001$).

3. Results

3.1. Epigallocatechin Gallate and Resveratrol Show Antiviral Activity on Enteroviruses

To evaluate whether selected polyphenolic compounds have antiviral effects on the chosen human enteroviruses (CVB1, CVB3, CVA9), we performed a cytopathic effect (CPE) inhibition assay on A549 cells. A high amount of CVB1 virus (10^7 PFU/mL) was pre-treated with 10-fold serial dilutions of each compound for 1 h at 37 °C before adding to cells. Untreated virus and mock infection were used as positive and negative controls in the assay, respectively. The CPE analysis showed that Epigallocatechin gallate (EGCG) and Resveratrol (RES) as free molecules have a potent inhibitory effect on virus infection (Figure 1A,B). At a concentration of 6.5 μM of EGCG (Figure 1A, left) and 880 μM of RES (Figure 1B, left), CVB1 was efficiently inhibited. A significant toxicity could not be detected for any of the tested concentrations of the compounds (Figure 1A,B, right).

Next, we tested EGCG and RES bound to gold nanoparticles (Figure 1A,B, middle). The functionalized gold with EGCG or RES both showed antiviral activity. Nevertheless, RES-AuNPs were more efficient in inhibiting CVB1 infection than EGCG-AuNPs (RES ligand concentration 3.44×10^{-1} μM versus EGCG ligand concentration 5.61×10^{-1} μM). However, the necessary concentrations of ligand bound to AuNPs needed for virus inactivation were several orders of magnitude lower than the free polyphenols.

TEM images showed that the RES particles were smaller than the EGCG-AuNPs (Figure 1C, left). Automated determination of average core diameter from TEM images using BioImageXD software resulted in 131.5 ± 7.1 and 78.6 ± 2.3 nm for EGCG-AuNP and RES-AuNP, respectively. DLS analysis of the nanoparticles showed similar diameters as the TEM images, indicating that only one layer of polyphenol was attached. The zeta potential of the nanoparticles was −35 and −40 mV for the RES-AuNPs and the EGCG-AuNPs, respectively. The determination of gold content by ICP-MS showed a 3-fold higher concentration of gold for RES-AuNPs as compared to EGCG-AuNPs (Figure 1C).

We calculated the number of polyphenol molecules per AuNPs considering the nanoparticle diameter. Moreover, we assumed from the DLS versus TEM data that we have only one monolayer of molecules, which are oriented parallel to the surface, as observed previously for aromatic ring systems [17], and approximating the area of the polyphenol molecules from their molecule length and width, as measured by the Avogadro software. The calculations resulted in 47,239 EGCG molecules per AuNP and 19,122 RES molecules per AuNP. By considering the concentration of gold determined by ICP-MS and the diameter of the AuNP from TEM, the concentration of ligands was calculated to be 5.61 μM for EGCG and 34.4 μM for RES (see detailed calculations in the Supplementary Materials). The calculated ligand concentrations were confirmed by an indirect quantitative analysis. For this analysis, EGCG and RES ligands present on the AuNP surface were replaced by an exchange with cysteine. The thiol group of cysteine has a stronger, quasi-covalent binding affinity to gold than the polyphenols. After incubation of EGCG-AuNP or RES-AuNP with a solution of cysteine, the remaining free thiol groups were determined photometrically using a colorimetric reaction with Ellman reagent. A 1:1 ratio of cysteine to polyphenol was assumed. The concentration of EGCG and RES determined by the Ellman test was 5.5 ± 0.1 μM for EGCG and 42.9 ± 1.1 μM for RES, respectively. In the following assays, we have used the calculated concentration.

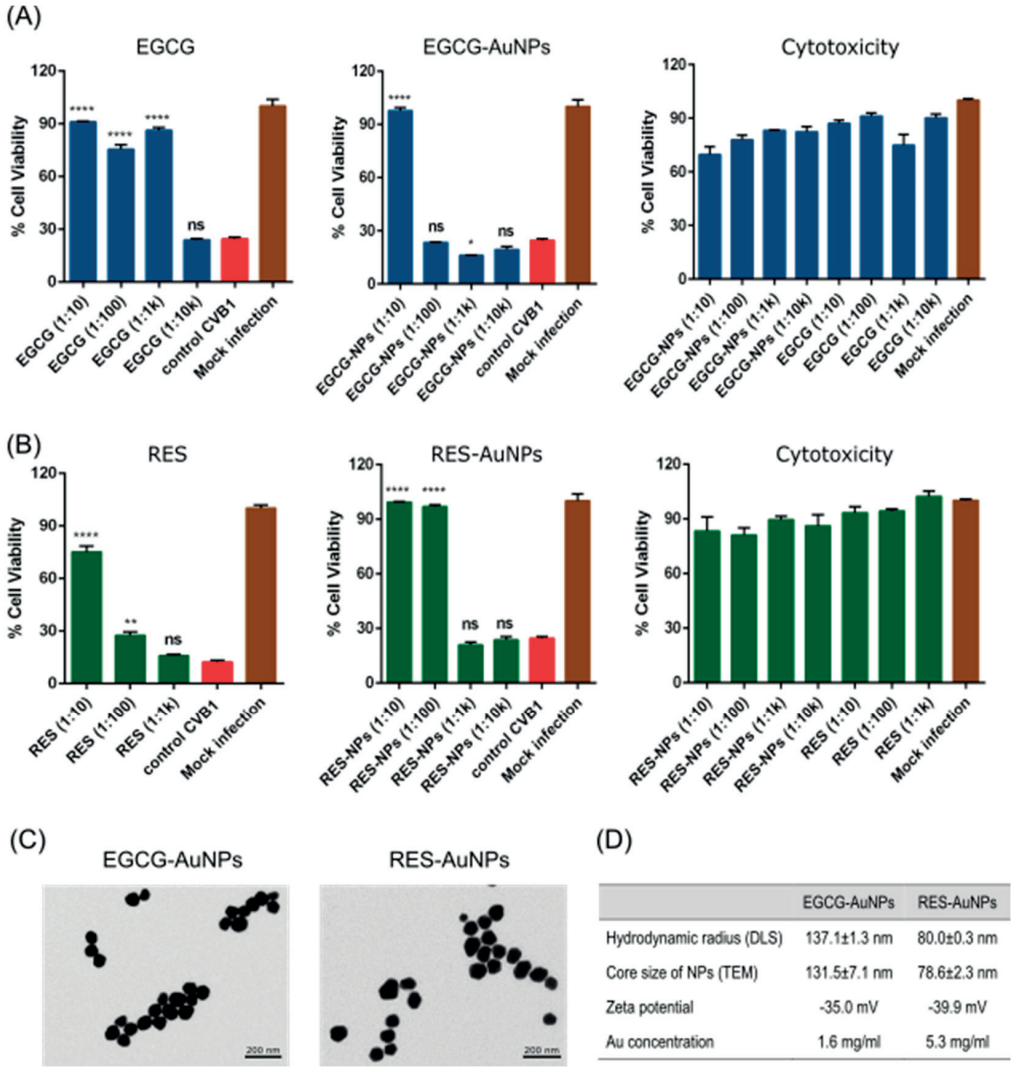

	EGCG-AuNPs	RES-AuNPs
Hydrodynamic radius (DLS)	137.1±1.3 nm	80.0±0.3 nm
Core size of NPs (TEM)	131.5±7.1 nm	78.6±2.3 nm
Zeta potential	-35.0 mV	-39.9 mV
Au concentration	1.6 mg/ml	5.3 mg/ml

Figure 1. Polyphenols and polyphenol-functionalized nanoparticles block virus infection. (**A**) Epigallocatechin gallate (EGCG) and (**B**) Resveratrol (RES) and polyphenol-functionalized nanoparticles (AuNPs) were screened against CVB1 using the CPE inhibition assay to evaluate infection and cytotoxicity of the polyphenolic compounds. The test samples and the virus control are normalized against the mock infection. N = 3 replicates for each dilution of the samples tested. Average values + standard error of the mean (SEM) are shown. * $p < 0.05$, ** $p < 0.01$and **** $p < 0.0001$ versus the virus control (analyzed using the one-way ANOVA with Bonferroni tests). (**C**) Transmission electron microscopy images of EGCG-AuNPs and RES-AuNPs. (**D**) Physico-chemical characteristics of the polyphenol-functionalized AuNPs. The mean core size of the nanoparticles was calculated using the BioImage XD software by processing TEM images containing 684 (EGGC-AuNPs) and 2411 (RES-AuNPs) nanoparticles, respectively. The results of the TEM and DLS are expressed as average values ± standard error of the mean (SEM). Hydrodynamic size and zeta potential were evaluated from three separate readings using a Malvern Zetasizer. Au concentration was obtained using ICP-MS. Scale bars = 200 nm.

3.1.1. Detailed Antiviral Efficacy Studies

Once the preliminary screening results confirmed the antiviral activity of the polyphenols and the polyphenol-functionalized nanoparticles for CVB1, the antiviral efficacy on different enteroviruses was calculated as 50% effective concentrations (EC_{50}) by regression analysis from their dose–response curves. The antiviral studies were performed using the CPE inhibition assay, where we incubated the compounds with high amounts of CVB3 (2×10^7 PFU/mL) for 1 h at 37 °C. As shown in Figure 2A and Table 2, both polyphenols

and the corresponding nanoparticles protected the A549 cells from CVB3 infection in a dose-dependent manner. The EC_{50} value for EGCG was 3.411 μM, 32 times more effective than RES (107.894 μM). Interestingly, the ligands bound to AuNPs (0.051 μM for EGCG and 0.004 μM for RES) were 67 or 26,974 times more potent than the free polyphenols, respectively. The RES-AuNPs were in this case 13 times more potent than EGCG-AuNPs against CVB3 infection.

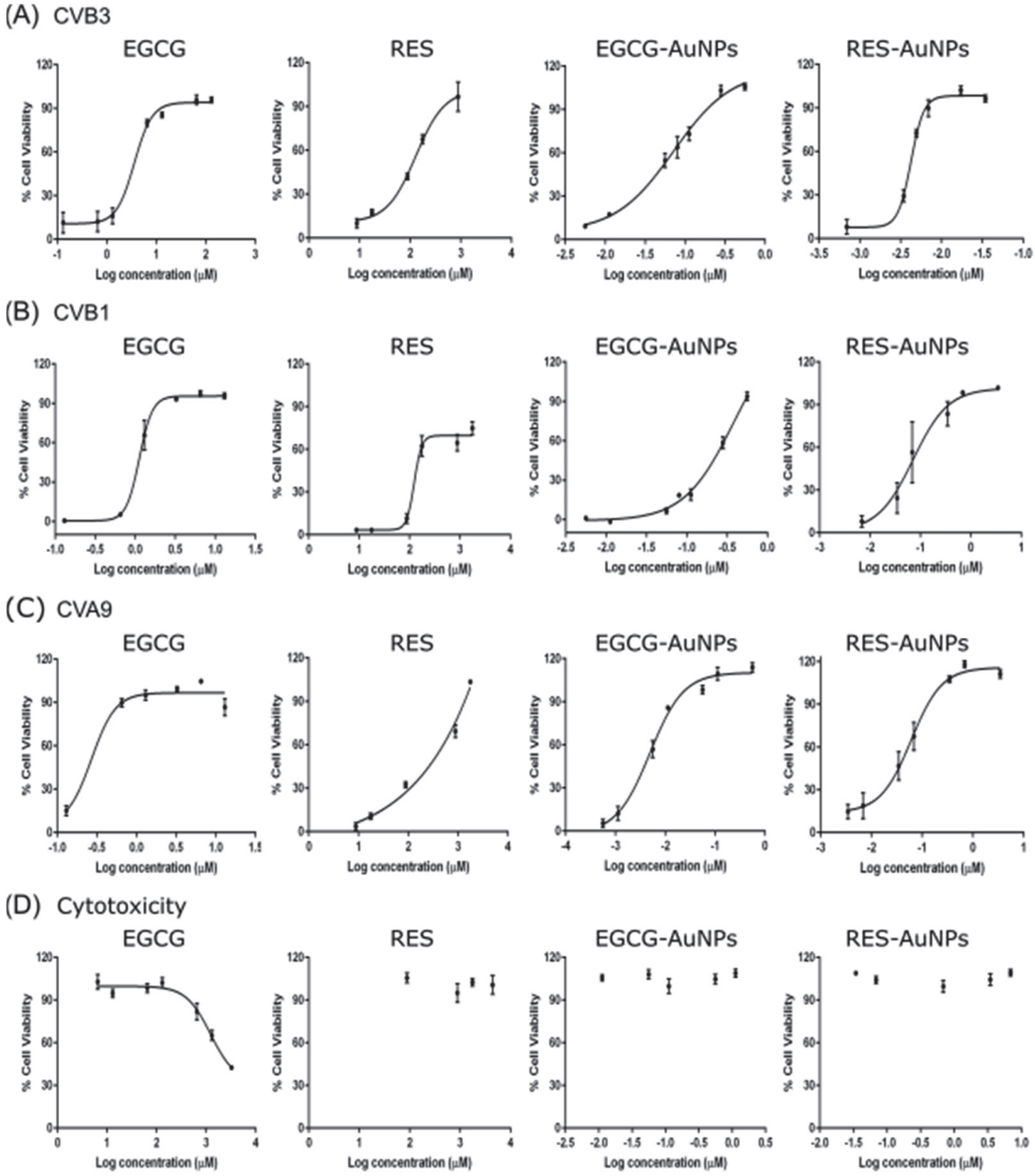

Figure 2. Dose–response curves for studying the antiviral efficacy of Epigallocatechin gallate (EGCG) and Resveratrol (RES) and polyphenol-functionalized nanoparticles (AuNPs), against (**A**) CVB3, (**B**) CVB1 and (**C**) CVA9 and their (**D**) cytotoxicity, using the CPE inhibition assay. Drug concentration of the compounds are shown as Log (10) of μM on the *x*-axis. The results are mean of two independent experiments and are expressed as average values ± standard error of the mean (SEM).

Table 2. Antiviral activity and cytotoxicity of polyphenols and polyphenol-functionalized AuNPs.

Virus	Compounds	EC_{50} (μM)	Fold Improvement	CC_{50} (μM)	SI
CVB3	NP-EGCG	0.051	67	>1.122	>22.000
	EGCG	3.411		2218.196	650.306
	NP-Res	0.004	26,974	>6.880	>1720.000
	Res	107.894		>4400.000	>40.780
CVB1	NP-EGCG	0.237	5	>1.122	>4.734
	EGCG	1.140		2218.196	1945.785
	NP-Res	0.068	2101	>6.880	>101.176
	Res	142.889		>4400.000	>30.793
CVA9	NP-EGCG	0.004	67	>1.122	>280.500
	EGCG	0.266		2218.196	8339.082
	NP-Res	0.039	8471	>6.880	>176.410
	Res	330.369		>4400.000	>13.318

EC_{50}—50% effective concentration, CC_{50}—50% cytotoxic concentration, SI—selectivity index.

We also tested the compounds for inhibition of other enteroviruses, using highly concentrated CVB1 (2×10^7 PFU/mL) and CVA9 (2×10^8 PFU/mL) enteroviruses. Figure 2B,C and Table 2 show that EGCG is 3 and 13 times more effective for CVB1 and CVA9 respectively, than for CVB3. In general, the RES ligand was less effective compared to the EGCG ligand. The results also show that the ligands have better efficacy when functionalized on the gold nanoparticle for RES. Depending on the virus and the ligand, there was a 5- to 26,974-fold improvement in efficacy (Table 2). Usually, the improvement in efficacy was better for RES than for EGCG. This can be due to an increased solubility of RES when bound on nanoparticles.

Since the polyphenols and functionalized AuNPs both exhibited potent antiviral activity, we tested if the inhibitory effect was due to bound ligands and not due to free ligands present in the solution. This was confirmed by pelleting the functionalized AuNPs by ultracentrifugation and testing the pellet for the antiviral activity. The antiviral activity of the NP solution was similar to the activity in the resuspended pellet of AuNPs, confirming that antiviral efficacy was not related to detached ligands (Supplementary Figure S1).

Detailed cytotoxicity studies using the CPE inhibition assay on uninfected cells were repeated under the same conditions as used for the antiviral studies (Figure 2D). Mock infection, having no virus or compounds, was used as a control for the assay. As shown in Figure 2D, none of the compounds reduced the viability of A549 cells at the effective antiviral concentrations, thus verifying the antiviral potential of the compounds. The 50% cytotoxic concentrations (CC_{50}) calculated by regression analysis from the dose–response curves are shown in Table 2. The results showed no toxicity for RES or for both AuNPs, while for EGCG, we detected toxicity at a very high concentration (CC_{50}: 2.218 mM). Thus, the selectivity index (SI) deduced from the ratio of CC_{50}/EC_{50} is incalculable for compounds other than EGCG. For EGCG, the SI values are very high for all tested viruses (Table 2). Based on the high (or incalculable) SI values, it can be said that these compounds effectively protect the A549 cells from the tested enterovirus infections with no toxicity.

3.1.2. EGCG and RES Show Long-Term Antiviral Efficacy at Different Temperatures

To investigate the antiviral efficacy of the polyphenols further, we performed antiviral tests for the functionalized AuNPs at different temperatures and different periods of incubation (Figure 3A). First, the functionalized AuNPs were pre-incubated with the virus at 8, 21 and 37 °C. Untreated viruses in PBS-$MgCl_2$ buffer incubated at the same temperatures were used as an experimental control. Virus infectivity was measured after incubating the polyphenols with viruses for 6, 24, 48 and 72 h using the CPE assay. The results showed that the observed effective concentrations of EGCG-AuNPs (ligand concentration 5.61×10^{-1} μM) and RES-AuNPs (ligand concentration 3.44 μM) inhibited infection at the tested temperatures, at least for the whole period for which the untreated

virus was showing infectivity. Namely, in the control experiment with the untreated virus, it was observed that the virus infectivity was decreasing with time, more quickly at higher temperatures, as expected.

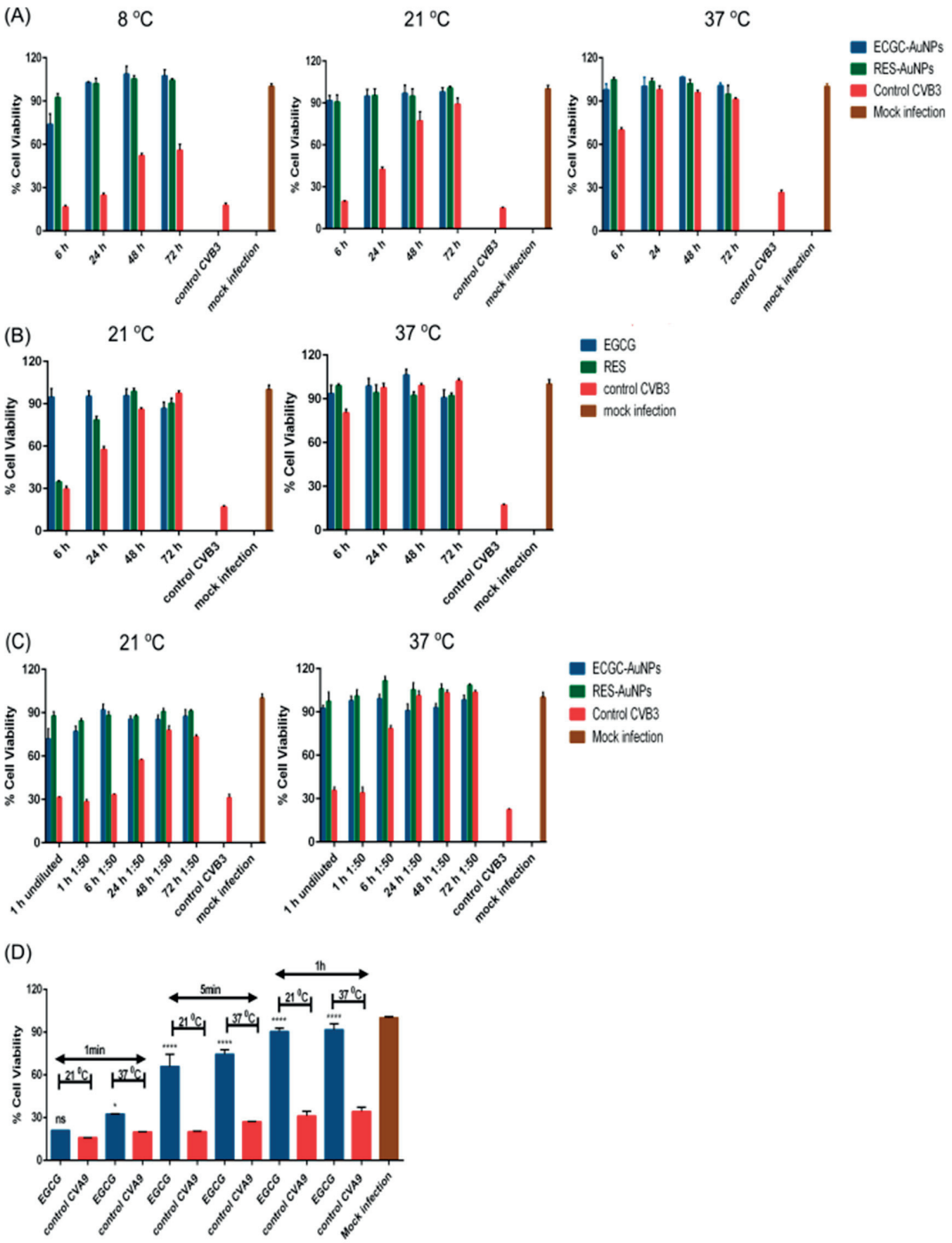

Figure 3. Effect of time and temperature (**A**,**B**,**D**) and dilution (**C**) on antiviral activity of polyphenols and polyphenol-functionalized nanoparticles (AuNPs). (**A**,**B**) EGCG-AuNPs (ligand concentration 5.61×10^{-1} μM), RES-AuNPs (ligand concentration 3.44 μM), EGCG (650 μM) and RES (880 μM) were incubated with CVB3 (4.4×10^{8} PFU/mL) at different temperatures over 72 h. Sample fractions were collected at 6, 24, 48 and 72 h and a CPE was performed from them.

(**C**) The effect of dilution on the antiviral activity of polyphenol-functionalized nanoparticles (AuNPs) after an initial preincubation of 1 h between CVB3 (4.4×10^8 PFU/mL) with EGCG-AuNPs (ligand concentration 5.61×10^{-1} μM) and RES-AuNPs (ligand concentration 3.44 μM). (**D**) EGCG (6.5 μM) and CVA9 (2×10^7 PFU/mL) were incubated at different time intervals (1 min, 5 min and 1 h) and at different temperatures (21 and 37 °C). Results (**A**–**D**) are expressed as the number of viable cells left, detected by crystal violet staining. Every experiment had an experimental virus control that was used to assess the infectivity of the virus at each point and a mock infection showing the status of viable cells. Experiments 3A and 3B were performed twice with $n = 3$, and experiments 3C and 3D were performed once, with $n = 3$ and $n = 2$, respectively. The results are expressed as average values + standard error of the mean (SEM). Experiments 3A, 3B and 3C were analyzed by two-way ANOVA and 3D by one-way ANOVA, followed by the Bonferroni test (* $p < 0.05$, and **** $p < 0.0001$).

The experiments were repeated with the ligands at 21 and 37 °C (Figure 3B). The results were similar to those with AuNPs. Interestingly, RES could not rescue cells from infection before 6 h at 21 °C, but was already quite effective after 24 h. We then tested whether the antiviral efficacy was lost if the solution was diluted after the initial incubation with the virus (Figure 3C). The hypothesis was that strong dilution may disconnect the virus and ligand or ligand-NP and lead to a re-established infectivity. After 1 h of incubation of the virus with functionalized AuNPs at 37 and 21 °C, we diluted the solution 50 times and continued the incubation. Samples were collected from diluted solutions at different time points (1, 6, 24, 48 and 72 h) and tested for infectivity on A549 cells. The CPE analysis of diluted and control virus samples (normalized to contain comparable amounts of virus) showed that the 50-times diluted samples maintained the antiviral activity very well, and similarly to undiluted samples (Figure 3C). Similar results were observed with EGCG and RES without AuNPs even when diluted (data not shown).

We also wanted to understand the effectiveness of polyphenols at shorter incubation time intervals at 21 and 37 °C (Figure 3D). The results showed that already, 1 min of incubation slightly increased the cell viability, as indicated by reduced lytic viral activity. This effect was more apparent at 37 °C. After 5 min of incubation, cell viability increased strongly at both temperatures, and 1 h of incubation already showed full protection. These results thus confirm that the polyphenols show good antiviral efficacy at various temperatures and after a short contact time.

3.2. Mechanism of Action

To understand if the compounds acted as inhibitors for virus attachment or in other steps of infection, we performed a simple time of addition study. In the assay, cells were first infected with CVB3 for 1 h at 37 °C and then the compounds were added, followed by overnight incubation. As shown in Figure 4A, polyphenols did not exhibit any antiviral activity when added 1 h post-infection (p.i.). This excludes antiviral action on intracellular processes.

Three possible mechanisms of pre-entry action were studied: (1) the polyphenols and polyphenol-functionalized nanoparticles stabilize the virus and prevent its opening (and release of genome), (2) the compounds prevent binding of the virions to the cell surface and (3) the capsid is disrupted or damaged by the polyphenols, and thus, the genome is prematurely released from the virions.

A potential increase in capsid stability of the virions was tested in a thermal stability assay, PaSTRy [15,22]. In the assay, gradual heating of the virus up to 90 °C induces the uncoating and release of the viral RNA to the solution, typically between 40 and 50 °C for enteroviruses [22]. Non-fluorescent SGII in the medium intercalates within the double-stranded regions in the viral RNA and emits fluorescence upon binding [33]. Increase in capsid stability would lead to a higher melting temperature, whereas lower melting temperature would suggest destabilization.

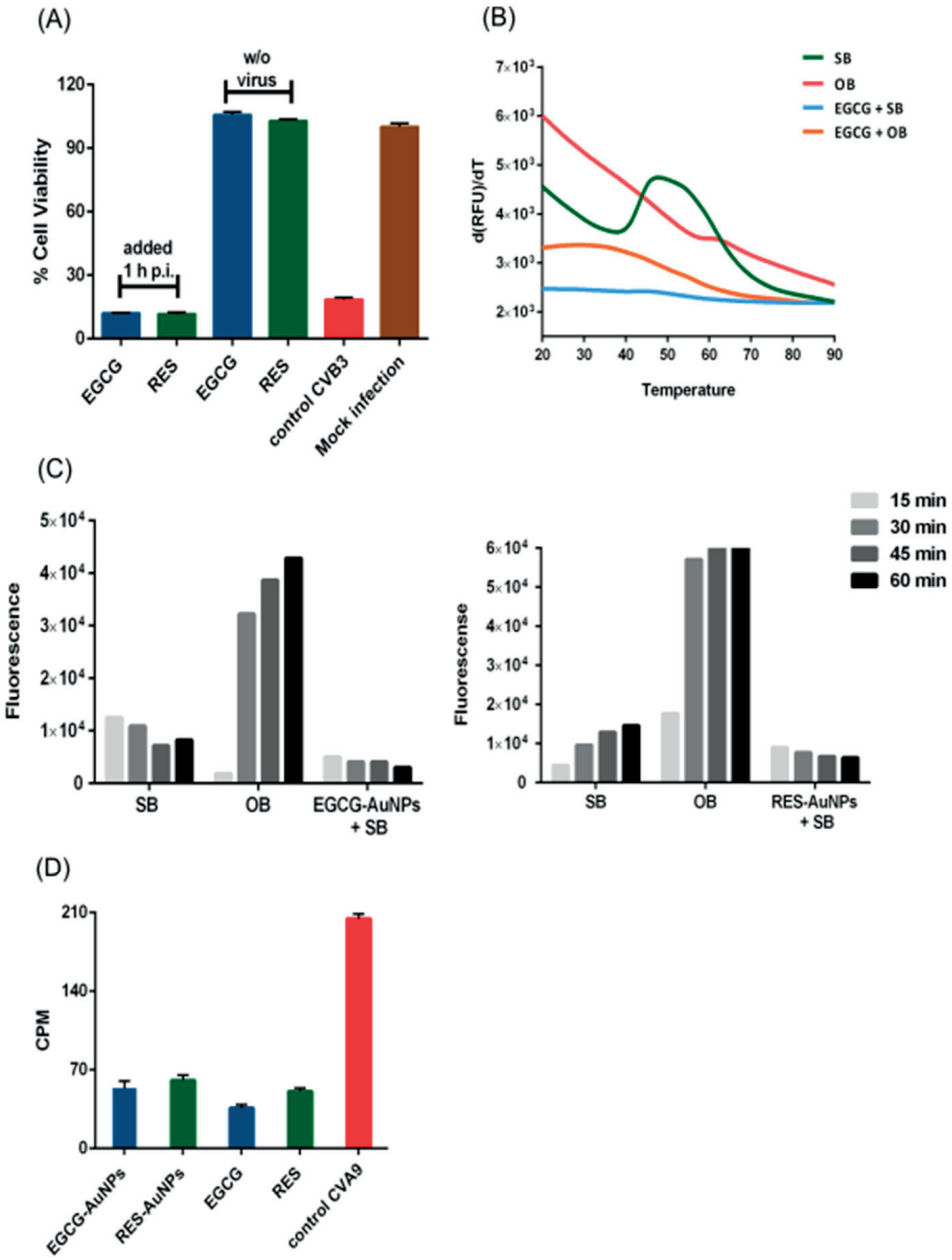

Figure 4. Studies on mechanism of antiviral activity of polyphenols and polyphenol-conjugated nanoparticles (AuNPs). (**A**) Time of addition assay, where the polyphenols EGCG (65 μM) and RES (880 μM) were added to cells 1 h post-infection. The results are the mean of two independent experiments, with $n = 5$. Average values + standard errors of the mean (SEM) are shown. (**B**) The PaSTRy assay measures the thermal stability of CVB3 (0.5 μg) in the presence of the EGCG (65 μM). The tests were performed in the presence of the storage buffer (SB; PBS with 2 mM $MgCl_2$) and opening buffer (OB; 20 mM NaCl, 6 mM KH_2PO_4, 12 mM K_2HPO_4 and 0.01% faf-BSA), depicted as blue and orange color, respectively. This is a representative result from three experiments, with $n = 3$. (**C**) The Uncoating assay shows that EGCG-AuNPs and RES-AuNPs lower the release of the viral RNA from virions and prevent expansion of the virions. The assay is based on real-time fluorescence spectroscopy, which detects high fluorescence of SGII when it is bound to the viral genome, either free RNA released from the virions or virion-bound RNA when SGII can enter an expanded virus.

Here, CVB3 (0.5 μg) was incubated with SB or OB as controls or with SB in the presence of EGCG-AuNPs (ligand concentration 5.61×10^{-2} μM; left graph) or RES-AuNPs (ligand concentration 3.44×10^{-1} μM; right graph). The fluorescence values have been subtracted with the measurement of RNAse in the assay, and the difference between the calculations, which is the net release of RNA, has been plotted in the graphs. Both the graphs are a representative result from three experiments. (**D**) The binding assay measures the binding of metabolically radio-labeled virus onto the cells in the presence of compounds on ice. Control CVA9 is the binding measured from the virus without polyphenols. Average values of radioactivity (CPM, counts per minute) + standard error of the mean (SEM) are shown from one representative experiment that was performed twice with similar results, with $n = 3$.

Untreated CVB3 in a storage buffer (PBS $MgCl_2$) had a transition temperature of 42 °C (Figure 4B), while in an opening buffer, the fluorescence was maximal already without heating [16,21]. The opening buffer promotes virus opening by releasing the pocket factor with a combination of albumin and low sodium/high potassium content. When 0.5 μg of CVB3 was pre-incubated with a concentration of 65 μM EGCG, strikingly, low fluorescence was recorded and no transition could be observed in the tested temperature range, probably because EGCG stabilized the virion and prevents genome release (Figure 4B). If the opening buffer was added to the EGCG-treated virus, the initial fluorescence was higher but still lower than in the absence of EGCG and, again, no significant transition was observed during the heating.

To study the mechanism of this unexpected stabilization in detail, we used our previously developed real-time spectroscopy uncoating assay, which can detect the viral genome at various stages of uncoating in vitro at physiological temperature, 37 °C. This assay relies on the fact that SGII is able to bind to the virus RNA inside the expanded capsid and outside the broken capsid, but the dye is excluded from the intact capsid [16,21]. Thus, this approach enables us to detect the expanded, primed state and the fully opened state of the virus, while the intact virus would show no fluorescence. For this assay, CVB3, polyphenol-functionalized nanoparticles and SGII were mixed in a buffer, and the fluorescence was measured. The control virus in the storage buffer revealed a low background fluorescence that did not change much during the 1 h experiment at 37 °C, suggesting that the virus is relatively stable at 37 °C in this buffer (Figure 4C), as expected from earlier studies [16]. The assay includes a subsequent addition of RNAse to the samples that degrades the released RNA. The RNase molecule is too large (72 kDa) to enter the primed virus particles and digest the viral genome, hence allowing to distinguish fully open capsids from partially damaged ones. SGII is small enough (0.45 kDa) to enter, bind to the genome and emit fluorescence [15]. The values after RNAse addition were subtracted from the fluorescence values without RNAse, thus providing the net RNA released from the viruses in the assay. The presence of EGCG-AuNPs or RES-AuNPs caused an even lower overall fluorescence compared to the control virus sample in this assay, suggesting that the functionalized AuNPs prevented expansion that normally occurs to some extent in the storage buffer at 37 °C. The fluorescence did not change with time, confirming that the functionalized AuNPs prevented opening and RNA release. The results were similar if the free polyphenols were added instead of polyphenol-functionalized AuNPs (data not shown).

To test whether the presence of ligands also prevents binding of the virus to the surface receptors of A549 cells, we performed a binding assay using a metabolically radiolabeled virus. Radioactive ^{35}SMet/Cys-CVA9 was first incubated with the compounds for 1 h, followed by binding them to A549 cells for another 1 h on ice, and continuing by thorough washings. Measurement of the radioactivity from the virus bound to the cell surface in the presence of the compounds revealed that both the ligands and the functionalized nanoparticles drastically reduced binding of the virus to the cell surface (Figure 4D). The results altogether suggest that the EGCG, RES and their functionalized AuNPs interact directly with the capsid, stabilize it strongly and hence prevent the infection by both preventing uncoating and receptor binding.

Polyphenols Cause Clustering and Aggregation of the Enteroviruses

With a sucrose gradient, viruses can be separated into intact, empty and expanded/intermediate particles [15,16]. Such a separation was performed with the radioactive ^{35}SMet/Cys-CVA9, pre-incubated with EGCG or RES for 1 h at 37 °C (Figure 5A). Fresh virus control without the polyphenols and without preliminary incubation at 37 °C showed a typical single peak of intact viruses covering about 4–5 fractions in the bottom part of the gradient. Incubation of the control virus in the storage buffer for 1 h at 37 °C showed no significant difference to the fresh virus. Only a small peak broadening can be observed due to the presence of some expanded virions [15]. Strikingly, when the virus was treated with the polyphenols, there was a complete loss of radioactivity. We assume that the clustering of the virus induced by the polyphenols led to aggregates, which precipitated or adhered to the walls of the tubes. Myllynen et al. [15] observed a similar loss of radioactivity when vulnerable virus preparations were aggregated during fractionation in a $CsCl_2$ gradient.

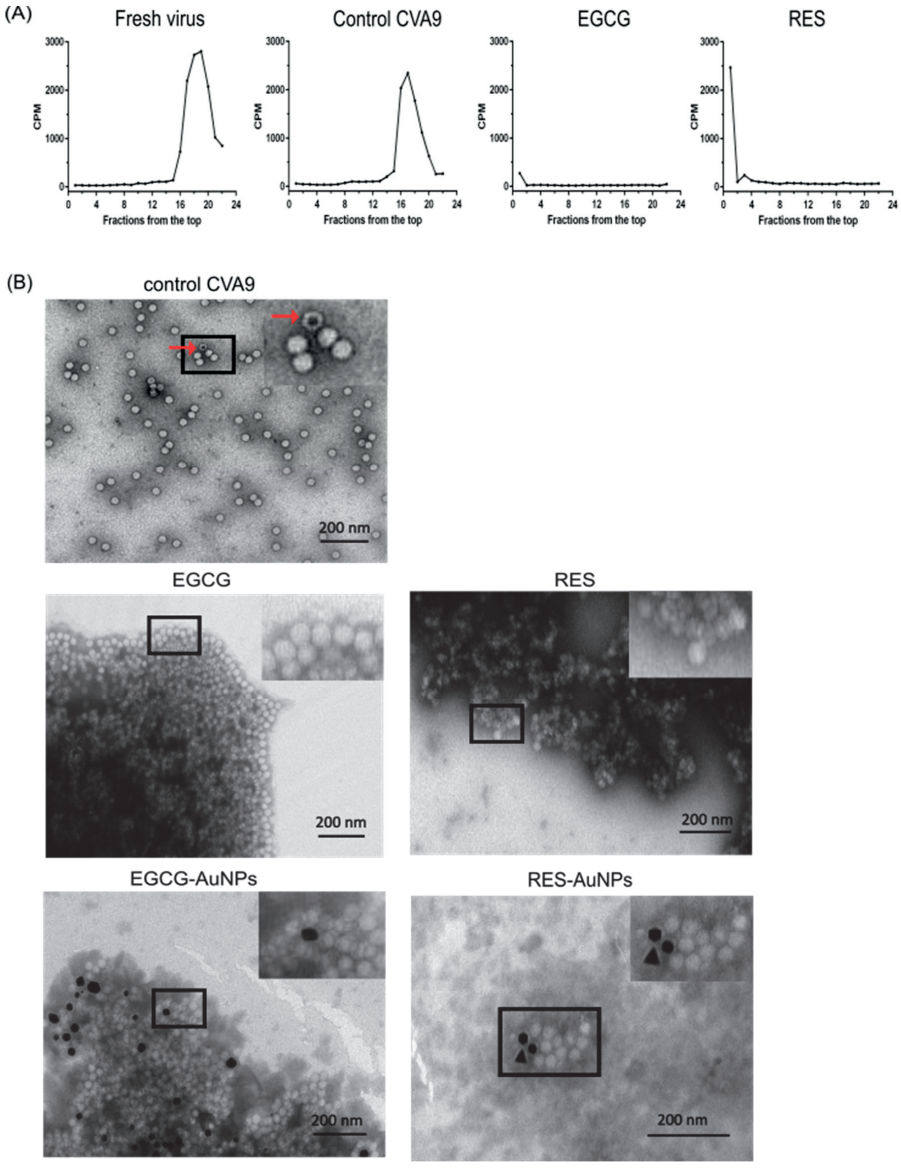

Figure 5. *Cont.*

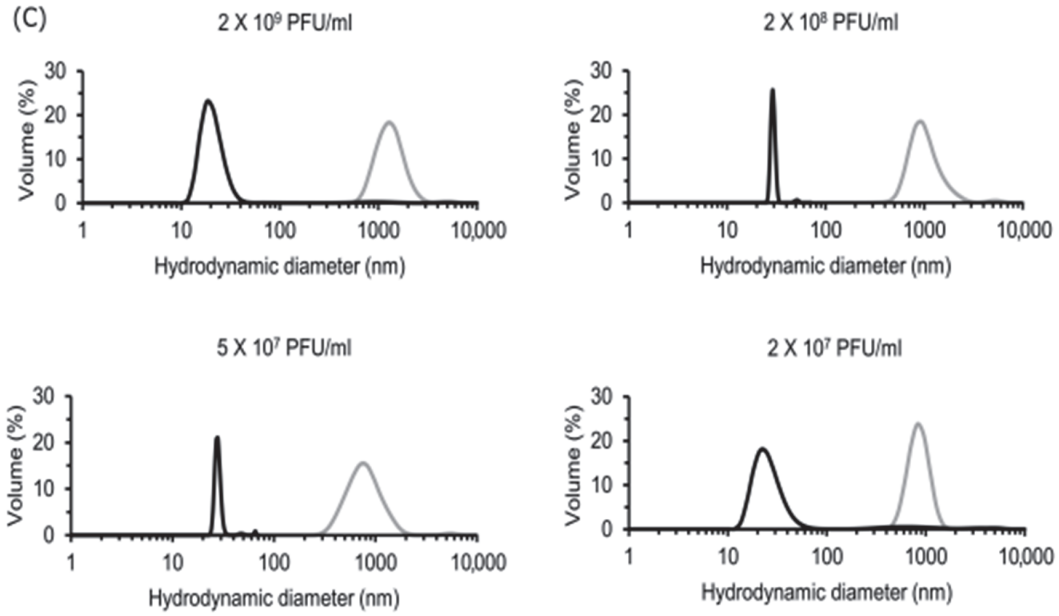

Figure 5. Aggregation/clustering of enteroviruses identified using (**A**) sucrose gradient (5–20%) separation of the metabolically radiolabeled CVA9 after incubation with the polyphenols for 1 h at 37 °C, and (**B**) negatively stained TEM images of CVA9 (1.6×10^{10} PFU/mL) and CVA9 treated with EGCG (650 μM), RES (880 μM), EGCG-AuNPs (ligand concentration 5.61×10^{-1} μM) and RES-AuNPs (ligand concentration 3.44 μM). Scale bar, 200 nm. The viral particles with a dark inner center (marked with a red arrow in the control CVA9 TEM image) can be easily differentiated as empty/broken virus capsids. (**C**) Dynamic light scattering analysis of EGCG (6.5 μM) with different dilutions of CVA9.

To test our hypothesis, we pretreated the virus with polyphenols or polyphenol-functionalized AuNPs for 1 h and then visualized them under the transmission electron microscope. Figure 5B shows negatively stained control viruses and viruses treated with polyphenols and polyphenol-functionalized AuNPs. Control viruses mostly showed single viruses distributed homogenously over the grid. Intact virus particles have the stain around the capsid and have a bright center, whereas those that are expanded, or broken/empty allow the stain to enter the capsid and have a darker appearance or dark center, respectively (some empty virions are indicated in Figure 5B). In the presence of the polyphenols or polyphenol-functionalized AuNPs, virus particles appeared only in large aggregates. Interestingly, the viruses inside the aggregates seemed to be intact, and empty virus particles were rarely seen. However, some uneven coloring of the virions was observed. These results confirmed that, in addition to stabilization of the particles, the polyphenols cause clustering of the viruses.

To observe the clustering of the viruses in a more robust way in solution, we performed DLS after EGCG treatment. We detected the virus in DLS with a hydrodynamic diameter of ~22 nm, which is a little lower than expected for CVA9 (Figure 5C). However, this peak could be detected in a very reproducible manner, and we observed only a few aggregates in the virus samples by DLS. After treating the virus samples with EGCG, the virus-associated peak completely disappeared, and particles were detected only in the size range of 650–1240 nm, further confirming that, indeed, polyphenols cause aggregation of the enteroviruses. The virus was then diluted using 10-fold dilutions while keeping the EGCG concentration constant. The aggregates appeared upon every dilution, indicating that a high concentration of viruses was not a prerequisite for aggregate forming. A similar size distribution was observed in all tested dilutions.

We also studied if the clustering with a lower titer of the virus would still cause a similar drop of infectivity. We did this by drastically reducing the CVB3 concentration to 2×10^5 PFU/mL, which is 100 times less than in the previous experiment (Supplementary Figure S2). Despite the dilution of 100 times, we observed an efficient antiviral effect.

3.3. Discovery of Multiple Ligand Binding Sites on the Surface of CVA9 and CVB3

The docking poses were visualized from the 2-fold (Figure 6) and 3-fold (Figure 7) axes of symmetry, respectively. From the PyVOL calculations, the hydrophobic pockets (HPs) were visibly smaller in CVB3 (subfigures B and D from Figures 1 and 2) compared to CVA9 (subfigures A and C from Figures 6 and 7). More specifically, in CVB3, the buried HP site was found to be composed of VP1 residue positions 93, 95, 190–194, 205–212 and 258–261 (residue numbering according to 6GZV). The analogous pocket in CVA9, however, consisted of residues 95–98, 115, 117, 144, 146, 170, 181, 183, 186–188, 192, 193, 210, 212–216 and 219 in CVA9 (residue numbering according to 1D4M). Abdelnabi and co-workers' work describes the Butcher-Neyts pocket that comprise VP1 residue positions 73, 76, 77, 78, 234 and 236, and VP3 residue positions 234–236 in CVB3 [25]. While CVA9 and CVB3 shared identical residue loci for the VP3 component of the Butcher-Neyts pocket, CVB3 had VP1 mutations M76F and E77T and VP3 mutations D234Q and K236F (using CVA9 as a reference). EGCG was the only compound found to bind the Butcher-Neyts pocket in CVA9, albeit with dissimilar contact residues, consisting of D158, D159, Y160, W162, Q163 and R222 from VP1, and the VP3 residues Q233, D234, N235 and R237 (Figure 7A). In our experimental set-up, the Butcher-Neyts pocket was more completely exposed within the docking grid box covering the 3-fold axis protomers, which explains the absence of bound ligands within the grids designed for the 2-fold axis of symmetry.

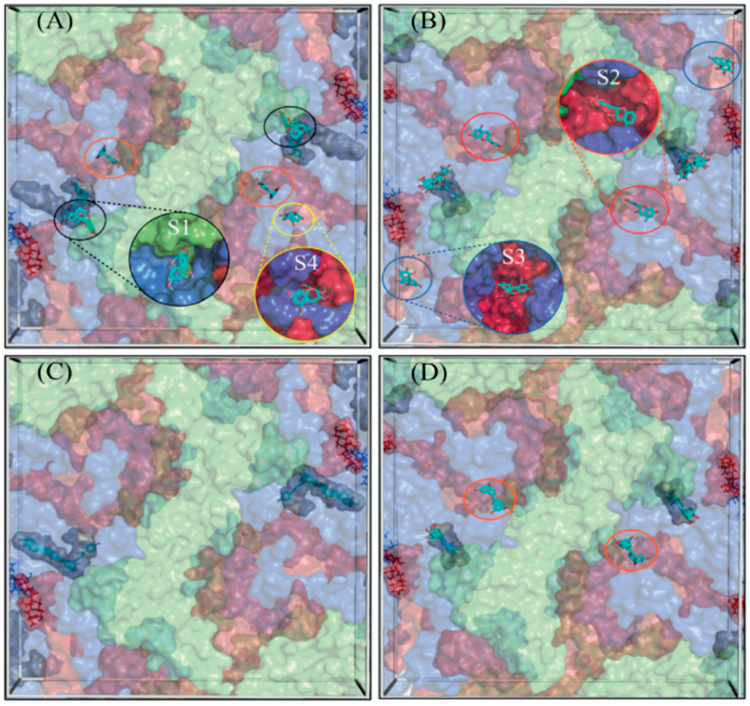

Figure 6. Docking grid boxes centered at the 2-fold axis, for EGCG (top subfigures) and RES (bottom subfigures). CVA9 is on the left (**A**,**C**) while CVB3 is on the right (**B**,**D**). The hydrophobic pocket is represented as a grey surface, while the residues for the Butcher-Neyts pocket are represented as lines. Capsid proteins VP1–VP3 are colored blue, light green and red, respectively. VP4 is not shown. Docked poses are represented as sticks. The binding sites S1, S2 and S3 are colored black, red and blue. Tentative site S4 is in circled in yellow. The additional binding site (S4) was found using EGCG (Figure 1A, circled in yellow) in CVA9 only. There is less statistical support for this site, as only one ligand pose was found in this region. However, with a favorable binding energy (−7 kcal/mol) and an estimated six hydrogen bonds, it cannot be completely ignored. The binding surface for the potential S4 site comprises VP1 residues T274, R275, K276, T280, V281, T282, T283 and V284, and VP3 residues N57, Q59, R86, D92, S93 and V94. As these residues are recorded only from one observation, it is not a consensus for S4.

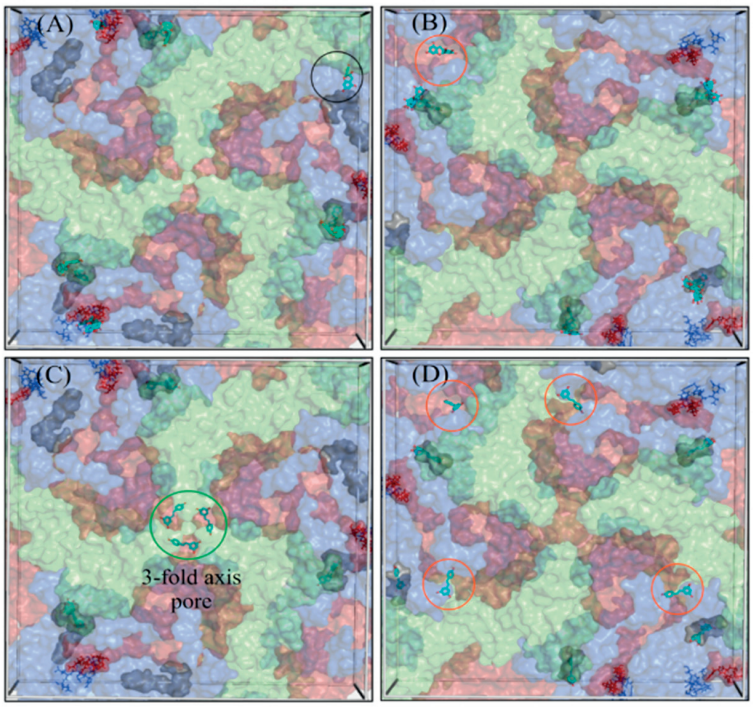

Figure 7. Docking grid boxes centered at the 2-fold axis, for EGCG (top subfigures) and RES (bottom subfigures). CVA9 is on the left (**A**,**C**) while CVB3 is on the right (**B**,**D**). The hydrophobic pocket is represented as a grey surface, while the residues for the Butcher-Neyts pocket are represented as lines. Capsid proteins VP1–VP3 are colored blue, light green and red, respectively. VP4 is not shown. Docked poses are represented as sticks. The binding sites S1, S2 and S3 are colored black, red and blue. Tentative site S4 is in circled in yellow. The additional binding site (S4) was found using EGCG (Figure 1A, circled in yellow) in CVA9 only. There is less statistical support for this site, as only one ligand pose was found in this region. However, with a favorable binding energy (−7 kcal/mol) and an estimated six hydrogen bonds, it cannot be completely ignored. The binding surface for the potential S4 site comprises VP1 residues T274, R275, K276, T280, V281, T282, T283 and V284, and VP3 residues N57, Q59, R86, D92, S93 and V94. As these residues are recorded only from one observation, it is not a consensus for S4.

Four novel binding sites were found, each with the support of more than one ligand pose, and were named S1, S2, S3 and the 3-fold axis pore, based on consensus residues shared across ligand-contacting surfaces. A fifth one—tentatively named S4—had a lower level of support, as it was bound only once. S1 was detected only in CVA9 and comprised the VP1 residues Y208, G209, N211, F262, S263, V264 and D265, and VP2 residues M132, G133, G134, G138, Q139, A140 and F141, from a consensus of all 16 detected ligand poses at that site. S2 was present in both CVA9 and CVB3. In CVA9, S2 comprised VP1 residues F202 and T283, and VP3 residues R86, L87, Q88, P137, G138, A139, Q181, D182, E183, T185, S186, A187, G188 and Y189, and was derived from two poses. In CVB3, S2 is composed of VP1 residue F199 and VP3 residues P86, G140, A186, G187, G188 and F189, obtained from a consensus of residue contacts derived from 12 ligand poses. The 3-fold axis pore was detected in the CVA9 capsid only in the case of RES (Figure 8). Its consensus ligand-contacting surfaces (derived from four poses) are composed of VP2 residues R12, E27, K116, R193 and T194, VP3 residues A124, A126, T127, I158, G159 and L160 and the VP4 residue L68 in CVA9. In the same figure, the three ligand binding sites subtending the 3-fold axis with a similar rotational symmetry provide support for an actual binding site. Upon closer inspection, these sites were found to be connected, as part of a larger cavity. Access to this hollow space in CVA9 is lined with residues such as methionine (VP3), phenylalanine

(VP2) and aspartic acid (VP3). The fact that these all have titratable side chains suggests that pH may play a role in driving the pore dynamics.

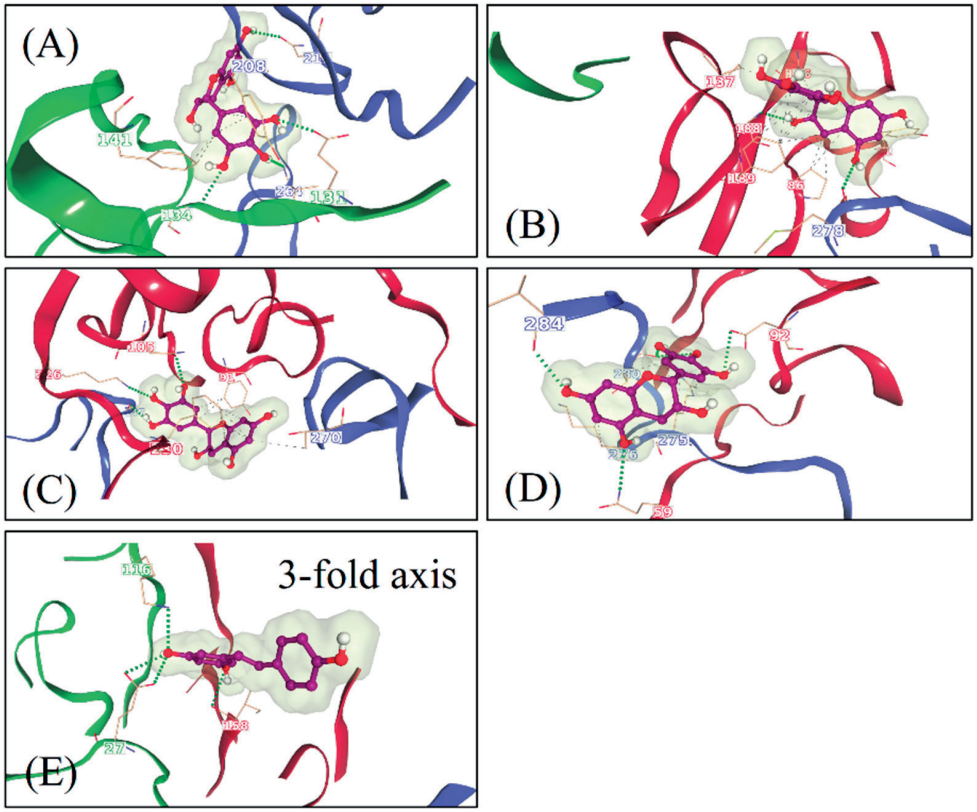

Figure 8. Protein–ligand interactions for example poses obtained at the newly determined binding sites, namely for EGCG at sites (**A**) S1 in CAV9, (**B**) S2 in CBV3, (**C**) S3 in CBV3, (**D**) S4 in CAV9 and (**E**) RES at the 3-fold axis pore in CAV9. Hydrogen bonds and hydrophobic interactions are depicted as dashed green and grey lines, respectively. Interacting residues are labeled, and the capsid proteins VP1–VP3 are colored blue, light green and red, respectively.

For a closer inspection of the non-bonded interactions occurring for RESV and EGCG, single ligand poses docked at each of the newly found sites are depicted in Figure 8. Their favorable binding energy scores and multiplicity of binding locations, combined to the formation of multiple H-bonding interactions, provide good support for the stability of these compounds for each of the Coxsackievirus strains. For instance, using the binding locations described in Figures 6 and 7, EGCG forms four H-bonding interactions involving VP1 and VP2 in CAV9 at S1, two H-bonds at S2 in CBV3 involving VP1 and VP3, three H-bonds at S3 in CBV3 involving VP1 and VP3 and five potential H-bonds at S4 in CAV9. Similarly, RES forms five potential H-bonding interactions with residues from VP2 and VP3 at the 3-fold axis pore in CAV9. While there are many more ligand binding poses from both the strains and binding sites, only one pose is shown per site, as an example.

RES and EGCG Show Differential Binding Patterns for CVA9 and CVB3

RES has fewer H-bond acceptors compared to EGCG, in addition to having a smaller size and larger hydrophobicity, as detailed in the Discussion Section. All docked poses (across ligands and strains) are summarized in Figure 9 in terms of ligand binding energies, their aggregated number of H-bonds and hydrophobic interactions at each of the six sites (S1, S2, S3, 3-fold, Butcher-Neyts pocket and HP). Our results suggest that there are both specific and shared binding sites for EGCG and RES, with strain also playing a role. Ligand binding at the sites S1 and the pore found at the 3-fold axis was only noted in CVA9. The

S1 site was bound by EGCG only with CVA9. In the case of S2, EGCG showed strain bivalence, although the calculated affinity was slightly higher in CVA9. RES also bound to S2, but only in the CVB3 strain. RES displayed slightly higher estimated affinity compared to EGCG for the same site. Binding to the S3 site was achieved only by EGCG in CVB3. Binding at the pore found at the 3-fold axis was only observed in the case of RES, only in CVA9. EGCG was found to be bound to the Butcher-Neyts pocket only in CVA9. HP was bound by both compounds in both strains. The most favorable binding energies were recorded for both EGCG and RES in the HP of CVA9, most likely due to the shape and partial charges present within the deeper hydrophobic tunnel. RES however displayed the highest affinities for the HP, which suggests more favorable binding poses due to the linear ligand shape. Both compounds performed worse in the CVB3 HP compared to CVA9, most likely due to the shallower hydrophobic pocket. The binding energies recorded at sites S1, S2, S3 and 3-fold axes are generally lower than those observed in the HP, most likely due to a decreased exposure to protein surfaces.

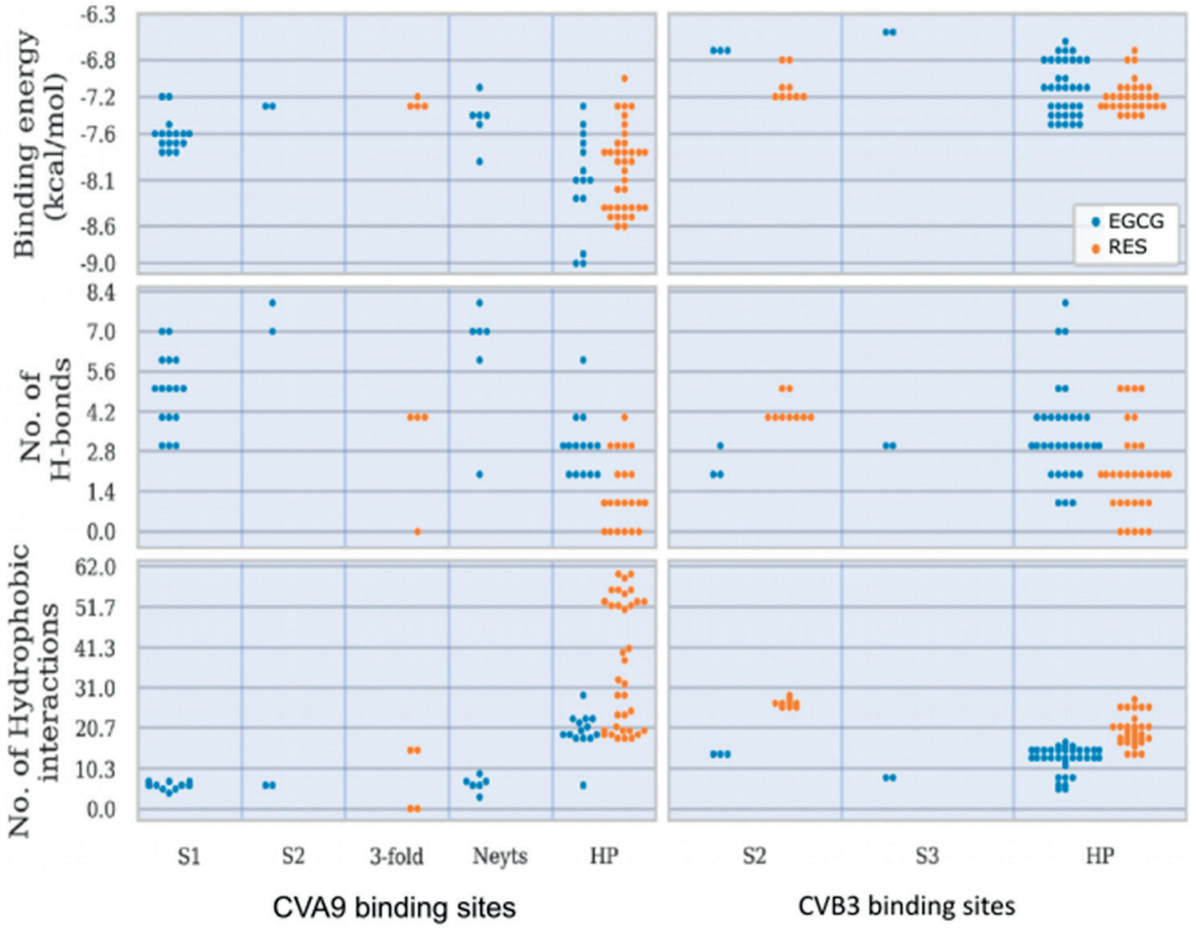

Figure 9. Summary of the binding characteristics of EGCG and RES at each of the six binding sites across CVA9 and CVB3. Each dot is an experimental unit, for which the binding energy, number of H-bonds and number of hydrophobic interactions are shown for CVA9 (left subfigures) and CVB3 (right subfigures). HP—hydrophobic pocket, Neyts—the Butcher-Neyts pocket.

Overall, EGCG bound to more sites in both CVA9 and CVB3. However, RES showed high selectivity for the hydrophobic pocket. The high number of binding sites for both compounds (compounded by the capsid symmetries) may entail a noticeable dysfunction of viral capsid behavior, especially more so in CVA9 due to the comparatively higher

number of sites and the lower binding energies for the HP region. This also explains the difference in inhibition efficacy of EGCG as compared to RES.

4. Discussion

There is a great need for broad-acting non-toxic antivirals that reduce the virus load in the body or on surfaces. Present and future pandemics as well as the yearly occurring epidemics cause high economic costs due to hospitalizations and absence from workplaces and from schools. Enteroviruses still lack a clinically accepted antiviral for treatment or disinfection of hands and surfaces. Therefore, we studied two polyphenols, EGCG from green tea and RES from red grapes and other fruits, as soluble polyphenols and polyphenol-functionalized gold nanoparticles and explored the mechanism of action for the molecules on three very stable, non-enveloped enteroviruses (CVA9, CVB1 and CVB3).

Our results showed that EGCG and RES have strong antiviral efficacy against the three enterovirus serotypes. Antiviral efficacy in general was already known for the two polyphenols before [34], but not for enteroviruses. The EC_{50} values were in the range of 0.266–3.411 μM for EGCG and 107.894–330.369 μM for RES, thus suggesting a good efficacy already at low concentrations. The CC_{50} showed no cytotoxicity. The polyphenols bound to the AuNPs showed EC_{50} values in the range of 0.004–0.237 μM for EGCG and 0.004–0.068 μM for RES.

Most antivirals target cellular replication steps of the viruses, such as promoting apoptosis and via inhibiting Nf-kB or MAPK pathways and replication [5,35,36]. Most studies on the polyphenols as antivirals for enteroviruses focus on EV71 and observe antiviral action past entry and during replication of the viruses. Our results reveal that both EGCG and Resveratrol act as entry and attachment inhibitors by binding to enterovirus surfaces. This was confirmed by the time of addition CPE assay when polyphenols pre-incubated with viruses showed inhibition, while drugs added after entry to cells had no effect. In silico docking data further showed that these polyphenols could bind to multiple areas on the virion surface. Other drugs binding directly to enterovirus capsids, such as pleconaril, target the hydrophobic pocket that is normally housed by an aliphatic lipid such as palmitic or oleic acid [37,38]. The hydrophobic pocket has been associated with capsid stability and suggested to release its lipid upon viral RNA release [39]. We have recently shown that albumin treatment of enteroviruses Echovirus 1 and CVA9 do expand the virion, which is typically an event associated with emptying of the pocket. However, we showed that treatment with albumin, which may steal fatty acids from the virion, does not yet lead to virus uncoating but rather virus priming to an intermediary form, leading to virus RNA release only upon further cues, such as changes in concentration of key ions [16,21]. Here, we have studied three viruses, two of which show similarly spacious pockets, whereas the CVB3 Nancy strain has a collapsed pocket that cannot house large molecules. Consequently, CVA9 showed the highest estimated binding energies for both drugs in the HP. In addition, simulations showed that the HP is the preferable docking site for the drugs with the 73% of the docking poses associated with it.

A novel algorithm that was developed for this study to reveal the docking of the molecules on enterovirus surfaces considered larger areas around the 2- and 3-fold symmetry axis. Remarkably, the docking poses for the polyphenols, RES and EGCG on the viral capsids suggested the existence of multiple binding sites, as seen from the 2-fold (Figure 6) and 3-fold (Figure 7) axes of symmetry, respectively. It seemed that the binding locations were influenced by both the physico-chemical characteristics of the polyphenols, the geometric landscapes and partial charge distributions present within the capsid assemblies for each strain. While both compounds are polyphenolic, Resveratrol is classified by PubChem as smaller and more hydrophobic (2 heterocycles, an XLogP3 value of 3.1 and 3 H-bond acceptors) than EGCG (4 heterocycles, an XLogP3 value of 1.2 and 11 H-bond acceptors) [40], which we believe to be a main factor influencing the distribution of the ligand binding sites. The fact that the HPs detected in CVA9 are much deeper than those of CVB3 may explain the better fit of the smaller Resveratrol further inside the capsid

compared to EGCG. Altogether, three new sites were found, in addition to the known HP and the recently discovered pocket that we call the Butcher-Neyts pocket [25].

Our results suggest that there are both specific and shared binding sites for EGCG and RES, with the strain also playing a role. HP showed good binding by both viruses and both drugs, suggesting that it is the main attraction on the virion surface. Instead, S1 was only detected with EGCG in CVA9, while EGCG bound S2 in both CVA9 and CVB3. Resveratrol bound to S2 only in CVB3 but to the 3-fold axis only in CVA9, further suggesting that the structural differences of the drugs as well as of the virions dictate the docking to the virions.

The predicted binding energies were lower in the newly found docking sites in comparison to the canonical HP, probably due to its deep invagination and charges present in the pocket. In silico-determined binding energies only provide a general estimation of the affinity of ligand binding and are generally useful for doing preliminary ranking of docked ligands. However, the frequency of binding to a site can additionally assist in the evaluation of lower-scoring poses. Out of the 159 docking poses, the HP ranked first with 73% of poses assigned to it, followed by S1 (10%), S2 (9%), the Butcher-Neyts pocket (4%), the pore at the 3-fold axis (3%) and the S3 site (1%). As the Neyts pocket has already been independently proven experimentally, there are valid reasons to believe that S1, S2 and the 3-fold pore are actual novel binding sites, based on the closeness in percentage clustering, a partial overlap in the range of binding energies and the number of H-bonding interactions. There is less support for the S3 site and S4, even though both may occur.

It is no wonder that the multiple ligand binding sites on the capsid led to a strong antiviral effect directly on the virion. Our studies on the molecular mechanisms of the action showed that stabilization rather than premature RNA release occurred for enteroviruses. This was shown by several methods: (1) thermal assay, (2) our previously developed real-time uncoating assay, (3) radioactive gradient assay and (4) TEM. Stabilization and prevention of virus uncoating was evident even at higher temperatures. Our results also showed that ligand binding was accompanied by strong clustering of the virions in addition to prevention of virion uncoating in the clusters.

The fact that EGCG is a bigger molecule with more hydroxy groups can be the reason why, in comparison to RES, it is more efficient in inhibiting the enteroviruses. The number of hydroxy groups has been addressed before for the difference in antiviral action of the polyphenols, apigenin and luteolin [36]. Interestingly, Resveratrol being a nearly flat molecule (Supplementary Figure S3) is more closely attached to the surface of a gold nanoparticle. Previous experiments indicate that aromatic rings are oriented parallel to the gold surface [17]. EGCG has a nearly planar aromatic ring system with one ring perpendicular to the base (Supplementary Figure S3).

This indicates that partial immersion of the EGCG is possible and can be responsible for the increase in stability and the subsequent virus aggregation. On the other hand, the three-dimensional structure of the free EGCG molecule can cross-link several viruses by immersing into their binding pockets and inducing cross-linking of two viruses, explaining why the free EGCG is more efficient than the RES molecule. RES is six times more concentrated when bound to AuNPs as compared to EGCG. Moreover, the molecules are presented on smaller nanoparticles that have a strong surface curvature. Even if we assume that RES only penetrates slightly into the pockets because it is nearly parallel to the surface, the sheer number of interactions between virus and RES and the RES presentation by the more curved surface of nanoparticles can work as a cross-linker between multiple binding pockets on several viruses. This could explain why RES bound to nanoparticles is more efficient than the free molecule.

Another interesting fact that we observed in our infection experiments was that RES was slower to inhibit virus infection. After 6 h, its antiviral efficacy was still moderate, whereas after 24 h and later, it had reached full efficiency, while EGCG was very efficient already at earlier time points. This may be directly because RES has fewer docking sites on the virion surface. However, it may also be because it has less hydroxylic groups on its structure, leading to lower binding affinity.

Altogether, the two studied polyphenols showed great antiviral efficacy for all three studied enteroviruses. The discovered mechanism of action is that the polyphenols immerse in several binding sites on the virion surface, resulting in stabilization of the virions against opening, even in harsh conditions. In addition, formation of large clusters was observed, which might be another efficient way to lower the incidence of virions entering cells. Clustering and the resulting precipitation of the virus–polyphenol or polyphenol–AuNP clusters indicate a potential use for safe water clearing applications and for decontamination of surfaces. Future studies will focus on clarifying if the clustered viruses will be prevented from penetrating the mucus layer or be used as vaccines. Previous studies have also demonstrated the therapeutic potential of polyphenols such as EGCG and Curcumin, for treating protein aggregation diseases associated with peripheral neuropathy [41]. The mechanism by which EGCG works, to prevent the disease progression in case of amyloid fibril formation, is by stabilizing the protein after binding to it and forming soluble nontoxic aggregates [42,43]. EGCG interacts with amyloid-forming proteins through hydrophobic interactions or H-bonds, forming stable oligomers [44]. Similar interactions between the virus capsid and polyphenols have been described in our computational studies. Whether the mechanism behind virus stability/loss of infectivity and prevention of formation of amyloid aggregates reported previously is the same remains to be shown.

In general, it can be concluded that especially the AuNP-bound polyphenols might have interesting potential in future applications for (i) antiviral surface coatings, which can already reduce the viral load before it is transferred to the body surface and unintentionally up-taken, and (ii) as oral antivirals. The oral administration of the polyphenol-coated nanoparticles is especially interesting as the nanoparticle and the bound polyphenol are localized in the primary infection site for enteroviruses, in the gut, before they likely pass through the intestinal cell layer and hence can significantly reduce the viral load of the intestine. The systemic toxicity of these nanoparticles will be determined in future animal experiments. It requires consideration as the polyphenol-AuNPs due to their size and nearly neutral surface charge have optimal properties to penetrate the mucus layer of the intestinal tract [45,46].

5. Conclusions

Based on our findings, EGCG and RES effectively inhibit enterovirus infection, even after short encounters with the viruses and at various temperatures. Interestingly, the studied polyphenols have better efficacy when functionalized on gold nanoparticles, particularly for RES. The efficacy of the compounds was not compromised even when diluted 50 times. Mechanistic studies revealed that the polyphenols and polyphenol-functionalized AuNPs (i) cause clustering and stabilization of the virions, (ii) prevent the release of viral RNA and (iii) prevent the virus from binding to the cell surface. In silico docking experiments of these molecules against 2- and 3-fold symmetry axes of the capsid identified three novel binding sites in addition to the canonical hydrophobic pocket, and the Butcher-Neyts pocket. The presence of several binding sites for the polyphenols explains the strong increase in the stability. The strong clustering and inactivation of the virions may turn out to be helpful for future applications, for example, vaccination.

Supplementary Materials: The following are available online at https://www.mdpi.com/article/10.3390/pharmaceutics13081182/s1, Figure S1: Testing whether the antiviral efficacy was solely dependent on the ligand bound to the nanoparticles or from the unbound ligands possibly present in the nanoparticle preparation, Figure S2: Testing the antiviral efficacy of EGCG using lower viral titer of CVB3 (2×10^5 PFU/mL), Figure S3: 3D structure of (A) EGCG and (B) RES, Supplementary Calculations 1: calculation of number of ligands per nanoparticles, Supplementary Calculations 2: calculation of ligand concentration in AuNP stock solution. Supplementary Table S1: Parameters for the calculation of the number of ligands per AuNP, Supplementary Table S2: Parameters for the calculation of the ligand concentration bound to the AuNP in the stock solution.

Author Contributions: D.R., S.S., S.K. and V.M. conceptualized the study; D.R., S.S., O.S.A., V.L. (Valentino Laquintana), N.D., V.L. (Vili Lampinen), A.Z. and V.P.H. performed the investigations; V.M. acquired funding; S.K. and V.M. were the project administrators; O.S.A. and Ö.T.B. performed the programming; D.R., S.S., O.S.A., S.K. and V.M. wrote the manuscript; Ö.T.B., V.P.H., S.K. and V.M. reviewed and edited the manuscript. All authors have read and agreed to the published version of the manuscript.

Funding: This work was supported by the Jane and Aatos Erkko foundation (V.M.).

Institutional Review Board Statement: Not applicable.

Informed Consent Statement: Not applicable.

Data Availability Statement: Not applicable.

Acknowledgments: We would like to thank Amirbabak Sioofy-Khojine from Tampere University for helping with regression curves and EC_{50} and CC_{50} calculations.

Conflicts of Interest: The authors declare no conflict of interest.

References

1. Stone, V.M.; Hankaniemi, M.M.; Laitinen, O.H.; Sioofy-Khojine, A.B.; Lin, A.; Lozano, I.M.D.; Mazur, M.A.; Marjomäki, V.; Loré, K.; Hyöty, H.; et al. A hexavalent Coxsackievirus B vaccine is highly immunogenic and has a strong protective capacity in mice and nonhuman primates. *Sci. Adv.* **2020**, *6*, eaaz2433. [CrossRef] [PubMed]
2. Linnakoski, R.; Reshamwala, D.; Veteli, P.; Cortina-Escribano, M.; Vanhanen, H.; Marjomäki, V. Antiviral Agents From Fungi: Diversity, Mechanisms and Potential Applications. *Front. Microbiol.* **2018**, *9*, 2325. [CrossRef] [PubMed]
3. Filardo, S.; Di Pietro, M.; Mastromarino, P.; Sessa, R. Therapeutic potential of resveratrol against emerging respiratory viral infections. *Pharmacol. Ther.* **2020**, *214*, 107613. [CrossRef] [PubMed]
4. Vestergaard, M.; Ingmer, H. Antibacterial and antifungal properties of resveratrol. *Int. J. Antimicrob. Agents* **2019**, *53*, 716–723. [CrossRef] [PubMed]
5. Zhang, L.; Li, Y.; Gu, Z.; Wang, Y.; Shi, M.; Ji, Y.; Sun, J.; Xu, X.; Zhang, L.; Jiang, J.; et al. Resveratrol Inhibits Enterovirus 71 Replication and Pro-Inflammatory Cytokine Secretion in Rhabdosarcoma Cells through Blocking IKKs/NF-κB Signaling Pathway. *PLoS ONE* **2015**, *10*, e0116879.
6. Williamson, M.; McCormick, T.G.; Nance, C.L.; Shearer, W. Epigallocatechin gallate, the main polyphenol in green tea, binds to the T-cell receptor, CD4: Potential for HIV-1 therapy. *J. Allergy Clin. Immunol.* **2006**, *118*, 1369–1374. [CrossRef]
7. Kawai, K.; Tsuno, N.H.; Kitayama, J.; Okaji, Y.; Yazawa, K.; Asakage, M.; Hori, N.; Watanabe, T.; Takahashi, K.; Nagawa, H. Epigallocatechin gallate, the main component of tea polyphenol, binds to CD4 and interferes with gp120 binding. *J. Allergy Clin. Immunol.* **2003**, *112*, 951–957. [CrossRef]
8. Kim, M.; Kim, S.-Y.; Lee, H.W.; Shin, J.S.; Kim, P.; Jung, Y.-S.; Jeong, H.-S.; Hyun, J.-K.; Lee, C.-K. Inhibition of influenza virus internalization by (−)-epigallocatechin-3-gallate. *Antivir. Res.* **2013**, *100*, 460–472. [CrossRef]
9. Cottart, C.-H.; Nivet-Antoine, V.; Laguillier-Morizot, C.; Beaudeux, J.-L. Resveratrol bioavailability and toxicity in humans. *Mol. Nutr. Food Res.* **2009**, *54*, 7–16. [CrossRef]
10. Kučera, O.; Mezera, V.; Moravcova, A.; Endlicher, R.; Lotková, H.; Drahota, Z.; Červinková, Z. In VitroToxicity of Epigallocatechin Gallate in Rat Liver Mitochondria and Hepatocytes. *Oxidative Med. Cell. Longev.* **2015**, *2015*, 476180. [CrossRef]
11. Isbrucker, R.; Edwards, J.; Wolz, E.; Davidovich, A.; Bausch, J. Safety studies on epigallocatechin gallate (EGCG) preparations. Part 2: Dermal, acute and short-term toxicity studies. *Food Chem. Toxicol.* **2006**, *44*, 636–650. [CrossRef]
12. Yang, F.; Medik, Y.; Li, L.; Tian, X.; Fu, D.; Brouwer, K.L.R.; Wagner, K.; Sun, B.; Sendi, H.; Mi, Y.; et al. Nanoparticle Drug Delivery Can Reduce the Hepatotoxicity of Therapeutic Cargo. *Small* **2020**, *16*, e1906360. [CrossRef] [PubMed]
13. Meléndez-Villanueva, M.A.; Morán-Santibañez, K.; Sanmiguel, J.J.M.; Rangel-López, R.; Garza-Navarro, M.A.; Rodríguez-Padilla, C.; Zarate-Triviño, D.G.; Trejo-Ávila, L.M. Virucidal Activity of Gold Nanoparticles Synthesized by Green Chemistry Using Garlic Extract. *Viruses* **2019**, *11*, 1111. [CrossRef] [PubMed]
14. Huttunen, M.; Waris, M.; Kajander, R.; Hyypiä, T.; Marjomäki, V. Coxsackievirus A9 Infects Cells via Nonacidic Multivesicular Bodies. *J. Virol.* **2014**, *88*, 5138–5151. [CrossRef]
15. Myllynen, M.; Kazmertsuk, A.; Marjomäki, V. A Novel Open and Infectious Form of Echovirus 1. *J. Virol.* **2016**, *90*, 6759–6770. [CrossRef]
16. Ruokolainen, V.; Domanska, A.; Laajala, M.; Pelliccia, M.; Butcher, S.J.; Marjomäki, V. Extracellular Albumin and Endosomal Ions Prime Enterovirus Particles for Uncoating That Can Be Prevented by Fatty Acid Saturation. *J. Virol.* **2019**, *93*, 599. [CrossRef]
17. Mandal, S.; Bonifacio, A.; Zanuttin, F.; Sergo, V.; Krol, S. Synthesis and multidisciplinary characterization of polyelectrolyte multilayer-coated nanogold with improved stability toward aggregation. *Colloid Polym. Sci.* **2011**, *289*, 269–280. [CrossRef]
18. Sechi, M.; Sanna, V.; Pala, N.; Manconi, P.; Mariani, A.; Dedola, S.; Rassu, M.; Crosio, C.; Iaccarino, C.; Dessi, G. Single-step green synthesis and characterization of gold-conjugated polyphenol nanoparticles with antioxidant and biological activities. *Int. J. Nanomed.* **2014**, *9*, 4935–4951. [CrossRef] [PubMed]

19. Perrone, M.; Lopalco, A.; Lopedota, A.; Cutrignelli, A.; Laquintana, V.; Douglas, J.; Franco, M.; Liberati, E.; Russo, V.; Tongiani, S.; et al. Preactivated thiolated glycogen as mucoadhesive polymer for drug delivery. *Eur. J. Pharm. Biopharm.* **2017**, *119*, 161–169. [CrossRef]
20. Schmidtke, M.; Schnittler, U.; Jahn, B.; Dahse, H.-M.; Stelzner, A. A rapid assay for evaluation of antiviral activity against coxsackie virus B3, influenza virus A, and herpes simplex virus type 1. *J. Virol. Methods* **2001**, *95*, 133–143. [CrossRef]
21. Ruokolainen, V.; Laajala, M.; Marjomäki, V. Real-time Fluorescence Measurement of Enterovirus Uncoating. *Bio-Protocol* **2020**, *10*, e3582. [CrossRef]
22. Martikainen, M.; Salorinne, K.; Lahtinen, T.; Malola, S.; Permi, P.; Häkkinen, H.; Marjomäki, V. Hydrophobic pocket targeting probes for enteroviruses. *Nanoscale* **2015**, *7*, 17457–17467. [CrossRef]
23. Morris, G.M.; Huey, R.; Lindstrom, W.; Sanner, M.F.; Belew, R.K.; Goodsell, D.S.; Olson, A.J. AutoDock4 and AutoDockTools4: Automated docking with selective receptor flexibility. *J. Comput. Chem.* **2009**, *30*, 2785–2791. [CrossRef]
24. Hendry, E.; Hatanaka, H.; Fry, E.; Smyth, M.; Tate, J.; Stanway, G.; Santti, J.; Maaronen, M.; Hyypiä, T.; Stuart, D. The crystal structure of coxsackievirus A9: New insights into the uncoating mechanisms of enteroviruses. *Structure* **1999**, *7*, 1527–1538. [CrossRef]
25. Abdelnabi, R.; Geraets, J.A.; Ma, Y.; Mirabelli, C.; Flatt, J.W.; Domanska, A.; Delang, L.; Jochmans, D.; Kumar, T.A.; Jayaprakash, V.; et al. A novel druggable interprotomer pocket in the capsid of rhino- and enteroviruses. *PLoS Biol.* **2019**, *17*, e3000281. [CrossRef]
26. Hassan, N.M.; Alhossary, A.A.; Mu, Y.; Kwoh, C. Protein-Ligand Blind Docking using QuickVina-W with Inter-Process Spatio-Temporal Integration. *Sci. Rep.* **2017**, *7*, 15451. [CrossRef] [PubMed]
27. Tange, O. GNU Parallel: The Command-Line Power Tool. *Login* **2011**, *36*, 42–47.
28. Jubb, H.; Higueruelo, A.; Ochoa-Montaño, B.; Pitt, W.; Ascher, D.B.; Blundell, T.L. Arpeggio: A Web Server for Calculating and Visualising Interatomic Interactions in Protein Structures. *J. Mol. Biol.* **2017**, *429*, 365–371. [CrossRef] [PubMed]
29. Smith, R.H.B.; Dar, A.C.; Schlessinger, A. PyVOL: A PyMOL Plugin for Visualization, Comparison, and Volume Calculation of Drug-Binding Sites. *Biorxiv* **2019**, 816702. [CrossRef]
30. Muckelbauer, J.K.; Kremer, M.; Minor, I.; Tong, L.; Zlotnick, A.; Johnson, J.E.; Rossmann, M.G. Structure determination of coxsackievirus B3 to 3.5 Å resolution. *Acta Crystallogr. Sect. D Biol. Crystallogr.* **1995**, *51*, 871–887. [CrossRef]
31. Pei, J.; Kim, B.-H.; Grishin, N.V. PROMALS3D: A tool for multiple protein sequence and structure alignments. *Nucleic Acids Res.* **2008**, *36*, 2295–2300. [CrossRef]
32. Waterhouse, A.M.; Procter, J.; Martin, D.; Clamp, M.; Barton, G.J. Jalview Version 2–a multiple sequence alignment editor and analysis workbench. *Bioinformatics* **2009**, *25*, 1189–1191. [CrossRef]
33. Saarnio, V.K.; Salorinne, K.; Ruokolainen, V.P.; Nilsson, J.R.; Tero, T.-R.; Oikarinen, S.; Wilhelmsson, L.M.; Lahtinen, T.M.; Marjomäki, V.S. Development of functionalized SYBR green II related cyanine dyes for viral RNA detection. *Dye. Pigment.* **2020**, *177*, 108282. [CrossRef]
34. Orhan, D.D.; Özçelik, B.; Özgen, S.; Ergun, F. Antibacterial, antifungal, and antiviral activities of some flavonoids. *Microbiol. Res.* **2010**, *165*, 496–504. [CrossRef] [PubMed]
35. Du, N.; Li, X.; Bao, W.; Wang, B.; Xu, G.; Wang, F. Resveratrol-loaded nanoparticles inhibit enterovirus 71 replication through the oxidative stress-mediated ERS/autophagy pathway. *Int. J. Mol. Med.* **2019**, *44*, 737–749. [CrossRef] [PubMed]
36. Lv, X.; Qiu, M.; Chen, D.; Zheng, N.; Jin, Y.; Wu, Z. Apigenin inhibits enterovirus 71 replication through suppressing viral IRES activity and modulating cellular JNK pathway. *Antivir. Res.* **2014**, *109*, 30–41. [CrossRef]
37. Pevear, D.C.; Tull, T.M.; Seipel, M.E.; Groarke, J.M. Activity of Pleconaril against Enteroviruses. *Antimicrob. Agents Chemother.* **1999**, *43*, 2109–2115. [CrossRef]
38. Smyth, M.S.; Martin, J.H. Picornavirus Uncoating. *Mol. Pathol. MP* **2002**, *55*, 214–219. [CrossRef]
39. Smyth, M.; Pettitt, T.; Symonds, A.; Martin, J. Identification of the pocket factors in a picornavirus. *Arch. Virol.* **2003**, *148*, 1225–1233. [CrossRef] [PubMed]
40. Kim, S.; Chen, J.; Cheng, T.; Gindulyte, A.; He, J.; He, S.; Li, Q.; Shoemaker, B.A.; Thiessen, P.A.; Yu, B.; et al. PubChem 2019 update: Improved access to chemical data. *Nucleic Acids Res.* **2019**, *47*, D1102–D1109. [CrossRef]
41. Ferreira, N.; Saraiva, M.J.; Almeida, M. Natural polyphenols inhibit different steps of the process of transthyretin (TTR) amyloid fibril formation. *FEBS Lett.* **2011**, *585*, 2424–2430. [CrossRef] [PubMed]
42. Ferreira, N.; Cardoso, I.; Domingues, M.R.; Vitorino, R.; Bastos, M.; Bai, G.; Saraiva, M.J.; Almeida, M. Binding of epigallocatechin-3-gallate to transthyretin modulates its amyloidogenicity. *FEBS Lett.* **2009**, *583*, 3569–3576. [CrossRef]
43. Ferreira, N.; Saraiva, M.J.; Almeida, M.R. Epigallocatechin-3-Gallate as a Potential Therapeutic Drug for TTR-Related Amyloidosis: "In Vivo" Evidence from FAP Mice Models. *PLoS ONE* **2012**, *7*, e29933. [CrossRef] [PubMed]
44. del Amo, J.M.L.; Fink, U.; Dasari, M.; Grelle, G.; Wanker, E.E.; Bieschke, J.; Reif, B. Structural Properties of EGCG-Induced, Nontoxic Alzheimer's Disease Aβ Oligomers. *J. Mol. Biol.* **2012**, *421*, 517–524. [CrossRef]
45. Pearson, J.P.; Chater, P.I.; Wilcox, M.D. The properties of the mucus barrier, a unique gel–how can nanoparticles cross it? *Ther. Deliv.* **2016**, *7*, 229–244. [CrossRef] [PubMed]
46. de Sousa, I.P.; Steiner, C.; Schmutzler, M.; Wilcox, M.D.; Veldhuis, G.J.; Pearson, J.P.; Huck, C.; Salvenmoser, W.; Bernkop-Schnürch, A. Mucus permeating carriers: Formulation and characterization of highly densely charged nanoparticles. *Eur. J. Pharm. Biopharm.* **2015**, *97*, 273–279. [CrossRef]